

**SEPARATION OF DL-ASPARAGINE ENANTIOMERS
USING CRYSTALLIZATION INHIBITORS**



**A Thesis Submitted in Partial Fulfillment of Requirements for the
Degree of Doctor of Philosophy in Chemical Engineering
Suranaree University of Technology
Academic Year 2017**

การแยกดีแอลเอสพาราจีนอินเนนทีโอเมอร์โดยการตกผลึกด้วยสารยับยั้ง



วิทยานิพนธ์นี้เป็นส่วนหนึ่งของการศึกษาตามหลักสูตรปริญญาวิศวกรรมศาสตรดุษฎีบัณฑิต

สาขาวิชาวิศวกรรมเคมี

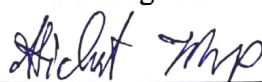
มหาวิทยาลัยเทคโนโลยีสุรนารี

ปีการศึกษา 2560

SEPARATION OF DL-ASPARAGINE ENANTIOMERS USING CRYSTALLIZATION INHIBITORS

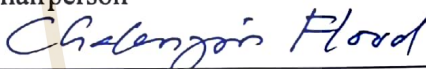
Suranaree University of Technology has approved this thesis submitted in partial fulfillments of the requirements for the Degree of Doctor of Philosophy.

Thesis Examining Committee




(Asst. Prof. Dr. Atichat Wongkoblap)

Chairperson




(Asst. Prof. Dr. Chalongsri Flood)

Member (Thesis Advisor)




(Prof. Dr. Adrian E. Flood)

Member



(Dr. Terasut Sookkumnerd)

Member



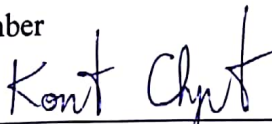
(Asst. Prof. Dr. Atthaphon Maneedaeng)

Member



(Asst. Prof. Dr. Lek Wantha)

Member



(Assoc. Prof. Flt. Lt. Dr. Kontorn Chamniprasart)



(Prof. Dr. Santi Maensiri)

Vice Rector for Academic Affairs
and Internationalization

Dean of Institute of Engineering

ปีติภมล คงสมัย : การแยกดีแอลแอสพาราจีนเอนทิโอเมอร์โดยการตกผลึกด้วยสาร
ยับยั้ง (SEPARATION OF DL-ASPARAGINE ENANTIOMERS USING
CRYSTALLIZATION INHIBITORS) อาจารย์ที่ปรึกษา : ผู้ช่วยศาสตราจารย์ ดร.ฉลองศรี
พลัด, 250 หน้า

ในปัจจุบันอุตสาหกรรมยา อาหารและการเกษตรมีผลิตภัณฑ์หลายอย่างที่อยู่ในรูปของสารประกอบไครรัลแต่มีเอนทิโอเมอร์ตัวเดียวจากสารผสมราซีมิกของกลุ่มเอนทิโอเมอร์ที่มีประโยชน์และสามารถนำไปใช้งานได้จริง ดังนั้นกระบวนการแยกเอนทิโอเมอร์จึงเป็นกระบวนการที่สำคัญ งานวิจัยนี้มีความสนใจในกระบวนการตกผลึกแบบเลือกตกซึ่งมีข้อดีคือเป็นกระบวนการที่ง่าย ประหยัดและได้ผลิตภัณฑ์ในปริมาณมาก แต่ข้อเสียของกระบวนการนี้คือนิวเคลียสของเอนทิโอเมอร์ที่ไม่ต้องการสามารถเกิดขึ้นได้เองในกระบวนการ ดังนั้นในงานวิจัยนี้จึงสนใจการใช้สารเติมแต่งเทลอร์เมคเพื่อยับยั้งการเกิดนิวเคลียสของเอนทิโอเมอร์ที่ไม่ต้องการ โดยศึกษาการตกผลึกของกรดอะมิโนชนิดดีแอลแอสพาราจีน โมโนไฮเดรตซึ่งเป็นกรดอะมิโนที่มีรูปแบบผลึกเป็นแบบคอนโกเมอร์พและได้ใช้สารเติมแต่งชนิดดีและแอลของกรดแอสปาดิก ดีและแอลของกรดกลูตามิก ดีและแอลเวอลีน และดีและแอลลิซีน สำหรับงานวิจัยนี้ได้ทำการศึกษาผลกระทบของสารเติมแต่งแต่ละชนิดต่อความสามารถในการละลาย ความกว้างของบริเวณที่ไม่เกิดผลึก อัตราการโตของผลึก การเกิดนิวเคลียส การตกผลึกแบบเลือกตก และการกระจายตัวของขนาดผลึกของดีและแอลแอสพาราจีน โมโนไฮเดรต

จากผลการศึกษาพบว่าความสามารถในการละลายของแอสพาราจีน โมโนไฮเดรตในน้ำเพิ่มขึ้นเมื่อมีการใช้สารเติมแต่ง โดยที่ความกว้างของบริเวณที่ไม่เกิดผลึกเพิ่มขึ้นเมื่ออัตราการลดอุณหภูมิเพิ่มขึ้น แต่เมื่อมีการใช้สารเติมแต่งจะส่งผลให้ความกว้างของบริเวณที่ไม่เกิดผลึกเกิดการเปลี่ยนแปลงอย่างไม่ชัดเจน เนื่องจากเป็นกระบวนการเกิดนิวเคลียสซึ่งเป็นการเกิดแบบสุ่ม นอกจากนี้ยังพบว่าอัตราการโตของผลึกแอลแอสพาราจีน โมโนไฮเดรตจากดีแอลแอสพาราจีน โมโนไฮเดรตจะลดลงอย่างชัดเจนเมื่อใช้สารเติมแต่งชนิดแอลของกรดของแอสปาดิก และแอลของกรดกลูตามิก แต่มีผลน้อยมากเมื่อใช้สารเติมแต่งชนิดแอลเวอลีนและแอลลิซีน

จากการศึกษากระบวนการการเกิดนิวเคลียสของดีแอลแอสพาราจีน โมโนไฮเดรตจากดีแอลแอสพาราจีน โมโนไฮเดรตในการบวนการตกผลึกโดยไม่อาศัยตัวล่อ พบว่าแอลของกรดแอสปาดิก และแอลของกรดกลูตามิกสามารถยับยั้งการเกิดนิวเคลียสของแอลแอสพาราจีน โมโนไฮเดรตได้ และมีผลในทางเดียวกันเมื่อใช้สารเติมแต่งชนิดดีของกรดแอสปาดิกและดีของกรดกลูตามิกในการ

ยับยั้งการเกิดนิวเคลียสของดีแอสพาราจีน โมโนไฮเดรตเนื่องจากมีชนิดของอิแนนทิโอเมอร์เป็นแบบเดียวกัน แต่ดีและแอลแวลีน และดีและแอลลิวซีนแทบจะไม่มีผลต่อการเกิดนิวเคลียสของดีและแอลแอสพาราจีน โมโนไฮเดรต และจากการทดลองพบว่าสารเติมแต่งแอลของกรดแอสปาติกและแอลของกรดกลูตามิกยังยับยั้งการตกผลึกของดีแอสพาราจีน โมโนไฮเดรตบางส่วนซึ่งไม่ได้เป็นชนิดของอิแนนทิโอเมอร์ชนิดเดียวกัน

จากการศึกษากระบวนการตกผลึกแบบเลือกตกของแอลแอสพาราจีน โมโนไฮเดรตจากสารละลายดีแอลแอสพาราจีน โมโนไฮเดรตโดยใช้สารเติมแต่งชนิดดีของกรดแอสปาติกและดีของกรดกลูตามิกพบว่าเมื่อมีการใช้สารเติมแต่ง ช่วงเวลาที่แอลแอสพาราจีน โมโนไฮเดรตตกผลึกในรูปแบบบริสุทธิ์และปริมาณของแอลแอสพาราจีน โมโนไฮเดรตที่บริสุทธิ์เพิ่มขึ้น ในทางตรงกันข้ามถ้าใช้ปริมาณสารเติมแต่งมากเกินไปจะส่งผลให้ปริมาณของผลิตภัณฑ์แอลแอสพาราจีน โมโนไฮเดรตลดลง เนื่องจากความสามารถในการละลายของแอลแอสพาราจีน โมโนไฮเดรตในน้ำสูงขึ้น นอกจากนี้ยังได้ทำการศึกษาการกระจายตัวของขนาดผลึกในกระบวนการตกผลึกแบบเลือกตก จากการทดลองพบว่าอัตราการโตของผลึกจะลดลงเมื่อค่าการอิมิตวียังขูดสัมพัทธ์ลดลง และเมื่อใช้สารเติมแต่งจะทำให้ค่าอัตราการโตของผลึกลดลงมากขึ้น ซึ่งจากผลการทดลองนี้ทำให้ทราบว่า การใช้สารเติมแต่งจะส่งผลให้เวลาที่ในการตกผลึกของแอลแอสพาราจีน โมโนไฮเดรตที่บริสุทธิ์นานขึ้น และได้ปริมาณของผลิตภัณฑ์มากขึ้น แต่ในทางกลับกันการใช้สารเติมแต่งนี้จะส่งผลให้ขนาดของผลึกมีอัตราการโตช้าลง

สาขาวิชา วิศวกรรมเคมี

ปีการศึกษา 2560

ลายมือชื่อนักศึกษา ชัชวาลย์ อม

ลายมือชื่ออาจารย์ที่ปรึกษา Chalongin Hood

ลายมือชื่ออาจารย์ที่ปรึกษาร่วม Adha Fai

PEETIKAMOL KONGSAMAI : SEPARATION OF DL-ASPARAGINE
ENANTIOMERS USING CRYSTALLIZATION INHIBITORS. THESIS
ADVISOR : ASST. PROF. CHALONGSRI FLOOD, Ph.D., 250 PP.

PREFERENTIAL CRYSTALLIZATION/TAILOR-MADE ADDITIVES/CRYSTAL
GROWTH RATE/ NUCLEATION/INDUSTRIAL CRYSTALLIZATION

Many products from the pharmaceutical, food and agrochemical industries are chiral compounds. Normally, only one enantiomer from racemic mixture is wanted because the other enantiomer did not have a benefit, and sometimes it is harmful. Therefore, the separation of enantiomers is interesting. This research is interested in preferential crystallization (PC) because this method is easy to operate, low cost, and gives a high yield of product. However, the main problem of this method is the spontaneous primary nucleation of counter enantiomer.

In this research, we investigated the use of tailor-made additives, which is any additive that can change the crystallization in a desired way. We investigated the effect of these additives to the solubility, metastable zone width (MSZW), crystal growth rate, nucleation rate, the PC process, and crystal size distribution (CSD) by using DL-asparagine monohydrate (DL-Asn·H₂O), which is a racemic mixture in a conglomerate forming system, to produce pure L-Asn·H₂O by using D-/L-aspartic acid (D-/L-Asp), D-/L-glutamic acid (D-/L-Glu), D-/L-valine (D-/L-Val), D-/L-leucine (D-/L-Leu) as additives.

The solubility of D-/L-/DL-Asn·H₂O increased when using additives. The additives change the MSZW of D-/L-/DL-Asn·H₂O but they did not show a clear trend. The crystal growth rate of L-Asn·H₂O from DL-Asn·H₂O decreased when using L-Asp


and L-Glu. The nucleation of L-Asn·H₂O in DL-Asn·H₂O was inhibited by L-Asp and L-Glu, the nucleation of D-Asn·H₂O was inhibited by D-Asp, and D-Glu. D-/L-Val and D-/L-Leu showed very limited inhibition for this process. From crystal growth and nucleation, L-Asp and L-Glu inhibited the crystallization pathway of L-Asn·H₂O, which has the same absolute configuration. However, these additives also slightly inhibited the crystallization pathway of D-Asn·H₂O which has a different absolute configuration.

In the PC of L-Asn·H₂O from DL-Asn·H₂O with and without D-amino acid additives, the time of pure L-Asn·H₂O crystallization increased when using D-Asp and D-Glu additives. The yield of L-Asn·H₂O, during the crystallization of only L-Asn·H₂O without D-Asn·H₂O nucleation, also increased when using D-Asp and D-Glu. The time available for production of pure L-Asn·H₂O increased when the amount of D-Asp and D-Glu increased, but when using a very high amount of these additives, the yield is lower than when a small amount of additive was used because these additives also increase the solubility, which is related to the yield.

The CSD during the PC was studied. The crystal growth rate decreased when the relative supersaturation decreased, and the crystal growth rate is lower when using additives. From these results, the time of pure L-Asn·H₂O crystallized is longer and the yield is higher when using the D-Asp and D-Glu additives; however, the crystal growth rate of L-Asn·H₂O is lower when compared with the process without additives.

School of Chemical Engineering

Academic Year 2017

Student's Signature 

Advisor's Signature Chalangan Flood

Co-Advisor's Signature 

ACKNOWLEDGEMENTS

I would like to express my deepest gratitude to my advisor, Asst. Prof. Dr. Chalongsri Flood, and Prof. Dr. Adrian Evan Flood, for their support and guidance throughout my PhD studies. I really appreciate that they are very patient and have faith in me. I truly appreciate their constructive criticism to bring the best out of me and to prepare me well for both professional and personal development for the future.

I would also like to extend my appreciation to Prof. Dr. Joop H. ter Horst from University of Strathclyde, UK, for his invaluable guidance during my research experience in the Netherlands, and also thanks to all of the intensified reaction and separation systems group at Delft University of Technology.

I would like to express my gratitude to Asst. Prof. Dr. Atichat Wonkoblalab, Dr. Terasut Sookkumnerd, Asst. Prof. Dr. Lek Wantha, Asst. Prof. Dr. Atthaphon Maneedaeng, and Dr. Apichit Svang-Ariyaskul for their kind agreement to serve on my committee for the thesis proposal and thesis examination, and also for their wonderful questions and guidance.

I would like to thank all of the lecturers at School of Chemical Engineering, Suranaree University of Technology (SUT) for their advice and support. I would also like to thank all of the academic members in the School of Chemical Engineering, for their teaching, support, and encouragement.

Special thanks to Mrs. Amporn Ladnongkhun for her skillful secretarial work and Mr. Saran Dokmaikun for his skillful technical work and assistance. I also thank the graduate students in the School of Chemical Engineering for their encouragement

and keeping me sane during difficult times, keeping me smiling and happy, and raising me up when I am down. I would like to thank my best friend, Miss Boonpradab Daengpradab, who always supported me during the most difficult time in my life.

I would also like to thank the Thailand Research Fund (TRF) through the Royal Golden Jubilee Ph.D. Program (RGJ-Ph.D.), grant number PHD/0097/2552, for the financial support.

Finally, I would like to give a big thank you to my family, especially my mother, Mrs. Thitimone Kongsamai, who raised me with endless love, unbounded support, and encouragement.

Peetikamol Kongsamai

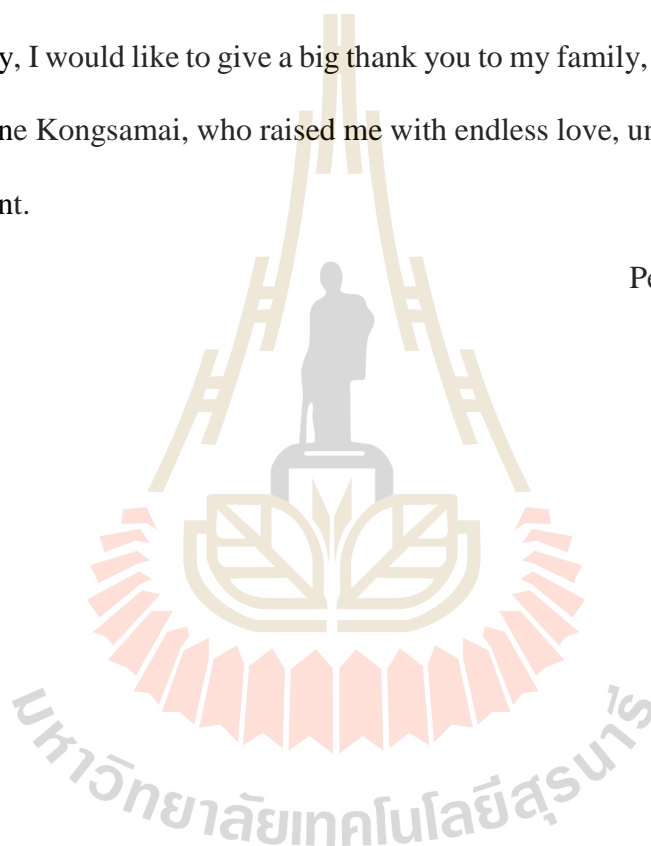


TABLE OF CONTENTS

	Page
ABSTRACT (THAI).....	I
ABSTRACT (ENGLISH).....	III
ACKNOWLEDGEMENTS.....	V
TABLE OF CONTENTS.....	VII
LIST OF TABLES.....	XVII
LIST OF FIGURES.....	XXIV
SYMBOLS AND ABBREVIATIONS.....	XLI
CHAPTER	
I INTRODUCTION.....	1
1.1 Introduction to Stereoisomer.....	1
1.2 Introduction to Racemate.....	3
1.3 Introduction to Amino Acids.....	5
1.4 Background and Significance of the Study.....	8
1.5 Research Objectives.....	11
1.6 Scope and Limitation of the research.....	12
1.7 Research Development.....	13
1.8 References.....	14

TABLE OF CONTENTS (Continued)

	Page
II SOLUBILITIES AND METSTABLE ZONE WIDTH OF ASPARAGINE MONOHYDRATE AND ASPARAGINE MONOHYDRATE WITH TAILOR-MADE ADDITIVES.....	19
2.1 Abstract.....	19
2.2 Introduction.....	20
2.3 Theory.....	24
2.3.1 Solubility.....	24
2.3.2 Supersaturation.....	24
2.3.3 Nucleation.....	26
2.3.4 Metastable Zone Width.....	26
2.3.5 Phase Diagram.....	27
2.4 Materials and Methods.....	29
2.4.1 Materials.....	29
2.4.2 Solubility Measurement by Gravimetric Method.....	29
2.4.3 Solubility Measurement by Refractive Index Method.....	30
2.4.4 Solubility, Metastable Zone Limit and Phase Diagram Measurement by Crystal 16.....	31

TABLE OF CONTENTS (Continued)

	Page
2.5	Results and Discussion.....33
2.5.1	Solubility of L-/DL-Asparagine Monohydrate in Water.....33
2.5.2	Phase Diagram for Aqueous Solutions of Asparagine.....36
2.5.3	Effect of Additives to Solubility of L-/DL-Asn·H ₂ O in Water.....38
2.5.4	Metastable zone width of L-/DL-Asn·H ₂ O in Water.....46
2.5.5	Effect of Additives to Solubility of L-/DL-Asn·H ₂ O in Water.....48
2.6	Conclusions.....49
2.7	References.....50

III EFFECT OF TAILOR-MADE ADDITIVES TO

THE CRYSTAL GROWTH RATE OF

L-ASPARAGINE MONOHYDRATE.....56

3.1	Abstract.....56
3.2	Introduction.....57
3.3	Theory.....59
3.3.1	Meaning of Crystal Growth.....59

TABLE OF CONTENTS (Continued)

	Page
3.3.2 Crystal Growth Model.....	60
3.3.3 Crystal Growth Kinetics.....	65
3.4 Materials and Methods.....	66
3.4.1 Materials.....	66
3.4.2 Single Crystal Growth Rate of L-Asn·H ₂ O in Supersaturated Solution of L- and DL-Asn·H ₂ O	66
3.5 Results and Discussion.....	68
3.5.1 Single Crystal Growth Rate of L-Asn·H ₂ O in Supersaturated Solution of L- and DL-Asn·H ₂ O.....	68
3.5.2 Single Crystal Growth Rate of L-Asn·H ₂ O in supersaturated solution of DL-Asn·H ₂ O with Tailor made additives.....	77
3.6 Conclusions.....	85
3.7 References.....	86
IV EFFECT OF TAILOR MADE ADDITIVES TO UNSEEDED CRYSTALLIZATION OF DL-ASPARAGINE MONOHYDRATE IN WATER.....	90
4.1 Abstract.....	90

TABLE OF CONTENTS (Continued)

	Page
4.2	Introduction.....91
4.3	Theory.....93
4.3.1	Nucleation.....93
4.3.2	Primary Nucleation.....94
4.3.3	Secondary Nucleation.....95
4.4	Materials and Methods.....97
4.4.1	Materials.....97
4.4.2	Apparatus.....97
4.4.3	Methods.....98
4.5	Results and Discussion.....100
4.5.1	Unseed Crystallization of DL-Asn·H ₂ O in Water.....100
4.5.2	Unseed Crystallization of DL-Asn·H ₂ O with D/L-Asp and D/L-Glu.....103
4.5.3	Unseed Crystallization of DL-Asn·H ₂ O with D/L-Leu and D/L-Val.....111
4.6	Conclusions.....114
4.7	References.....115

TABLE OF CONTENTS (Continued)

	Page
V PREFERENTIAL CRYSTALLIZATION OF L-ASPARAGINE MONOHYDRATE WITH THE INHIBITION BY TAILOR-MADE ADDITIVES.....	119
5.1 Abstract.....	119
5.2 Introduction.....	120
5.3 Theory.....	122
5.3.1 Preferential Crystallization.....	122
5.4 Materials and Methods.....	125
5.4.1 Materials.....	125
5.4.2 Apparatus.....	125
5.4.3 Preferential Crystallization of L-Asn·H ₂ O in Batch Crystallization.....	126
5.4.4 Tailor made Inhibition to the Preferential Crystallization of L-Asn·H ₂ O in a Small Batch Crystallization.....	127
5.4.5 Tailor made Inhibition to the Preferential Crystallization of L-Asn·H ₂ O in a Batch Crystallization.....	129

TABLE OF CONTENTS (Continued)

	Page
5.5 Results and Discussion.....	129
5.5.1 The Preferential Crystallization of L-Asn·H ₂ O in DL-Asn·H ₂ O Solution.....	129
5.5.2 Effect of Supersaturation Ratio to the Preferential Crystallization of L-Asn·H ₂ O from DL-Asn·H ₂ O.....	134
5.5.3 Effect of Seed Amount to the Preferential Crystallization of L-Asn·H ₂ O from DL-Asn·H ₂ O.....	137
5.5.4 Effect of Tailor-Made Additives to the Preferential Crystallization of L-Asn·H ₂ O from DL-Asn·H ₂ O.....	142
5.5.5 Effect of Amount of Additive to the Preferential Crystallization of L-Asn·H ₂ O from DL-Asn·H ₂ O.....	146
5.6 Conclusions.....	157
5.7 References.....	158

TABLE OF CONTENTS (Continued)

	Page
VI CRYSTAL SIZE DISTRIBUTION DURING THE	
PREFERENTIAL CRYSTALLIZATION OF	
L-ASPARAGINE MONOHYDRATE WITH THE	
INHIBITIONS BY TAILOR-MADE ADDITIVES.....	
	161
6.1 Abstract.....	161
6.2 Introduction.....	162
6.3 Theory.....	165
6.3.1 Particle Size Distribution.....	165
6.4 Materials and Methods.....	166
6.4.1 Materials.....	166
6.4.2 Apparatus.....	166
6.4.3 Particle Size Distribution during the Preferential Crystallization of L-Asn·H ₂ O in Batch Crystallization.....	169
6.5 Results and Discussion.....	170
6.5.1 The Analysis of Concentration and Product Purity....	170
6.5.2 The Crystal Size Distribution.....	176

TABLE OF CONTENTS (Continued)

	Page
6.5.3 Mean Crystal Size of L-Asn·H ₂ O and Crystal Growth Rate During the Preferential Crystallization.....	182
6.6 Conclusions.....	186
6.7 References.....	187
VII CONCLUSIONS AND RECOMMENDATIONS.....	189
7.1 Conclusions.....	189
7.2 Recommendations.....	193
APPENDICES	
APPENDIX A. RAW DATA OF SOLUBILITY AND METASTABLE ZONE WIDTH OF ASPRAGINE MONOHYDRATE WITH TAILOR-MADE ADDITIVES.....	194
APPENDIX B. RAW DATA OF CRYSTAL GROWTH RATE OF L-ASPARAGINE MONOHYDRATE FROM L-/DL-ASPARAGINE MONOHYDRATE WITHOUT AND WITH TAILOR-MADE ADDITIVES.....	202

TABLE OF CONTENTS (Continued)

	Page
APPENDIX C. RAW DATA OF UNSEED CRYSTALLIZATION OF DL-ASPARAGINE MONOHYDRATE WITH TAILOR-MADE ADDITIVES.....	205
APPENDIX D. RAW DATA OF PREFERENTIAL CRSYSTALLIZATION OF L-SAPARAGINE MONOHYDRATE WITH THE INHIBITIONS BY TAILOR-MADE ADDITIVES.....	212
APPENDIX E. CALCUALTION OF TOTAL CRYTAL COUNT BY FOCUS BEAM REFLECTANCE MEASUREMENT.....	225
APPENDIX F. RAW DATA OF CRYSTAL SIZE DISTRIBUTION DURING THE PREFERENTIAL CRSYTALLIZATION OF L-SAPARAGINE MONOHYDRATE WITH THE INHIBITIONS BY TAILOR-MADE ADDITIVES.....	230
APPENDIX G. LIST OF PUBLICATIONS.....	234
BIOGRAPHY.....	250

LIST OF TABLES

Table		Page
2.1	The solubility of inorganic compound at 20°C.....	20
2.2	Fitting parameter of solubility of L-/D-/DL-Asn·H ₂ O with any additives by quadratic equation.....	45
3.1	Measurements of the individual crystal growth rate of L-Asn·H ₂ O in L-Asn·H ₂ O supersaturation (S=1.10) at 30°C.....	71
3.2	Measurements of the individual crystal growth rate of L-Asn·H ₂ O in DL-Asn·H ₂ O supersaturation (S=1.10) at 30°C.....	71
3.3	The range of crystal growth rate of L-Asn·H ₂ O in L-/DL-Asn·H ₂ O supersaturated solution (S=1.10) at 30°C.....	72
3.4	Fitting parameters for the crystal growth rate distribution of L-Asn·H ₂ O grown in supersaturation of L- and DL-Asn·H ₂ O (S=1.10) at 30°C.....	74
3.5	Fitting parameters for the crystal growth rate distribution of L-Asn·H ₂ O grown in various supersaturation of L- and DL-Asn·H ₂ O at 30°C.....	76
3.6	Fitting parameters for the crystal growth rate distribution of L-Asn·H ₂ O grown in DL-Asn·H ₂ O solutions with D-amino acid additives at 30°C.....	80

LIST OF TABLES (Continued)

Table	Page
3.7	Fitting parameters for the crystal growth rate distribution of L-Asn·H ₂ O grown in DL-Asn·H ₂ O solutions with L-amino acid additives at 30°C.....83
4.1	The conditions for unseeded crystallization of DL-Asn·H ₂ O in water.....99
4.2	The number of initial solid product from unseeded crystallization of DL-Asn·H ₂ O when using L-/D-Leu, and L-/D-Val additives.....114
5.1	The conditions of preferential crystallization of L-Asn·H ₂ O.....127
5.2	The conditions of preferential crystallization of L-Asn·H ₂ O in small batch crystallization.....128
5.3	The conditions of preferential crystallization of L-Asn·H ₂ O with Tailor-made additives inhibition.....129
6.1	The conditions for preferential crystallization of L-Asn·H ₂ O for finding the particle size distribution.....170
6.2	Mean crystal size of L-Asn·H ₂ O in the preferential crystallization of L-Asn·H ₂ O in DL-Asn·H ₂ O from 1h to 7h.....184
6.3	The fitting parameter of crystal growth rate of L-Asn·H ₂ O in preferential crystallization of L-Asn·H ₂ O in DL-Asn·H ₂ O without and with D-Glu and D-Asp additives.....186

LIST OF TABLES (Continued)

Table		Page
A.1	Solubility of DL-Asn·H ₂ O in water from Gravimetric Method.....	195
A.2	Solubility of L- and DL-Asn·H ₂ O in water from and Refractive Index Method.....	195
A.3	Solubility and Metastable Zone Limit (cooling rate 0.3°C/min) of DL-Asn·H ₂ O in water by Crystal 16.....	195
A.4	Solubility and Metastable Zone Limit (cooling rate 0.1°C/min) of DL-Asn·H ₂ O in water by Crystal 16.....	196
A.5	Solubility and Metastable Zone Limit (cooling rate 0.3°C/min) of L-Asn·H ₂ O in water by Crystal 16.....	197
A.6	Solubility and Metastable Zone Limit (cooling rate 0.1°C/min) of L-Asn·H ₂ O in water by Crystal 16.....	197
A.7	Solubility and Metastable Zone Limit of D-Asn·H ₂ O in water with 5mol% of D-Asp by Crystal 16.....	198
A.8	Solubility and Metastable Zone Limit of L-Asn·H ₂ O in water with 5 mol% D-Asp by Crystal 16.....	198
A.9	Solubility and Metastable Zone Limit of D-Asn·H ₂ O in water with 5 mol% D-Glu by Crystal 16.....	199
A.10	Solubility and Metastable Zone Limit of L-Asn·H ₂ O in water with 5 mol% D-Glu by Crystal 16.....	199

LIST OF TABLES (Continued)

Table	Page
A.11 Solubility of L-Asn·H ₂ O in water with 10mol% L-Asp and L-Glu by Crystal 16.....	199
A.12 Solubility and Metastable Zone Limit of D-Asn·H ₂ O in water with 5 mol% D-Val by Crystal 16.....	200
A.13 Solubility and Metastable Zone Limit of L-Asn·H ₂ O in water with 5 mol% D-Val by Crystal 16.....	200
A.14 Solubility and Metastable Zone Limit of D-Asn·H ₂ O in water with 5 mol% D-Leu by Crystal 16.....	201
A.15 Solubility and Metastable Zone Limit of L-Asn·H ₂ O in water with 5 mol% D-Leu by Crystal 16.....	201
A.16 Solubility of DL-Asn·H ₂ O in water with 5 mol% L-Asp and L-Glu by Crystal 16.....	201
B.1 Crystal growth rate of L-Asn·H ₂ O in L-Asn·H ₂ O and DL-Asn·H ₂ O supersaturated solution.....	203
B.2 Crystal growth rate of L-Asn·H ₂ O in DL-Asn·H ₂ O supersaturated solution with 3mol% of additives.....	204
C.1 The purity of D-Asn·H ₂ O and yield of D-/L-Asn·H ₂ O in unseeded crystallization of DL-Asn·H ₂ O in water.....	205
C.2 The purity of D-Asn·H ₂ O and yield of D-/L-Asn·H ₂ O in unseeded crystallization of DL-Asn·H ₂ O with D-/L-Asp additives.....	206

LIST OF TABLES (Continued)

Table	Page
C.3	The purity of D-Asn·H ₂ O and yield of D-/L-Asn·H ₂ O in unseeded crystallization of DL-Asn·H ₂ O with D-/L-Glu additives.....207
C.4	The purity of D-Asn·H ₂ O in unseeded crystallization of DL-Asn·H ₂ O with D-/L-Leu additives.....208
C.5	The purity of D-Asn·H ₂ O in unseeded crystallization of DL-Asn·H ₂ O with L-Val additives.....209
C.6	The purity of D-Asn·H ₂ O in unseeded crystallization of DL-Asn·H ₂ O with D-Val additives.....210
D.1	The conditions of preferential crystallization of L-Asn·H ₂ O.....213
D.2	The result of preferential crystallization of L-Asn·H ₂ O in DL-Asn·H ₂ O for condition A1.....213
D.3	The result of preferential crystallization of L-Asn·H ₂ O in DL-Asn·H ₂ O for condition A2.....214
D.4	The result of preferential crystallization of L-Asn·H ₂ O in DL-Asn·H ₂ O for condition A3.....214
D.5	The result of preferential crystallization of L-Asn·H ₂ O in DL-Asn·H ₂ O for condition A4.....215
D.6	The result of preferential crystallization of L-Asn·H ₂ O in DL-Asn·H ₂ O for condition A5.....216

LIST OF TABLES (Continued)

Table	Page
D.7	The conditions of preferential crystallization of L-Asn·H ₂ O in small batch crystallization.....216
D.8	The result of preferential crystallization of L-Asn·H ₂ O in DL-Asn·H ₂ O for condition B1.....217
D.9	The result of preferential crystallization of L-Asn·H ₂ O in DL-Asn·H ₂ O for condition B2.....217
D.10	The result of preferential crystallization of L-Asn·H ₂ O in DL-Asn·H ₂ O for condition B3.....218
D.11	The result of preferential crystallization of L-Asn·H ₂ O in DL-Asn·H ₂ O for condition B4.....218
D.12	The result of preferential crystallization of L-Asn·H ₂ O in DL-Asn·H ₂ O for condition B5.....219
D.13	The conditions of preferential crystallization of L-Asn·H ₂ O With Tailor-made additives inhibition.....219
D.14	The result of preferential crystallization of L-Asn·H ₂ O in DL-Asn·H ₂ O for condition C1.....220
D.15	The result of preferential crystallization of L-Asn·H ₂ O in DL-Asn·H ₂ O for condition C2.....220
D.16	The result of preferential crystallization of L-Asn·H ₂ O in DL-Asn·H ₂ O for condition C3.....221

LIST OF TABLES (Continued)

Table	Page
D.17	The result of preferential crystallization of L-Asn·H ₂ O in DL-Asn·H ₂ O for condition C4.....222
D.18	The result of preferential crystallization of L-Asn·H ₂ O in DL-Asn·H ₂ O for condition C5.....223
D.19	The result of preferential crystallization of L-Asn·H ₂ O in DL-Asn·H ₂ O for condition C6.....224
E.1	The number of CaCO ₃ particle from FBRM.....227
E.2	The total number of CaCO ₃ particles in 500mL of solution.....229
F.1	The conditions for preferential crystallization of L-Asn·H ₂ O for finding the particle size distribution.....230
F.2	The conditions of preferential crystallization of L-Asn·H ₂ O from DL-Asn·H ₂ O without additives (D1).....230
F.3	The conditions of preferential crystallization of L-Asn·H ₂ O from DL-Asn·H ₂ O with D-Glu additives (D2).....231
F.4	The conditions of preferential crystallization of L-Asn·H ₂ O from DL-Asn·H ₂ O with D-Asp additives (D3).....232

LIST OF FIGURES

Figure	Page
1.1	Type of isomer.....2
1.2	Enantiomers of 2-butanol.....2
1.3	Hemihedral crystals of d- and l-sodium ammonium tartrate.....3
1.4	Crystalline of racemate (a) conglomerate, (b) racemic compound, and (c) solid solution.....4
1.5	Binary phase diagram of racemate crystalline forming (a) a conglomerate (b) a racemic mixture, and (c) a solid solution.....5
1.6	Binary phase diagram of (a) asparagine in water, (b) ibuprofen in hexane, and (c) atenolol in ethanol.....5
1.7	Amino acid structure.....6
1.8	Amino acids (a) nonpolar amino acids, (b) polar-uncharged amino acids, (c) charged amino acids, and (d) aromatic amino acids.....7
1.9	Structure of L-/D-alanine.....8
2.1	Solubility of potassium nitrate (KNO_3), copper sulfate ($CuSO_4$), and sodium chloride ($NaCl$) in aqueous solution.....21
2.2	Solubility of hexamethylenetetramine in different solvents.....21
2.3	Solubility of amino acid from Dalton and Schmidt (1935).....23
2.4	Solubility curve and the zone of concentration.....25
2.5	Metastable zone in crystallization process.....26

LIST OF FIGURES (Continued)

Figure	Page
2.6 Ternary phase diagram for conglomerates (left), and racemic compound systems (right).....	28
2.7 Ternary solubility phase diagram of threonine in water (left) and mandelic acid in eluent (right).....	28
2.8 The calibration curve between concentration of L-/DL-Asn·H ₂ O in water and refractive index (RI).....	30
2.9 Crystal16 equipment.....	31
2.10 Temperature profiles, and clear and cloud points using the Crystal16.....	33
2.11 The DL-Asn·H ₂ O solubility in water from Crystal 16, refractive index, and gravimetric methods.....	34
2.12 The TGA analyzer of DL-Asn from gravimetric method and DL-Asn·H ₂ O.....	35
2.13 Solubility of L-/DL-Asn·H ₂ O in water from Crystal16 and refractive index method.....	36
2.14 Phase diagram of a fixed amount of Asn·H ₂ O in water.....	37
2.15 Ternary solubility phase diagram of Asn·H ₂ O in water.....	37
2.16 The solubility of D-Asn·H ₂ O in water with D-Asp additives.....	38
2.17 The solubility of L-Asn·H ₂ O in water with D-Asp additives.....	39
2.18 The solubility of D-Asn·H ₂ O in water with D-Glu additives.....	40
2.19 The solubility of L-Asn·H ₂ O in water with D-Glu additives.....	40

LIST OF FIGURES (Continued)

Figure	Page
2.20	The solubility of D-Asn·H ₂ O in water with D-Val additives.....41
2.21	The solubility of L-Asn·H ₂ O in water with D-Val additives..... 42
2.22	The solubility of D-Asn·H ₂ O in water with D-Leu additives.....42
2.23	The solubility of L-Asn·H ₂ O in water with D-Leu additives.....43
2.24	The solubility of D-Asn·H ₂ O in water with D-amino acid additives.....43
2.25	The solubility of DL-Asn·H ₂ O in water with L-Asp additives.....44
2.26	The solubility of DL-Asn·H ₂ O in water with L-Glu additives.....44
2.27	The metastable zone width of L-Asn·H ₂ O in water.....47
2.28	The metastable zone width of DL-Asn·H ₂ O in water.....47
2.29	The metastable zone width of D-Asn·H ₂ O in water with D-amino acid additives.....48
2.30	The metastable zone width of D-Asn·H ₂ O in water with L-amino acid additives.....49
3.1	The Schematic of Rule of reversal.....58
3.2	The Schematic of selective inhibition of crystal by Tailor-made additives.....59
3.3	The three possible sites for molecules adsorb on crystal surface.....61
3.4	Formation of two-dimensional critical nucleus on a crystal surface in mononuclear model.....62
3.5	Development of a growth spiral from a screw dislocation.....63

LIST OF FIGURES (Continued)

Figure	Page
3.6	Concentration driving force in crystallization from solution.....64
3.7	Crystal shape of L-Asn·H ₂ O.....67
3.8	Growth cell equipment.....67
3.9	Experimental set up.....67
3.10	Crystal shape of L-Asn·H ₂ O in L-Asn·H ₂ O solution (S = 1.10).....68
3.11	Crystal shape of L-Asn·H ₂ O in DL-Asn·H ₂ O solution (S = 1.10).....69
3.12	Relationship between crystal size (length) of L-Asn·H ₂ O and time in solution (S = 1.10) of L-Asn·H ₂ O at 30°C.....70
3.13	Relationship between crystal size (length) of L-Asn·H ₂ O and time in solution (S = 1.10) of L-Asn·H ₂ O at 30°C.....70
3.14	Relationship between growth rate frequency and growth rate of L-Asn·H ₂ O crystals in L-Asn·H ₂ O solution (S=1.10) at 30°C.....73
3.15	Relationship between growth rate frequency and growth rate of L-Asn·H ₂ O crystals in DL-Asn·H ₂ O solution (S=1.10) at 30°C.....73
3.16	Relationship between growth rate frequency and growth rate of L-Asn·H ₂ O crystals in L-Asn·H ₂ O solution (S=1.10) at 30°C.....75
3.17	Relationship between growth rate frequency and growth rate of L-Asn·H ₂ O crystals in L-Asn·H ₂ O solution (S=1.10) at 30°C.....75
3.18	Relationship between crystal growth of L-Asn·H ₂ O in various supersaturation of L- and DL-Asn·H ₂ O solution at 30°C.....76

LIST OF FIGURES (Continued)

Figure	Page
3.19	Crystal shape of L-Asn·H ₂ O in DL-Asn·H ₂ O solution (S = 1.10) with 3 mol% of D-Asp additives.....77
3.20	Crystal shape of L-Asn·H ₂ O in DL-Asn·H ₂ O solution (S = 1.10) with 3 mol% of D-Glu additives.....78
3.21	Crystal shape of L-Asn·H ₂ O in DL-Asn·H ₂ O solution (S = 1.10) with 3 mol% of D-Leu additives.....78
3.22	Crystal shape of L-Asn·H ₂ O in DL-Asn·H ₂ O solution (S = 1.10) with 3 mol% of D-Val additives.....79
3.23	Relationship between growth rate frequency and growth rate of L-Asn·H ₂ O crystals in DL-Asn·H ₂ O solution with 3 mol% of D-amino acid additives at 30°C.....80
3.24	Crystal shape of L-Asn·H ₂ O in DL-Asn·H ₂ O solution (S = 1.10) with 3 mol% of L-Asp additives.....81
3.25	Crystal shape of L-Asn·H ₂ O in DL-Asn·H ₂ O solution (S = 1.10) with 3 mol% of L-Glu additives.....82
3.26	Crystal shape of L-Asn·H ₂ O in DL-Asn·H ₂ O solution (S = 1.10) with 3 mol% of L-Leu additives.....82
3.27	Crystal shape of L-Asn·H ₂ O in DL-Asn·H ₂ O solution (S = 1.10) with 3 mol% of L-Val additives.....83

LIST OF FIGURES (Continued)

Figure	Page
3.28 Relationship between growth rate frequency and growth rate of L-Asn·H ₂ O crystals in DL-Asn·H ₂ O solution with 3 mol% of L-amino acid additives at 30°C.....	84
3.29 The mean crystal growth rate of L-Asn·H ₂ O in L-Asn·H ₂ O and DL-Asn·H ₂ O solution without and with additives.....	85
4.1 Nucleation mechanism.....	94
4.2 Change in cluster size by attachment or detachment of molecules.....	95
4.3 %Purity of D-Asn·H ₂ O from DL-Asn·H ₂ O supersaturation without additives.....	100
4.4 % Yield of D-Asn·H ₂ O from DL-Asn·H ₂ O supersaturation at different temperature.....	101
4.5 % Yield of L-Asn·H ₂ O from DL-Asn·H ₂ O supersaturation at different temperature.....	102
4.6 % Yield of D-Asn·H ₂ O from DL-Asn·H ₂ O supersaturation at different supersaturation.....	102
4.7 % Yield of L-Asn·H ₂ O from DL-Asn·H ₂ O supersaturation at different supersaturation.....	103
4.8 %Purity of D-Asn·H ₂ O from DL-Asn·H ₂ O supersaturation with L-/D-Asp additives.....	104

LIST OF FIGURES (Continued)

Figure	Page
4.9	% Yield of D-Asn·H ₂ O from DL-Asn·H ₂ O supersaturation with L-/D-Asp additives.....104
4.10	% Yield of L-Asn·H ₂ O from DL-Asn·H ₂ O supersaturation with L-/D-Asp additives.....105
4.11	% maximum yield and maximum time of 100% purity of D-Asn·H ₂ O when using L-Asp additives.....106
4.12	% Purity of D-Asn·H ₂ O from DL-Asn·H ₂ O supersaturation with L-/D-Glu additives.....107
4.13	% Yield of D-Asn·H ₂ O from DL-Asn·H ₂ O supersaturation with L-/D-Glu additives.....107
4.14	% Yield of L-Asn·H ₂ O from DL-Asn·H ₂ O supersaturation with L-/D-Glu additives.....108
4.15	XRPD pattern of L-/DL-Asn·H ₂ O without and with L-Asp, and L-Glu additives.....109
4.16	FTIR pattern of L-/DL-Asn·H ₂ O without and with L-Asp, and L-Glu additives.....110
4.17	FT-Raman pattern of L-/DL-Asn·H ₂ O without and with L-Asp, and L-Glu additives.....111
4.18	% Purity of D-Asn·H ₂ O from DL-Asn·H ₂ O supersaturation with L-Leu additives.....112

LIST OF FIGURES (Continued)

Figure	Page
4.19	%Purity of D-Asn·H ₂ O from DL-Asn·H ₂ O supersaturation with D-Leu additives.....113
4.20	%Purity of D-Asn·H ₂ O from DL-Asn·H ₂ O supersaturation with L-Val additives.....113
4.21	%Purity of D-Asn·H ₂ O from DL-Asn·H ₂ O supersaturation with D-Val additives.....114
5.1	The procedure of preferential crystallization process.....123
5.2	The path way of enantiomer E1, and E2 in solution from the preferential crystallization process.....124
5.3	The path way of enantiomer E1, and E2 in solution from the preferential crystallization process when using Tailor-made additives.....124
5.4	The analysis of D-/L-Asn·H ₂ O in water from HPLC with Chirobiotic T column with a 40:60 vol% ethanol: water mobile phase.....126
5.5	Solid crystal of D-/L-Asn·H ₂ O in the preferential crystallization of L-Asn·H ₂ O in DL-Asn·H ₂ O (S=1.3) at 20°C.....131
5.6	Concentration of D-/L-Asn·H ₂ O in the preferential crystallization of L-Asn·H ₂ O in DL-Asn·H ₂ O (S=1.3) at 20°C.....131

LIST OF FIGURES (Continued)

Figure	Page
5.7 Ternary phase diagram of D-/L-Asn·H ₂ O in DL-Asn·H ₂ O solution (S=1.3) during the preferential crystallization of L-Asn·H ₂ O at 20°C.....	132
5.8 % <i>e.e.</i> of L-Asn·H ₂ O in the preferential Crystallization of L-Asn·H ₂ O in DL-Asn·H ₂ O (S=1.3) at 20°C.....	132
5.9 % Yield of D-/L-Asn·H ₂ O in the preferential crystallization of L-Asn·H ₂ O in DL-Asn·H ₂ O (S=1.3) at 20°C.....	133
5.10 The relationship between % yield and % <i>e.e.</i> of L-Asn·H ₂ O in the preferential crystallization of L-Asn·H ₂ O in DL-Asn·H ₂ O (S=1.3) at 20°C.....	133
5.11 Solid crystal of L-Asn·H ₂ O in the preferential crystallization of L-Asn·H ₂ O in DL-Asn·H ₂ O at 20°C by varying the supersaturation ratio.....	135
5.12 Solid crystal of D-Asn·H ₂ O in the preferential crystallization of L-Asn·H ₂ O in DL-Asn·H ₂ O at 20°C by varying the supersaturation ratio.....	135
5.13 % <i>e.e.</i> of L-Asn·H ₂ O in the preferential crystallization of L-Asn·H ₂ O in DL-Asn·H ₂ O at 20°C by varying the supersaturation ratio.....	136

LIST OF FIGURES (Continued)

Figure	Page
5.14 % Yield of L-Asn·H ₂ O in the preferential crystallization of L-Asn·H ₂ O in DL-Asn·H ₂ O at 20°C by varying the supersaturation ratio.....	136
5.15 The relationship between %yield and % <i>e.e.</i> of L-Asn·H ₂ O in the preferential crystallization of L-Asn·H ₂ O in DL-Asn·H ₂ O at 20°C by varying the supersaturation ratio.....	137
5.16 Solid crystal of L-Asn·H ₂ O in the preferential crystallization of L-Asn·H ₂ O in DL-Asn·H ₂ O (S=1.3) at 20°C by varying the L-Asn·H ₂ O seeds.....	139
5.17 Solid crystal of L-Asn·H ₂ O (excluding seeds amount) in the preferential crystallization of L-Asn·H ₂ O in DL-Asn·H ₂ O (S=1.3) at 20°C by varying the L-Asn·H ₂ O seeds.....	139
5.18 Solid crystal of D-Asn·H ₂ O in the preferential crystallization of L-Asn·H ₂ O in DL-Asn·H ₂ O (S=1.3) at 20°C by varying the L-Asn·H ₂ O seeds.....	140
5.19 % <i>e.e.</i> of L-Asn·H ₂ O in the preferential crystallization of L-Asn·H ₂ O in DL-Asn·H ₂ O (S=1.3) at 20°C by varying the L-Asn·H ₂ O seeds.....	140

LIST OF FIGURES (Continued)

Figure	Page
5.20 % Yield of L-Asn·H ₂ O in the preferential crystallization of L-Asn·H ₂ O in DL-Asn·H ₂ O (S=1.3) at 20°C by varying the L-Asn·H ₂ O seeds.....	141
5.21 The relationship between % yield and % <i>e.e.</i> of L-Asn·H ₂ O in the preferential crystallization of L-Asn·H ₂ O in DL-Asn·H ₂ O (S=1.3) at 20°C by varying the L-Asn·H ₂ O seeds.....	141
5.22 Solid crystal of L-Asn·H ₂ O in the preferential crystallization of L-Asn·H ₂ O in DL-Asn·H ₂ O with 5mol% of D-amino acid additives (S=1.3) at 30°C with D-amino acid additives.....	143
5.23 Solid crystal of D-Asn·H ₂ O in the preferential crystallization of L-Asn·H ₂ O in DL-Asn·H ₂ O with 5mol% of D-amino acid additives (S=1.3) at 30°C with D-amino acid additives.....	144
5.24 % <i>e.e.</i> of L-Asn·H ₂ O in the preferential crystallization of L-Asn·H ₂ O in DL-Asn·H ₂ O with 5 mol% of D-amino acid additives (S=1.3) at 30°C with D-amino acid additives.....	144
5.25 % Yield of L-Asn·H ₂ O in the preferential crystallization of L-Asn·H ₂ O in DL-Asn·H ₂ O with 5 mol% of D-amino acid additives (S=1.3) at 30°C with D-amino acid additives.....	145

LIST OF FIGURES (Continued)

Figure	Page
5.26 The relationship between % yield and % <i>e.e.</i> of L-Asn·H ₂ O in the preferential crystallization of L-Asn·H ₂ O in DL-Asn·H ₂ O with 5 mol% of D-amino acid additives (S=1.3) at 30°C with D-amino acid additives.....	146
5.27 Solid crystal of L-Asn·H ₂ O in the preferential crystallization of L-Asn·H ₂ O in DL-Asn·H ₂ O with D-Asp additives (S=1.3) at 20°C.....	148
5.28 Solid crystal of D-Asn·H ₂ O in the preferential crystallization of L-Asn·H ₂ O in DL-Asn·H ₂ O with D-Asp additives (S=1.3) at 20°C.....	149
5.29 Ternary phase diagram of D-/L-Asn·H ₂ O in DL-Asn·H ₂ O solution (S=1.3) during the preferential crystallization of L-Asn·H ₂ O at 20°C with 3 mol% of D-Asp additives.....	149
5.30 Ternary phase diagram of D-/L-Asn·H ₂ O in DL-Asn·H ₂ O solution (S=1.3) during the preferential crystallization of L-Asn·H ₂ O at 20°C with 5 mol% of D-Asp additives.....	150
5.31 Ternary phase diagram of D-/L-Asn·H ₂ O in DL-Asn·H ₂ O solution (S=1.3) during the preferential crystallization of L-Asn·H ₂ O at 20°C with 7 mol% of D-Asp additives.....	150
5.32 Ternary phase diagram of D-/L-Asn·H ₂ O in DL-Asn·H ₂ O solution (S=1.3) during the preferential crystallization of L-Asn·H ₂ O at 20°C with D-Asp additives.....	151

LIST OF FIGURES (Continued)

Figure	Page
5.33	% <i>e.e.</i> of L-Asn·H ₂ O in the preferential crystallization of L-Asn·H ₂ O in DL-Asn·H ₂ O with D-Asp additives (S=1.3) at 20°C.....151
5.34	% Yield of L-Asn·H ₂ O in the preferential crystallization of L-Asn·H ₂ O in DL-Asn·H ₂ O with D-Asp additives (S=1.3) at 20°C.....152
5.35	The relationship between % yield and % <i>e.e.</i> of L-Asn·H ₂ O in the preferential crystallization of L-Asn·H ₂ O in DL-Asn·H ₂ O with D-Asp additives (S=1.3) at 20°C.....152
5.36	% maximum of yield of L-Asn·H ₂ O in the preferential crystallization of L-Asn·H ₂ O in DL-Asn·H ₂ O without and with 3, 5, and 7% by mole of D-Asp additives at 20°C.....153
5.37	Solid crystal of L-Asn·H ₂ O in the preferential crystallization of L-Asn·H ₂ O in DL-Asn·H ₂ O with D-Glu additives (S=1.3) at 20°C.....154
5.38	Solid crystal of D-Asn·H ₂ O in the preferential crystallization of L-Asn·H ₂ O in DL-Asn·H ₂ O with D-Glu additives (S=1.3) at 20°C.....155
5.39	% <i>e.e.</i> of L-Asn·H ₂ O in the preferential crystallization of L-Asn·H ₂ O in DL-Asn·H ₂ O with D-Glu additives (S=1.3) at 20°C.....155
5.40	% Yield of L-Asn·H ₂ O in the preferential crystallization of L-Asn·H ₂ O in DL-Asn·H ₂ O with D-Glu additives (S=1.3) at 20°C.....156

LIST OF FIGURES (Continued)

Figure	Page
5.41	The relationship between %yield and % <i>e.e.</i> of L-Asn·H ₂ O in the preferential crystallization of L-Asn·H ₂ O in DL-Asn·H ₂ O with D-Glu additives (S=1.3) at 20°C.....156
6.1	Model of particle size distribution of D- and L-Asn·H ₂ O from the preferential crystallization of L-Asn·H ₂ O in DL-Asn·H ₂ O.....164
6.2	Particle size distribution and cumulative particle size distribution.....166
6.3	Experimental Setup.....167
6.4	Focus Beam Reflectance Measurement.....168
6.5	The screen of icFBRM 4.3 program for analyzing the crystal size distribution.....168
6.6	Concentration of L-Asn·H ₂ O in the preferential crystallization of L-Asn·H ₂ O in DL-Asn·H ₂ O without and with D-Glu and D-Asp additives.....172
6.7	Relative supersaturation of L-Asn·H ₂ O in the preferential crystallization of L-Asn·H ₂ O in DL-Asn·H ₂ O without and with D-Glu and D-Asp additives.....172
6.8	Concentration of D-Asn·H ₂ O in the preferential crystallization of L-Asn·H ₂ O in DL-Asn·H ₂ O without and with D-Glu and D-Asp additives.....173

LIST OF FIGURES (Continued)

Figure	Page
6.9	Solid crystal of L-Asn·H ₂ O in the preferential crystallization of L-Asn·H ₂ O in DL-Asn·H ₂ O without and with D-Glu and D-Asp additives.....173
6.10	Solid crystal of L-Asn·H ₂ O in the preferential crystallization of L-Asn·H ₂ O in DL-Asn·H ₂ O without and with D-Glu and D-Asp additives.....174
6.11	% <i>e.e.</i> of L-Asn·H ₂ O in the preferential crystallization of L-Asn·H ₂ O in DL-Asn·H ₂ O without and with D-Glu and D-Asp additives.....174
6.12	% Yield of L-Asn·H ₂ O in the preferential crystallization of L-Asn·H ₂ O in DL-Asn·H ₂ O without and with D-Glu and D-Asp additives.....175
6.13	The relationship between % <i>e.e.</i> and % Yield of L-Asn·H ₂ O in the preferential crystallization of L-Asn·H ₂ O in DL-Asn·H ₂ O without and with D-Glu and D-Asp additives.....175
6.14	The crystal size distribution of the preferential crystallization of L-Asn·H ₂ O in DL-Asn·H ₂ O solution by FBRM.....177
6.15	The cumulative oversize distribution of crystal in the preferential crystallization of L-Asn·H ₂ O in DL-Asn·H ₂ O solution by FBRM.....178

LIST OF FIGURES (Continued)

Figure	Page
6.16	The normalize of cumulative oversize distribution of crystal in the preferential crystallization of L-Asn·H ₂ O in DL-Asn·H ₂ O solution by FBRM.....178
6.17	The crystal size distribution of the preferential crystallization of L-Asn·H ₂ O in DL-Asn·H ₂ O solution with 5mol% D-Glu by FBRM.....179
6.18	The cumulative oversize distribution of crystal in the preferential crystallization of L-Asn·H ₂ O in DL-Asn·H ₂ O solution with 5 mol% D-Glu by FBRM.....179
6.19	The normalize of cumulative oversize distribution of crystal in the preferential crystallization of L-Asn·H ₂ O in DL-Asn·H ₂ O solution with 5 mol% D-Glu by FBRM.....180
6.20	The crystal size distribution of the preferential crystallization of L-Asn·H ₂ O in DL-Asn·H ₂ O solution with 5 mol% D-Asp by FBRM.....180
6.21	The cumulative oversize distribution of crystal in the preferential crystallization of L-Asn·H ₂ O in DL-Asn·H ₂ O solution with 5 mol% D-Asp by FBRM.....181
6.22	The normalize of cumulative oversize distribution of crystal in the preferential crystallization of L-Asn·H ₂ O in DL-Asn·H ₂ O solution with 5 mol% D-Asp by FBRM.....181

LIST OF FIGURES (Continued)

Figure	Page
6.23	The relationship between the crystal size and time of L-Asn·H ₂ O solid product in the preferential crystallization of L-Asn·H ₂ O in DL-Asn·H ₂ O without and with D-Glu and D-Asp additives.....185
6.24	The relationship between the crystal growth rate and time of L-Asn·H ₂ O solid product in the preferential crystallization of L-Asn·H ₂ O in DL-Asn·H ₂ O without and with D-Glu and D-Asp additives.....185
6.25	The relationship between the crystal growth rate and relative supersaturation of L-Asn·H ₂ O solid product in the preferential crystallization of L-Asn·H ₂ O in DL-Asn·H ₂ O without and with D-Glu and D-Asp additives.....186
E.1	The relationship between particle count number and time.....226
E.2	The particle size distribution of CaCO ₃227
E.3	The relationship between the number of particle from FBRM and mass of CaCO ₃228
E.4	The relationship between particle from FBRM and total number of particle in 1 g of solution.....229

SYMBOLS AND ABBREVIATIONS

a	=	Pre-exponential kinetic parameter, $m^{-1}s^{-1}$
A	=	Surface area of crystal, m^2
A_D	=	HPLC peak areas of D-Asn·H ₂ O
A_L	=	HPLC peak areas of L-Asn·H ₂ O
Asn·H ₂ O	=	Asparagine monohydrate
Asn	=	Asparagine
Asp	=	Aspartic acid
B	=	Thermodynamic parameter
B^0	=	Secondary nucleation rate, $\#/m^3 \cdot s$
C_D	=	Concentrations of D-Asn·H ₂ O, g/g-sol
C_L	=	Concentrations of L-Asn·H ₂ O, g/g-sol
C^*	=	Equilibrium concentration, g/g-sol
CaCO ₃	=	Calcium carbonate
CNT	=	Classical nucleation theory
CSD	=	Crystal size distribution
D	=	Diffusion coefficient, m^2/s
<i>e.e.</i>	=	Enantiomeric excess
FBRM	=	Focus beam reflectance measurement
FTIR	=	Fourier transform infrared spectroscopy
FT-Raman	=	Fourier transform Raman spectroscopy
G	=	Crystal growth rate, m/s

SYMBOLS AND ABBREVIATIONS (Continued)

Glu	=	Glutamic acid
HPLC	=	High pressure liquid chromatography
J	=	Nucleation rate, $\#/m^3 \cdot s$
K	=	Boltzmann constant, 1.38×10^{-23} J/K
k_a	=	Area shape factor
k_d	=	Coefficient of bulk mass transfer, m/s
k_g	=	Growth rate constant, m/s
k_D	=	Crystallization rate of D-enantiomer
k_L	=	Crystallization rate of L-enantiomer
k_v	=	Volume shape factor
L	=	Characteristic dimension that is increasing, m
Leu	=	Leucine
m	=	Crystal mass, g or kg
m_i	=	Mass of enantiomer i, g/g-sol
$m_{i,th}$	=	Maximum mass of enantiomer i, g/g-sol
M_T	=	Suspension density, g crystal/ g suspension
MSZW	=	Metastable zone width
n	=	Growth rate order
PSD	=	Particle size distribution
PC	=	Preferential crystallization
R_G	=	The increase of mass, $kg/m^2 \cdot s$
S	=	Supersaturation ratio

SYMBOLS AND ABBREVIATIONS (Continued)

T	=	Temperature, °C or K
t	=	Time, s or h
Val	=	Valine
XRPD	=	Powder X-ray diffraction
v_0	=	Molecular volume, m^3
γ	=	Interfacial energy, J/m^2
σ	=	Relative supersaturation
ω	=	Agitation speed, rpm
ρ	=	Density of the crystal, kg/m^3
Δ	=	Stagnant film or boundary layer, m
#	=	Crystal number

CHAPTER I

INTRODUCTION

1.1 Introduction to Stereoisomers

An isomer is one of a set of chemical molecules that have the same molecular formula but differences in their structure. Isomers can be classified into various types; these include “constitution isomers” where the molecules have the same molecular formula but are different in the way their atoms are connected (Bruice, 2014). Another type is “Stereoisomers”, sometimes called configurational isomers, which have the same molecular structure and the same sequence of bonds, but differences in the way their atoms are arranged in space. Stereoisomers can be divided into two types as shown in Figure 1.1. Diastereomers are a pair of compounds having the same sequence of bonds but they are not mirror images of each other. These two compounds have different angles of bonding. The physical, chemical and biological properties of these compound are different. The last one is enantiomers; the two compounds are nonsuperimposable mirror images of each other (for example 2-butanol as shown in Figure 1.2. We call this feature “chirality”. A chiral object is an object that cannot be superimposed on its mirror image. In this research, we focus on a chiral carbon which is a carbon atom that is bonded to four different types of atoms or groups of atoms; this may also be called an asymmetric carbon. The enantiomers have the same physical properties except optical activity, and the same chemical properties in achiral environments, but they are different in biological properties (because biological systems are not achiral). The two enantiomers which are mirror images of each other

can be classified by using many methods, such as the R and S system of enantiomers developed by Cahn, Ingold and Prelog (1966), or using the (+)- and (-)-notation (sometimes d- and l-) via the a polarimeter to see the optical activity of each enantiomer, whether it rotates the plane of polarization clockwise or counter clockwise. The d- and l- notation is less popular now since it can be confused with the D- and L- notation discussed next. The D and L notation is another classification of enantiomers which is commonly used with carbohydrates and amino acids. This notation was developed by Fischer and Rosanoff (1906), and uses the Fischer projection to determine the label for the specific enantiomer (in relation to the Fischer projections of D- and L-glyceraldehyde).

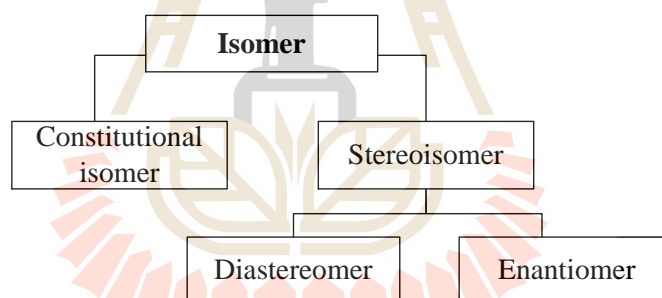


Figure 1.1 Type of isomer

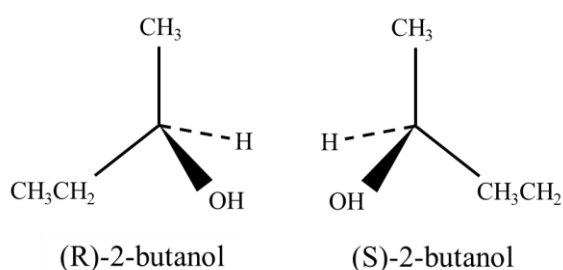


Figure 1.2 Enantiomers of 2-butanol

1.2 Introduction to Racemates and Racemic Mixtures

A racemic mixture is an equimolar mixture of two enantiomers. In 1847, the racemic mixture was discovered by Louis Pasteur who investigated the difference in shapes of d- and l-sodium ammonium tartrates as show in Figure 1.3.

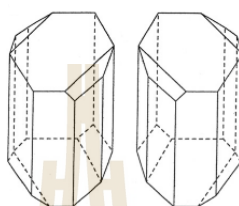


Figure 1.3 Hemihedral crystals of d- and l-sodium ammonium tartrate

(Manchester, 2007).

The crystal from a racemic mixture can be classified into three different types, consisting of conglomerate, racemic compound, and solid solution (Jacques et al., 1981). A conglomerate is a mechanical mixture of the enantiomers. This type is only 5-10% of racemates in nature (Lorenz et al., 2006). 90-95% of racemic mixtures are racemic compounds (also call true racemates) where the two enantiomers are arranged in the crystal lattice in equimolar quantities. The last type is a solid solution or pseudoracemate, where the two enantiomers coexist in the crystal, but in unequal amounts, and not in a structured way (as in a true racemate). The crystalline types of these racemates are shown in Figure 1.4.

These crystalline forms have differences in their binary phase diagrams, as shown in Figure 1.5 (Srisanga and ter Horst, 2010). The binary phase diagram shows the relationship between the mole fraction of the R-enantiomer in the mixture of R- and

S-enantiomers, and the melting temperature of the mixture. The binary phase diagrams of a conglomerate forming system can be divided into four regions, consisting of liquid solution (L), solid S-enantiomorph (S) with L, solid R-enantiomorph (R) with L, and solid R-enantiomorph and S-enantiomorph mixture (R+S). For a racemic compound, there are six regions, consisting of S+L, R+L, solid RS racemic compound (RS)+L, S+RS, and R+RS. For a solid solution, there are two regions consist of L, and RS. From these diagrams, the conglomerate and racemic compound types of crystal of racemic mixture have a pure crystal of solid enantiomer which is R-enantiomer, or S-enantiomer. Srisanga and ter Horst (2010) investigated the phase diagram screening for several crystalline racemates using asparagine, ibuprofen, and atenolol for conglomerate, racemic compound, and solid solution respectively, as shown in Figure 1.6.

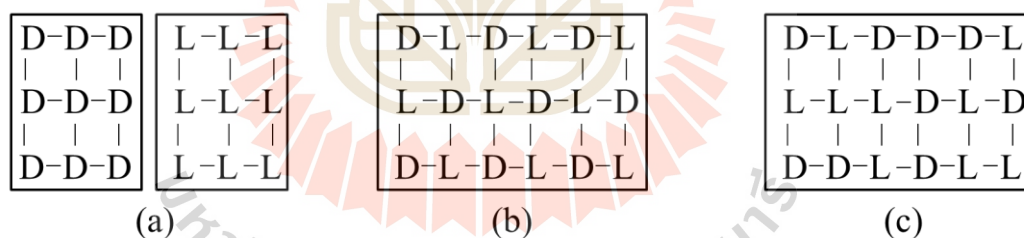


Figure 1.4 Crystalline forms of racemates (a) conglomerate, (b) racemic compound, and (c) solid solution.

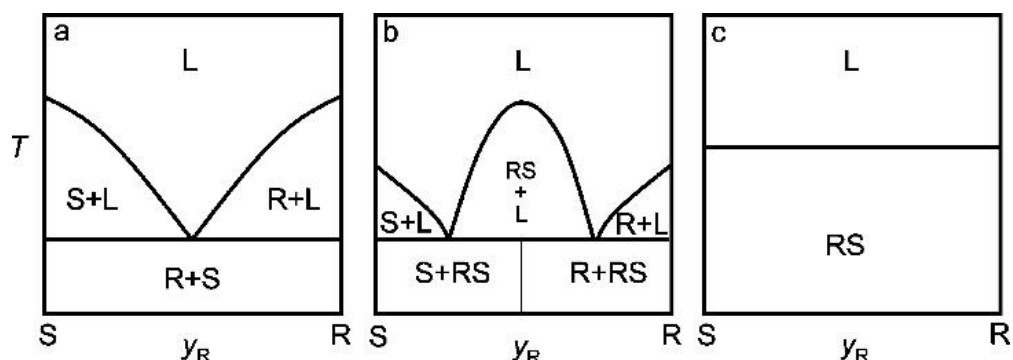


Figure 1.5 Binary phase diagram of racemate crystalline forming (a) a conglomerate (b) a racemic mixture, and (c) a solid solution (adapted from Srisanga and ter Horst (2010)).

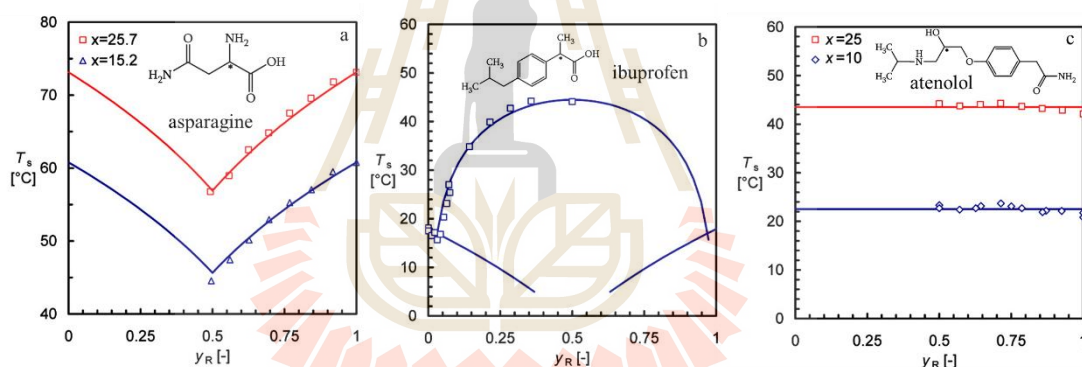


Figure 1.6 Phase diagram screens of (a) asparagine in water, (b) ibuprofen in hexane, and (c) atenolol in ethanol (Srisanga and ter Horst, 2010).

1.3 Introduction to Amino Acids

Amino acids are small organic molecules which are important to living organisms via being a building block of proteins, are precursors for many biologically active molecules, serve as an energy source, and relate to gene expression and cellular signaling (Kessel and Ben-Tal, 2010) etc. All amino acids contain an amine, carboxylic

acid, and an alkyl group or side chain; these groups are bonded to a chiral carbon atom as shown in Figure 1.7. There are many types of amino acids in nature, but only 20 of them are building blocks of proteins. The 20 natural amino acids can be divided into 4 types according to their side chain, as shown in Figure 1.8. Nonpolar amino acids include glycine, alanine, valine, leucine, isoleucine, methionine, and proline. Polar-uncharged amino acids include serine, threonine, cysteine, asparagine, and glutamine. Polar-charged amino acid include aspartic acid, glutamic acid, lysine, arginine, and histidine. Aromatic amino acids include phenylalanine, tyrosine, and tryptophan.

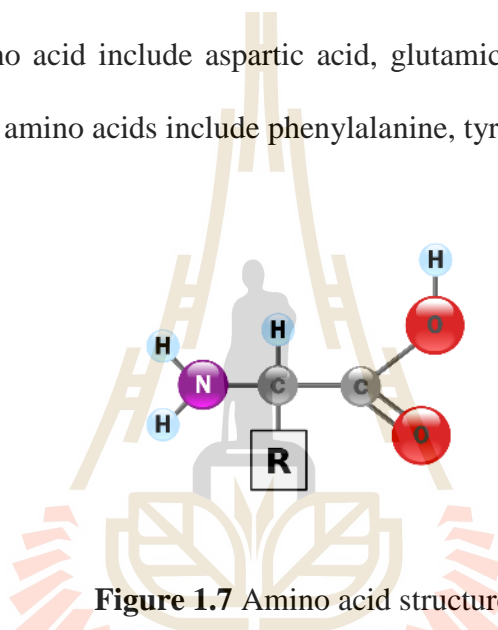


Figure 1.7 Amino acid structure

Some amino acids are nonessential amino acids because they can be synthesized by our body; these include alanine, asparagine, aspartic acid, glutamic acid, serine, arginine, cysteine, glutamine, glycine, proline, and tyrosine. Essential amino acids cannot be synthesized by our body and must be obtained from foods. This type includes histidine, isoleucine, leucine, lysine, methionine, phenylalanine, threonine, tryptophan, and valine.

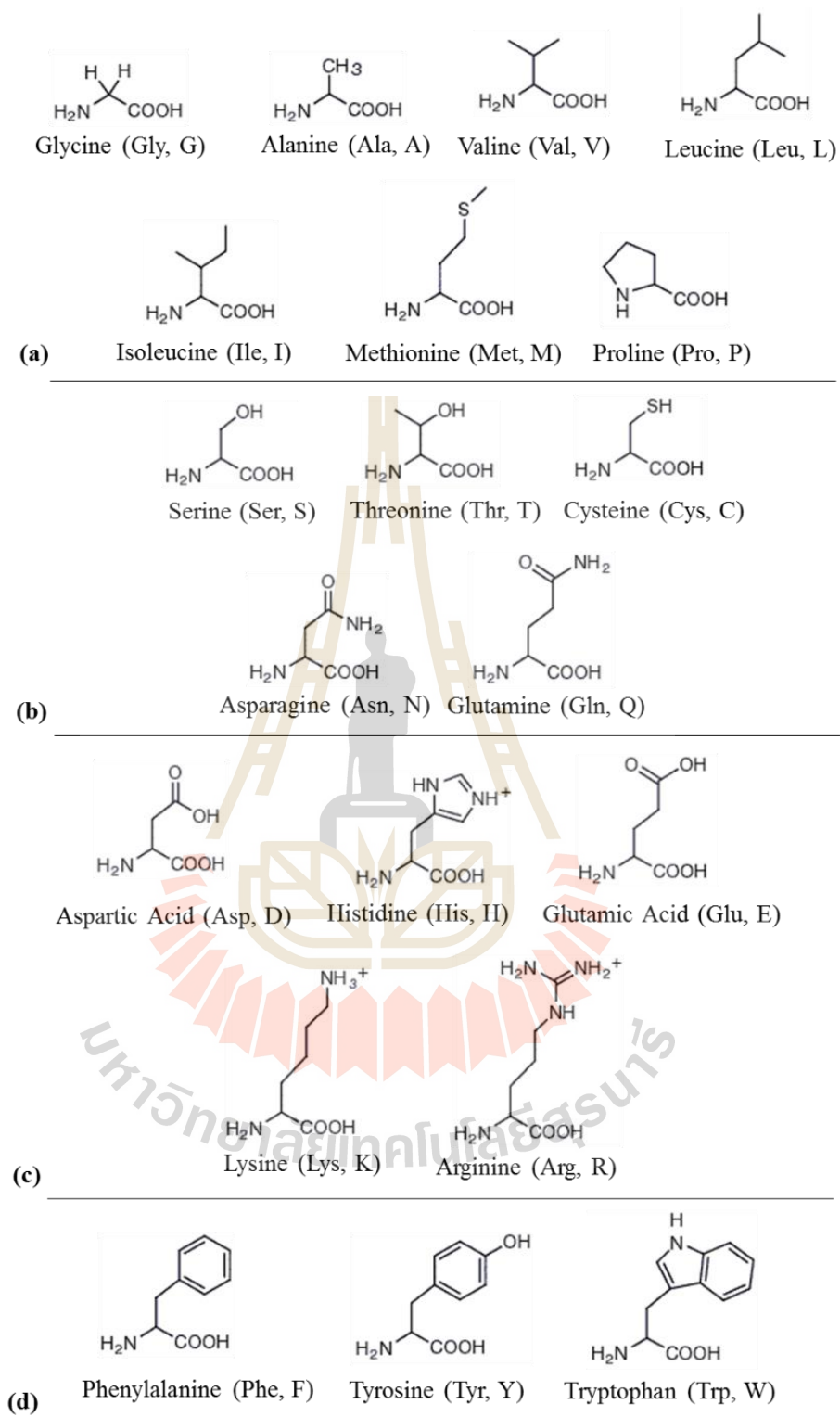


Figure 1.8 Amino acids (a) nonpolar amino acids, (b) polar-uncharged amino acids, (c) charged amino acids, and (d) aromatic amino acids.

Every amino acid (except glycine) is a chiral molecule, and thus occurs potentially as two different enantiomers. They are normally called L- and D-forms of the amino acid. Only L-amino acids are building blocks of proteins and some D-amino acids are found in cell walls of bacteria, but not in bacterial proteins. The two chiral forms of an amino acid are shown in Figure 1.9 for D- and L-alanine. Normally, only the L-amino acid can be found in nature, but amino acids from chemical synthesis probably contain both D- and L-amino acids as a racemic mixture.

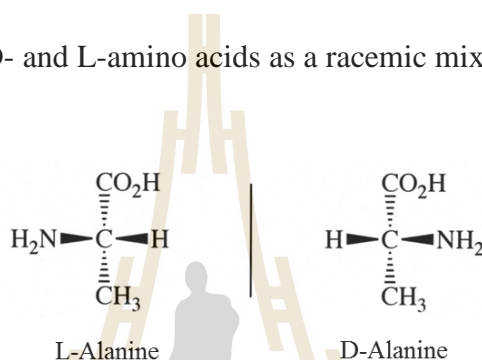


Figure 1.9 Structure of L-/D-alanine.

1.4 Background and Significance of the Study

Many products in the pharmaceutical, food, and agrochemical industries are chiral compounds. However, the chemical synthesis of chiral materials produces products that are usually a racemic mixture of enantiomers; 50% is the preferred enantiomer and 50% is the counter enantiomer. Normally, the counter enantiomer has no beneficial effect but does increase the drug loading on the body. In some cases, the counter enantiomer is harmful; R-thalidomide was used as a sedative and sleeping drug for pregnant women, however, S-thalidomide was found to be teratogenic and caused birth defects in thousands of babies (Eriksson et al., 2001). Therefore, the separation of enantiomers is essential in many industries, but particularly in the pharmaceutical industry.

There are many processes to separate enantiomers. Chiral membrane separation uses a chiral-modified membrane which allows the desired enantiomer to selectively diffuse through the membrane (Yoshikawa et al., 2013). Chiral chromatography separation uses an enantioselective chiral stationary phase to separate enantiomers (Francotte, 2001; Lorenz et al., 2006). However, crystallization has unprecedented selectivity and potentially leads to an enantiopure product within a single process step if the crystallization of the counter enantiomer can be avoided. This can be done through the formation of diastereomeric salts which changes the enantiomers to diastereomers which have different physical properties and enable separation by crystallization (Kozma, 2002). However, this requires an additional separation step to recover the resolving agent.

Preferential crystallization (PC) is a single step process that is easy and low cost for separating enantiomers. This process is suitable for separation of a racemic mixture that is a conglomerate forming system, meaning the equilibrium product is a mechanical mixture of the two enantiomorphs (Jacques et al., 1981). PC achieves separation in a single process step through seeding the preferred enantiomer to the supersaturated racemic solution; the preferred enantiomer will crystallize at a higher rate than the counter enantiomer, and significant yield and enantiopurity can be achieved if the nucleation and growth of the counter enantiomer from the supersaturated solution can be avoided. PC has been applied to chiral species such as glutamic acid (Buhse et al., 1999), asparagine (Petruševska-Seebach et al., 2011), threonine (Profir and Matsuoka, 2000) and methionine hydrochloride (Srimahaprom and Flood, 2013). However, this method has a serious problem which is the spontaneous nucleation and growth of the counter enantiomer (Jacques et al., 1981; Matsuoka, 1997; Profir and Matsuoka, 2000;

Beilles et al., 2001; Angelov et al., 2008; Czapla et al., 2009; Elsner et al., 2009). This may occur after prolonged batch times where the solution has a high supersaturation of the counter enantiomer in comparison to the preferred enantiomer (Profir and Matsuoka, 2000). Many researchers have tried to circumvent this problem, for instance by using coupled batch crystallizers – crystallizing the preferred enantiomer in one crystallizer and the counter enantiomer in another crystallizer, with exchange of solution between the two crystallizers (Elsner et al., 2009), coupled batch crystallizers with seeding of the preferred enantiomer in one crystallizer and allowing nucleation of the counter enantiomer in another crystallizer maintained at a different temperature (Levilain et al., 2012; Eicke et al., 2013), coupled batch crystallizers with a membrane between the crystallizers to prevent transport of crystals from one crystallizer to another (Svang-Ariyaskul et al., 2009), and racemization of the solute species to equalize the concentrations of the preferred and counter enantiomer (Würges et al., 2009; Petruševska-Seebach et al., 2009).

Another way to circumvent the crystallization of the counter enantiomer is to use tailor made additives to inhibit the nucleation and growth of the counter enantiomer. This will be most suitable if the resolution is done in a fully batch system, and crystallization or recycling of the counter enantiomer is not required. A tailor-made additive is any additive which is intelligently designed to change the crystallization process in a desired way. It may inhibit either growth or nucleation, or more rarely promote growth or nucleation, or it may alter the shape or morphology of the crystals. Addadi et al. proposed the rule of reversal, which suggests that additives most easily adsorb on the surface of the crystal that has the same absolute configuration as the additive (Addadi et al., 1981; Addadi et al., 1982). The rule thus states that the chiral

additive will inhibit the crystallization of the enantiomorph similar in chirality to the additive. There are many studies about effect of tailor made additives to the crystallization such as effect of D- and L-lysine additives on DL-glutamic acid (Buhse et al., 1999; Kondepudi and Culha, 1998; Kondepudi and Crook, 2005).

These ideas encourage the author to develop the preferential crystallization process with tailor-made additives to increase the purity and yield of the preferred enantiomer. Moreover, the effect of additives to solubility, metastable zone width, crystal growth rate, and nucleation is also studied to deepen knowledge of crystallization with additives.

In this research we used asparagine, which is an amino acid, to study the preferential crystallization process because almost all amino acids are chiral compounds. We also used other amino acid as Tailor-made additives because their chemical structures are close to the structure of the asparagine enantiomers.

1.5 Research Objectives

This thesis will use experimental data to study the crystallization of L-asparagine monohydrate ($L\text{-Asn}\cdot\text{H}_2\text{O}$) from $L\text{-Asn}\cdot\text{H}_2\text{O}$ and $DL\text{-Asn}\cdot\text{H}_2\text{O}$ solution. We also investigate the effect of amino acid additives as tailor-made additives for crystallization of $L\text{-Asn}\cdot\text{H}_2\text{O}$. In addition, we use eight types of additives consisting of D- and L- Aspartic acid (Asp), D- and L-glutamic acid (Glu), D- and L-leucine (Leu) and D- and L-valine (Val). This includes the measurement and analysis of the thermodynamic and kinetic properties. The specific objectives of this research are as follows:

1.5.1 To determine the solubility of L-Asn·H₂O, and DL-Asn·H₂O as a function of temperature. Also, to study the effect of amino acid additives to the solubility of L- and DL-Asn·H₂O.

1.5.2 To determine the metastable zone width of L-Asn·H₂O and DL-Asn·H₂O without and with amino acid additives. This phenomenon depends on the concentration of the solute, the cooling rate, and temperature.

1.5.3 To investigate the crystal growth rate of L-Asn·H₂O in L-Asn·H₂O, and DL-Asn·H₂O supersaturation, and also the effect of amino acid additives to inhibit or promote crystal growth rate of L-Asn·H₂O, or change the morphology of the L-Asn·H₂O crystal.

1.5.4 To study the unseeded crystallization of DL-Asn·H₂O with amino acid additives. These additives may change the crystallization pathway by inhibiting the nucleation of D- or L-Asn·H₂O.

1.5.5 To study the preferential crystallization of L-Asn·H₂O from DL-Asn·H₂O solution. Moreover, tailor-made additives are used to increase the yield and purity of the product.

1.5.6 To investigate the effect of tailor-made additives to the particle size distribution of L-Asn·H₂O from DL-Asn·H₂O solution. This investigation will show the relationship between the nucleation, crystal growth and inhibition by additives simultaneously.

1.6 Scope and Limitation of the research

The solubility DL-Asn·H₂O was studied by three methods, consisting of the gravimetric method, the refractive index method, and a turbidity measurement using

the Crystal16 (Technobis, the Netherlands). We also used the Crystal16 to find the solubility of L-Asn·H₂O and L-/DL-Asn·H₂O with and without amino acid additives. The metastable zone width and induction time of L-Asn·H₂O and DL-Asn·H₂O with additives were also measured by the Crystal16.

In the growth kinetic study, the L-Asn·H₂O crystal growth was performed in a small cell. The growth occurred in stagnant conditions and we assumed that no nucleation, no breakage, and no agglomeration occurred during the crystallization process. The crystal growth was observed using a microscope.

In unseeded crystallization, the enantiopurity of product was analyzed by chiral High Pressure Liquid Chromatography (HPLC). The product also was analyzed by powder X-ray diffraction (XRD), Fourier transform Raman spectroscopy (FT-Raman), and Fourier transform infrared spectroscopy (FTIR).

In the preferential crystallization section, the product yield and enantiopurity were analyzed by chiral HPLC and the particle size distribution of solid product was analyzed by Focused Beam Reflectance Measurement (FBRM).

1.7 Research Development

This thesis is divided into 7 chapters. **Chapter I** is an introduction; it gives some introduction to stereoisomers, racemic mixtures, amino acids, and describes the background, significance, objectives and scope of the research. **Chapter II** reports the solubility and the metastable zone width of L-Asn·H₂O and DL-Asn·H₂O as a function of temperature, and concentration. The effect of tailor-made additives to the solubility of L-Asn·H₂O and DL-Asn·H₂O is also reported. The crystal growth rate of L-Asn·H₂O from L-Asn·H₂O, DL-Asn·H₂O, and DL-Asn·H₂O with additives is presented in

Chapter III. This chapter also shows the growth rate of L-Asn·H₂O in L-/DL-Asn·H₂O solution in different levels of supersaturation. In **Chapter IV**, the crystallization of DL-Asn·H₂O without seeding is reported. Moreover, the effect of tailor-made additives to the crystallization of DL-Asn·H₂O is also presented. In **Chapter V**, the effect of supersaturation, and seed amount to the preferential crystallization (PC) of L-Asn·H₂O in DL-Asn·H₂O were studied, and the effect of tailor-made additives to the preferential crystallization of L-Asn·H₂O in DL-Asn·H₂O was also studied. In **Chapter VI**, the crystal size distribution during the preferential crystallization was studied and the effect of additives to the crystal size distribution was also studied. Finally, **Chapter VII** concludes the results from this thesis and gives some recommendations for future study.

1.8 References

- Addadi, L., Van Mil, J., and Lahav, M. 1981. Useful impurities for optical resolutions. 2. Generality and mechanism of the rule of reversal. **Journal of the American Chemical Society** 103 (5):1249-1251.
- Addadi, L., Weinstein, S., Gati, E., Weissbuch, I., and Lahav, M. 1982. Resolution of conglomerates with the assistance of tailor-made impurities. Generality and mechanistic aspects of the "rule of reversal". A new method for assignment of absolute configuration. **Journal of the American Chemical Society** 104 (17):4610-4617.
- Angelov, I., Raisch, J., Elsner, M. P., and Seidel-Morgenstern, A. 2008. Optimal operation of enantioseparation by batch-wise preferential crystallization. **Chemical Engineering Science** 63 (5):1282-1292.

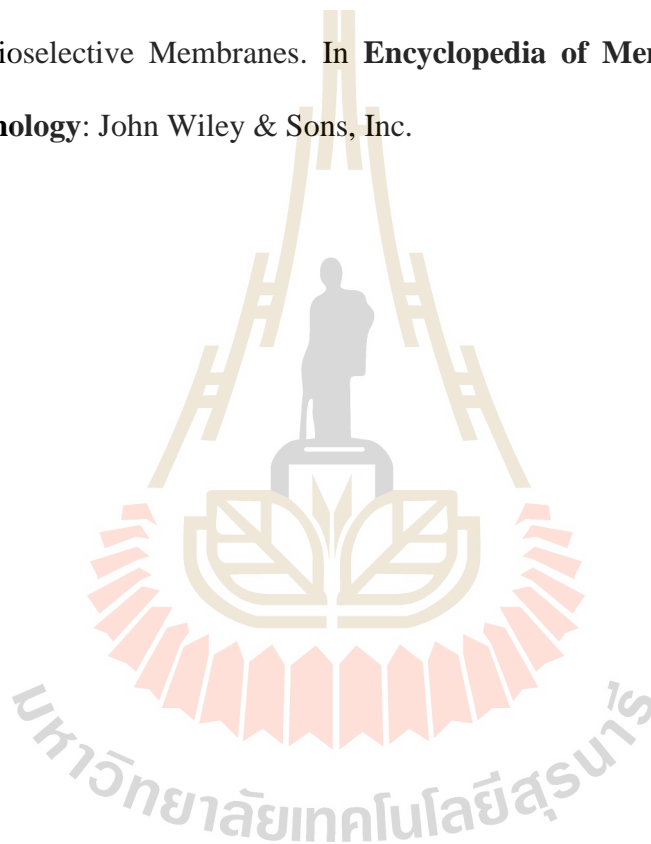
- Beilles, S., Cardinael, P., Ndzié, E., Petit, S., and Coquerel, G. 2001. Preferential crystallisation and comparative crystal growth study between pure enantiomer and racemic mixture of a chiral molecule: 5-ethyl-5-methylhydantoin. **Chemical Engineering Science** 56 (7):2281-2294.
- Bruice, P. Y. 2014. **Organic Chemistry**. edited by Paula Yurkanis Bruice. 7 ed. Upper Saddle River, NJ: Pearson.
- Buhse, T., Kondepudi, D. K., and Hoskins, B. 1999. Kinetics of chiral resolution in stirred crystallization of D/L-glutamic acid. **Chirality** 11 (4):343-348.
- Czapla, F., Haida, H., Elsner, M. P., Lorenz, H., and Seidel-Morgenstern, A. 2009. Parameterization of population balance models for polythermal auto seeded preferential crystallization of enantiomers. **Chemical Engineering Science** 64 (4):753-763.
- Eicke, M. J., Levilain, G., and Seidel-Morgenstern, A. 2013. Efficient Resolution of Enantiomers by Coupling Preferential Crystallization and Dissolution. Part 2: A Parametric Simulation Study to Identify Suitable Process Conditions. **Crystal Growth and Design** 13 (4):1638-1648.
- Elsner, M. P., Ziomek, G., and Seidel-Morgenstern, A. 2009. Efficient separation of enantiomers by preferential crystallization in two coupled vessels. **AIChE Journal** 55 (3):640-649.
- Eriksson, T., Björkman, S., and Höglund, P. 2001. Clinical pharmacology of thalidomide. **European Journal of Clinical Pharmacology** 57 (5):365-376.
- Francotte, E. R. 2001. Enantioselective chromatography as a powerful alternative for the preparation of drug enantiomers. **Journal of Chromatography A** 906 (1-2):379-397.

- Jacques, J., Collet, A., and Wilen, S. H. 1981. **Enantiomers, Racemates, and Resolutions**. New York: Wiley.
- Kessel, A., and Ben-Tal, N. 2010. **Introduction to Proteins Structure, Function, and Motion**. 0 vols: CRC Press.
- Kondepudi, D. K., and Crook, K. E. 2005. Theory of conglomerate crystallization in the presence of chiral impurities. **Crystal Growth and Design** 5 (6):2173-2179.
- Kondepudi, D. K., and Culha, M. 1998. Chiral interaction and stochastic kinetics in stirred crystallization of amino acids. **Chirality** 10:238-245.
- Kozma, D. 2002. **CRC Handbook of Optical Resolutions via Diastereomeric Salt Formation**: CRC Press.
- Levilain, G., Eicke, M. J., and Seidel-Morgenstern, A. 2012. Efficient Resolution of Enantiomers by Coupling Preferential Crystallization and Dissolution. Part 1: Experimental Proof of Principle. **Crystal Growth and Design** 12 (11):5396-5401.
- Lorenz, H., Perlberg, A., Sapoundjiev, D., Elsner, M. P., and Seidel-Morgenstern, A. 2006. Crystallization of enantiomers. **Chemical Engineering and Processing: Process Intensification** 45 (10):863-873.
- Manchester, K. L. 2007. Louis Pasteur, fermentation, and a rival. **South African Journal of Science** 103:377-380.
- Matsuoka, M. 1997. Purity Drop in Optical Resolution of Racemic Mixtures. In **Separation and Purification by Crystallization**: American Chemical Society, 59-72.

- Petruševska-Seebach, K., Seidel-Morgenstern, A., and Elsner, M. P. 2011. Preferential crystallization of L-asparagine in water. **Crystal Growth and Design** 11 (6):2149-2163.
- Petruševska-Seebach, K., Würges, K., Seidel-Morgenstern, A., Lütz, S., and Elsner, M. P. 2009. Enzyme-assisted physicochemical enantioseparation processes—Part II: Solid–liquid equilibria, preferential crystallization, chromatography and racemization reaction. **Chemical Engineering Science** 64 (10):2473-2482.
- Profir, V. M., and Matsuoka, M. 2000. Processes and phenomena of purity decrease during the optical resolution of dl-threonine by preferential crystallization. **Colloids and Surfaces A: Physicochemical and Engineering Aspects** 164 (2–3):315-324.
- Srimahaprom, W., and Flood, A. E. 2013. Crystal growth rates and optical resolution of dl-methionine hydrochloride by preferential crystallization from aqueous solution. **Journal of Crystal Growth** 362:88-92.
- Srisanga, S., and ter Horst, J. H. 2010. Racemic Compound, Conglomerate, or Solid Solution: Phase Diagram Screening of Chiral Compounds. **Crystal Growth and Design** 10 (4):1808-1812.
- Svang-Ariyaskul, A., Koros, W. J., and Rousseau, R. W. 2009. Chiral separation using a novel combination of cooling crystallization and a membrane barrier: Resolution of DL-glutamic acid. **Chemical Engineering Science** 64 (9):1980-1984.

Würges, K., Petrusevska, K., Serci, S., Wilhelm, S., Wandrey, C., Seidel-Morgenstern, A., Elsner, M. P., and Lütz, S. 2009. Enzyme-assisted physicochemical enantioseparation processes: Part I. Production and characterization of a recombinant amino acid racemase. **Journal of Molecular Catalysis B: Enzymatic** 58 (1-4):10-16.

Yoshikawa, M., Higuchi, A., Hoek, E. M. V., and Tarabara, V. V. 2013. Enantioselective Membranes. In **Encyclopedia of Membrane Science and Technology**: John Wiley & Sons, Inc.



CHAPTER II

SOLUBILITIES AND METASTABLE ZONE WIDTH OF ASPARAGINE MONOHYDRATE AND ASPARAGINE MONOHYDRATE WITH TAILOR-MADE ADDITIVES

2.1 Abstract

The essential information for the design of crystallization processes consists of solubility, metastable zone width (MSZW), nucleation rate, and growth rate. This chapter investigates the solubility and MSZW of L-/D-/DL-asparagine monohydrate ($\text{Asn}\cdot\text{H}_2\text{O}$) in water. Moreover, the change in the solubility and MSZW due to the use of additives was also studied. The solubility of DL-Asn $\cdot\text{H}_2\text{O}$ was measured by 3 methods, the gravimetric method, the refractive index method (RI), and the turbidity method (using the Crystal16 from Technobis). The solubilities resulting from these methods are very similar; thus, the solubility can be found from any common method depending on the chemicals involved and the equipment available. Moreover, this research used D-/L-aspartic acid (Asp), D-/L-glutamic acid (Glu), D-/L-leucine (Leu), and D-/L-valine (Val) as additives to change the solubility and metastable zone width of L-Asn $\cdot\text{H}_2\text{O}$. The solubility of Asn $\cdot\text{H}_2\text{O}$ in water is increased when using 5 mol% of additives because the additives associate with the solute in the solution. The cooling rate is the main effect to the width of the metastable zone, with higher cooling rates leading to larger MSZW. The additives also effect the MSZW of L-/DL-Asn $\cdot\text{H}_2\text{O}$ in water. However, the results are very scattered because the metastable zone relies on

nucleation which is a stochastic process. Therefore, the trend of these MSZW are not clear, but they still depend on some of the variables considered.

2.2 Introduction

Crystallization is a process to transform solute in the solution phase into the crystal phase. This process is one of the most popular separation and purification processes in the chemical industry and related industries. The solubility and metastable zone are basic pieces of information for the design of crystallization processes. The main variables which have an effect on the solubility of a species are the type of chemical, as shown in Table 2.1, temperature, as shown in Figure 2.1, and solvent, as shown in Figure 2.2.

Table 2.1 The solubility of inorganic compound at 20°C.

Compound	Solubility (g anhydrous/100g H ₂ O)
Calcium chloride	74.5
Calcium iodide	204
Calcium nitrate	129
Calcium hydroxide	0.17
Calcium sulfate	0.2
Ammonium sulfate	75.4
Copper sulfate	20.7
Lithium sulfate	34
Magnesium sulfate	35.5
Silver sulfate	0.7

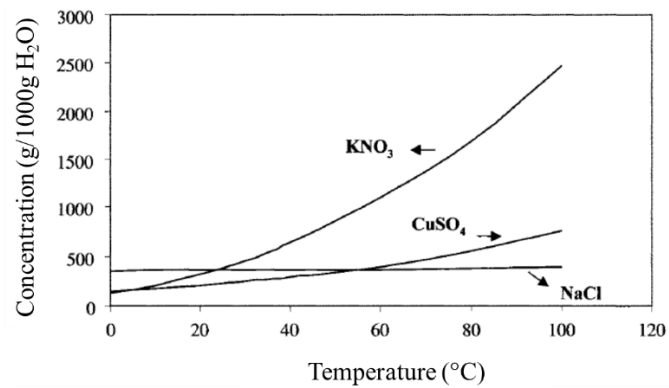


Figure 2.1 Solubility of potassium nitrate (KNO₃), copper sulfate (CuSO₄), and sodium chloride (NaCl) in aqueous solution (Myerson, 2002).

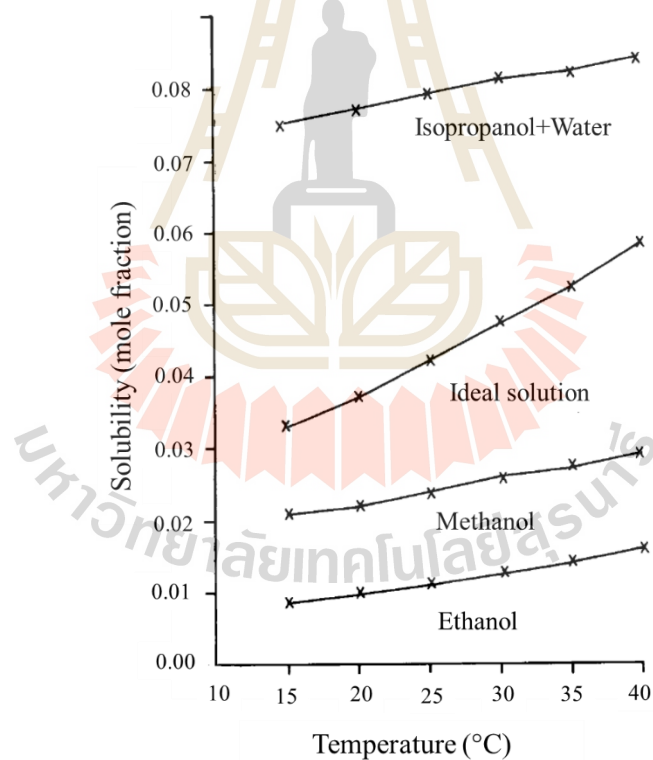


Figure 2.2 Solubility of hexamethylenetetramine in different solvents (Myerson et al., 1986; Myerson, 2002).

There are many techniques to find the solubility. The solubility measurement techniques are classified into isothermal and polythermal methods. For isothermal methods, the solubility is measured at a constant temperature; examples are the gravimetric method (Dunn et al., 1933; Dalton and Schmidt, 1935; Nozaki and Tanford, 1963; Lorenz et al., 2002; Lorenz and Seidel-Morgenstern, 2002; Lorenz et al., 2003; Sapoundjiev et al., 2006), the refractive index method (Lawson and Ingham, 1969; Wingefors and Liljenzin, 1981; Buckley, 1999; Flood and Puagsa, 2000) and the chromatography method (Flood and Puagsa, 2000). For the polythermal method, the solubility is usually found by slowly heating a solution which has a known amount of solute and solvent, with the solubility usually found by determining the time at which a clear solution has been created. Examples of polythermal methods to find solubility are the differential scanning calorimetry (DSC) method (Shibuya et al., 1993; Huang and Chen, 2000; Mohan et al., 2002; Lorenz and Seidel-Morgenstern, 2002), and the turbidity method (ter Horst et al., 2009; Maosoongnern et al., 2012; Reus et al., 2015).

Many researchers have determined the solubility of amino acid enantiomers (including pure enantiomers and racemic mixtures) of particular species, and other chiral compounds (Dunn et al., 1933; Dalton and Schmidt, 1935; Nozaki and Tanford, 1963; Lorenz et al., 2002; Lorenz and Seidel-Morgenstern, 2002; Lorenz et al., 2003; Sapoundjiev et al., 2006). For example, the solubility of amino acids in pure enantiomer form and racemic mixture form in aqueous solution is shown in Figure 2.3, from Dalton and Schmidt (1935).

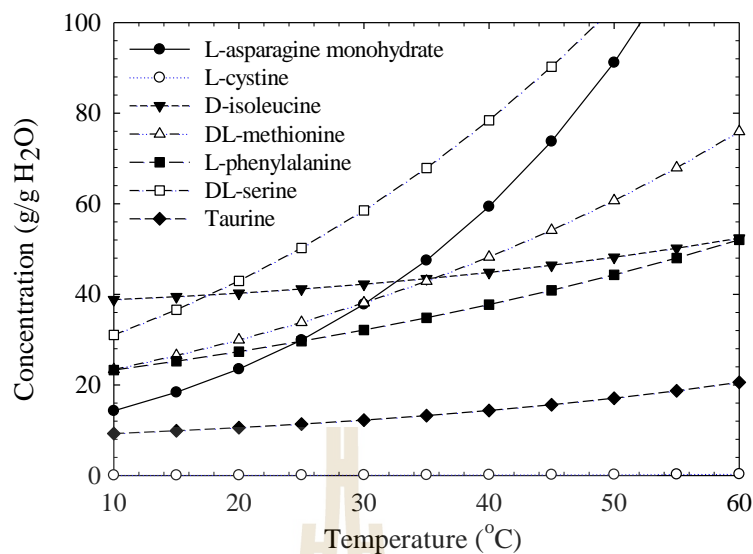


Figure 2.3 Solubility of pure enantiomers and racemic mixture of amino acids in aqueous solution (Dalton and Schmidt (1935)).

The metastable zone width (MSZW) is the zone between the saturation temperature and the temperature at which the first nuclei are found at a constant cooling rate (Mullin, 2001; Kadam et al., 2012). The importance of this zone is that the crystals in a solution within this zone can grow without significant nucleation occurring. There is much research that determined the MSZW using many methods; normally the solution is cooled at a constant cooling rate until the nucleation occurs (Zhou et al., 2016; Wang et al., 2015; Mersmann and Bartosch, 1998; Kadam et al., 2012; Kulkarni et al., 2013; Nývlt, 1983; Hussain et al., 2001; Herden et al., 2001; Wang et al., 2002; Barrett and Glennon, 2002; Titz-Sargut and Ulrich, 2002; Ulrich and Strege, 2002; O'Grady et al., 2007; Kobari et al., 2013).

This research focuses on the effect of tailor-made additives to the crystallization of Asn·H₂O enantiomers. The solubility and metastable zone width are fundamental information which we should know to further investigate these effects. This research

investigates the solubility of DL-Asn·H₂O using three different methods consisting of the gravimetric method, the refractive index method, and the turbidity method. The metastable zone width is also studied using the turbidity method by the Crystal16 equipment. Determination of the effect of amino acid additives to the solubility and metastable zone width of Asn species is the main objective in this chapter.

2.3 Theory

2.3.1 Solubility

Solubility, or the concentration of a saturated solution, is a physical property of a chemical substance. It is the maximum amount of solute that can dissolve in the solvent at constant set of conditions (e.g. temperature, and pressure). The solubility of a substance fundamentally depends on the physical and chemical properties of the solute and solvent such as temperature, pressure, and solvent composition.

2.3.2 Supersaturation

Supersaturation is an excess of the solute in solution (Randolph and Larson, 1988). This occurs by reduction of the solution temperature until it is lower than the saturation temperature for the solute in that solution. The supersaturation zone is shown in Figure 2.4. The supersaturation zone is above the solubility curve and the undersaturated region is below the solubility curve.

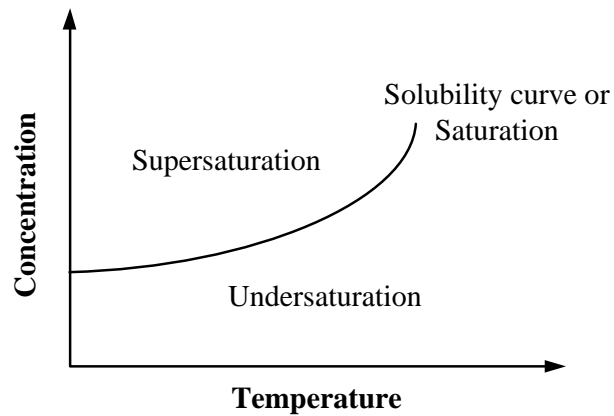


Figure 2.4 Solubility curve and the zones of concentration.

Supersaturation is often expressed as a concentration difference, as in Equation

(2.1)

$$\Delta C = C - C^* \quad (2.1)$$

and the supersaturation ratio in Equation (2.2)

$$S = \frac{C}{C^*} \quad (2.2)$$

and the relative supersaturation in Equation (2.3)

$$\sigma = \frac{C - C^*}{C^*} = S - 1 \quad (2.3)$$

where ΔC is the concentration difference (concentration driving force), C is solution concentration, C^* is the equilibrium concentration at a given temperature, S is the supersaturation ratio, and σ is relative supersaturation.

2.3.3 Nucleation

Nucleation is one step of crystallization from solution in which new crystals are produced. Nucleation can be divided into two mechanisms, primary nucleation and secondary nucleation. Primary nucleation occurs in the absence of crystalline surfaces, but secondary nucleation occurs in the presence of crystals due to their interaction with the environment such as crystallizer wall, impellers etc. (Myerson, 2002). The details of nucleation are described in Chapter IV.

2.3.4 Metastable Zone Width

The metastable zone is the zone in which nucleation usually does not spontaneously occur in supersaturated solutions. In batch crystallization processes, the operation is usually undertaken in the metastable zone to control the crystal size of the product (limiting growth to only the seed crystals) and avoid large amounts of nucleation. The metastable zone is shown in Figure 2.5, this zone is in between solubility curve and metastable limit.

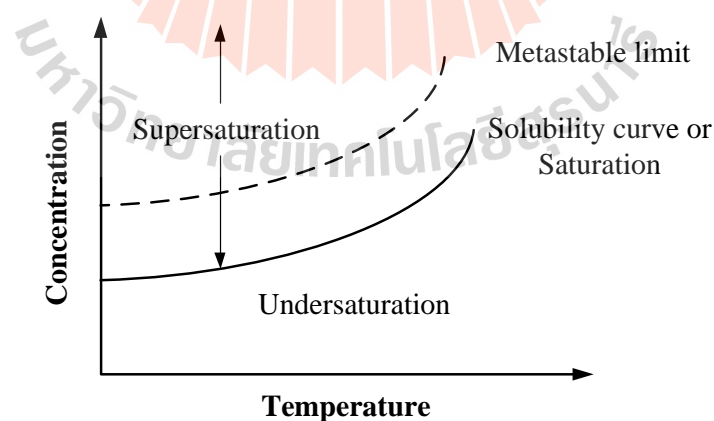


Figure 2.5 Metastable zone in crystallization process.

2.3.5 Phase Diagram

The solid-liquid equilibria (SLE) is a fundamental knowledge to design and optimize the crystallization process (Lorenz and Seidel-Morgenstern, 2002; Lorenz et al., 2003). This is especially true in processes to separate racemic mixtures, such as preferential crystallization or separation via diastereomeric salt formation. These separation methods are very important in the pharmaceutical industry. The binary phase diagram can divide the type of racemic mixture (Srisanga and ter Horst, 2010) as shown in Figure 1.6 in Chapter I. The ternary phase can also be used to classify the types of racemic mixture, as shown in Figure 2.6. For a conglomerate system, the ternary phase diagram can be divided into four regions consisting of two regions with pure solid enantiomer with liquid phases (liquid + E₁ enantiomorph, and liquid+E₂ enantiomorph), a single liquid phase region, and a region with a liquid phase in equilibrium both with E₁ and E₂ enantiomorphs. For the racemic compound system, the ternary phase diagram can be divided into six regions consisting of a region where the pure solid enantiomorphs are in equilibrium with liquid phases (liquid + E₁ enantiomorph, and liquid + E₂ enantiomorph), a region with a single liquid phase, a region with a liquid phase in equilibrium with both the racemic compound solid phase and the E₁ enantiomorph, a region with a liquid phase in equilibrium with both the racemic compound solid phase and the E₂ enantiomorph, and a region where the liquid phase is in equilibrium with only the racemic compound solid phase.

In Figure 2.7, the ternary phase diagram of threonine in water, a conglomerate forming system is shown. The ternary phase diagram of mandelic acid (MA) in eluent (95:5 vol%, 0.05 mol/L of ammonium acetate: acetonitrile) is also shown; this system is a racemic compound system.

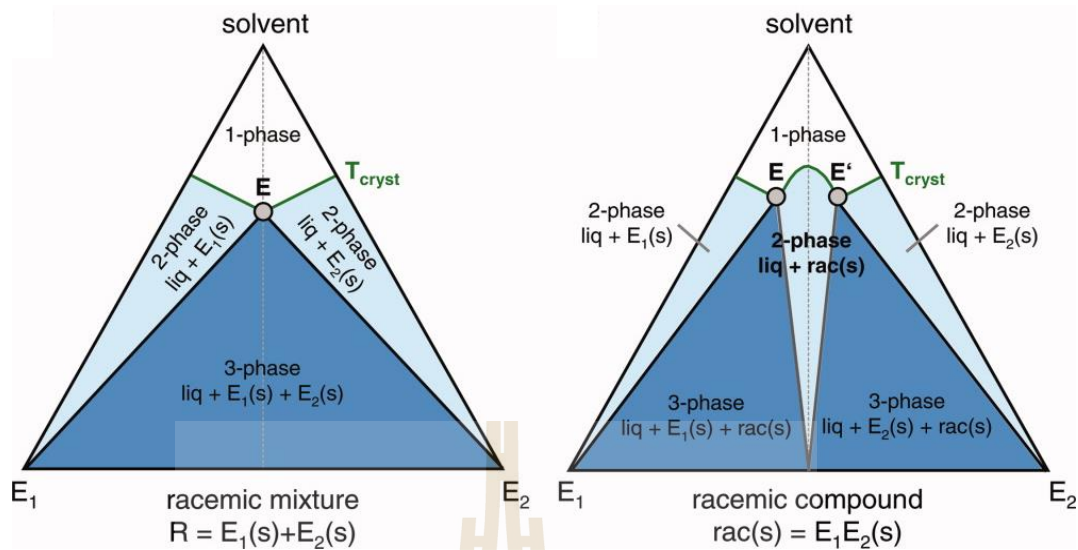


Figure 2.6 Ternary phase diagram for conglomerates (left), and racemic compound systems (right) (Elsner et al., 2009).

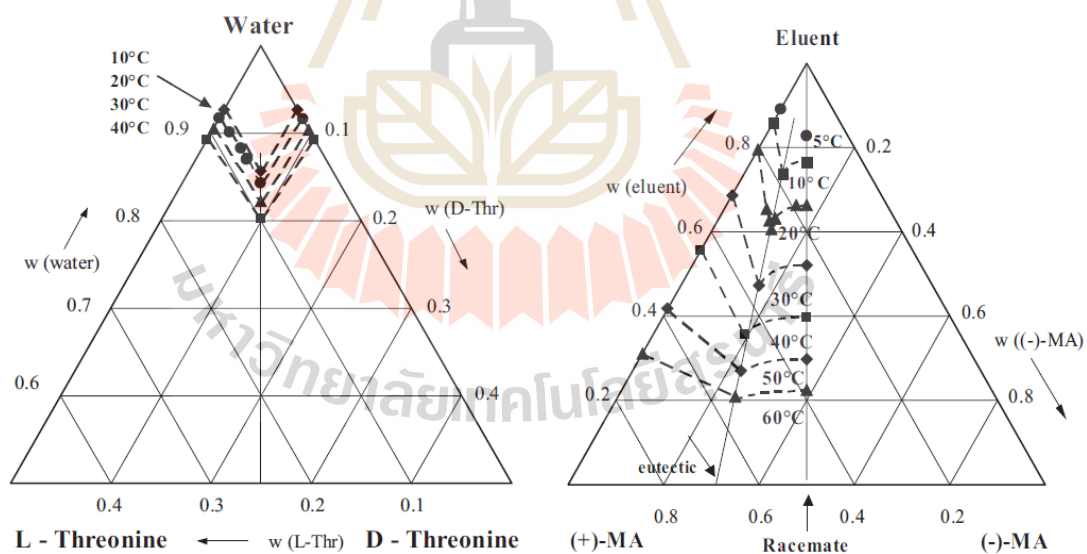


Figure 2.7 Ternary solubility phase diagram of threonine in water which is a conglomerate system (left) and mandelic acid in eluent (95:5 vol% 0.05 mol/L of ammonium acetate: acetonitrile) which is a racemic compound system (right) (Lorenz et al., 2003).

2.4 Materials and Methods

2.4.1 Materials

DL-asparagine monohydrate (DL-Asn·H₂O, 99+ wt%), L-asparagine monohydrate (L-Asn·H₂O, 99+ wt%) and D-asparagine monohydrate (D-Asn·H₂O, 99+ wt%), were purchased from Sigma-Aldrich. D-aspartic acid (D-Asp, 99+wt%), D-glutamic acid (D-Glu, 99+wt%), D-valine (D-Val, 98+wt%), D-leucine (D-Leu, 99 wt%), L-aspartic acid (L-Asp, 98+wt%), L-glutamic acid (L-Glu, 99+wt%), L-valine (L-Val, 98+wt%), and L-leucine (L-Leu, 99 wt%) were purchased from ACROS. These reagents were used without further purification. Deionized water was used as the solvent.

2.4.2 Solubility Measurement by Gravimetric Method

An excess amount of the solute DL-Asn·H₂O was added into water at a given temperature. The suspension was stirred using a magnetic stirrer. Every 1 h (from 1 h to 5 h) after stirring was begun the suspended solution was sampled and filtered through a membrane filter to retain only the pure liquid solution. The liquid solution was kept in a vial with a cap and weighed. This solution was dried in an oven at 90 °C for 24 h. This evaporates the water (solvent) leaving only the DL-Asn solid product. Weighing this solid product allows the construction of the solubility line. This solubility measurement was performed at 20, 25, 30, 35, and 40°C and then the solubility curve was constructed. Because the DL-Asn·H₂O is a monohydrate form of the solid product, but the oven drying may remove the crystal water, so there may be a conversion from the monohydrate form in the solid product to the anhydrous form. To check this, we also analyzed the composition in the solid product by using Thermal Gravimetric Analysis (TGA, Mettler Toledo, USA).

2.4.3 Solubility Measurement by Refractive Index Method

This method used a refractometer to find the solubility by determination of the refractive index of saturated solution. The calibration curve between the concentration of L-/DL-Asn·H₂O in water and the refractive index value was constructed as shown in Figure 2.8. The equation of the calibration curves between relative supersaturation and concentration of DL-Asn·H₂O, and L-Asn·H₂O are shown in Equation (2.1), and Equation (2.2) respectively. To investigate the solubility, an excess amount of L-/DL-Asn·H₂O was added in water at a given temperature. The suspension was stirred by a magnetic stirrer. Every 1 h (from 1 h to 5 h) after stirring was begun, the suspension was sampled and filtered through a membrane filter to retain only the liquid solution. The liquid solution was kept at 30°C for 1 h and the refractive index was measured using a refractometer (RFM340 Automatic Digital Refractometer, Bellingham + Stanley, USA) with ± 0.00004 accuracy. This solubility measurement was investigated at 20, 25, 30, 35, and 40°C and then the solubility curve was constructed.

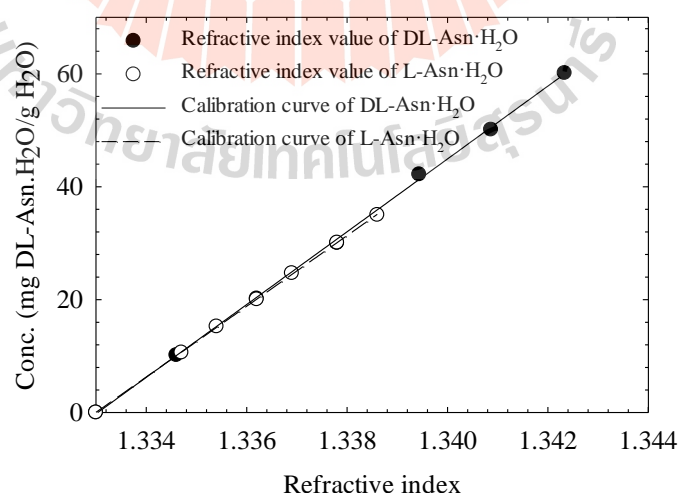


Figure 2.8 The calibration curve between concentration of L-/DL-Asn·H₂O in water and refractive index (RI).

$$C = 6449RI - 8597 \quad (2.1)$$

$$C = 6262RI - 8347 \quad (2.2)$$

where C is concentration of DL-/L-Asn·H₂O (mg/gH₂O) and RI is the refractive index value.

2.4.4 Solubility, Metastable Zone Limit, and Phase Diagram

Measurement by Crystal16

Crystal16 (Technobis, Amsterdam), as shown in Figure 2.9, is equipment to measure solubility, nucleation points, metastable zone limits etc., by detection of turbidity changes in the solution caused by temperature variations. To start the experiment, a known amount of L-/DL-Asn·H₂O was prepared in exactly 1 mL of water in a 1.8 mL vial which was then placed in the Crystal16.

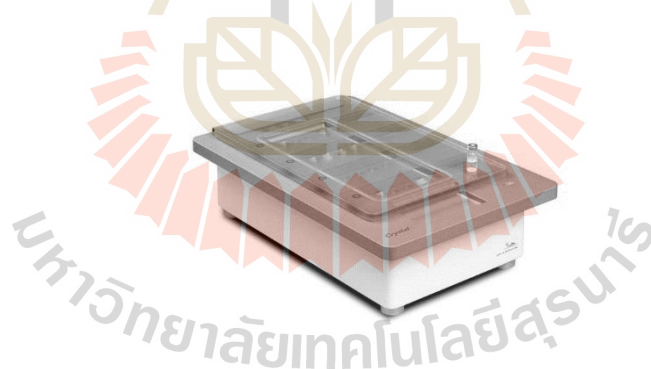


Figure 2.9 Crystal16 equipment.

The Crystal16 was programmed to heat and cool the solution at a particular rate for determination of the solubility and metastable zone limit, as shown in Figure 2.10. The suspension was heated to 60°C to completely dissolve the solute using a heating rate 0.1°C/min. In this heating step, the first time that 100% transmission was reported is the clear point, which determines the solubility point. After

heating to 60°C and holding at this temperature for 1 h, the solution was cooled by using a cooling rate of 0.1°C/min to find the cloud point, which is the metastable zone limit. The process was done for 3 repeating loops to find three clear points and three cloud points. For the clear point temperature, we averaged these data to find the solubility. For the cloud point temperature, the point that nucleation occurs, the data are very scattered. This is because nucleation is a stochastic process. Therefore, we used the highest temperature from the three cloud point data to represent the metastable zone limit.

To study the effect of additives, we studied the effect of D-/L-Asp, D-/L-Glu, D-/L-Leu, and D-/L-Val on the solubility and metastable zone width of D-/L-Asn·H₂O; normally the solubility of D-Asn·H₂O and L-Asn·H₂O must be the same, and also the zone width of the two compounds should also be the same. Thus, the effect of D-amino acid additives to the D-Asn·H₂O must be similar to the effect of L-amino acid additives to L-Asn·H₂O and the effect of L-amino acid additives to the D-Asn·H₂O must be similar to effect of D-amino acid additives to L-Asn·H₂O (because these systems are mirror images). We used additives at 5 mol% compared to the Asn·H₂O used. Moreover, the effect of L-Asp and L-Glu additives to the solubility of DL-Asn·H₂O was also studied.

We also find the phase diagram of Asn·H₂O in water where we vary the mass fraction of D-/L-Asn·H₂O in water by fixing the total amount of Asn·H₂O 0.1 g in 1 g of water. The clear points were measured using the Crystal16.

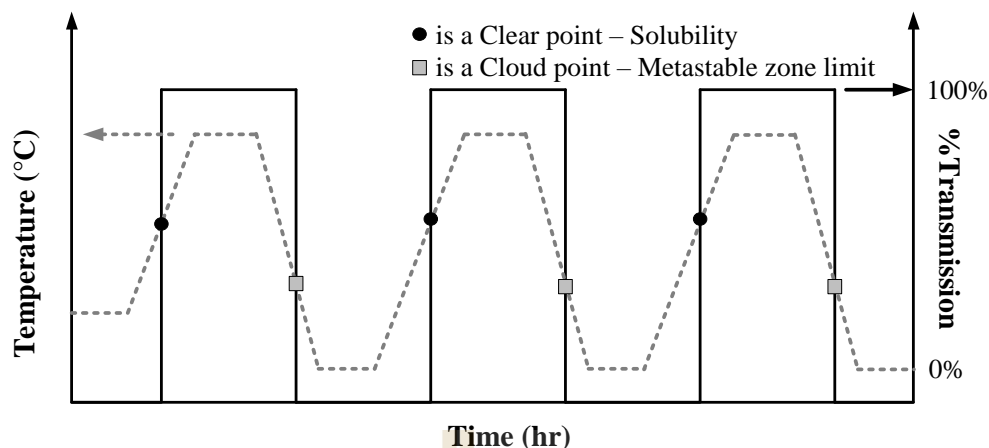


Figure 2.10 Temperature profiles, and clear and cloud points using the Crystal16.

2.5 Results and Discussion

2.5.1 Solubility of L-/DL-Asn·H₂O in Water

The solubility of DL-Asn·H₂O in water was measured by three methods; the gravimetric method, the refractive index method, and using the Crystal16. Results are shown in Figure 2.11. The DL-Asn·H₂O solubility in water using the refractive index method and the Crystal16 are very close.

The solubility of DL-Asn·H₂O found using the gravimetric method is clearly lower than the others because the solid product from the gravimetric method is DL-Asn, not DL-Asn·H₂O. This procedure removes water from the crystal product, so anhydrous DL-Asn forms. To confirm this effect, the solid product was analyzed by TGA to observe the decomposition of the solid at 100°C which is the boiling point of water, as shown in Figure 2.12. Therefore, we recalculated the solubility of DL-Asn·H₂O from the gravimetric method (taking into account the lost water molecule) and the result is also shown in Figure 2.11. The recalculated result shows that the

solubility from the gravimetric method is close to the refractive index method, and slightly different to the solubility of DL-Asn·H₂O found from the Crystal16 equipment.

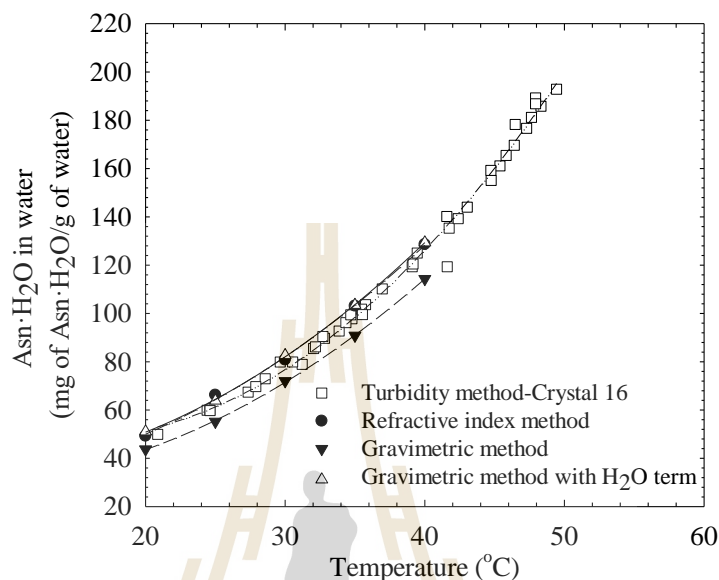


Figure 2.11 The DL-Asn·H₂O solubility in water from Crystal16, refractive index, and gravimetric methods.

The solubility of L-Asn·H₂O in water was also measured by the refractive index method and the Crystal16 equipment; results are shown in Figure 2.13. The solubility of L-/DL-Asn·H₂O in water were fitted with a quadratic equation as shown in Equation (2.3) and Equation (2.4) for L-Asn·H₂O, and DL-Asn·H₂O respectively.

$$C = 0.0538T^2 - 1.6934T + 37.3778 \quad (2.3)$$

$$C = 0.1222T^2 - 3.6113T + 75.2052 \quad (2.4)$$

where C is concentration of L-/DL-Asn·H₂O in water (mg/gH₂O), and T is the saturation temperature (°C)

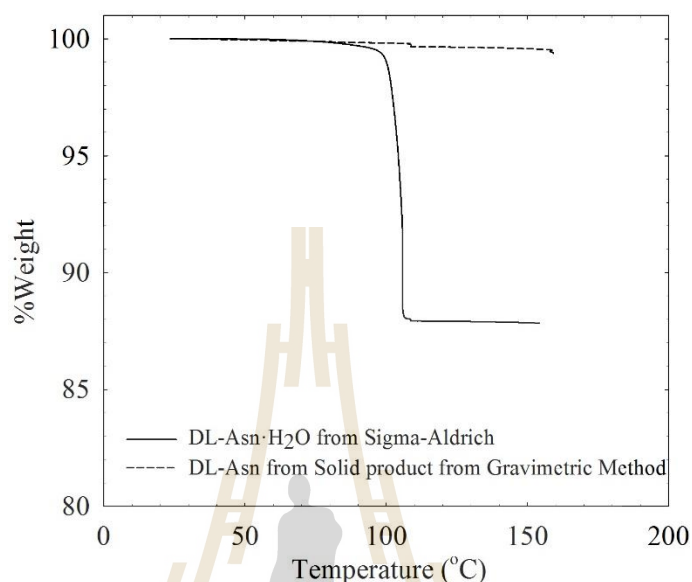


Figure 2.12 The TGA analysis of DL-Asn from the gravimetric method and DL-Asn·H₂O.

The solubility of DL-Asn·H₂O is slightly more than twice the L-Asn·H₂O solubility, and thus, this system only approximately follows the Meyerhoffer solubility rule (Izumi and Blackmond, 2009).

The current data agrees well with the single data point for aqueous systems of Orella and Kirwan (1991), 8.7 mg L-Asn·H₂O/g H₂O at 25°C. However the data for the L-Asn·H₂O is around 4-5% lower than equivalent results of Dalton and Schmidt (1935): however, that study is over 80 years old, and perhaps the purification of the amino acids was more difficult at that point. Solubility data over the entire range of temperatures measured agree very well with the recent data of Binev et al. (2016).

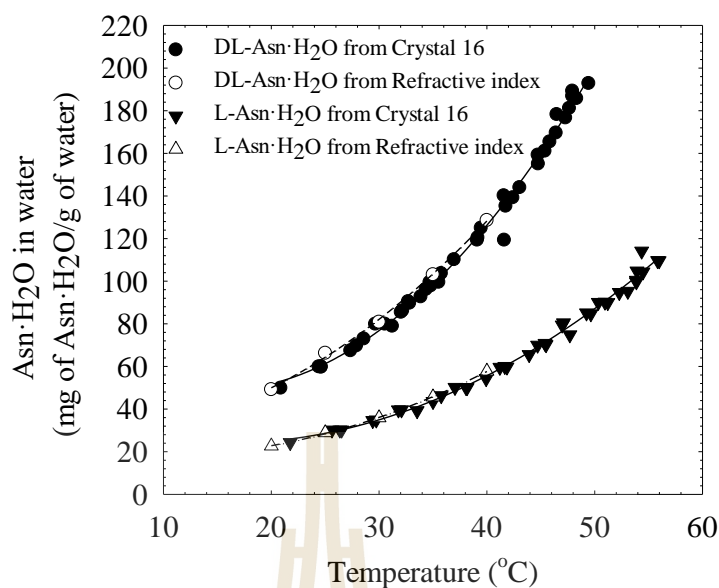


Figure 2.13 Solubility of L-/DL-Asn·H₂O in water from Crystal16 and refractive index method.

2.5.2 Phase Diagrams for Aqueous Solutions of Asparagine

The phase diagram of Asn·H₂O in water is shown in Figure 2.14. The racemic mixture of DL-Asn·H₂O is a conglomerate, where Srisanga and ter Horst (2010) and our experimental data confirm this result. The diagram shows that at a constant total amount of Asn·H₂O solute in water, the saturation temperature of 100% D- or L-Asn·H₂O is higher than the mixture of D-/L-Asn·H₂O. This means the solubility of the racemic mixture is higher than that of pure D-/L-Asn·H₂O.

The ternary solubility phase diagram of Asn·H₂O in water is shown in Figure 2.15. The ternary phase diagram shows that when the temperature is increased the solubility is also increased. The ternary phase diagram can be used as information to predict the yield of product in preferential crystallization which we discuss in Chapter V.

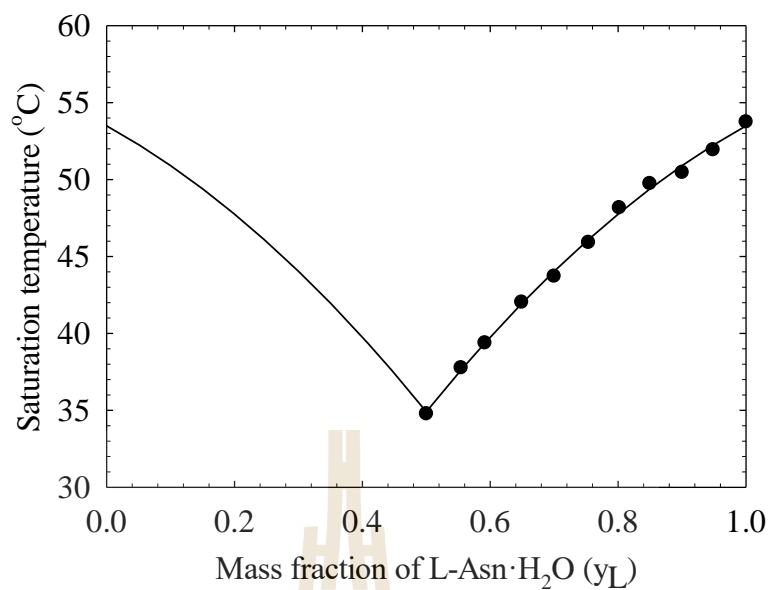


Figure 2.14 Phase diagram of a fixed amount of Asn·H₂O in water.

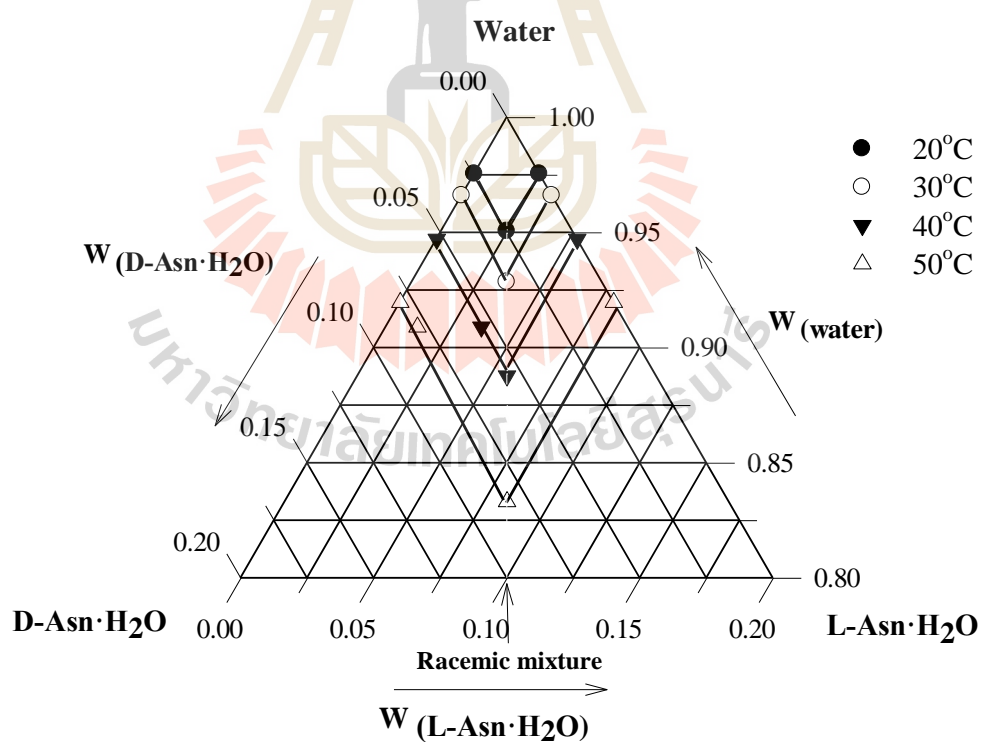


Figure 2.15 Ternary solubility phase diagram of Asn·H₂O in water.

2.5.3 Effect of Additives to Solubility of L-/DL-Asn·H₂O in Water

The solubility of L-Asn·H₂O with L-amino acid additives is the same as the solubility of D-Asn·H₂O with equivalent D-amino acid additives. Also, the solubility of L-Asn·H₂O with D-amino acid additives is the same as the solubility of D-Asn·H₂O with L-amino acid additives (because the systems are mirror images). The effect of the amino acid additives which have the same absolute configuration is studied. The effect of D-Asp to the solubility of D-Asn·H₂O is shown in Figure 2.16; D-Asp increases the solubility of D-Asn·H₂O when compared to the solubility of pure D-Asn·H₂O (or L-Asn·H₂O).

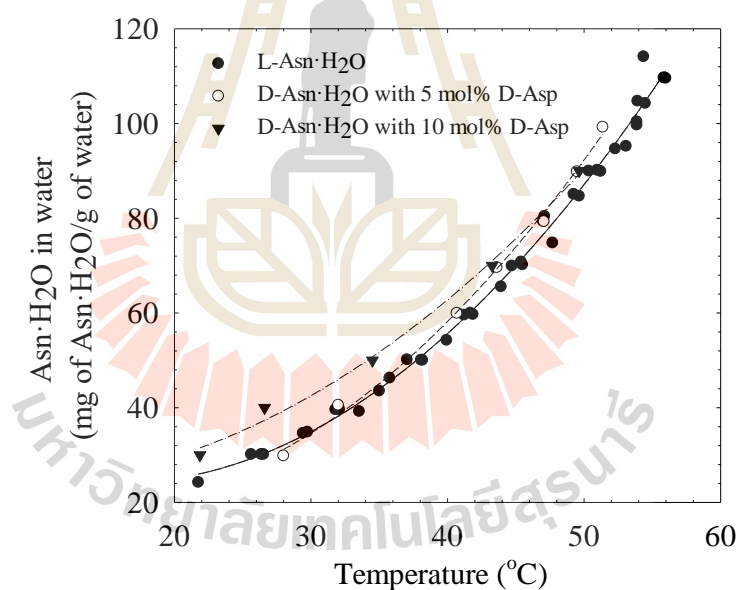


Figure 2.16 The solubility of D-Asn·H₂O in water with D-Asp additives.

The increase of D-Asp additive to 10 mol% also showed an increasing of the solubility. Figure 2.17 shows the effect of D-Asp to L-Asn·H₂O; the solubility of L-Asn·H₂O increases when using D-Asp additives. These results show that the

solubility of D-/L-Asn·H₂O is always increased when using Asp additives although using with same/different absolute configuration. This is because these additives associate with the solute in the solution and did not show any effect of the same absolute configuration to the enantiomer.

The solubility of D-Asn·H₂O with D-Glu additive is shown in Figure 2.18. The solubility of D-Asn·H₂O increases when using the additives, especially for the use of 10 mol% of D-Glu additive compared to the D-Asn·H₂O used. The solubility of L-Asn·H₂O with D-Glu additive is also slightly more than the solubility of L-Asn·H₂O without additives, as shown in Figure 2.19. This also confirms the result that the solubility of L-Asn·H₂O with additives increases because the association of additives and solute in the solution and did not show any effect of the same absolute configuration to the enantiomer.

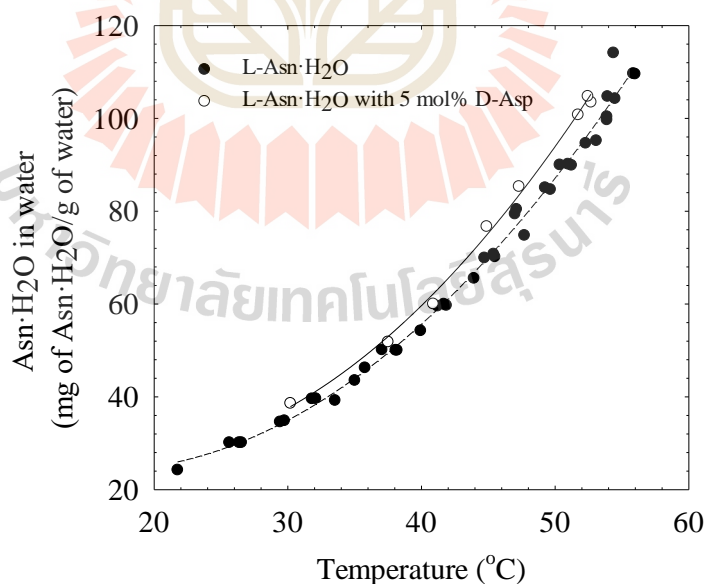


Figure 2.17 The solubility of L-Asn·H₂O in water with D-Asp additives.

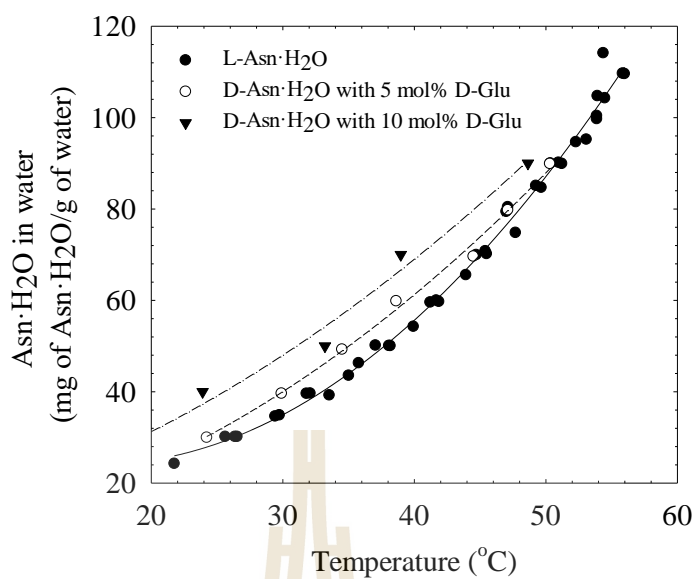


Figure 2.18 The solubility of D-Asn·H₂O in water with D-Glu additives.

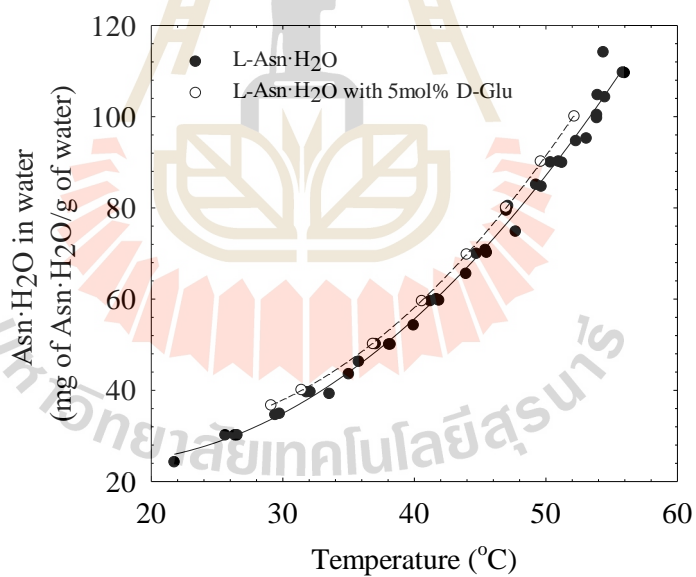


Figure 2.19 The solubility of L-Asn·H₂O in water with D-Glu additives.

The effect of D-Val to D-Asn·H₂O and L-Asn·H₂O are shown in Figure 2.20 and 2.21 respectively. These results show that D-Val has almost no effect on the solubility of D-/L-Asn·H₂O.

The solubility of D-Asn·H₂O and L-Asn·H₂O with D-Leu additive are shown in Figure 2.22 and Figure 2.23 respectively. Both figures show a slightly increase in the solubility when using D-Leu as an additive because the additives associate with the solute in the solution.

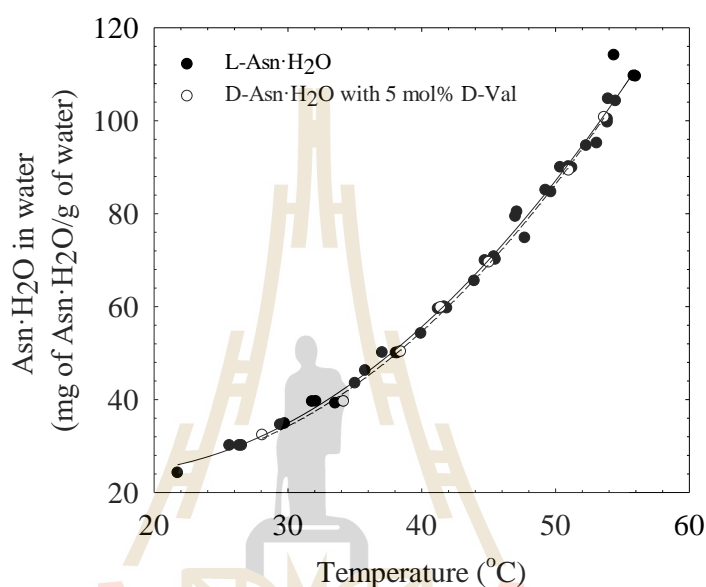


Figure 2.20 The solubility of D-Asn·H₂O in water with D-Val additives.

The effect of additives on L- and D-Asn·H₂O is almost the same for the same chemical although with different enantiomers. Thus, we can also summarize the effect of D-amino acid additives to the solubility of D-Asn·H₂O as shown in Figure 2.24. The solubility of D-/L-Asn·H₂O with additives are higher than without additives because the additives associate with the solute in the solution, so, the solubility is increased. Moreover, we did not see any effect on the solubility for additives that have the same absolute configuration to the enantiomer of Asn·H₂O.

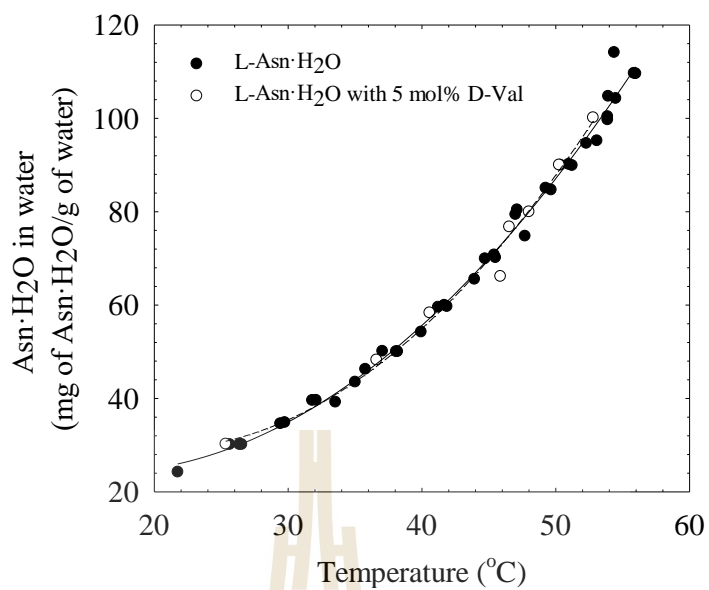


Figure 2.21 The solubility of L-Asn·H₂O in water with D-Val additives.

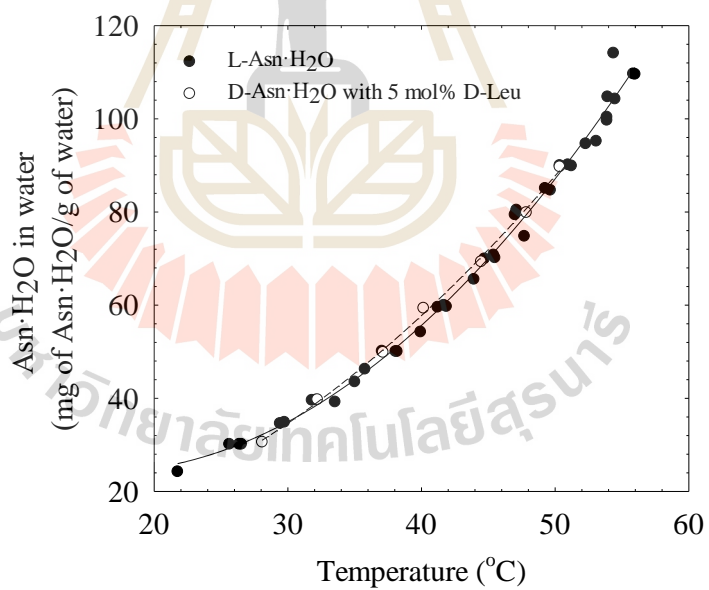


Figure 2.22 The solubility of D-Asn·H₂O in water with D-Leu additives.

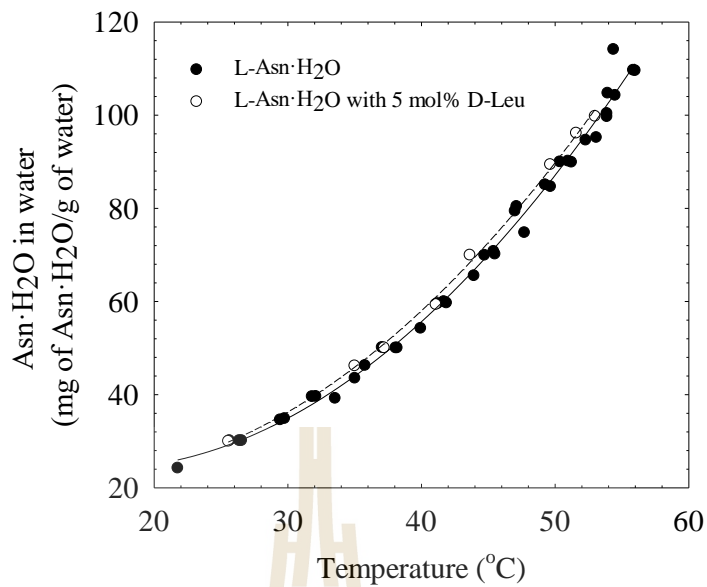


Figure 2.23 The solubility of L-Asn·H₂O in water with D-Leu additives.

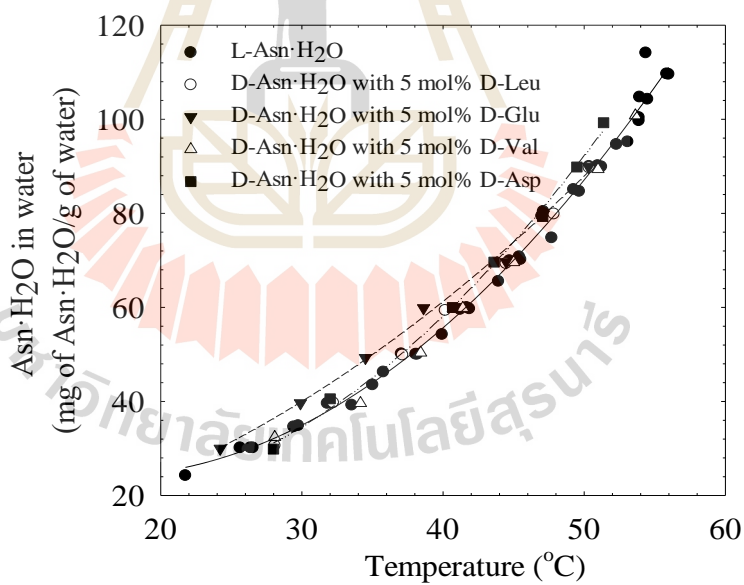


Figure 2.24 The solubility of D-Asn·H₂O in water with D-amino acid additives.

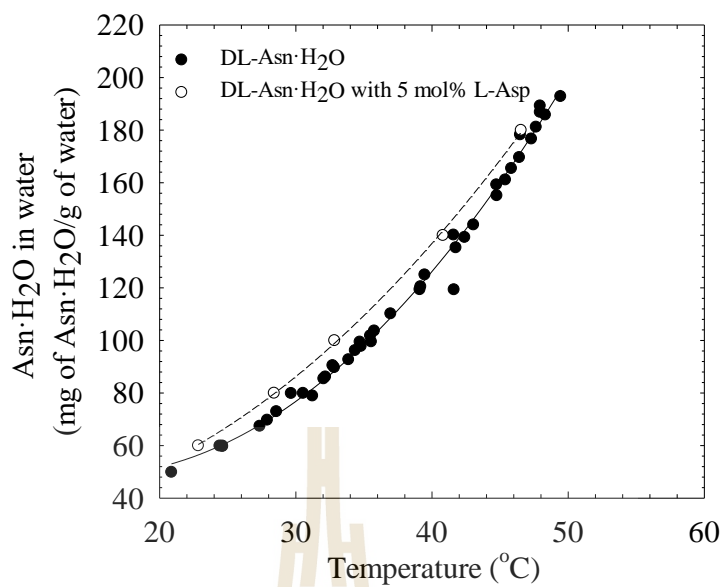


Figure 2.25 The solubility of DL-Asn·H₂O in water with L-Asp additives.

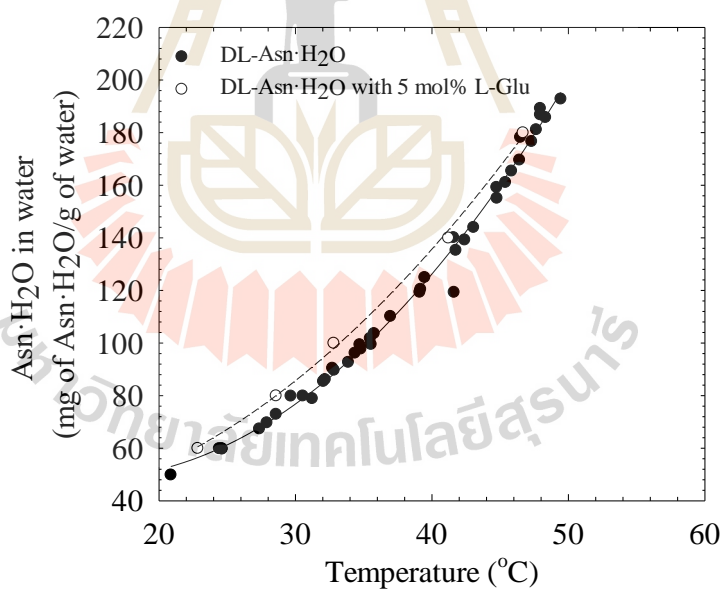


Figure 2.26 The solubility of DL-Asn·H₂O in water with L-Glu additives.

The solubility of DL-Asn·H₂O with L-Asp and L-Glu are also shown in Figure 2.25 and Figure 2.26 respectively. These results show similar trends to the effect of additives on D-Asn·H₂O, which we have discussed previously.

We can summarize the curve fitting of L-/D-/DL-Asn·H₂O with any additives with the quadratic equation shown in Equation (2.5); the fitting parameters are shown in Table 2.2 – 2.3.

$$C = aT^2 + bT + c \quad (2.5)$$

Table 2.2 Fitting parameters of solubility of L-/D-Asn·H₂O without and with different additives by equation (2.5).

Conditions	Additives	Amount of additives	a	b	c
L-Asn·H ₂ O	-	-	0.0538	-1.6934	37.3778
D-Asn·H ₂ O	D-Glu	5%	0.027	0.2379	8.6392
	D-Asp	5%	0.0527	-1.3344	27.2532
	D-Val	5%	0.0566	-1.922	41.0268
	D-Leu	5%	0.0343	-0.0875	6.4383
	D-Glu	10%	0.0213	0.6101	10.5618
	D-Asp	10%	0.0369	-0.5559	26.0572

Table 2.3 Fitting parameters of solubility of L-/DL-Asn·H₂O with different additives by equation (2.5).

Conditions	Additives	Amount of additives	a	b	c
L-Asn·H ₂ O	D-Glu	5%	0.0654	-2.5544	55.6963
	D-Asp	5%	0.061	-2.0642	44.579
	D-Val	5%	0.0664	-2.6903	56.3814
	D-Leu	5%	0.0501	-1.3353	31.2319
DL-Asn·H ₂ O	-	-	0.1222	-3.6113	75.2052
	D-Glu	5%	0.0868	-1.0792	39.9373
	D-Asp	5%	0.085	-0.8861	36.3176

2.5.4 Metastable zone width of L-/DL-Asn·H₂O in Water

The metastable zone widths of L- and DL-Asn·H₂O in water are shown in Figure 2.27, and Figure 2.28 respectively. The metastable zone width depends on the cooling rate of the solution. A higher cooling rate results in a larger metastable zone width. It is necessary to have an accurate metastable zone width in crystallizer design, to be able to control the crystal size and avoid nucleation. Thus, finding the metastable zone should be done at a low cooling rate. The metastable zone widths of L-/DL-Asn·H₂O show that a low cooling rate (0.1°C/min) has a smaller MSZW (in terms of ΔT) than when using a higher cooling rate of 0.3°C/min. The metastable zone widths of DL-Asn·H₂O in water are significantly larger than the results of Binev et al. (2016). However, the metastable zone width is found from the first nuclei occurring; thus, the results are very scattered which is a result of nucleation being a highly stochastic process.

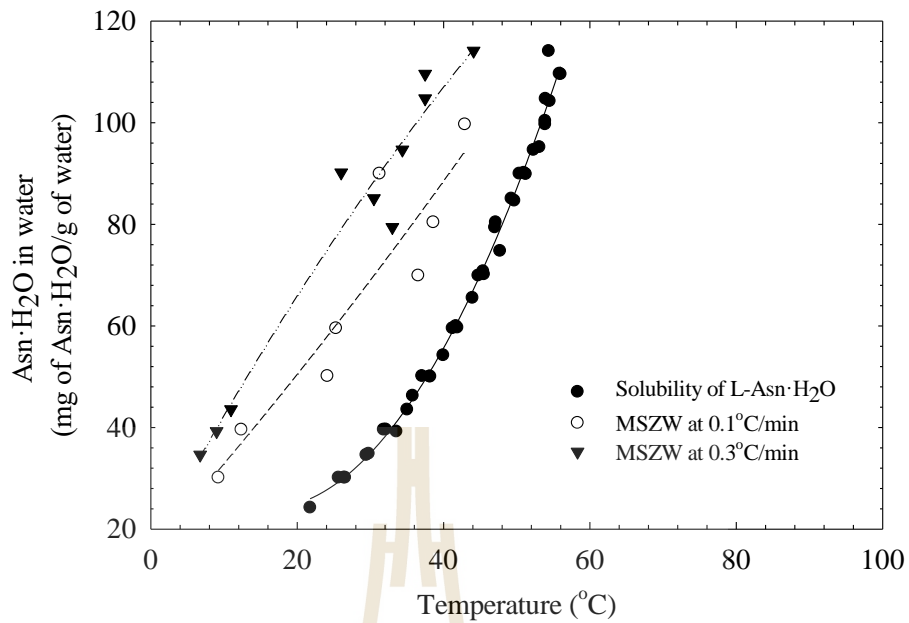


Figure 2.27 The metastable zone width of L-Asn·H₂O in water.

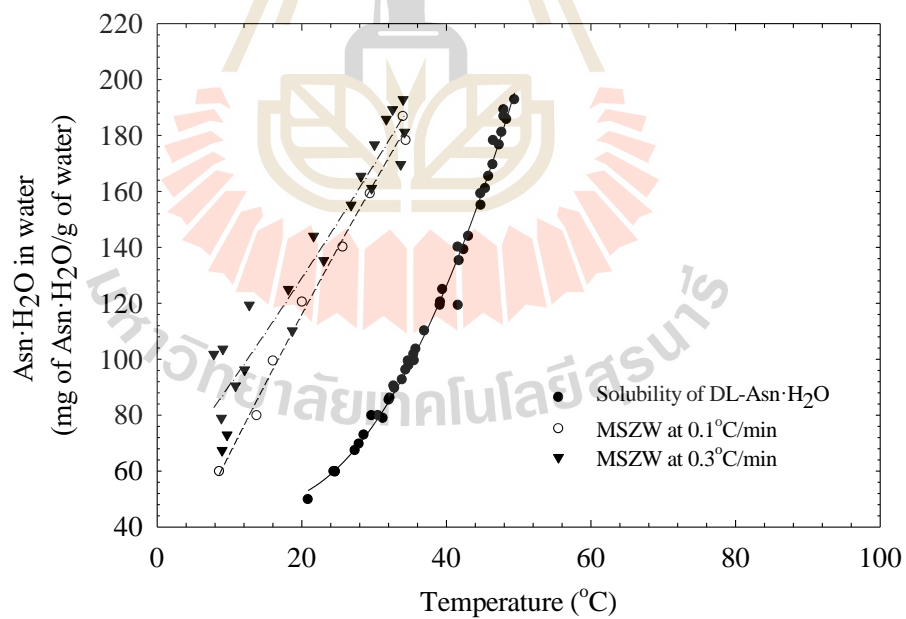


Figure 2.28 The metastable zone width of DL-Asn·H₂O in water.

2.5.5 Effect of Additives to Metastable Zone Width of L-/DL-Asn·H₂O in Water

The metastable zone width of D-Asn·H₂O with D-amino acid additives is shown in Figure 2.29, and the metastable width of L-Asn·H₂O with D-amino acid additives is shown in Figure 2.30. These results show that the metastable zone limits of D-/L-Asn·H₂O with D-amino acid additives are very scattered because the metastable zone relies on nucleation which is a stochastic process. In Chapter IV, we discuss the effect of additives on the nucleation of D-/L-Asn·H₂O which is also related to the metastable zone width as part of the nucleation process.

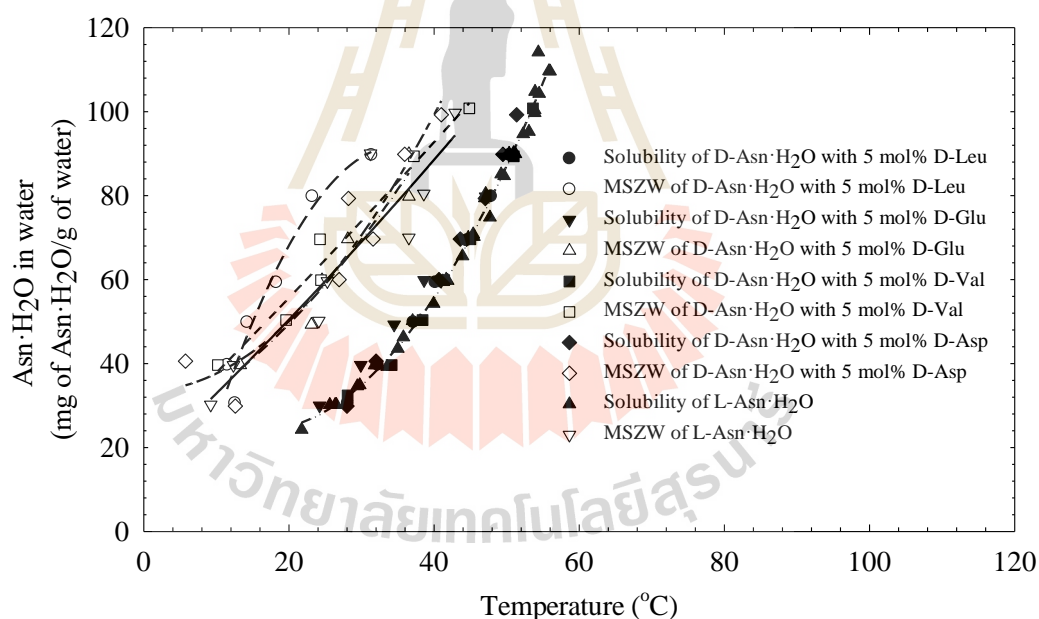


Figure 2.29 The metastable zone width of D-Asn·H₂O in water with D-amino acid additives.

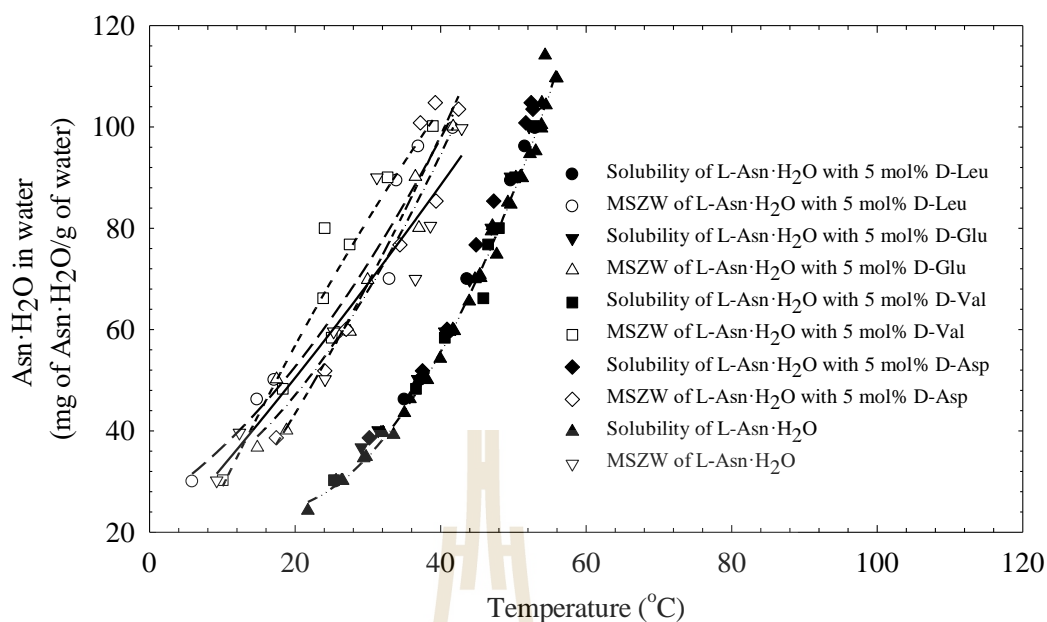


Figure 2.30 The metastable zone width of L-Asn·H₂O in water with D-amino acid additives.

2.6 Conclusions

The solubility can be found from many methods depending on the equipment available and the type of chemical species being investigated. The solubility of DL-Asn·H₂O is almost twice that of either L-Asn·H₂O or D-Asn·H₂O. Asparagine monohydrate is a conglomerate forming system which is easy to separate by preferential crystallization. The solubility of D-/L-Asn·H₂O with additives are higher than without additives because the additives associate with the solute in the solution, so, the solubility is increased. We did not see any effect on the solubility for additives that have the same absolute configuration to the enantiomer of Asn being investigated. The cooling rate has a significant effect on the width of metastable zone. A high cooling rate made the metastable zone wider compared to a low cooling rate. The real process prefers a metastable zone limit for a low cooling rate, which is safer for a real process

to control the crystal size and avoid nucleation. The metastable zone width of D/L-Asn·H₂O when using D-amino acid additives are very scattered because the nucleation event is highly stochastic. These additives have an effect on the metastable zone width of D-/L-Asn·H₂O, although because of the stochastic nature of the event makes the absolute change a little unclear.

2.7 References

- Barrett, P., and Glennon, B. 2002. Characterizing the Metastable Zone Width and Solubility Curve Using Lasentec FBRM and PVM. **Chemical Engineering Research and Design** 80 (7):799-805.
- Binev, D., Seidel-Morgenstern, A., and Lorenz, H. 2016. Continuous Separation of Isomers in Fluidized Bed Crystallizers. **Crystal Growth and Design** 16 (3):1409-1419.
- Buckley, J. S. 1999. Predicting the Onset of Asphaltene Precipitation from Refractive Index Measurements. **Energy & Fuels** 13 (2):328-332.
- Dalton, J. B., and Schmidt, C. L. A. 1935. The solubilities of certain amino acids and related compounds in water, the densities of their solutions at twenty-five degrees, and the calculated heats of solution and partial molal volumes. II. **The Journal of Biological Chemistry** 109:241.
- Dunn, M. S., Ross, F. J., and Read, L. S. 1933. The solubility of the amino acids in water. **The Journal of Biological Chemistry** 103:579-595.
- Elsner, M. P., Ziomek, G., and Seidel-Morgenstern, A. 2009. Efficient separation of enantiomers by preferential crystallization in two coupled vessels. **AIChE Journal** 55 (3):640-649.

- Flood, A. E., and Puagsa, S. 2000. Refractive Index, Viscosity, and Solubility at 30 °C, and Density at 25 °C for the System Fructose + Glucose + Ethanol + Water. **Journal of Chemical & Engineering Data** 45 (5):902-907.
- Herden, A., Mayer, C., Kuch, S., and Lacmann, R. 2001. About the Metastable Zone Width of Primary and Secondary Nucleation. **Chemical Engineering & Technology** 24 (12):1248-1254.
- Huang, C., and Chen, Y. 2000. Measurements and model prediction of the solid–liquid equilibria of organic binary mixtures. **Chemical Engineering Science** 55 (16):3175-3185.
- Hussain, K., Thorsen, G., and Malthe-Sørensen, D. 2001. Nucleation and metastability in crystallization of vanillin and ethyl vanillin. **Chemical Engineering Science** 56 (7):2295-2304.
- Izumi, T., and Blackmond, D. G. 2009. The double solubility rule holds for racemizing enantiomers. **Chemistry** 15 (13):3065-3068.
- Kadam, S. S., Kulkarni, S. A., Coloma Ribera, R., Stankiewicz, A. I., ter Horst, J. H., and Kramer, H. J. M. 2012. A new view on the metastable zone width during cooling crystallization. **Chemical Engineering Science** 72:10-19.
- Kobari, M., Kubota, N., and Hirasawa, I. 2013. Deducing primary nucleation parameters from metastable zone width and induction time data determined with simulation. **CrystEngComm** 15 (6):1199-1209.
- Kulkarni, S. A., Kadam, S. S., Meekes, H., Stankiewicz, A. I., and ter Horst, J. H. 2013. Crystal Nucleation Kinetics from Induction Times and Metastable Zone Widths. **Crystal Growth and Design** 13 (6):2435-2440.

- Lawson, D. D., and Ingham, J. D. 1969. Estimation of Solubility Parameters from Refractive Index Data. **Nature** 223 (5206):614-615.
- Lorenz, H., Sapoundjiev, D., and Seidel-Morgenstern, A. 2002. Enantiomeric Mandelic Acid Systems Melting Point Phase Diagram. **Journal of Chemical and Engineering Data** 47:1280-1284.
- Lorenz, H., Sapoundjiev, D., and Seidel-Morgenstern, A. 2003. Solubility Equilibria in Chiral Systems and Their Importance for Enantioseparation. **Engineering in Life Sciences** 3 (3):132-136.
- Lorenz, H., and Seidel-Morgenstern, A. 2002. Binary and ternary phase diagrams of two enantiomers in solvent systems. **Thermochimica Acta** 382 (1–2):129-142.
- Maosoongnern, S., Diaz Borbon, V., Flood, A. E., and Ulrich, J. 2012. Introducing a Fast Method to Determine the Solubility and Metastable Zone Width for Proteins: Case Study Lysozyme. **Industrial & Engineering Chemistry Research** 51 (46):15251-15257.
- Mersmann, A., and Bartosch, K. 1998. How to predict the metastable zone width. **Journal of Crystal Growth** 183 (1):240-250.
- Mohan, R., Lorenz, H., and Myerson, A. S. 2002. Solubility Measurement Using Differential Scanning Calorimetry. **Industrial & Engineering Chemistry Research** 41 (19):4854-4862.
- Mullin, J. W. 2001. **Crystallization**. 4th edition ed. Oxford: Butterworth-Heinemann.
- Myerson, A. S. 2002. **Handbook of Industrial Crystallization**. Second Edition ed. Woburn: Butterworth-Heinemann.

- Myerson, A. S., Decker, S. E., and Fan, W. 1986. Solvent selection and batch crystallization. **Industrial & Engineering Chemistry Process Design and Development** 25 (4):925-929.
- Nozaki, Y., and Tanford, C. 1963. The solubility of amino acids and related compounds in aqueous urea solutions. **The Journal of Biological Chemistry** 238 (2):9.
- Nývlt, J. 1983. Induction period of nucleation and metastable zone width. **Collection of Czechoslovak Chemical Communications** 48 (7):1977-1983.
- O'Grady, D., Barrett, M., Casey, E., and Glennon, B. 2007. The Effect of Mixing on the Metastable Zone Width and Nucleation Kinetics in the Anti-Solvent Crystallization of Benzoic Acid. **Chemical Engineering Research and Design** 85 (7):945-952.
- Orella, C. J., and Kirwan, D. J. 1991. Correlation of amino acid solubilities in aqueous aliphatic alcohol solutions. **Industrial & Engineering Chemistry Research** 30 (5):1040-1045.
- Randolph, A. D., and Larson, M. A. 1988. **Population Balances: Theory of Particulate Processes**. San Diego: Academic Press.
- Reus, M. A., van der Heijden, A. E. D. M., and ter Horst, J. H. 2015. Solubility Determination from Clear Points upon Solvent Addition. **Organic Process Research & Development** 19 (8):1004-1011.
- Sapoundjiev, D., Lorenz, H., and Seidel-Morgenstern, A. 2006. Solubility of Chiral Threonine Species in Water/Ethanol Mixtures. **Journal of Chemical and Engineering Data** 51:1562-1566.

- Shibuya, H., Suzuki, Y., Yamaguchi, K., Arai, K., and Saito, S. 1993. Measurement and prediction of solid-liquid phase equilibria of organic compound mixtures. **Fluid Phase Equilibria** 82:397-405.
- Srisanga, S., and ter Horst, J. H. 2010. Racemic Compound, Conglomerate, or Solid Solution: Phase Diagram Screening of Chiral Compounds. **Crystal Growth and Design** 10 (4):1808-1812.
- ter Horst, J. H., Deij, M. A., and Cains, P. W. 2009. Discovering New Co-Crystals. **Crystal Growth & Design** 9 (3):1531-1537.
- Titiz-Sargut, S., and Ulrich, J. 2002. Influence of Additives on the Width of the Metastable Zone. **Crystal Growth and Design** 2 (5):371-374.
- Ulrich, J., and Strege, C. 2002. Some aspects of the importance of metastable zone width and nucleation in industrial crystallizers. **Journal of Crystal Growth** 237–239, Part 3:2130-2135.
- Wang, L., Feng, H., Peng, J., Dong, N., Li, W., and Dong, Y. 2015. Solubility, Metastable Zone Width, and Nucleation Kinetics of Sodium Dichromate Dihydrate. **Journal of Chemical & Engineering Data** 60 (1):185-191.
- Wang, X., Wang, X. J., and Ching, C. B. 2002. Solubility, metastable zone width, and racemic characterization of propranolol hydrochloride. **Chirality** 14 (4):318-324.
- Wingefors, S., and Liljenzin, J.-O. 1981. Development of a correlation between the non-polar solubility parameter, refractive index and molecular structure. I. Aliphatic hydrocarbons. **Journal of Chemical Technology and Biotechnology** 31 (1):115-121.

Zhou, K., Yan, Y., An, L., Xiang, D., and Wang, H. 2016. Solubility, Density, and Metastable Zone Width of Pyridoxine Hydrochloride in Water and Ethanol Solvent Mixtures. **Journal of Chemical & Engineering Data** 61 (1):307-312.



CHAPTER III

EFFECT OF ADDITIVES ON THE CRYSTAL GROWTH RATE OF L-ASPARAGINE MONOHYDRATE

3.1 Abstract

Crystal growth is an essential mechanism in crystallization processes. This Chapter investigates the crystal growth rate of L-asparagine monohydrate (L-Asn·H₂O) in L-Asn·H₂O and DL-Asn·H₂O solutions containing additives. The experiments were performed in a small cell crystallizer. The crystal growth rate of L-Asn·H₂O in supersaturated solutions of L-Asn·H₂O and DL-Asn·H₂O was investigated at the supersaturation ratios (S) of 1.05, 1.10, and 1.15 respectively. The crystal growth rate of L-Asn·H₂O increases when the supersaturation ratio increases for growth in both L-Asn·H₂O and DL-Asn·H₂O solution. However, the crystal growth rate of L-Asn·H₂O in DL-Asn·H₂O solution is slower than in pure L-Asn·H₂O solution. Eight types of amino acid enantiomers were used as additives to change the crystallization process, particularly for the crystal growth rate of L-Asn·H₂O in this chapter. The additives used were D- and L-aspartic acid (Asp), D- and L-glutamic acid (Glu), D- and L-leucine (Leu), and D- and L-valine (Val). Additives were used at a concentration of 3 mol% (relative to the amount of DL-Asn·H₂O) in DL-Asn·H₂O supersaturated solutions. The additives have no significant effect on the shape of the L-Asn·H₂O seed crystals, partly because the experiment time of 80 min is too short to see a significant change in the shape of the relatively large seed crystals. However, the additives have an effect to the

crystal growth rate of L-Asn·H₂O. D-Leu and L-Val appear to slightly promote the crystal growth rate of L-Asn·H₂O, while D-/L-Asp, and D-/L-Glu decrease the crystal growth rate of L-Asn·H₂O in DL-Asn·H₂O solution. Moreover, L-Asp and L-Glu significantly decrease the crystal growth rate of L-Asn·H₂O in DL-Asn·H₂O solution, in agreement with the rule of reversal.

3.2 Introduction

The spontaneous nucleation of the counter enantiomer is the main problem in the preferential crystallization process (Jacques et al., 1981; Matsuoka, 1997; Profir and Matsuoka, 2000; Beilles et al., 2001; Angelov et al., 2008; Czapla et al., 2009; Elsner et al., 2009; Kongsamai et al., 2017). Therefore, the prolongation of the crystallization time of the pure preferred enantiomer is an interesting research topic. This research uses tailor-made additives to inhibit the nucleation and growth of the counter enantiomer. The research group in Weizmann Institute of Science, Israel, proposed the rule of reversal (Addadi et al., 1981a; Van Mil et al., 1981; Addadi et al., 1981b; Addadi et al., 1982b; Addadi et al., 1985; Weissbuch et al., 1986; Lahav and Leiserowitz, 1993; Weissbuch et al., 1995; Meir and Leslie, 2015). This rule predicts the inhibition of an enantiomer solute by an enantiomer of a similar species, which is the same absolute configuration as the solute, as shown in the scheme in Figure 3.1. Normally, the crystallization rate of the D-enantiomer and the L-enantiomer in a solution that is a racemic mixture are the same, as shown by $k_D = k_L$, where k_D is the crystallization rate constant of the D-enantiomer and k_L is the crystallization rate constant of the L-enantiomer. If a tailor-made additive is dissolved in this racemic mixture, i.e. the

L'-enantiomer (of a related species), it will inhibit the crystallization rate of the L-enantiomer. Thus, k_L is lower than k_D .

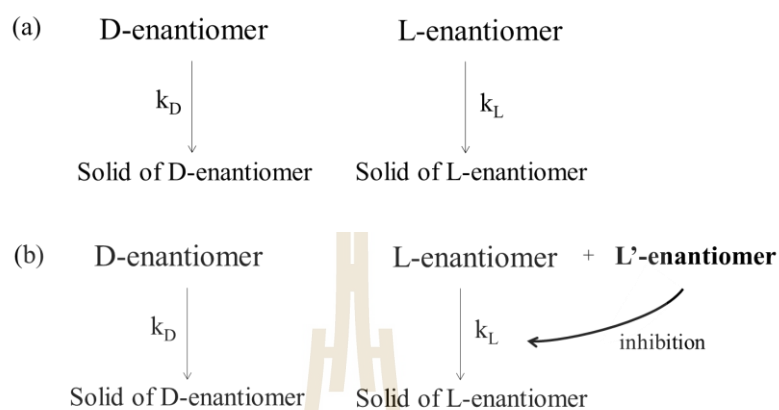


Figure 3.1 The rule of reversal (a) crystallization of racemic mixture and (b) crystallization of racemic mixture with L'-enantiomer additives (adapted from Addadi et al. (1981b)).

Addadi et al. (1982a) proposed that the morphology of an enantiomer changes due to the use of tailor-made additives, as shown in Figure 3.2. The selective adsorption of the additive onto the faces of the crystal makes the crystal shape change. However, the solid crystal is still a pure enantiomer. However, this shape change is only clearly visible after the crystal is exposed to the additive for 1-2 days. This means that the shape does not change significantly if the growth time is small.

In this chapter, we studied the crystal growth rate of L-Asn·H₂O in pure L-Asn·H₂O and DL-Asn·H₂O solutions by varying the initial supersaturation level. The effect of amino acid additives to the crystal growth rate of L-Asn·H₂O in DL-Asn·H₂O supersaturation is investigated. The experiment was conducted in a small cell stagnant crystallizer to prevent the secondary nucleation, and it can be assumed that the

concentration of the solution does not change significantly since the surface area of seed crystal is very small in comparison to the amount of solute in the solution phase.

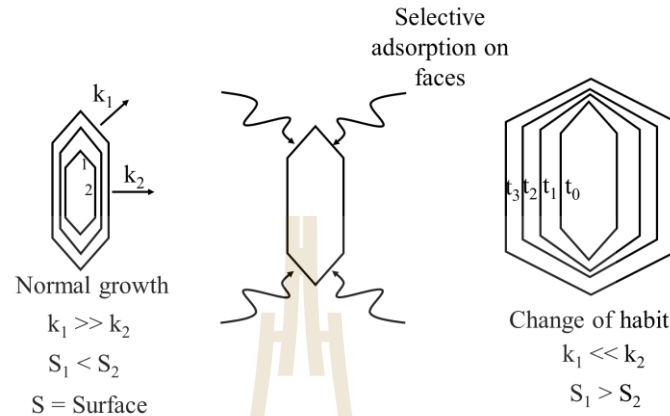


Figure 3.2 The Schematic of selective inhibition of a crystal by tailor-made additives (adapted from Addadi et al. (1982a)).

3.3 Theory

3.3.1 Meaning of Crystal Growth

Crystal growth is one of the mechanisms that has a significant effect on the particle size distribution in the crystallizers. The conditions and rate of crystal growth are also significant to product purity and crystal habit (Myerson, 2002). There are many descriptions of crystal growth but it is normally described by the rate of change in some dimension of the crystal with respect to time. It is usual to define the crystal growth rate via Equation (3.1)

$$G = \frac{dL}{dt} \quad (3.1)$$

where G is crystal growth rate (m/s), L is the characteristic dimension that is increasing (m), and t is the growth time (s). We can also define the crystal growth rate through the measurement of the rate of mass change of the crystal, as shown in equation (3.2) from Myerson (2002).

$$R_G = \frac{1}{A} \frac{dm}{dt} = 3 \frac{k_v}{k_a} \rho G = 3 \frac{k_v}{k_a} \rho \frac{dL}{dt} \quad (3.2)$$

where R_G is the increase of mass ($\text{kg}/\text{m}^2 \cdot \text{s}$), m is the crystal mass (kg), A is the surface area of crystal (m^2), k_v is the volume shape factor (-), k_a is the area shape factor (-), and ρ is the density of the crystal (kg/m^3) (Wantha, 2011).

3.3.2 Crystal Growth Model

In 1927, Kossel proposed that crystals grow in a layer by layer fashion as shown in Figure 3.3. There are three sites where molecules can be attached on the crystal surface. At site A, the molecule is attached at only one site, at site B, the molecule is attached onto two sites, and at site C, the molecule is attached to three sites, and this is usually called a kink site (Myerson, 2002). The molecules normally adsorb on the location where there are the maximum number of nearest neighbors. However, this theory still cannot describe what is the rate controlling factor in the crystal growth rate.

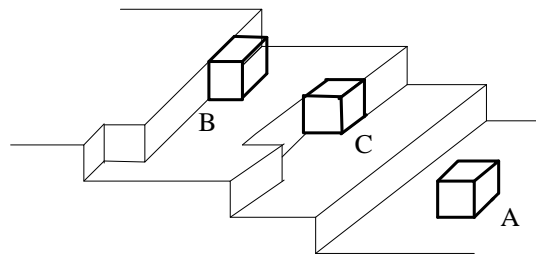


Figure 3.3 The three possible sites for molecules adsorb on crystal surface (adapted from Myerson (2002)).

Several two-dimensional growth rate theories have been proposed. The growth rate in these models occurs from molecules continually adsorbing on the surface of the crystal, and diffusing and colliding with each other to form two-dimensional aggregates as shown in Figure 3.4; this model is known as the mononuclear model. They assume that the surface nuclei spreads across the surface at an infinite velocity, so that a single nucleus is enough to create a layer. However, the collision and spread of molecules may not be able to form a complete layer before another surface nuclei forms. Therefore the polynuclear model was proposed, where the nucleus does not spread but the layer is formed by the formation of sufficient nuclei to cover the layer (Myerson, 2002).

Based on the mononuclear model and polynuclear model, the birth and spread model has been proposed. This model assumes that the spreading of nuclei at a finite rate, and that nuclei can form at any location including incomplete layers, and that there is no intergrowth between the nuclei. This model can predict that the growth rate increases with the supersaturation and temperature increase, but is independent of crystal size. However, the mononuclear, polynuclear and birth and spread models are

rarely used because the growth rate is not a simple function with temperature and must use some semi-empirical relation to obtain a relationship as show in equation (3.3).

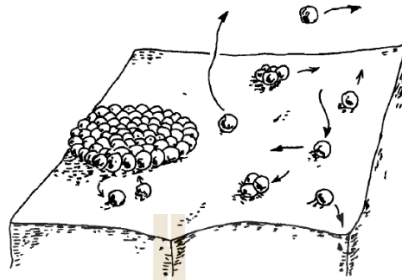


Figure 3.4 Formation of two-dimensional critical nucleus on a crystal surface in mononuclear model (Myerson, 2002).

$$G = C_1(S - I)^{2/3} [\ln(S)]^{1/6} \exp\left[\frac{-C_2}{T^2 \ln(S)}\right] \quad (3.3)$$

where G is crystal growth rate (m/s), S is supersaturation ratio, C_1 and C_2 are the empirical parameters obtained from experimental data.

Burton-Cabrera-Frank (BCF) proposed that screw dislocations can provide a way of propagating steps for growth, and thus the surface becomes a spiral staircase as shown in Figure 3.5. The BCF model can provide the growth rate equation via equation (3.4).

$$G = K_1 T (S - I) \ln(S) \tanh\left[\frac{K_2}{T \ln(S)}\right] \quad (3.4)$$

where K_1 and K_2 are system constants.

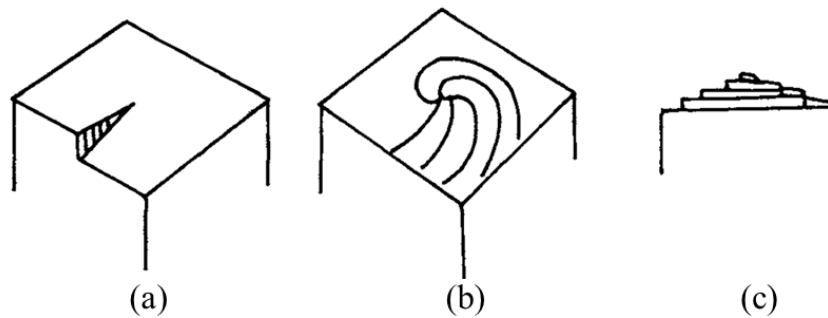


Figure 3.5 Development of a growth spiral from a screw dislocation (Myerson, 2002)

Chernov (1961) proposed the Chernov bulk diffusion model which is a model that can link the crystal growth theory and industrial crystallization. This model considered bulk diffusion as the limiting step of crystal growth. The concentration of solute in solution decreases at the crystal-liquid interface as it becomes part of the crystal.

We can combine the bulk diffusion model and the surface diffusion (or surface integration) model to predict an overall growth rate mechanism. A schematic diagram of the solute concentration in crystal growth model is shown in Figure 3.6. In the range of bulk diffusion, the rate of mass increase of crystal can be provided by Equation (3.5). The surface integration is given by Equation (3.7).

$$\frac{dm}{dt} = k_d A \frac{dC}{dx} = k_d A (C - C_i) \quad (3.5)$$

where
$$k_d = \frac{D}{\delta} \quad (3.6)$$

Therefore,
$$\frac{dm}{dt} = k_i A (C_i - C^*)^i \quad (3.7)$$

where m is crystal mass, t is time, A is surface area of the crystal, C is bulk concentration, C_i is interfacial concentration, C^* is equilibrium concentration, k_d is a coefficient of bulk mass transfer, D is the diffusion coefficient, δ is the stagnant film or boundary layer thickness, k_i is the rate constant of the surface integration process and i is a parameter between 1 and 2.

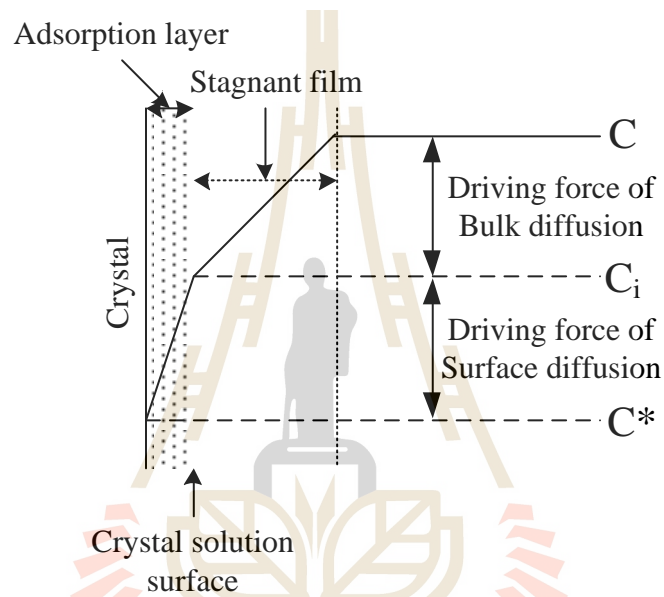


Figure 3.6 Concentration driving force in crystallization from solution
(adapted from Mullin (2001)).

From the bulk diffusion and surface integration equations, the overall growth rate equation can be modelled as Equation (3.8).

$$\frac{dm}{dt} = K_G A (C - C^*)^n \quad (3.8)$$

where

$$\frac{1}{K_G} = \frac{1}{k_d} + \frac{1}{k_i} \quad (3.9)$$

From Equation (3.8) and (3.9), if $k_d \ll k_i$, the bulk diffusion is the limiting step but if $k_i \ll k_d$, the surface integration is the limiting step for crystal growth.

3.3.3 Crystal Growth Kinetics

There are many theories that can predict the crystal growth rate, but they are still difficult to use in real industrial crystallizers. To overcome this issue, the power law model is used to empirically correlate the growth rate with the supersaturation (Mullin, 2001; Myerson, 2002) as shown in Equation (3.10).

$$G = k_g \sigma^n \quad (3.10)$$

where G is the crystal growth rate, k_g is the growth rate constant, σ is relative supersaturation, and n is the growth rate order. If $n=1$ the mass transfer from bulk phase controls the crystal growth rate, and if $1 < n < 2$ surface integration at least partially controls crystal growth rate. (Randolph and Larson, 1988; Flood, 2009).

Moreover, the crystal growth rate is temperature dependent as shown in Equation (3.11) which is an Arrhenius relationship (Myerson, 2002).

$$k_g = A \exp\left(-\frac{E_G}{RT}\right) \quad (3.11)$$

where A is a constant, R is the ideal gas constant, E_G is activation energy, and T is the crystal growth temperature.

3.4 Materials and Methods

3.4.1 Materials

DL-asparagine monohydrate (DL-Asn·H₂O, 99+ wt%), L-asparagine monohydrate (L-Asn·H₂O, 99+ wt%) and D-asparagine monohydrate (D-Asn·H₂O, 99+ wt%), were purchased from Sigma-Aldrich. D-aspartic acid (D-Asp, 99+wt%), D-glutamic acid (D-Glu, 99+wt%), D-valine (D-Val, 98+wt%), D-leucine (D-Leu, 99 wt%), L-aspartic acid (L-Asp, 98+wt%), L-glutamic acid (L-Glu, 99+wt%), L-valine (L-Val, 98+wt%), and L-leucine (L-Leu, 99 wt%) were purchased from ACROS. These reagents were used without further purification. Deionized water was used as the solvent.

3.4.2 Single Crystal Growth Rate of L-Asn·H₂O in Supersaturated Solution of L- and DL-Asn·H₂O

The solution phase, a supersaturated solution of L-Asn·H₂O was prepared in water in a Schott bottle. The solution was heated to 58 °C to completely dissolve the solute. After heating the solution for 20 min, the solution was rapidly cooled down to 30°C, which was the crystal growth temperature. Nine L-Asn·H₂O crystals, as shown in Figure 3.7, with approximate aspect ratios of L: W: T of 1: 0.47: 0.35, were attached onto a cover glass by glue and placed in a 50 cm³ small cell which was temperature-controlled using a jacket on the cell. The jacket used water from a constant temperature bath as shown in Figure 3.8. The crystal growth of L-Asn·H₂O was started by adding the supersaturated solution of L-Asn·H₂O into the small cell. The size of the crystal was measured every 10 min until 80 min using a microscope connected to a camera to capture the pictures of the crystal using the DinoCapture 2.0 software as shown in Figure 3.9. The crystal growth rate of L-Asn·H₂O was

investigated in L-Asn·H₂O and DL-Asn·H₂O at supersaturation ratios (S) of 1.05, 1.10, and 1.15 at 30°C. The effect of additives was also studied using 3 mol% of additives in DL-Asn·H₂O, S=1.10, at 30°C

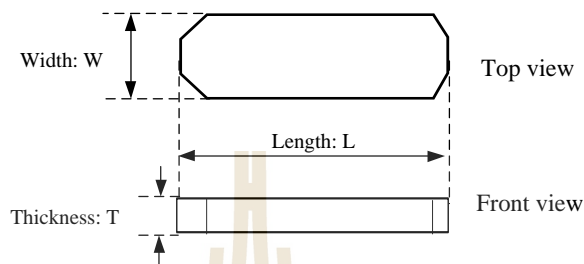


Figure 3.7 Crystal shape of L-Asn·H₂O.

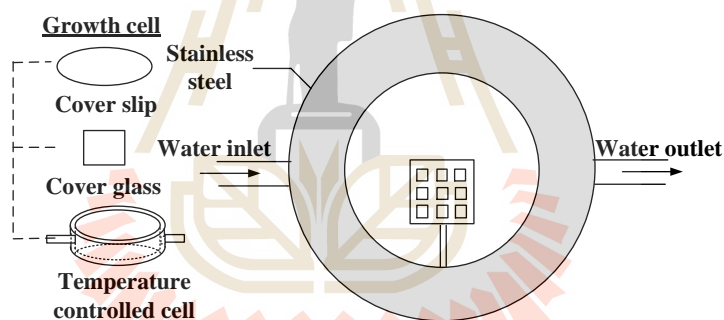


Figure 3.8 Growth cell equipment.

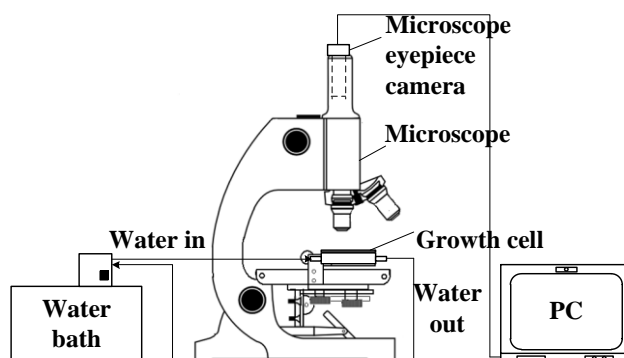


Figure 3.9 Experimental set up.

3.5 Results and Discussion

3.5.1 Single Crystal Growth Rate of L-Asn·H₂O in Supersaturated Solution of L- and DL-Asn·H₂O

The L-Asn·H₂O crystal in the supersaturated solution of L-/DL-Asn·H₂O was captured and measured by the DinoCapture 2.0 software. The crystals of L-Asn·H₂O in the supersaturated solution of L-Asn·H₂O and DL-Asn·H₂O are shown in Figure 3.10 and Figure 3.11, respectively. We used the length of the principal axis of the crystal to find the crystal growth rate. This can be converted to any other measure of growth rate by considering the exact shape of the crystals, which are quite consistent in these experiments.

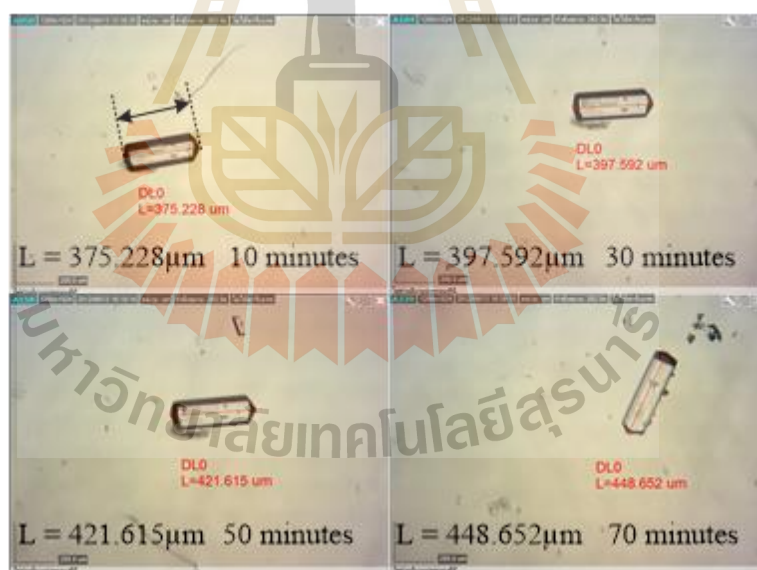


Figure 3.10 Crystal shape of L-Asn·H₂O in L-Asn·H₂O solution ($S = 1.10$).

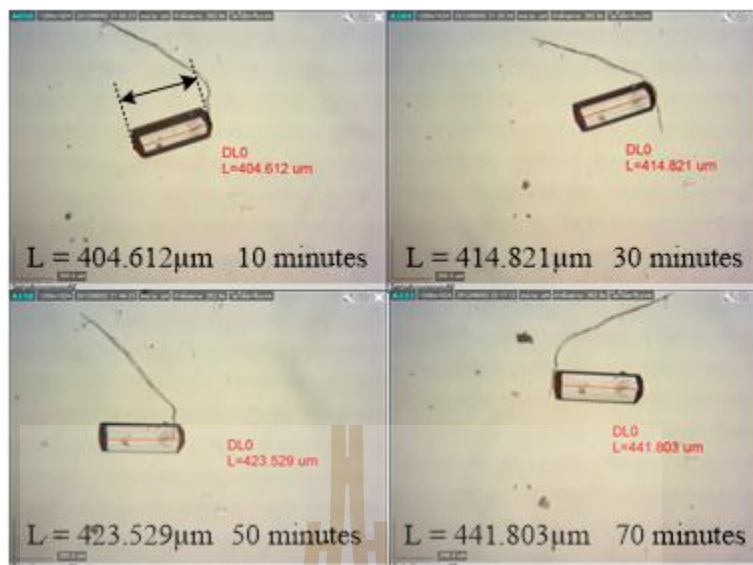


Figure 3.11 Crystal shape of L-Asn·H₂O in DL-Asn·H₂O solution (S = 1.10).

The relationship between the crystal size of L-Asn·H₂O crystal and time in the supersaturated solution of L-Asn·H₂O and DL-Asn·H₂O solution at S=1.10 is plotted in Figure 3.12 and Figure 3.13 respectively. These graphs show that when time increased the crystal size increases as a linear relationship. The crystal growth rate can be found from the slope of the graph.

The crystal growth rate of L-Asn·H₂O crystals are shown in Table 3.1 and Table 3.2 for the crystal growth in L-Asn·H₂O and DL-Asn·H₂O respectively. These results can be classified into crystal growth rate ranges, as shown in Table 3.3.

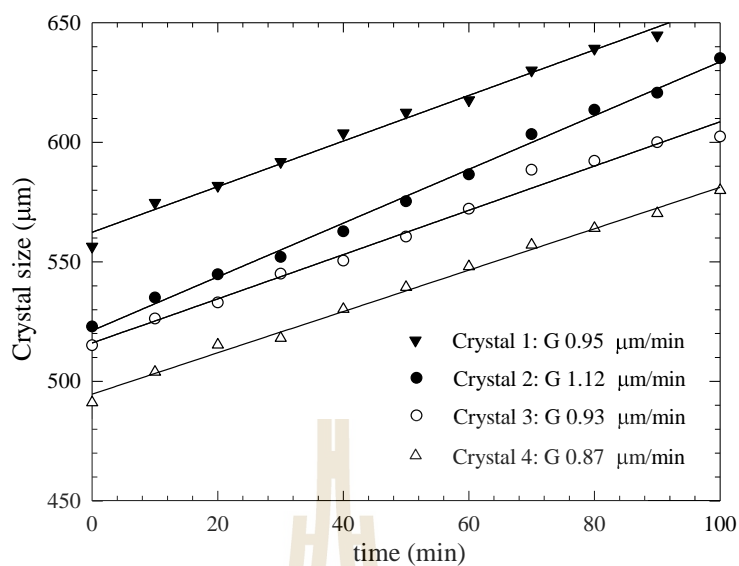


Figure 3.12 Relationship between crystal size (length) of L-Asn·H₂O and time in solution ($S = 1.10$) of L-Asn·H₂O at 30°C.

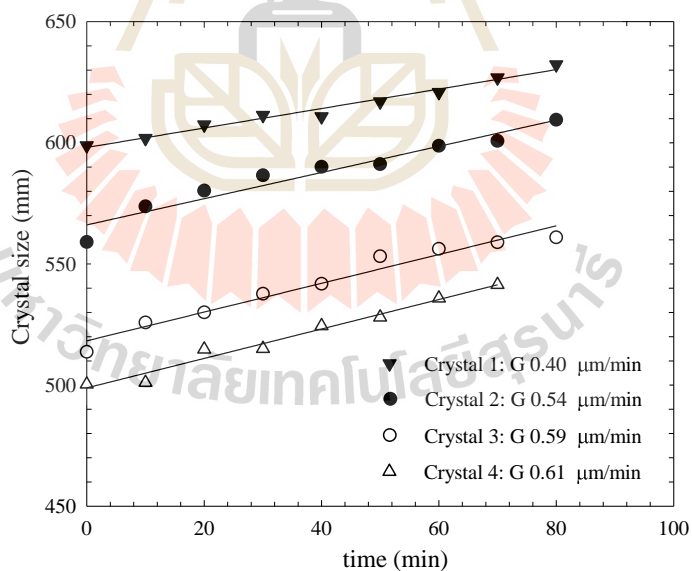


Figure 3.13 Relationship between crystal size (length) of L-Asn·H₂O and time in solution ($S = 1.10$) of DL-Asn·H₂O at 30°C

Table 3.1 Measurements of the individual crystal growth rate of L-Asn·H₂O in L-Asn·H₂O supersaturation (S=1.10) at 30°C.

Sorted crystal growth rate of L-Asn·H ₂ O in L-Asn·H ₂ O saturated solution (μm/min)					
0.7333	0.8654	0.9255	0.9601	1.0060	1.0741
0.7554	0.8678	0.9301	0.9618	1.0171	1.0907
0.7606	0.8938	0.9359	0.9682	1.0180	1.1173
0.8104	0.8949	0.9529	0.9741	1.0291	1.1236
0.8222	0.9117	0.9530	0.9848	1.0342	1.1444
0.8550	0.9118	0.9554	0.9960	1.0736	1.2026

Table 3.2 Measurements of the individual crystal growth rate of L-Asn·H₂O in DL-Asn·H₂O supersaturation (S=1.10) at 30°C.

Sorted crystal growth rate of L-Asn·H ₂ O in L-Asn·H ₂ O saturated solution (μm/min)					
0.3790	0.4817	0.5628	0.6028	0.6408	0.7080
0.4015	0.4937	0.5819	0.6078	0.6420	0.7271
0.4367	0.5217	0.5853	0.6084	0.6463	0.7366
0.4373	0.5247	0.5871	0.6167	0.6575	0.7594
0.4411	0.5293	0.5910	0.6325	0.6598	0.9455
0.4647	0.5445	0.6018	0.6377	0.6892	

These crystal growth rate data can be plotted as growth rate distributions, growth rate frequency vs growth rate of L-Asn·H₂O, as shown in Figure 3.14 and Figure 3.15, and also modeled based on the normal distribution in Equation (3.12).

Table 3.3 The range of crystal growth rate of L-Asn·H₂O in L-/DL-Asn·H₂O supersaturated solution (S=1.10) at 30°C

Crystal growth rate range (μm/min)	No. of L-Asn·H ₂ O crystals		f _G	
	in L-Asn·H ₂ O	in DL-Asn·H ₂ O	in L-Asn·H ₂ O	in DL-Asn·H ₂ O
0.0 - 0.1	0	0	0	0
0.1 - 0.2	0	0	0	0
0.2 - 0.3	0	0	0	0
0.3 - 0.4	0	1	0	10
0.4 - 0.5	0	7	0	70
0.5 - 0.6	0	9	0	90
0.6 - 0.7	0	13	0	130
0.7 - 0.8	3	4	30	40
0.8 - 0.9	7	0	70	0
0.9 - 1.0	14	1	140	10
1.0 - 1.1	8	0	80	0
1.1 - 1.2	3	0	30	0
1.2 - 1.3	1	0	10	0
1.3 - 1.4	0	0	0	0
1.4 - 1.5	0	0	0	0

$$f_G(G) = a \cdot \exp\left(-\frac{(G - G_0)^2}{2\sigma_G^2}\right) \quad (3.12)$$

where f_G is the growth rate frequency, which is the number of crystals having a growth rate within a particular range divided by width of the range, G is the crystal growth rate, G_0 is the mean growth rate of the distribution, σ_G is the standard deviation of the growth rate distribution, and a is a parameter relating only to the total number of samples in the distribution (Kongsamai et al., 2013; Kongsamai et al., 2017). While there is no *a priori* knowledge of the shape of the growth rate distribution, the distribution found are relatively narrow and fit the normal distribution quite well.

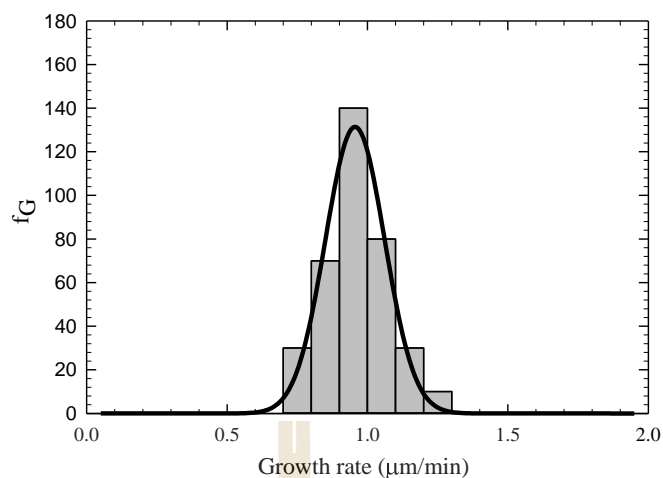


Figure 3.14 Relationship between growth rate frequency and growth rate of L-Asn·H₂O crystals in L-Asn·H₂O solution ($S=1.10$) at 30°C.

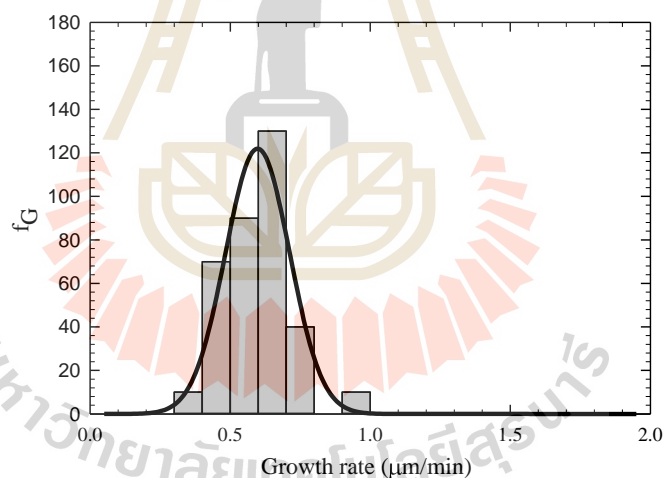


Figure 3.15 Relationship between growth rate frequency and growth rate of L-Asn·H₂O crystals in DL-Asn·H₂O solution ($S=1.10$) at 30°C.

The mean crystal growth rate of L-Asn·H₂O in L-Asn·H₂O and DL-Asn·H₂O is shown in Table 3.4. The growth rate of L-Asn·H₂O in L-Asn·H₂O solution is the higher. For the same supersaturation of L-Asn·H₂O, the growth rate from

DL-Asn·H₂O solutions was substantially reduced, with an almost 50% reduction in growth rate at a low supersaturation condition. One explanation for this difference is that the counter enantiomer acts as an inhibitor to the growth of the preferred enantiomer. It is possible that even in compounds where the conglomerate is the stable crystal form, the association of the preferred and counter enantiomer (as would be seen in the racemate form) is still strong enough that the counter enantiomer of the additive is an inhibitor. It can also adsorb to the surface of the crystal and inhibit the growth of the conglomerate form. Another possible explanation is that racemic dimers of Asn (associations of D- and L- molecules) in solution hinders the supply of L- monomers to the surface of the crystal and thus lower the crystal growth rate.

Table 3.4 Fitting parameters for the crystal growth rate distribution of L-Asn·H₂O grown in supersaturation of L- and DL-Asn·H₂O (S=1.10) at 30°C.

Parameter	L-Asn·H ₂ O in L-Asn·H ₂ O solution	L-Asn·H ₂ O in DL-Asn·H ₂ O solution
G ₀ (μm/min)	0.96	0.6
σ _G	0.11	0.11
R ²	0.9835	0.9423

Moreover, differences in the level of supersaturation were also studied.

The crystal growth rate of L-Asn·H₂O in L- and DL-Asn·H₂O at S= 1.05, 1.10, and 1.15 were investigated. The growth rate distribution of L-Asn·H₂O in L- and DL-Asn·H₂O are shown in Figure 3.16 and Figure 3.17, respectively. Table 3.5 shows the influence of supersaturation on the mean crystal growth rate of L-Asn·H₂O in L- and DL-Asn·H₂O.

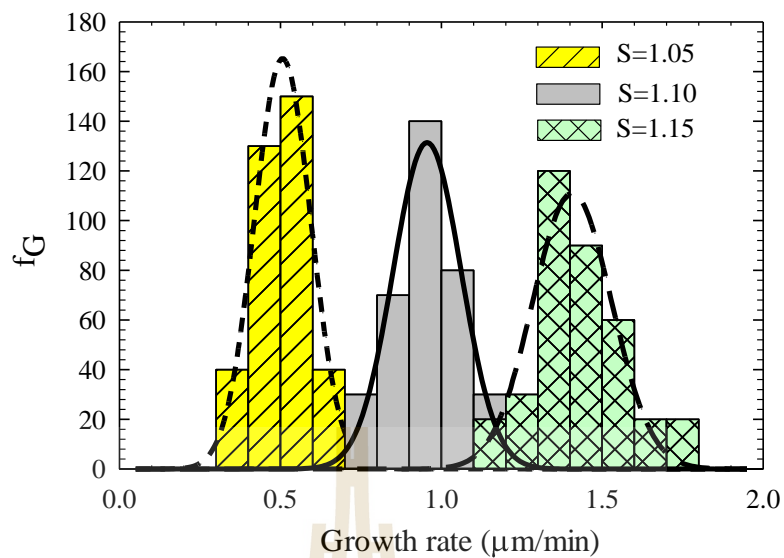


Figure 3.16 Relationship between growth rate frequency and growth rate of L-Asn·H₂O crystals in L-Asn·H₂O solution ($S=1.10$) at 30°C.

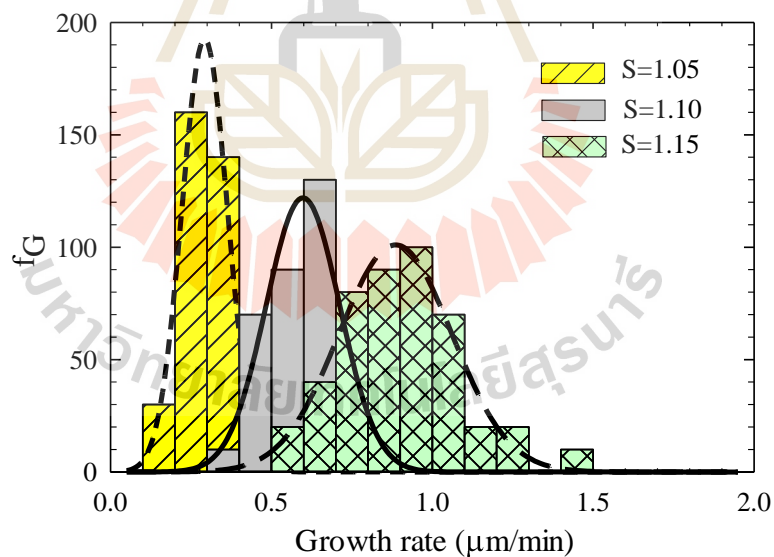


Figure 3.17 Relationship between growth rate frequency and growth rate of L-Asn·H₂O crystals in DL-Asn·H₂O solution ($S=1.10$) at 30°C.

Table 3.5 Fitting parameters for the crystal growth rate distribution of L-Asn·H₂O grown in various supersaturation levels in L- and DL-Asn·H₂O at 30°C.

Parameter	L-Asn·H ₂ O in L-Asn·H ₂ O solution			L-Asn·H ₂ O in DL-Asn·H ₂ O solution		
	1.05	1.1	1.15	1.05	1.1	1.15
G ₀ (μm/min)	0.51	0.96	1.41	0.29	0.60	0.89
σ _G	0.09	0.11	0.12	0.07	0.11	0.18
R ²	0.9972	0.9835	0.9360	0.9985	0.9423	0.9765

Figure 3.18 shows the relationship between the crystal growth rate and supersaturation ratio of L-Asn·H₂O in L-/ DL-Asn·H₂O solution. The fitting results are shown in Equation (3.13), and (3.14) for crystal growth rate of L-Asn·H₂O in L-Asn and DL-Asn supersaturated solution, respectively. This effect shows that the crystal growth rate increases when supersaturation increases.

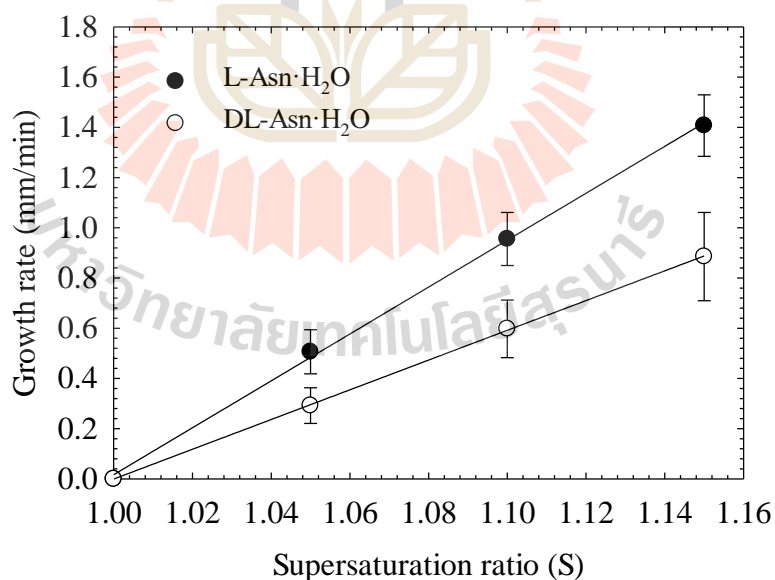


Figure 3.18 Relationship between crystal growth of L-Asn·H₂O in various supersaturations of L- and DL-Asn·H₂O solution at 30°C.

$$G = 9.4843*(S-1) \quad (3.13)$$

$$G = 5.9177*(S-1) \quad (3.14)$$

3.5.2 Single Crystal Growth Rate of L-Asn·H₂O in supersaturated solutions of DL-Asn·H₂O with tailor-made additives.

The size of L-Asn·H₂O crystal, as shown in Figure 3.19 – 3.21, was measured in the supersaturated solution of DL-Asn·H₂O with 3 mol% of D-amino acid additives; the additives consist of D-Asp, D-Glu, D-Leu, D-Val respectively. These results show that the shape of the crystal is not changing significantly, so, the prediction of growth rate by use of the length of the principal axis of the crystal is acceptable.

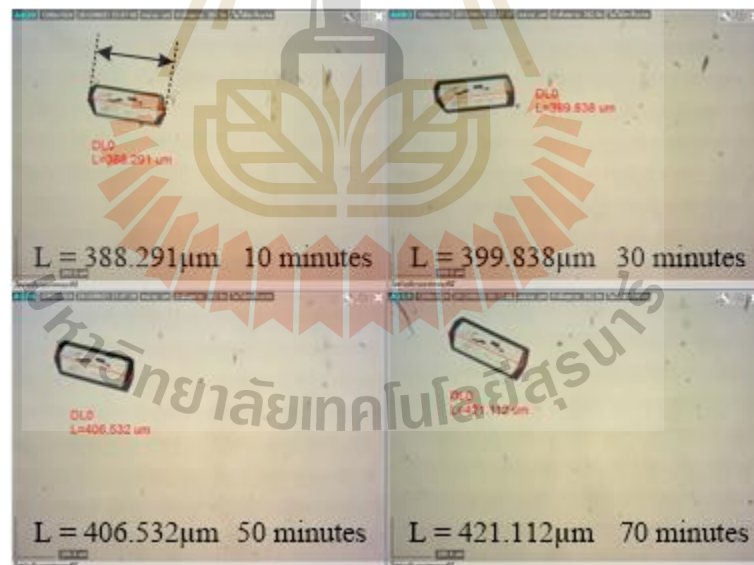


Figure 3.19 Crystal shape of L-Asn·H₂O in DL-Asn·H₂O solution (S = 1.10) with 3 mol% of D-Asp additive.

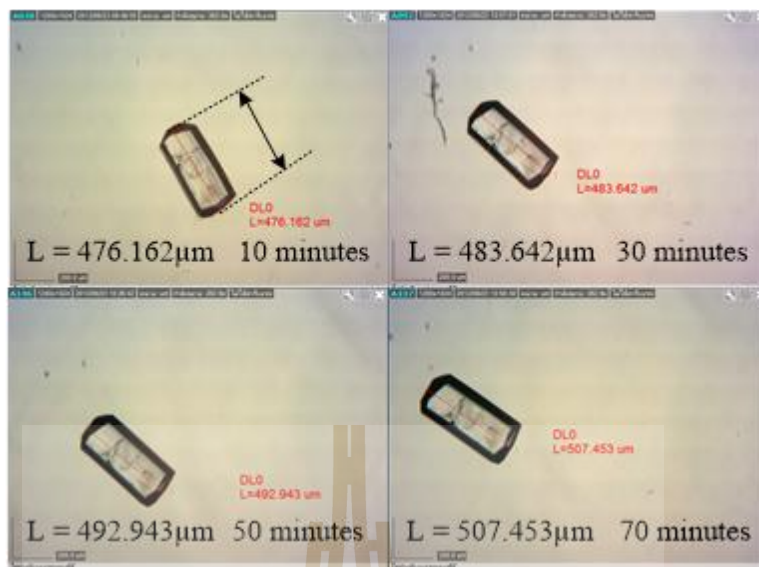


Figure 3.20 Crystal shape of L-Asn·H₂O in DL-Asn·H₂O solution ($S = 1.10$) with 3 mol% of D-Glu additive.



Figure 3.21 Crystal shape of L-Asn·H₂O in DL-Asn·H₂O solution ($S = 1.10$) with 3 mol% of D-Leu additive.

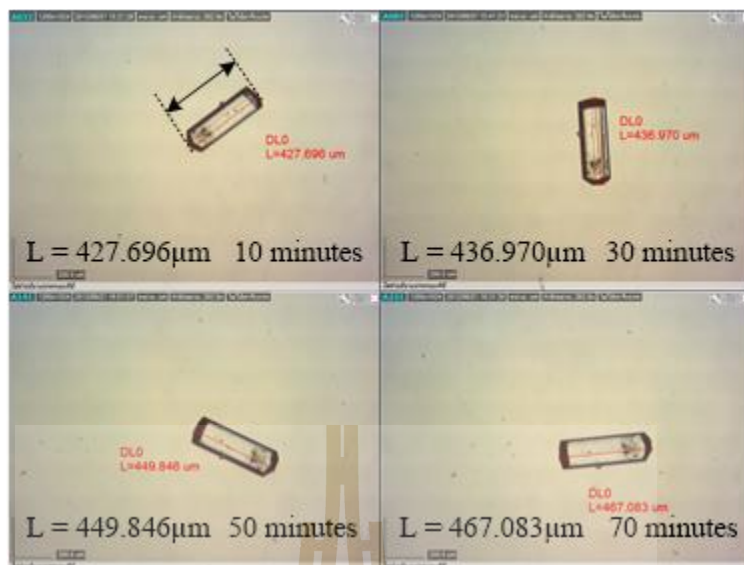


Figure 3.22 Crystal shape of L-Asn·H₂O in DL-Asn·H₂O solution ($S = 1.10$) with 3 mol% of D-Val additive.

The crystal growth rate frequency of L-Asn·H₂O in DL-Asn·H₂O with D-amino acid additives is shown in Figure 3.23. The mean crystal growth rate can be determined, and is tabulated in Table 3.6, based on the normal distribution in Equation (3.12). D-Val has no effect on the crystal growth rate of L-Asn·H₂O crystals. D-Leu slightly promotes the crystal growth rate of L-Asn·H₂O but not significantly. Therefore, D-Val and D-Leu additives have essentially no effect on the crystal growth rate of L-Asn·H₂O crystals. However, D-Glu and D-Asp additives inhibit the crystal growth rate of L-Asn·H₂O in DL-Asn·H₂O supersaturated solution; this is to be expected since the molecules have a similar side chain and thus it is more likely to act as an inhibitor. This is similar to D-Asn·H₂O in DL-Asn·H₂O solution inhibiting the crystal growth of L-Asn·H₂O, as described in Section 3.5.1.

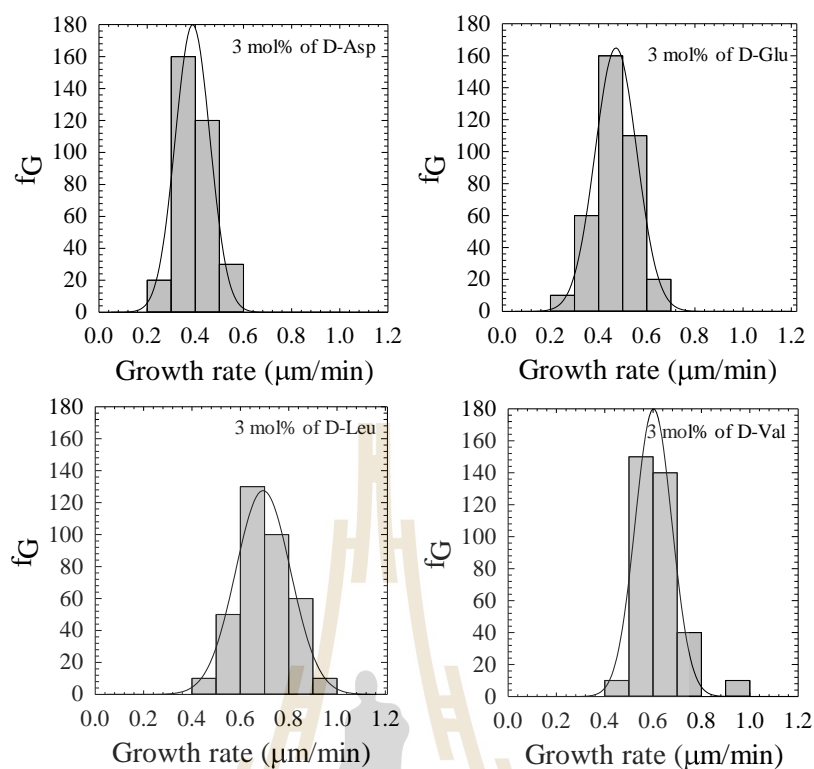


Figure 3.23 Relationship between growth rate frequency and growth rate of L-Asn·H₂O crystals in DL-Asn·H₂O solution with 3 mol% of different D-amino acid additives at 30°C.

Table 3.6 Fitting parameters for the crystal growth rate distribution of L-Asn·H₂O grown in DL-Asn·H₂O solutions with different D-amino acid additives at 30°C.

Parameter	DL-Asn·H ₂ O with 3mol% of D-amino acid additives				
	without additives	D-Asp	D-Glu	D-Leu	D-Val
Go (μm/min)	0.60	0.39	0.47	0.69	0.60
σ _G	0.11	0.07	0.09	0.11	0.08
R ²	0.9423	0.9903	0.9995	0.9824	0.9844

The crystal size of L-Asn·H₂O in DL-Asn·H₂O with 3 mol% of L-amino acid additives (L-Asp, L-Glu, L-Leu, and L-Val) is shown in Figure 3.24 – 3.26.

The frequency of the crystal growth rates is shown in Figure 3.28, and the mean crystal growth rates are tabulated in Table 3.7. L-Leu additives do not significantly change the crystal growth rate of L-Asn·H₂O in DL-Asn·H₂O solution. The crystal growth of L-Asn·H₂O in DL-Asn·H₂O solution increases when using L-Val as an additive. The reason for this is not known, although the additive appears to have no significant effect on the solubility of L-Asn·H₂O. It is possible that the molecule interrupts the associations between D- and L-Asn molecules in solution (Kongsamai et al., 2017). L-Glu and L-Asp additives significantly decrease the crystal growth rate of L-Asn·H₂O in DL-Asn·H₂O solution. This follows the rule of reversal; these additives have the same absolute configuration as L-Asn·H₂O, and are also have side chains similar to asparagine.



Figure 3.24 Crystal shape of L-Asn·H₂O in DL-Asn·H₂O solution ($S = 1.10$) with 3 mol% of L-Asp additives.

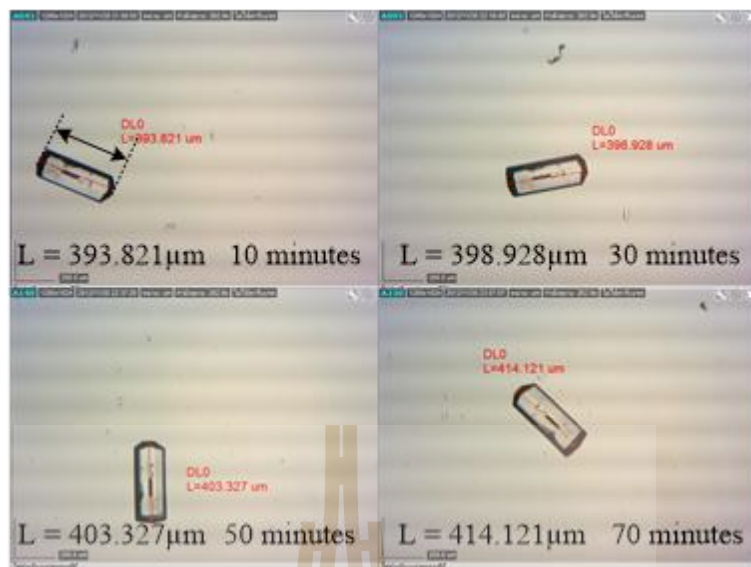


Figure 3.25 Crystal shape of L-Asn·H₂O in DL-Asn·H₂O solution ($S = 1.10$) with 3 mol% of L-Glu additives.



Figure 3.26 Crystal shape of L-Asn·H₂O in DL-Asn·H₂O solution ($S = 1.10$) with 3 mol% of L-Leu additives.

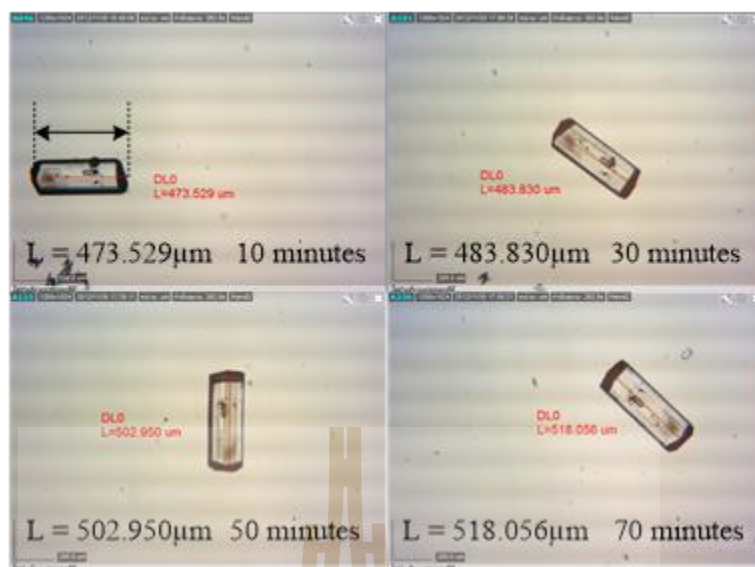


Figure 3.27 Crystal shape of L-Asn·H₂O in DL-Asn·H₂O solution ($S = 1.10$) with 3 mol% of L-Val additives.

Table 3.7 Fitting parameters for the crystal growth rate distribution of L-Asn·H₂O grown in DL-Asn·H₂O solutions with L-amino acid additives at 30°C.

Parameter	DL-Asn·H ₂ O with 3mol% of L-amino acid additives				
	without additives	L-Asp	L-Glu	L-Leu	L-Val
G_0 ($\mu\text{m}/\text{min}$)	0.60	0.19	0.28	0.62	0.73
σ_G	0.11	0.06	0.06	0.12	0.07
R^2	0.9423	0.9643	0.9974	0.9829	0.8964

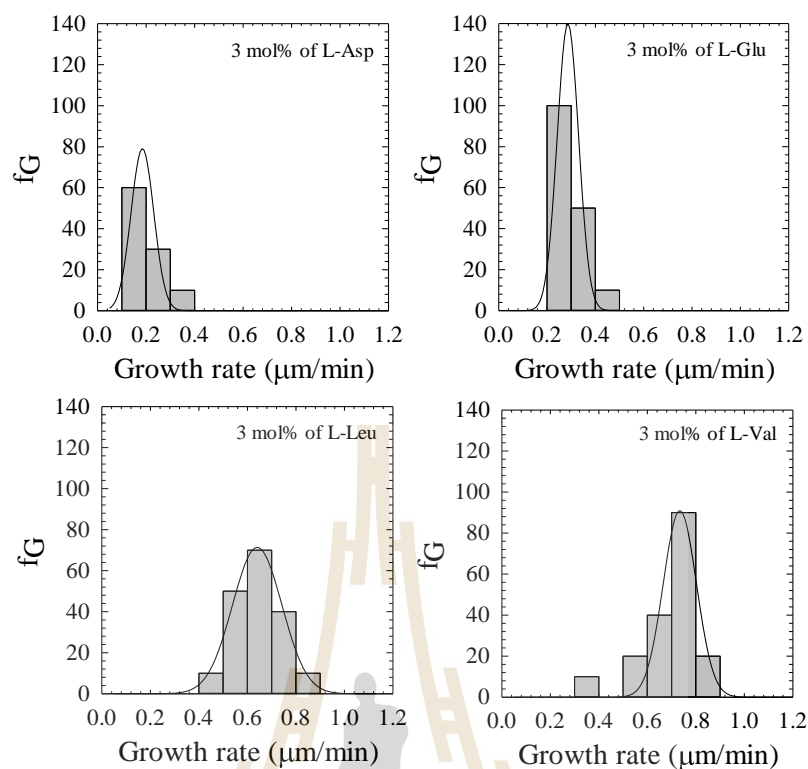


Figure 3.28 Relationship between growth rate frequency and growth rate of L-Asn·H₂O crystals in DL-Asn·H₂O solution with 3 mol% of L-amino acid additives at 30°C.

Finally, the summary of crystal growth rate of L-Asn·H₂O in L-Asn·H₂O, DL-Asn·H₂O and DL-Asn·H₂O with amino acid additives are shown in Figure 3.29. The dashed line is the mean crystal growth rate of L-Asn·H₂O in DL-Asn·H₂O solution.

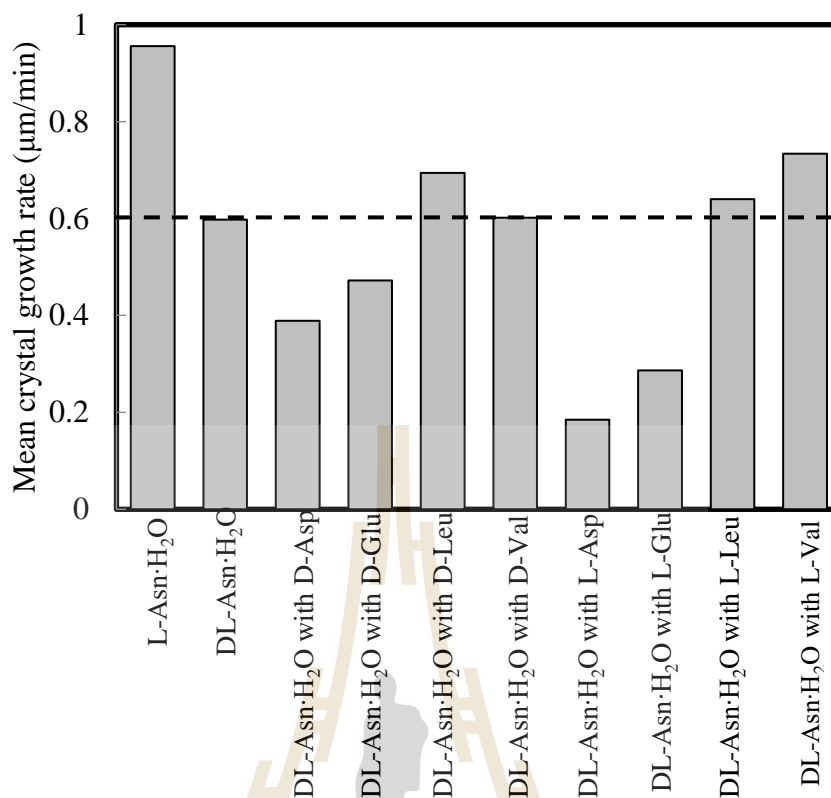


Figure 3.29 The mean crystal growth rates of L-Asn·H₂O in L-Asn·H₂O, and DL-Asn·H₂O solution without and with additives.

3.6 Conclusions

Crystal growth rates are key to crystallization processes. The growth rate of L-Asn·H₂O in L-Asn·H₂O, DL-Asn·H₂O and DL-Asn·H₂O with additives was presented in this chapter. The crystal growth rate of L-Asn·H₂O increases when increasing the supersaturation of L-Asn·H₂O and DL-Asn·H₂O. The crystal growth rate of L-Asn·H₂O in DL-Asn·H₂O is lower than in L-Asn·H₂O solution for all supersaturation values. D-Val, D-Leu, and L-Leu additives have almost no effect to the crystal growth of L-Asn·H₂O but L-Val increase the crystal growth rate of L-Asn·H₂O in DL-Asn·H₂O solutions. D/L-Asp and D/L-Glu clearly inhibit the crystal growth rate

of L-Asn·H₂O in DL-Asn·H₂O solution. This is especially true for L-Asp and L-Glu additives because they have a similar side chain to L-Asn, and also have the same absolute configuration.

3.7 References

- Addadi, L., Berkovitch-Yellin, Z., Domb, N., Gati, E., Lahav, M., and Leiserowitz, L. 1982a. Resolution of conglomerates by stereoselective habit modifications. **Nature** 296:21-26.
- Addadi, L., Berkovitch-Yellin, Z., Weissbuch, I., van Mil, J., Shimon, L. J. W., Lahav, M., and Leiserowitz, L. 1985. Growth and Dissolution of Organic Crystals with "Tailor-Made" Inhibitors—Implications in Stereochemistry and Materials Science. **Angewandte Chemie International Edition in English** 24 (6):466-485.
- Addadi, L., Gati, E., and Lahav, M. 1981a. Useful impurities for optical resolutions. 3. An improved Pasteur-type resolution of conglomerates and a new empirical method for assignment of absolute configuration. **Journal of the American Chemical Society** 103 (5):1251-1252.
- Addadi, L., Van Mil, J., and Lahav, M. 1981b. Useful impurities for optical resolutions. 2. Generality and mechanism of the rule of reversal. **Journal of the American Chemical Society** 103 (5):1249-1251.
- Addadi, L., Weinstein, S., Gati, E., Weissbuch, I., and Lahav, M. 1982b. Resolution of conglomerates with the assistance of tailor-made impurities. Generality and mechanistic aspects of the "rule of reversal". A new method for assignment of

- absolute configuration. **Journal of the American Chemical Society** 104 (17):4610-4617.
- Angelov, I., Raisch, J., Elsner, M. P., and Seidel-Morgenstern, A. 2008. Optimal operation of enantioseparation by batch-wise preferential crystallization. **Chemical Engineering Science** 63 (5):1282-1292.
- Beilles, S., Cardinael, P., Ndzié, E., Petit, S., and Coquerel, G. 2001. Preferential crystallisation and comparative crystal growth study between pure enantiomer and racemic mixture of a chiral molecule: 5-ethyl-5-methylhydantoin. **Chemical Engineering Science** 56 (7):2281-2294.
- Czapla, F., Haida, H., Elsner, M. P., Lorenz, H., and Seidel-Morgenstern, A. 2009. Parameterization of population balance models for polythermal auto seeded preferential crystallization of enantiomers. **Chemical Engineering Science** 64 (4):753-763.
- Elsner, M. P., Ziomek, G., and Seidel-Morgenstern, A. 2009. Efficient separation of enantiomers by preferential crystallization in two coupled vessels. **AIChE Journal** 55 (3):640-649.
- Flood, A. E. 2009. **Industrial crystallization from solution: A primer**. Thailand: Suranaree University of Technology.
- Jacques, J., Collet, A., and Wilen, S. H. 1981. **Enantiomers, Racemates, and Resolutions**. New York: Wiley.
- Kongsamai, P., Maneedaeng, A., and Flood, A. E. 2013. Effect of Additives to the Crystal Growth Rate. Paper read at **the 5th Regional Conference on Chemical Engineering**, at Pattaya, Thailand.

- Kongsamai, P., Maneedaeng, A., Flood, C., ter Horst, J. H., and Flood, A. E. 2017. Effect of additives on the preferential crystallization of L-asparagine monohydrate. **The European Physical Journal Special Topics** 226 (5):823-835.
- Lahav, M., and Leiserowitz, L. 1993. Tailor-made auxiliaries for the control of nucleation, growth and dissolution of two- and three-dimensional crystals. **Journal of Physics D: Applied Physics** 26 (8B):B22.
- Matsuoka, M. 1997. Purity Drop in Optical Resolution of Racemic Mixtures. In **Separation and Purification by Crystallization**: American Chemical Society, 59-72.
- Meir, L., and Leslie, L. 2015. A lifelong Odyssey: from structural and morphological engineering of functional solids to bio-chirogenesis and pathological crystallization. **Physica Scripta** 90 (11):118003.
- Mullin, J. W. 2001. **Crystallization**. 4th edition ed. Oxford: Butterworth-Heinemann.
- Myerson, A. S. 2002. **Handbook of Industrial Crystallization**. Second Edition ed. Woburn: Butterworth-Heinemann.
- Profir, V. M., and Matsuoka, M. 2000. Processes and phenomena of purity decrease during the optical resolution of dl-threonine by preferential crystallization. **Colloids and Surfaces A: Physicochemical and Engineering Aspects** 164 (2-3):315-324.
- Randolph, A. D., and Larson, M. A. 1988. **Population Balances: Theory of Particulate Processes**. San Diego: Academic Press.

- Van Mil, J., Gati, E., Addadi, L., and Lahav, M. 1981. Useful impurities for optical resolutions. 1. Crystallization of photopolymerizing dienes in the presence of their chiral topochemical products. **Journal of the American Chemical Society** 103 (5):1248-1249.
- Wantha, L. 2011. **Polymorphism and solution-mediated transformation of DL-methoionine**, School of Chemical Engineering, Suranaree University of Technology.
- Weissbuch, I., Popovitz-Biro, R., Lahav, M., Leiserowitz, L., and Rehovot. 1995. Understanding and control of nucleation, growth, habit, dissolution and structure of two- and three-dimensional crystals using 'tailor-made' auxiliaries. **Acta Crystallographica Section B** 51 (2):115-148.
- Weissbuch, I., Shimon, L. J. W., Landau, E. M., Popovitz-Biro, R., Berkovitch-Yellin, Z., Addadi, L., Lahav, M., and Leiserowitz, L. 1986. 'Tailormade' auxiliaries for nucleation, growth and dissolution of organic crystals. In **Pure and Applied Chemistry**, 947.

CHAPTER IV

EFFECT OF TAIOR-MADE ADDITIVES TO UNSEEDED CRYSTALLIZATION OF DL-ASPARAGINE MONOHYDRATE IN WATER

4.1 Abstract

Amino acid production from chemical synthesis will almost always create a product in the form of a racemic mixture which contains the preferred amino acid enantiomer at only 50% of the total content. Hence, the separation of enantiomers is important. Preferential crystallization (PC) is a popular process to separate enantiomers because it potentially gives high yields with low cost of operation. To improve this process, tailor-made additives have been employed to inhibit the nucleation and growth of the counter enantiomer. This research investigates the effect of D-/L-aspartic acid (Asp), D-/L-glutamic acid (Glu), D-/L-Valine (Val), and D-/L-Leucine (Leu) in unseeded crystallization of DL-Asn·H₂O in a small crystallizer. The result of unseeded crystallization of DL-Asn·H₂O without any additives is always 50% L-Asn·H₂O and 50% D-Asn·H₂O, crystallized at almost the same time and rate. The yield of solid product increases when increasing the crystallization temperature at constant supersaturation ratio and supersaturation ratio at constant temperature. The L-Asp additive clearly inhibits the nucleation of L-Asn·H₂O in DL-Asn·H₂O crystallization and D-Asp inhibits D-Asn·H₂O. A higher amount of L-Asp can increase the total crystallization time of pure D-Asn·H₂O, by comparing between 3, 5, and 7 mol% of

L-Asp additives. However, the yield of D-Asn·H₂O from DL-Asn·H₂O with 7 mol% of L-Asp additives is lower than with 5 mol% of L-Asp additives. The L-Glu additive also shows same trend as the L-Asp additive, although it cannot completely inhibit L-Asn·H₂O, as was possible with L-Asp. For the results of D-/L-Leu, and D-/L-Val additives to unseeded crystallization of DL-Asn·H₂O, they did not follow the rule of reversal; the initial crystallization of Asn·H₂O is very scattered because the effects of these additives are very small. Thus, the trend of the inhibition is not clear.

4.2 Introduction

Preferential crystallization (PC) is a process to separate the preferred enantiomer from a racemic mixture that contains two enantiomers (the preferred enantiomer and the counter enantiomer) by seeding the preferred enantiomer into a supersaturated solution of the racemic mixture. This process is mainly used to separate a racemic mixture in a conglomerate forming system, which is a mechanical mixture of the two enantiomorphs; examples include glutamic acid, asparagine (Petruševska-Seebach et al., 2011), threonine (Profir and Matsuoka, 2000), and methionine hydrochloride (Srimahaprom and Flood, 2013). The advantages of this process are high yield of product, it is easy to operate, and low cost. However, the disadvantage is the spontaneous nucleation and growth of counter enantiomer. Many researchers have tried to fix this problem by using many methods, such as using a heating unit to dissolve small crystals from the nucleation of counter enantiomer (Eicke et al., 2009), coupled batch crystallization units to crystallize preferred enantiomer and counter enantiomer in each crystallizer and exchange the solution between these crystallizer (Elsner et al., 2009), using a membrane in the coupled batch to ensure that only solution can exchange

between the crystallizers (Svang-Ariyaskul et al., 2009), the use of cyclic auto-seed polythermal preferential crystallization in coupled batch crystallizers (Czapla et al., 2010).

This research involves the use of Tailor-made additives. A tailor-made additive is any additive that can change the crystallization in a desired way, including by promoting or inhibiting the nucleation or growth rates, or by changing the morphology of the crystals (Kongsamai et al., 2017). In 1980-1999, the use of tailor-made additives was proposed and studied by many researchers in the Weizmann Institute of Science in Israel. In 1982, Addadi et. al. proposed the rule of reversal, in which an enantiomer can adsorb on another enantiomer which is similar in absolute configuration, and cannot adsorb on the enantiomer which is different in absolute configuration (Addadi et al., 1982b). This rule may also be applied to nucleation, with the additive inhibiting the nuclei growing to the critical size for crystal growth. Moreover, this tailor-made additive also changes the morphology of enantiomers which are same absolute configuration to additives (Addadi et al., 1982a). Kondepudi et. al. showed the effect of S-lysine (Lys) additives to the crystallization of S-glutamic acid (Glu). The results also showed that primary nucleation rate and growth rate are retarded when using additives but there is almost no change in the secondary nucleation rate (Kondepudi and Culha, 1998), and also showed the effect of D-/L-Lys (i.e. R-/S-Lys) to the unseeded crystallization of DL-Glu in a stirred batch crystallizer (Buhse et al., 1999). In 2005, this research group used the theory of nucleation, crystal growth, and Langmuir adsorption to simulate the effect of L-Lys to the crystallization of DL-Glu (Kondepudi and Crook, 2005). Doki et. al. found that L-cysteine (Cys) can inhibit the nucleation of L-Asn and also used this additive to inhibit L-Asn in DL-Asn and also

using pulse heating to dissolve the L-Asn nuclei, and obtained a D-Asn solid product (Doki et al., 2004). Yokota et. al. used L-arginine (Arg) to crystallize pure D-Glu in a conglomerate form from DL-Glu; this species normally crystallizes as a racemic compound but also has a metastable conglomerate form (Yokota et al., 2006). Gou et al. (2012) used hydroquinine-4-methyl-2-quinolyether (HMQ) to inhibit the nucleation of RS-mandelic acid (MA) which is normally crystallized as a racemic compound and produced only as pure R-/S-MA when enantiopure seeds are used. They assumed that HMQ has a strong hydrogen bond with MA which can inhibit the primary nucleation of RS-MA.

This research investigated the effect of tailor-made additives to the nucleation of D-/L-Asn·H₂O from DL-Asn·H₂O in unseeded crystallization, and also studied the inhibition effect on the induction time of L-Asn·H₂O in water.

4.3 Theory

4.3.1 Nucleation

Nucleation is the formation of new crystallites (nuclei) in a supersaturated solution. The nucleation is generally classified into primary and secondary nucleation as shown in Figure 4.1. Primary nucleation is the formation of crystals in a clear liquid, and secondary nucleation is when nuclei occur from liquid with the assistance of parent crystals of the solute (Lewis et al., 2015).

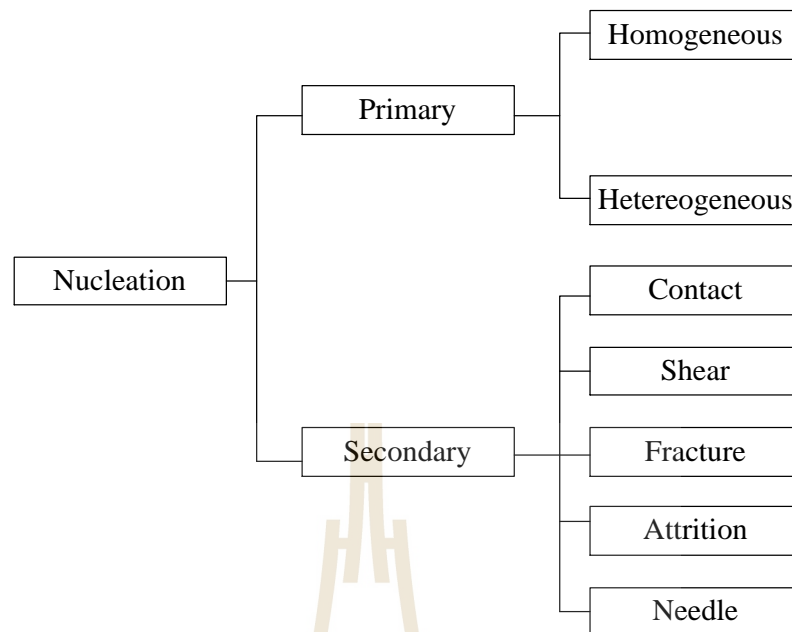


Figure 4.1 Nucleation mechanism (Randolph and Larson, 1988)

4.3.2 Primary Nucleation

From Figure 4.1, primary nucleation can be divided into two types; homogeneous nucleation and heterogeneous nucleation. For homogeneous nucleation, this mechanism occurs when the nuclei form from a clear solution without any external nucleation site. The classical nucleation theory (CNT) can be used to explain this mechanism. The molecules of the solute are formed in to a group which is called a cluster, and then a nucleus is formed, as shown in Figure 4.2.

The primary nucleation rate can be expressed as

$$J = AS \exp\left(-\frac{B}{\ln^2 S}\right) \quad (4.1)$$

where J is the nucleation rate ($\#/m^3 \cdot s$), S is the supersaturation ratio, A is the pre-exponential kinetic parameter ($m^{-1}s^{-1}$), and B is a thermodynamic parameter, and is defined as

$$B = \frac{16\pi v_0^2 \gamma^3}{3(kT)^3} \quad (4.2)$$

where v_0 is the molecular volume, γ is the interfacial energy (J/m^2), k is the Boltzmann constant and is equal to $1.38 \cdot 10^{-23}$ J/K, and T is absolute temperature (K).

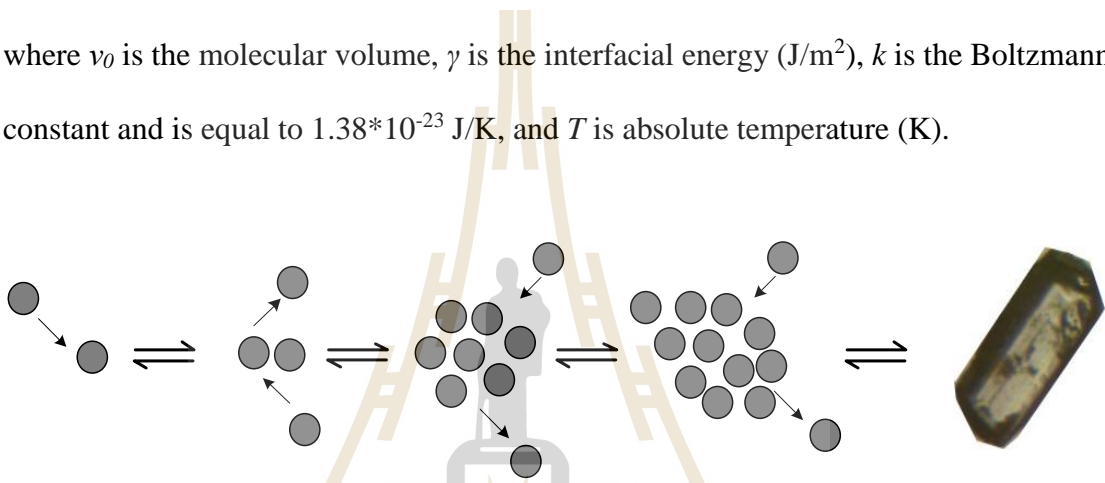


Figure 4.2 Change in cluster size by attachment or detachment of molecules

(adapted from Lewis et al. (2015) and Davey et al. (2013)).

However, most primary nucleation occurs by a heterogeneous mechanism, because in a real system it is very difficult to avoid the presence of any dust particles (Lewis et al., 2015). Heterogeneous nucleation requires a lower supersaturation than homogeneous nucleation to achieve a particular nucleation rate (Dirksen and Ring, 1991).

4.3.3 Secondary Nucleation

Secondary nucleation mechanisms are shown in Figure 4.1. The mechanism of secondary can be separated into three areas; the parent crystal, the

absorbed layer, and the solute molecule in the bulk solution. Contact nuclei are formed from contacts, including crystal-crystal, crystal-vessel wall, crystal-impeller etc. This contact will remove the absorbed layer of the growing surface of the crystal. Then these absorbed layers can form a nucleus if the amount of solute in the absorbed layer is larger than the critical nuclei size. Shear nucleation occurs when the fluid velocity relative to the crystal velocity is large, and some of the absorbed layer is removed and then these absorbed layers form a nucleus, as in the contact nuclei mechanism. Fracture and attrition concern the breakage of the parent crystal. Fracture nucleation is caused by the breakage of crystal crystals due to collisions. The attrition nuclei are the formation of attrition fragments from larger crystals. The nuclei from attrition are very much smaller than the parent crystals. Needle breeding occurs because of dendritic growth on the parent crystal (Flood, 2009).

For design and analysis purposes, secondary nucleation is most often modeled with empirical models of the form

$$B^0 = k_N \sigma^a T^b \omega^c M_T^d \quad (4.3)$$

where B^0 is the secondary nucleation rate, σ is the relative supersaturation, T is absolute temperature (K), ω is the agitation speed, M_T is the suspension density (g crystal/ g suspension), and k_N , a , b , c , and d are empirical constants obtained from experimental measurements (Flood, 2009).

4.4 Materials and Methods

4.4.1 Materials

DL-asparagine monohydrate (DL-Asn·H₂O, 99+ wt%), L-asparagine monohydrate (L-Asn·H₂O, 99+ wt%) and D-asparagine monohydrate (D-Asn·H₂O, 99+ wt%), were purchased from Sigma-Aldrich. D-aspartic acid (D-Asp, 99+ wt%), D-glutamic acid (D-Glu, 99+ wt%), D-valine (D-Val, 98+ wt%), D-leucine (D-Leu, 99 wt%), L-aspartic acid (L-Asp, 98+ wt%), L-glutamic acid (L-Glu, 99+ wt%), L-valine (L-Val, 98+ wt%), and L-leucine (L-Leu, 99 wt%) were purchased from ACROS. These reagents were used without further purification. Deionized water was used as the solvent.

4.4.2 Apparatus

A 50 mL batch crystallizer with temperature control via a jacket was used for unseeded crystallizations. A water bath (F32-ME, Julabo, Germany) was used to control the temperature of the jacket and therefore the crystallizer. A magnetic stirrer was used at 400 rpm to agitate the suspension.

The purity of solid products was analysed by HPLC (1260 Infinity, Agilent Technologies) with a Chirobiotic T column. The HPLC analysis was performed at 25°C using a 40:60 vol% ethanol: water mixture as a mobile phase with a flow rate of 0.25 mL/min and using UV detection at 210 nm. The injection volume was 5 µL. For analysing the composition in the crystal, (specifically, whether or not the additive incorporates into the crystal) we used powder X-ray diffraction (XRD D2 Phaser, Bruker, USA), Fourier transform Raman spectroscopy (FT-Raman, Vertex 70 + RAM II, Bruker, USA), and Fourier transform infrared spectroscopy (FTIR, T27/Hyp2000, Bruker, USA).

4.4.3 Methods

DL-Asn·H₂O without and with additives was prepared in 40 g of water in a crystallizer. All conditions are shown in Table 4.1. The solution was stirred by a magnetic stirrer with a stirrer speed of 400 rpm. The solution was heated to 55°C and kept at this temperature for 20 minutes to completely dissolve the asparagine and additives. The solution was cooled to the crystallization temperature using a water bath with a cooling rate of 1°C/min. When the solution reached the crystallization temperature then the crystallization time started. Spontaneous nucleation occurred in the solution at some point after the crystallization time started. The solution was sampled between 1 to 10 hours using a 5 mL syringe, and harvesting only the solid product by using membrane filter (Nylon 0.45 micron). Filtered samples were kept in a desiccator for 1-2 days to remove the liquid. The solid product was weighed and prepared to analyze the composition using HPLC.

The solid crystal was analyzed by HPLC and the %enantiopurity of D-Asn·H₂O can be found from Equation (4.4), and the %yield from Equation (4.5).

$$\% \text{ purity} = \frac{C_D}{C_D + C_L} \times 100\% = \frac{A_D}{A_D + A_L} \times 100\% \quad (4.4)$$

where C_L and C_D are the concentrations of L-Asn·H₂O and D-Asn·H₂O in the solid product respectively. A_L and A_D are HPLC peak areas of L-Asn·H₂O and D-Asn·H₂O in the solid product.

$$\% \text{ yield}_i = \frac{m_i}{m_{i,th}} \times 100\% \quad (4.5)$$

where i represents one of the enantiomers, L-Asn·H₂O or D-Asn·H₂O. m_i is the mass of enantiomer i in solid product and $m_{i,th}$ is the maximum mass of enantiomer i which could be obtained at equilibrium. The maximum mass, $m_{i,th}$, is the difference between half of the DL-Asn·H₂O concentration and the saturation concentration of D- or L-Asn·H₂O.

We also used XRD, FTIR, FT-Raman to analyze the composition of the solid product to confirm that there was no additive impurity in the solid product.

Table 4.1 The conditions used for unseeded crystallizations of DL-Asn·H₂O in water.

Supersaturation ratio of DL-Asn·H ₂ O	Crystallization Temperature (°C)	Additives	Amount of additives
1.5	20	-	-
1.5	30	-	-
1.5	35	-	-
1.7	30	-	-
1.5	30	L-Asp	3%
1.5	30	L-Asp	5%
1.5	30	L-Asp	7%
1.5	30	D-Asp	5%
1.5	30	L-Glu	3%
1.5	30	L-Glu	5%
1.5	30	L-Glu	7%
1.5	30	D-Glu	5%
1.5	30	L-Leu	5%
1.5	30	D-Leu	5%
1.5	30	L-Val	5%
1.5	30	D-Val	5%

4.5 Results and Discussion

4.5.1 Unseeded Crystallization of DL-Asn·H₂O in Water

The crystallization of pure DL-Asn·H₂O in water is always 50% D- and L-Asn·H₂O. Therefore, the purity of D-Asn·H₂O is 50% by weight and mole along the crystallization time as shown in Figure 4.3 for all supersaturation and temperature.

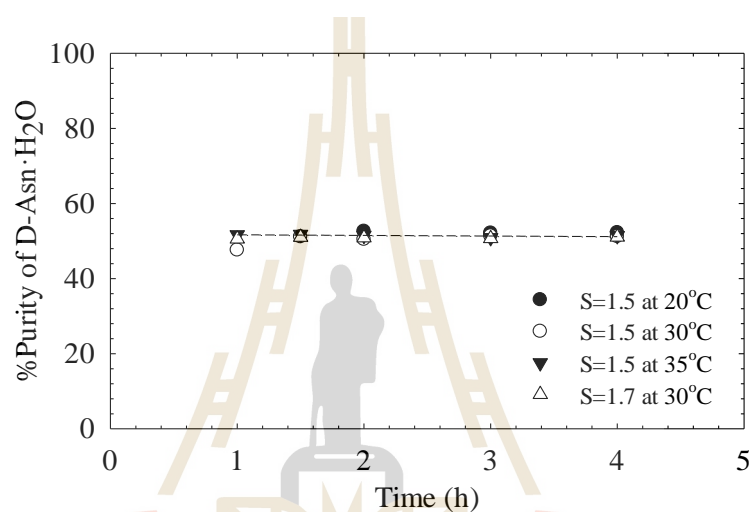


Figure 4.3 %Purity of D-Asn·H₂O from DL-Asn·H₂O supersaturated solution without additives.

At the same supersaturation ratio, for higher crystallization temperature the yield of D-Asn·H₂O and L-Asn·H₂O increases faster than at lower crystallization temperature, as shown in Figure 4.4 and Figure 4.5, respectively. The yield of D-Asn·H₂O and L-Asn·H₂O product did not approach to 100% because the yield from Equation (4.5) is based on the maximum amount of D- and L-Asn·H₂O ($m_{i,th}$) that can be produced which calculated from the difference between amount of D- and L-Asn·H₂O in DL-Asn·H₂O supersaturation (half of DL-Asn·H₂O concentration) and the saturated solution of D-/ and L-Asn·H₂O at the crystallization temperature.

However, the solubility of D- and L-Asn·H₂O is slightly lower than a half of solubility of the DL-Asn·H₂O and the nucleation of D-/L-Asn·H₂O from DL-Asn·H₂O supersaturation is probably limited at the half of DL-Asn·H₂O saturated solution at crystallization temperature. Hence, the difference between amount of D- and L-Asn·H₂O in DL-Asn·H₂O supersaturation (half of DL-Asn·H₂O concentration) and the saturated solution of D-/ and L-Asn·H₂O in DL-Asn·H₂O supersaturation (half of DL-Asn·H₂O concentration) at crystallization temperature are significantly lower than $m_{i,th}$. Thus, the yield is lower than 100%. However, if the crystallization time is longer, the yield may be approach to close 100%.

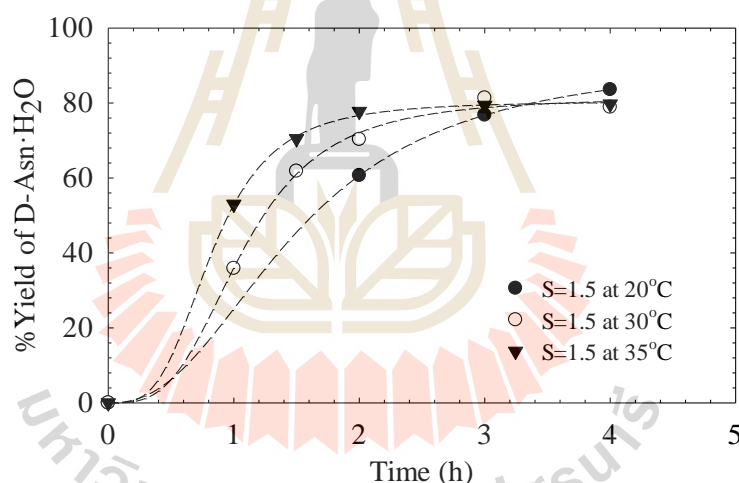


Figure 4.4 % Yields of D-Asn·H₂O from DL-Asn·H₂O supersaturated solution at different temperature.

At the same crystallization temperature, when the supersaturation ratio increases the rate of D-/L-Asn·H₂O crystallization is faster than at a lower supersaturation ratio, as shown in Figure 4.6 and Figure 4.7.

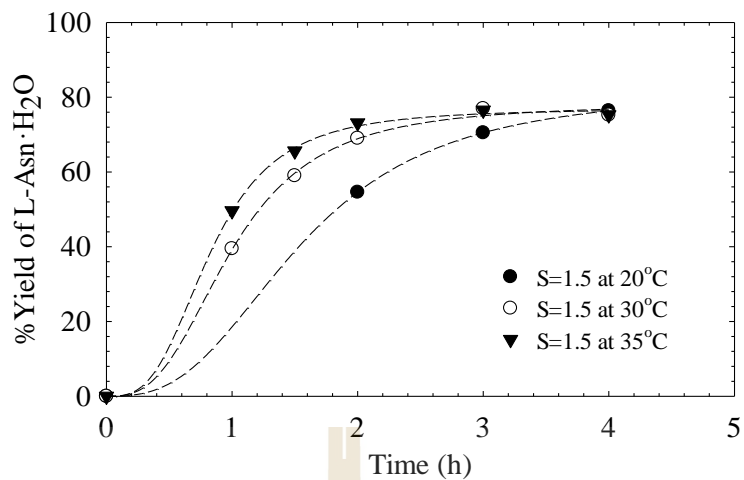


Figure 4.5 % Yield of L-Asn·H₂O from DL-Asn·H₂O supersaturated solution at different temperatures.

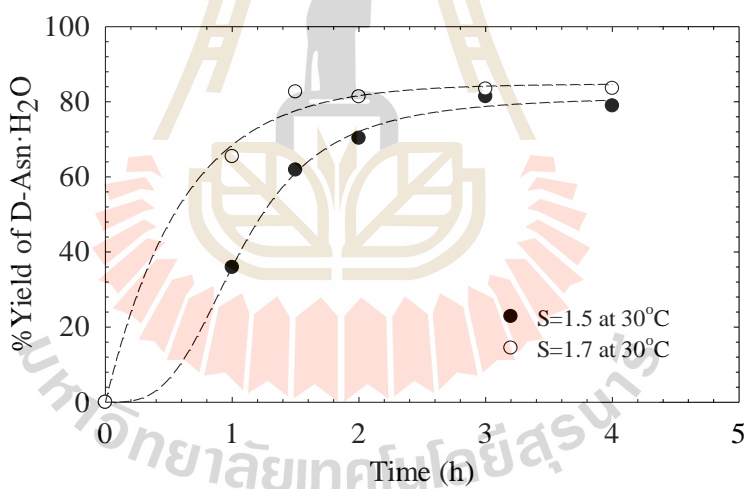


Figure 4.6 % Yield of D-Asn·H₂O from DL-Asn·H₂O supersaturated solution at different initial supersaturation.

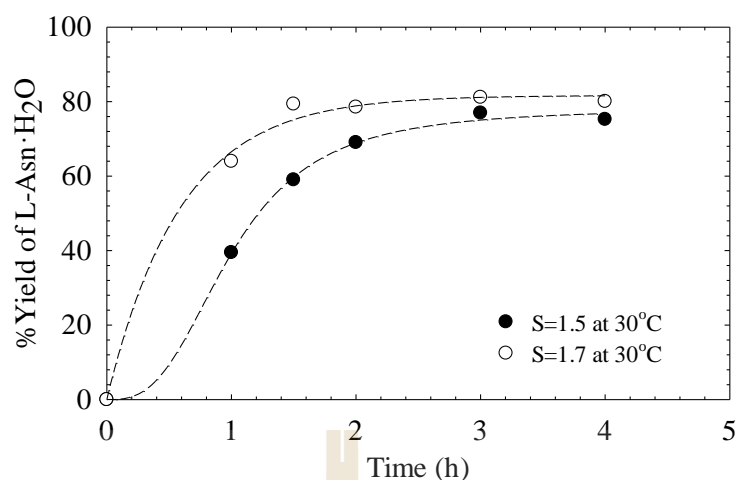


Figure 4.7 % Yield of L-Asn·H₂O from DL-Asn·H₂O supersaturated solution at different initial supersaturation.

4.5.2 Unseeded Crystallization of DL-Asn·H₂O with D- and L-Asp and D- and L-Glu

The %purity of the D-Asn·H₂O solid product from unseeded crystallization of DL-Asn·H₂O with D-/L-Asp is shown Figure 4.8. The D-Asp additive inhibited the nucleation of D-Asn·H₂O from the DL-Asn·H₂O and L-Asp inhibited the nucleation L-Asn·H₂O from DL-Asn·H₂O. As the amount of L-Asp additive increases the inhibition time of the crystallization of L-Asn·H₂O increases.

The rate of increase of the D-Asn·H₂O product is lower when using a higher amount of L-Asp additives because the L-Asp additive does not only inhibit the nucleation of L-Asn·H₂O but also inhibits the nucleation and growth of D-Asn·H₂O, as shown in Figure 4.9.

The %yield of L-Asn·H₂O from DL-Asn·H₂O solutions with L-Asp as an additive is shown in Figure 4.10. This clearly shows the effect of L-Asp additives to

inhibit the nucleation of L-Asn·H₂O; the progression of the yield of L-Asn·H₂O is lower when using a higher amount of the L-Asp additive.

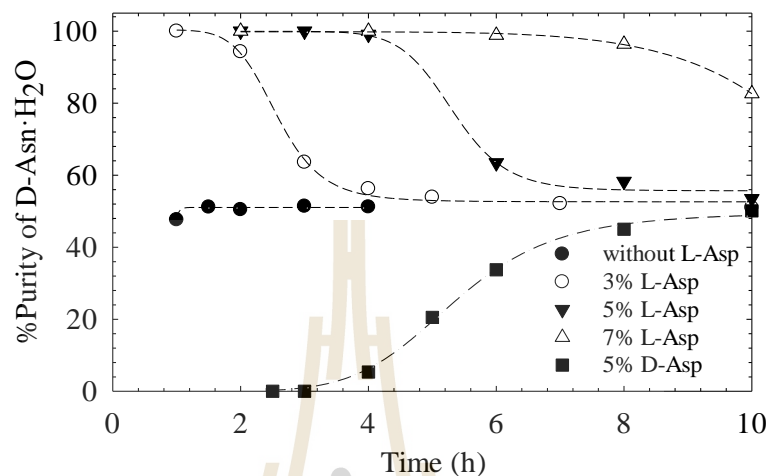


Figure 4.8 %Purity of D-Asn·H₂O from DL-Asn·H₂O supersaturated solution with L-/D-Asp additives.

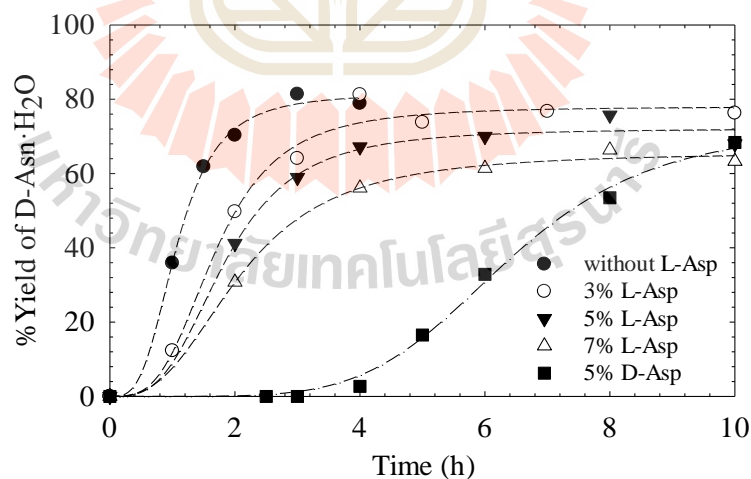


Figure 4.9 %Yield of D-Asn·H₂O from DL-Asn·H₂O supersaturated solution with L-/D-Asp additives.

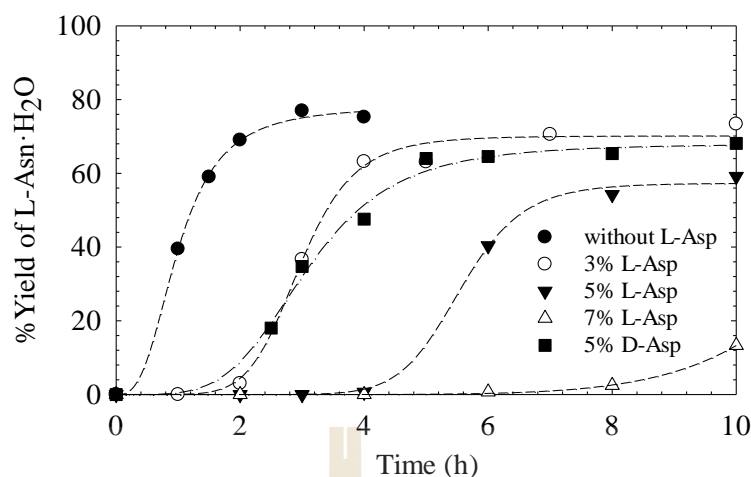


Figure 4.10 % Yield of L-Asn·H₂O from DL-Asn·H₂O supersaturated solution with L-/D-Asp additives.

The effect of L-Asp additives to the unseeded crystallization when varying amounts of additives were used is summarized in Figure 4.11. The maximum yield of pure D-Asn·H₂O solid product at 5 mol% is highest, because at 3mol% L-Asp additive, the spontaneous nucleation of L-Asn·H₂O occurs faster than when using 5 mol% L-Asp additives. However, using of 7 mol% L-Asp increases the maximum time at 100% purity of D-Asn·H₂O, but it inhibits the nucleation of D-Asn·H₂O also. Moreover, the additives also change the solubility by increasing the solubility line as shown in Chapter II, so the supersaturation ratio when using additives is lower than when not using additives. In the same way, use of a higher amount of additives results in a solution with a lower supersaturation ratio than when using a lower amount of additives.

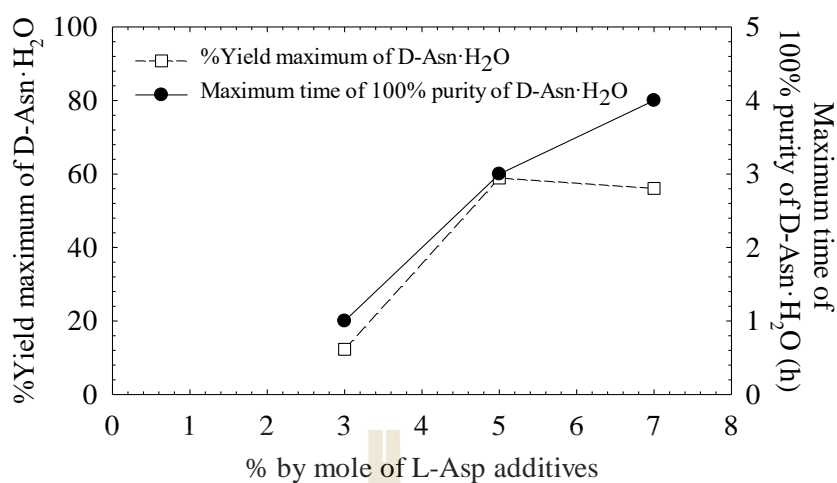


Figure 4.11 %Maximum yield and maximum time of 100%purity of D-Asn·H₂O when using L-Asp additives.

The effect of L-Glu additives to the unseeded crystallization of DL-Asn·H₂O is shown in Figure 4.12 to Figure 4.14. The L-Glu additive inhibits the nucleation of L-Asn·H₂O, and D-Glu inhibits the nucleation of D-Asn·H₂O. The amount of L-Glu increases the time before the decrease in purity to 50%, although the L-Glu additive does not completely inhibit the nucleation of L-Asn·H₂O.

The yield of D-Asn·H₂O solid product decreases when an increased amount of L-Glu additive is used because while L-Glu inhibits L-Asn·H₂O it also slightly inhibits the nucleation of D-Asn·H₂O. This occurs even though D-Asn·H₂O is not the same absolute configuration to the L-Glu additive.

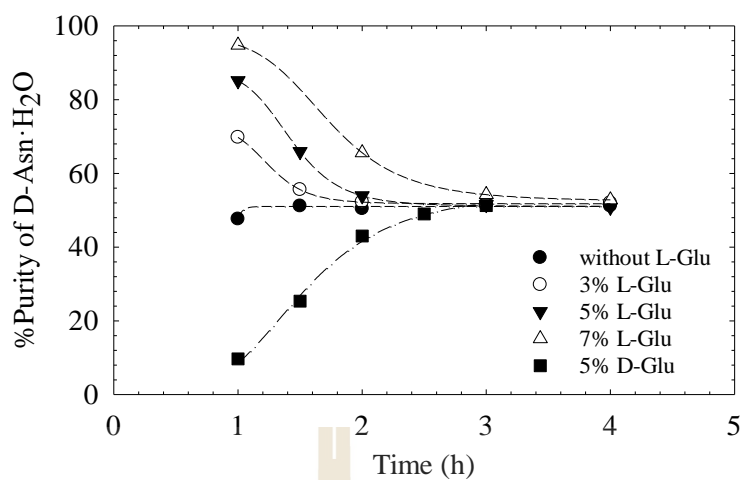


Figure 4.12 % Purity of D-Asn·H₂O from DL-Asn·H₂O supersaturated solution with L-/D-Glu additives.

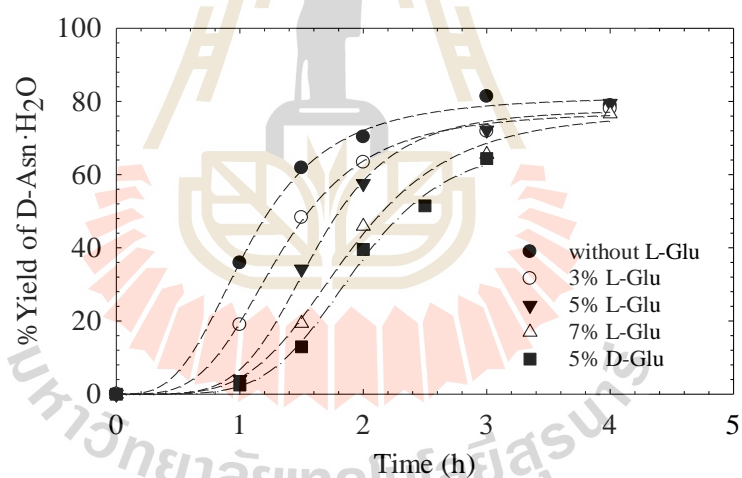


Figure 4.13 % Yield of D-Asn·H₂O from DL-Asn·H₂O supersaturated solution with L-/D-Glu additives.

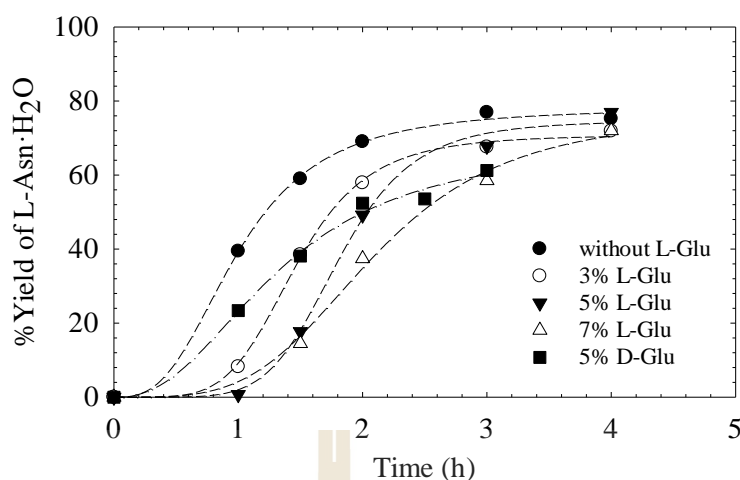


Figure 4.14 % Yield of L-Asn·H₂O from DL-Asn·H₂O supersaturated solution with L-/D-Glu additives.

The solid product enantiopurity was analyzed by HPLC. In order to confirm the solid crystal does not have a significant amount of additives in the structure, we used XRPD, FTIR, and FT-Raman to analyze the composition in the solid product, as shown in Figure 4.15 – 4.17 for XRPD, FTIR, and FT-Raman, respectively. We tried to confirm these results because some articles proposed that the additive is clearly combined in the solid product of D-/L-Asn·H₂O, and showed the crystal in the form of a solid solution (Addadi et al., 1982a; Kojo and Tanaka, 2001; Kojo et al., 2004).

The analysis from these techniques shows that the L-Asn·H₂O and DL-Asn·H₂O spectra are the same because they are essentially the same chemical species but different in enantiomer – the techniques cannot resolve the D- and L- forms of a species. The composition of the solid product from unseeded crystallization of DL-Asn·H₂O with L-Asp, and L-Glu additives are similar to the composition of L-/DL-Asn·H₂O, and they did not show the peak of pure L-Asp or L-Glu in the solid product by comparing between the composition of solid product in unseeded

crystallization of DL-Asn·H₂O with L-Asp additives and pure L-Asp, and between the composition of solid product in unseeded crystallization of DL-Asn·H₂O with L-Glu additives and pure L-Glu.

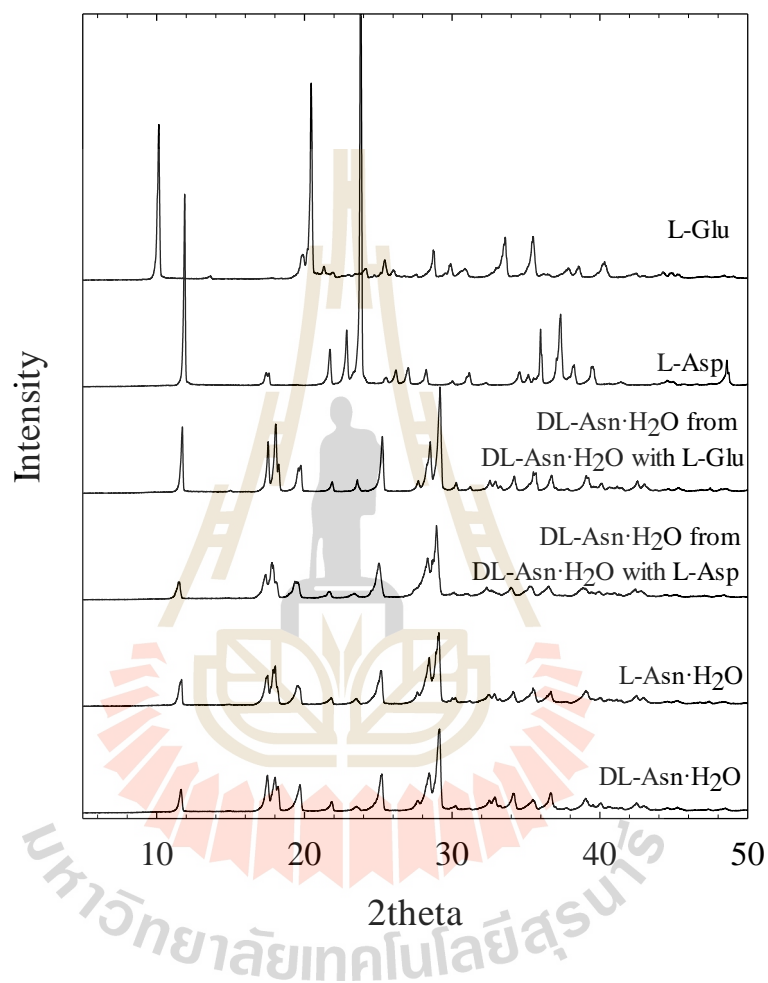


Figure 4.15 XRPD pattern of L-/DL-Asn·H₂O without and with L-Asp and L-Glu additives.

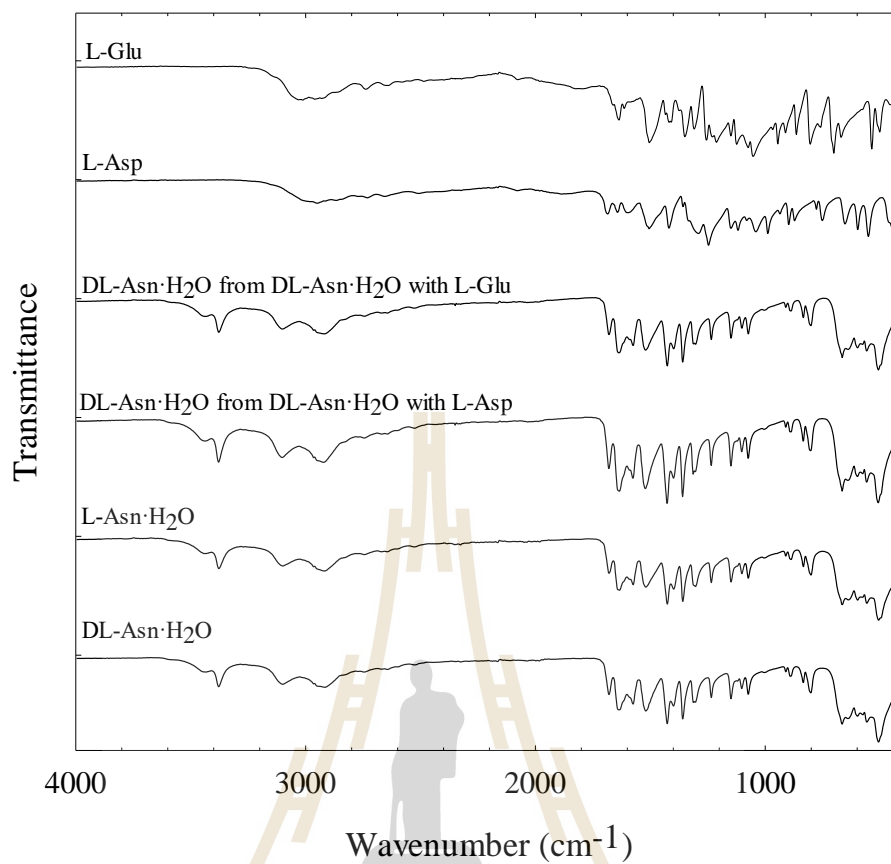


Figure 4.16 FTIR pattern of L-/DL-Asn·H₂O with and without L-Asp, and L-Glu additives.

มหาวิทยาลัยเทคโนโลยีสุรนารี

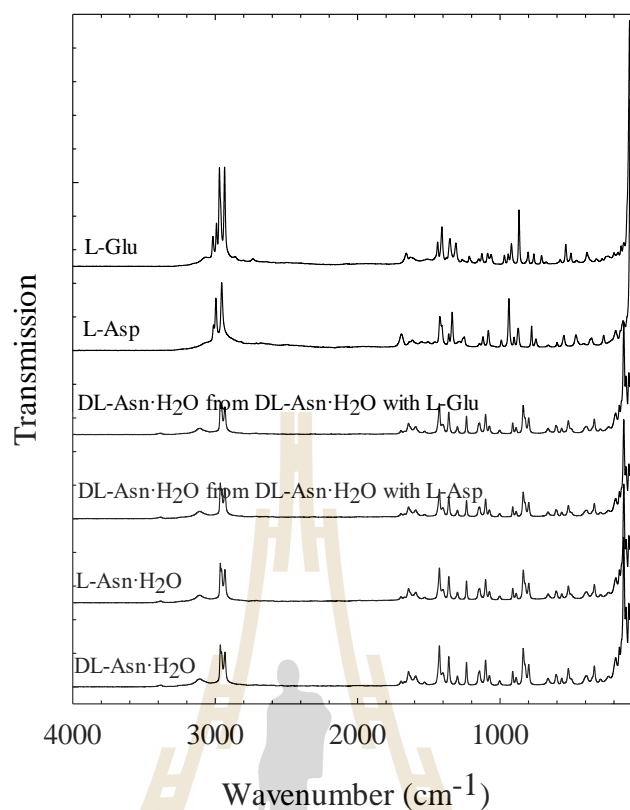


Figure 4.17 FT-Raman pattern of L-/DL-Asn·H₂O with and without L-Asp, and L-Glu additives.

4.5.3 Unseeded Crystallization of DL-Asn·H₂O with D/L-Leu and D/L-Val

The unseeded crystallization of DL-Asn·H₂O with D-/L-Asp and D-/L-Glu additives follows to the rule of reversal, where D-enantiomer additives inhibit the D-enantiomer and vice versa. However, the additives L-Leu, D-Leu, L-Val, and D-Val do not follow the rule of reversal, as shown in Figure 4.18 – 4.21.

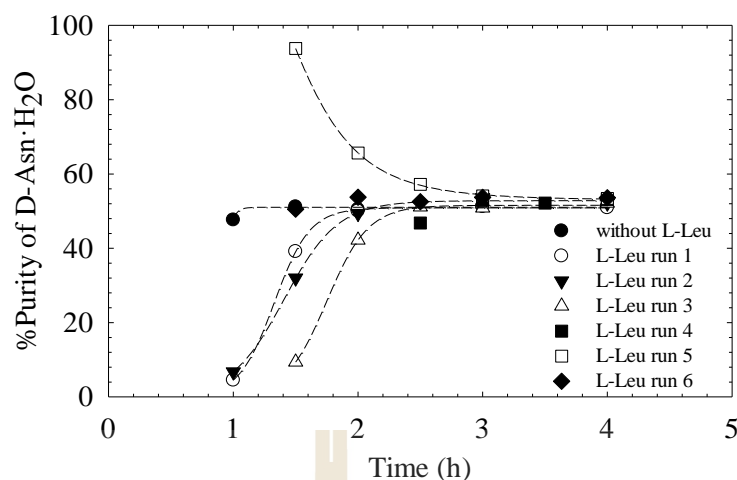


Figure 4.18 %Purity of D-Asn·H₂O from DL-Asn·H₂O supersaturated solution with L-Leu additives.

The purity of D-Asn·H₂O solid product shown in these figures does not follow the rule of reversal. By this rule, the L-Leu additive in the DL-Asn·H₂O system should inhibit L-Asn·H₂O and not inhibit D-Asn·H₂O, however the results show the inhibition of both D- and L-Asn·H₂O, or else a random product produced initially; the initial solid product was pure L-Asn·H₂O (3 times), a racemic mixture of D- and L-Asn·H₂O (2 times), and D-Asn·H₂O (1 time). The summary of initial crystallization of D-/L-/DL-Asn·H₂O with L-/D-Leu, and L-/D-Val are shown in Table 4.2. The results are very random because the nucleation is a stochastic process so, the nucleation of D-/L-Asn·H₂O can occur at different times or rate. These results cannot show an exact trend because there are effects of these additives to the crystallization of D-/L-Asn·H₂O, but it is very small effect. Thus, the trend of inhibition varies.

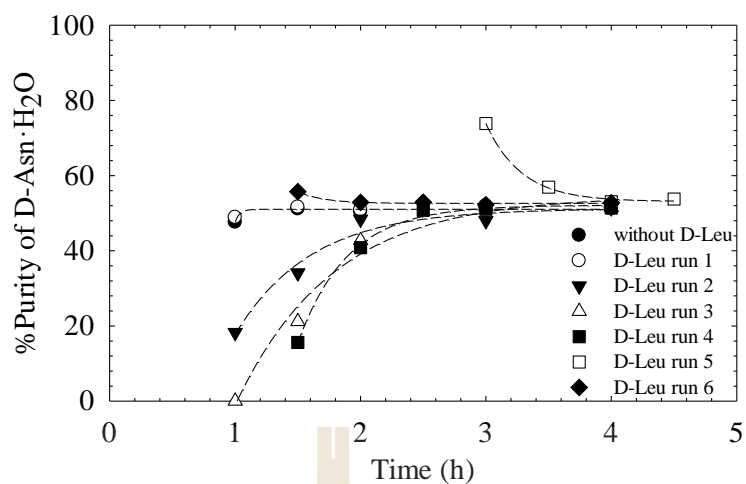


Figure 4.19 %Purity of D-Asn·H₂O from DL-Asn·H₂O supersaturated solution with D-Leu additives.

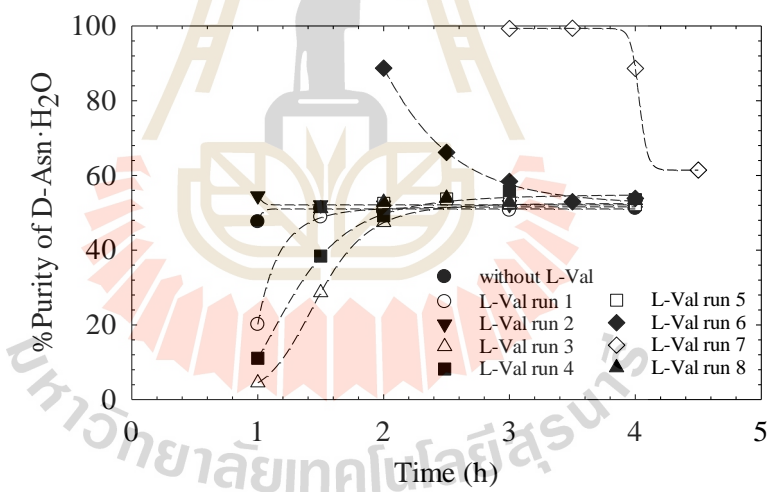


Figure 4.20 %Purity of D-Asn·H₂O from DL-Asn·H₂O supersaturation with L-Val additives.

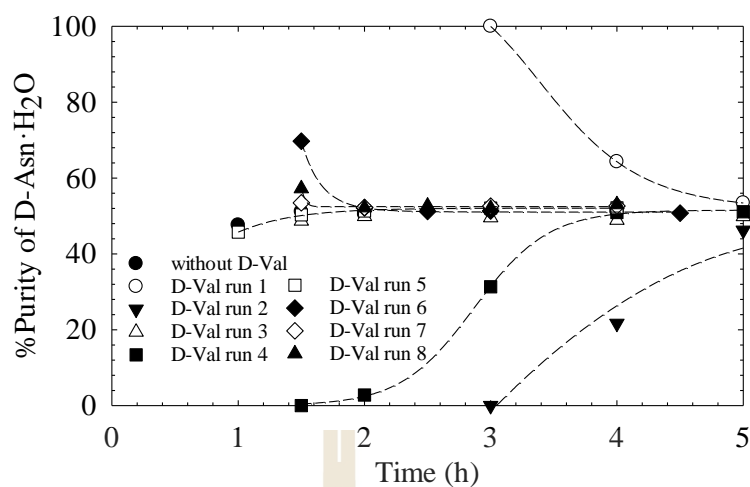


Figure 4.21 %Purity of D-Asn·H₂O from DL-Asn·H₂O supersaturated solution with D-Val additives.

Table 4.2 The number of initial solid product from unseeded crystallization of DL-Asn·H₂O when using L-/D-Leu, and L-/D-Val additives.

Additives	No. of the initial solid product in the crystallization of DL-Asn·H ₂ O			Total runs
	L-Asn·H ₂ O	D-Asn·H ₂ O	DL-Asn·H ₂ O	
L-Leu	3	1	2	6
D-Leu	3	1	2	6
L-Val	3	2	3	8
D-Val	2	2	4	8

4.6 Conclusions

The unseeded crystallization of DL-Asn·H₂O without any additives is always 50% L-Asn·H₂O and 50% D-Asn·H₂O crystallized at almost the same time and rate. The yield of solid product increases when increasing the crystallization temperature and supersaturation ratio. The additive L-Asp clearly inhibits the nucleation of L-Asn·H₂O in DL-Asn·H₂O crystallization and D-Asp clearly inhibits D-Asn·H₂O. A higher

amount of L-Asp can increase the crystallization time of pure D-Asn·H₂O crystallized by comparing between 3, 5, and 7 mol% of L-Asp additives. However, the yield of D-Asn·H₂O from DL-Asn·H₂O with 7 mol% of L-Asp additives is lower than 5 mol% of L-Asp additives. The L-Glu additive also shows the same trend as the L-Asp additive, although the inhibition is not 100% inhibiting L-Asn·H₂O. The results of D-/L-Leu, and D-/L-Val additives to the unseeded crystallization of DL-Asn·H₂O do not follow to the rule of reversal. The initial crystallization of Asn·H₂O is very scattered because the effects of these additives are very small. Thus, the trend of the inhibition is not significantly clear.

4.7 References

- Addadi, L., Berkovitch-Yellin, Z., Domb, N., Gati, E., Lahav, M., and Leiserowitz, L. 1982a. Resolution of conglomerates by stereoselective habit modifications. **Nature** 296 (5852):21-26.
- Addadi, L., Weinstein, S., Gati, E., Weissbuch, I., and Lahav, M. 1982b. Resolution of conglomerates with the assistance of tailor-made impurities. Generality and mechanistic aspects of the "rule of reversal". A new method for assignment of absolute configuration. **Journal of the American Chemical Society** 104 (17):4610-4617.
- Buhse, T., Kondepudi, D. K., and Hoskins, B. 1999. Kinetics of chiral resolution in stirred crystallization of D/L-glutamic acid. **Chirality** 11 (4):343-348.

- Czapla, F., Polenske, D., Klukas, L., Lorenz, H., and Seidel-Morgenstern, A. 2010. Cyclic auto-seeded polythermal preferential crystallization—Effect of impurity accumulation. **Chemical Engineering and Processing: Process Intensification** 49 (1):22-28.
- Davey, R. J., Schroeder, S. L. M., and ter Horst, J. H. 2013. Nucleation of Organic Crystals—A Molecular Perspective. **Angewandte Chemie International Edition** 52 (8):2166-2179.
- Dirksen, J. A., and Ring, T. A. 1991. Fundamentals of crystallization: Kinetic effects on particle size distributions and morphology. **Chemical Engineering Science** 46 (10):2389-2427.
- Doki, N., Yokota, M., Sasaki, S., and Kubota, N. 2004. Simultaneous crystallization of D- and L-asparagines in the presence of a Tailor-made additive by natural cooling combined with pulse heating. **Crystal Growth and Design** 4 (6):1359-1363.
- Eicke, M. J., Seidel-Morgenstern, A., and Elsner, M. P. 2009. Preferential Crystallization Including Fines Dissolution: How to Kill Two Birds with One Stone. In **ICheaP-9 - 9th International Conference on Chemical and Process Engineering, AIDIC Conference Series** edited by Sauro Pierucci. Rome, Italy, 111-120.
- Elsner, M. P., Ziomek, G., and Seidel-Morgenstern, A. 2009. Efficient separation of enantiomers by preferential crystallization in two coupled vessels. **AIChE Journal** 55 (3):640-649.
- Flood, A. E. 2009. **Industrial crystallization from solution: A primer**. Thailand: Suranaree University of Technology.

- Gou, L., Lorenz, H., and Seidel-Morgenstern, A. 2012. Investigation of a chiral additive used in preferential crystallization. **Crystal Growth and Design** 12 (11):5197-5202.
- Kojo, S., and Tanaka, K. 2001. Enantioselective crystallization of d,l-amino acids induced by spontaneous asymmetric resolution of d,l-asparagine. **Chemical Communications** (19):1980-1981.
- Kojo, S., Uchino, H., Yoshimura, M., and Tanaka, K. 2004. Racemic d,l-asparagine causes enantiomeric excess of other coexisting racemic d,l-amino acids during recrystallization: a hypothesis accounting for the origin of l-amino acids in the biosphere. **Chemical Communications** (19):2146-2147.
- Kondepudi, D. K., and Crook, K. E. 2005. Theory of conglomerate crystallization in the presence of chiral impurities. **Crystal Growth and Design** 5 (6):2173-2179.
- Kondepudi, D. K., and Culha, M. 1998. Chiral interaction and stochastic kinetics in stirred crystallization of amino acids. **Chirality** 10:238-245.
- Kongsamai, P., Maneedaeng, A., Flood, C., ter Horst, J. H., and Flood, A. E. 2017. Effect of additives on the preferential crystallization of L-asparagine monohydrate. **The European Physical Journal Special Topics** 226 (5):823-835.
- Lewis, A., Seckler, M., Kramer, H., and van Rosmalen, G. 2015. **Industrial Crystallization: Fundamentals and Applications**: Cambridge University Press.
- Petruševska-Seebach, K., Seidel-Morgenstern, A., and Elsner, M. P. 2011. Preferential crystallization of L-asparagine in water. **Crystal Growth and Design** 11 (6):2149-2163.

- Profir, V. M., and Matsuoka, M. 2000. Processes and phenomena of purity decrease during the optical resolution of dl-threonine by preferential crystallization. **Colloids and Surfaces A: Physicochemical and Engineering Aspects** 164 (2–3):315-324.
- Randolph, A. D., and Larson, M. A. 1988. **Population Balances: Theory of Particulate Processes**. San Diego: Academic Press.
- Srimahaprom, W., and Flood, A. E. 2013. Crystal growth rates and optical resolution of dl-methionine hydrochloride by preferential crystallization from aqueous solution. **Journal of Crystal Growth** 362:88-92.
- Svang-Ariyaskul, A., Koros, W. J., and Rousseau, R. W. 2009. Chiral separation using a novel combination of cooling crystallization and a membrane barrier: Resolution of DL-glutamic acid. **Chemical Engineering Science** 64 (9):1980-1984.
- Yokota, M., Doki, N., and Shimizu, K. 2006. Chiral separation of a racemic compound induced by transformation of racemic crystal structures: DL-glutamic acid. **Crystal Growth and Design** 6 (7):1588-1590.

CHAPTER V

PREFERENTIAL CRYSTALLIZATION OF L-ASPARAGINE MONOHYDRATE WITH THE INHIBITIONS BY TAILOR-MADE ADDITIVES

5.1 Abstract

The separation of enantiomers by preferential crystallization is very popular because of easy operation and low cost of production. However, the problem of this process is the spontaneous nucleation of the counter enantiomer. In this research, tailor made additives were used to inhibit the nucleation and crystal growth of the counter enantiomer. This chapter investigated the separation of the amino acid L-asparagine monohydrate (L-Asn·H₂O) from DL-Asn·H₂O using seeding with L-Asn·H₂O crystals. We used the additives D-aspartic acid (D-Asp), D-glutamic acid (D-Glu), D-leucine (D-Leu), and, D-valine (D-Val) to study the inhibition of D-Asn·H₂O in the preferential crystallization processes. In these experiments, the effect of supersaturation and L-Asn·H₂O seeds on the preferential crystallization process were studied. In addition, the effect of additives and the concentration of additives (3, 5, and 7 mol% additives) on the process were studied. When the supersaturation ratio of DL-Asn·H₂O increases the crystallization rate (including both the nucleation and crystal growth rate) also increases. The purity of the L-Asn·H₂O product from DL-Asn·H₂O is lower when using a high initial supersaturation ratio, but the yield is low for very low initial supersaturation ratio. The yield of L-Asn·H₂O increases when an increasing amount of

L-Asn·H₂O seeds is used, however, this does not make the nucleation rate larger nor the induction time of D-Asn·H₂O smaller. Using 5 mol% of D-Val and D-Leu additives did not change the crystallization pathway of D- and L-Asn·H₂O in the preferential crystallization of L-Asn·H₂O from DL-Asn·H₂O solution. However, 5 mol% of D-Glu and D-Asp additives increases the time available to produce a pure L-Asn·H₂O solid product by inhibiting the nucleation of the counter enantiomer of D-Asn·H₂O. The yield of L-Asn·H₂O also increases when using D-Glu and D-Asp additives, especially for the D-Asp additive. An increasing amount of the D-Asp additive increases the time available for pure L-Asn·H₂O crystallization. The total yield of L-Asn·H₂O decreases when using a higher amount of additives compared to DL-Asn·H₂O without additives, because the additives inhibit both D- and L-Asn·H₂O and change the solubility of DL-Asn·H₂O. The time available to crystallize pure L-Asn·H₂O crystals from the preferential crystallization using D-Glu additives increases when the amount of D-Glu increases; nevertheless, the maximum yield of pure L-Asn·H₂O product is very similar for D-Glu additive between 3-7 mol%.

5.2 Introduction

The preferential crystallization process is a common process used to separate enantiomers. This process is suitable for separation of a racemic mixture of the two enantiomers (Jacques et al., 1981) assuming the racemic mixture is a conglomerate forming system. Preferential crystallization achieves separation in a single process step through seeding of the preferred enantiomer to the supersaturated racemic solution; the preferred enantiomer will crystallize at a higher rate than the counter enantiomer, and significant yield and enantiopurity can be achieved if the nucleation and growth of the

counter enantiomer from the supersaturated solution can be avoided. PC has been applied to chiral species such as glutamic acid (Buhse et al., 1999), asparagine (Petruševska-Seebach et al., 2011), threonine (Profir and Matsuoka, 2000) and methionine hydrochloride (Srimahaprom and Flood, 2013). However, this method has a serious problem, which is the spontaneous nucleation and growth of the counter enantiomer (Jacques et al., 1981; Matsuoka, 1997; Profir and Matsuoka, 2000; Beilles et al., 2001; Angelov et al., 2008; Czaplá et al., 2009; Elsner et al., 2009). This may occur after prolonged batch times where the solution has a high supersaturation of the counter enantiomer in comparison to the preferred enantiomer (Profir and Matsuoka, 2000). Many researchers have tried to circumvent this problem, for instance by using coupled batch crystallizers – crystallizing the preferred enantiomer in one crystallizer and the counter enantiomer in another crystallizer, with exchange of solution between the two crystallizers (Elsner et al., 2009), coupled batch crystallizers with seeding of the preferred enantiomer in one crystallizer and allowing nucleation of the counter enantiomer in another crystallizer maintained at a different temperature (Levilain et al., 2012; Eicke et al., 2013), coupled batch crystallizers with a membrane between the crystallizers to prevent transport of crystals from one crystallizer to another (Svang-Ariyaskul et al., 2009), and racemization of the solute species to equalize the concentrations of the preferred and counter enantiomer (Würges et al., 2009; Petruševska-Seebach et al., 2009).

In this research, we used the tailor-made additives to inhibit the nucleation and crystal growth rate of the counter enantiomer to increase the time of crystallization of only the preferred enantiomer, and therefore increasing the yield of the product that can be produced at high purity. We investigate the preferential crystallization of L-Asn·H₂O

from DL-Asn·H₂O in water. The effect of supersaturation ratio and the amount of L-Asn·H₂O seed crystals was studied. The effect of D-aspartic acid (D-Asp), D-glutamic acid (D-Glu), D-leucine (D-Leu), and, D-valine (D-Val) additives to inhibit the nucleation and growth of D-Asn·H₂O as a counter enantiomer during the preferential crystallization of L-Asn·H₂O in DL-Asn·H₂O was investigated. We also studied the effect of the concentration of the additives on the preferential crystallization process by focusing on the product yield and crystallization of the pure preferred enantiomer (L-Asn·H₂O).

5.3 Theory

5.3.1 Preferential Crystallization

The preferential crystallization (PC) process is shown in Figure 5.1. A supersaturated solution of a racemic mixture of E1 and E2 enantiomers, where E1 is the preferred enantiomer and E2 is the counter enantiomer, is prepared in the crystallizer. Then E1 is seeded in to the crystallizer. The E1 seed will crystallize from the solution due to crystal growth and secondary nucleation. After a prolonged time period of the batch the counter enantiomer, E2, occurs due to primary nucleation, so the process must stop before the E2 enantiomer occurs to maintain the enantiopurity of the product.

We also show the pathway of the PC process in the ternary phase diagram between E1, E2, and solvent, as shown in Figure 5.2. The process starts at the point A, which is a racemic mixture of the enantiomers in a saturated solution at the temperature $T_{\text{cryst}} + \Delta T$. The E1 seeds are added to this supersaturated solution at the crystallization temperature. After seeding, the E1 enantiomer in the liquid phase

transfers to the solid crystal phase; therefore, the concentration of the E1 enantiomer in the solution decreases from point A to point X. At point X, the spontaneous nucleation of enantiomer E2, which is the counter enantiomer, will occur. Then the concentration of E1 and E2 in the solution phase decreases until point C, which is a racemic mixture at the crystallization temperature.

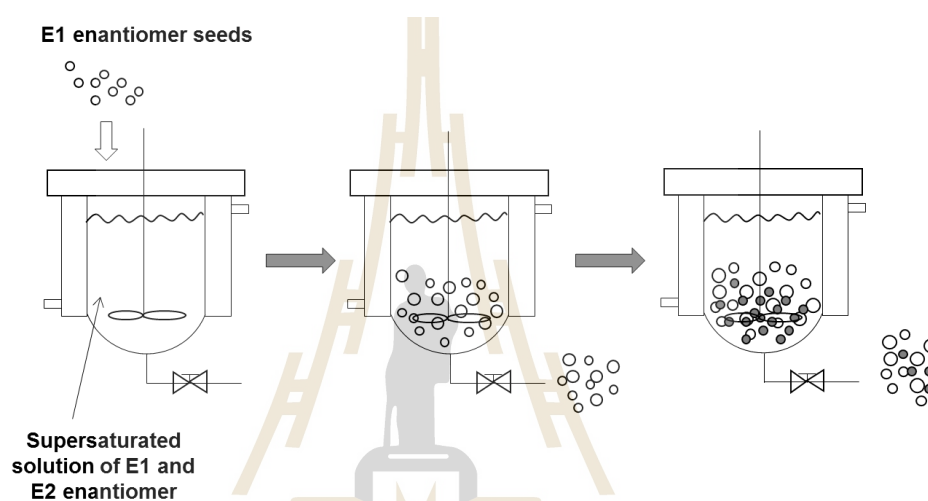


Figure 5.1 The procedure of preferential crystallization process.

This research uses tailor-made additives to develop this process by dissolving a small amount of the additives in the solution at the temperature $T_{\text{cryst}} + \Delta T$. The pathway of this process is shown in ternary phase diagram in Figure 5.3. The E1 seeds were added to this supersaturated solution after the solution was rapidly cooled to the crystallization temperature. The E1 enantiomer in the solution decreased until point X^* , where the pathway is longer than when the preferential crystallization is performed without additives, and then the nucleation of the counter enantiomer, E2 occurred at this point. Then the system moved to the point C which, is a racemic mixture of enantiomer E1 and E2 at the crystallization temperature. From this pathway, the

amount of E1 crystallized, before the nucleation of E2, increased when using the additives, so, the yield of the product increased.

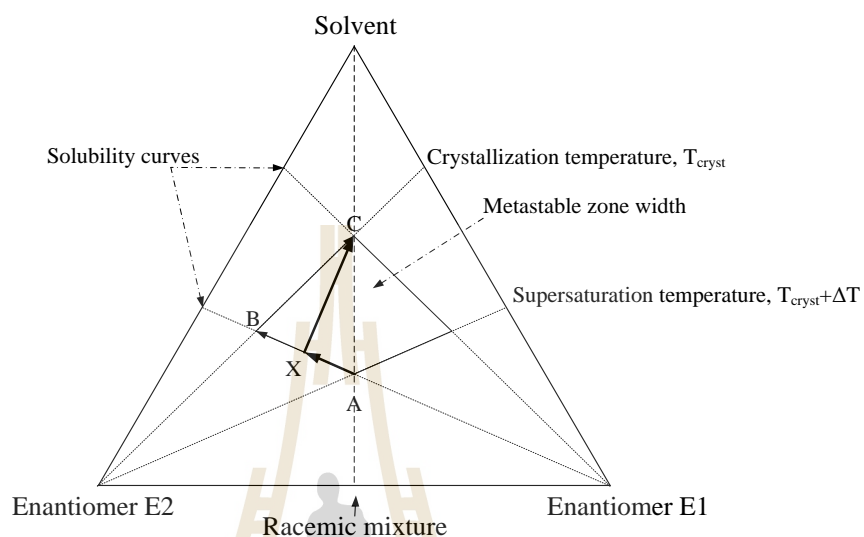


Figure 5.2 The path way of the preferential crystallization process (adapted from Elsner et al. (2009)).

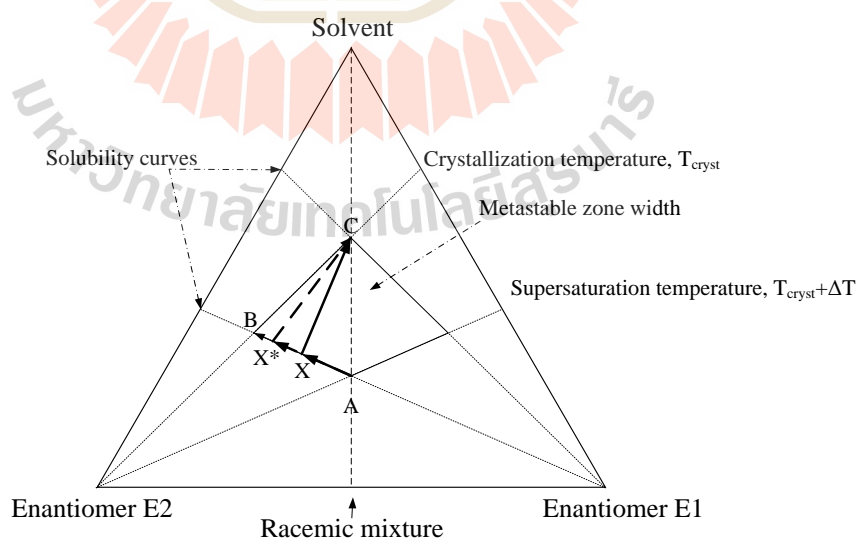


Figure 5.3 The path way of the preferential crystallization process when using Tailor-made additives.

5.4 Materials and Methods

5.4.1 Materials

DL-asparagine monohydrate (DL-Asn·H₂O, 99+ wt%), L-asparagine monohydrate (L-Asn·H₂O, 99+ wt%) and D-asparagine monohydrate (D-Asn·H₂O, 99+ wt%), were purchased from Sigma-Aldrich. D-aspartic acid (D-Asp, 99+wt%), D-glutamic acid (D-Glu, 99+wt%), D-valine (D-Val, 98+wt%), D-leucine (D-Leu, 99 wt%), L-aspartic acid (L-Asp, 98+wt%), L-glutamic acid (L-Glu, 99+wt%), L-valine (L-Val, 98+wt%), and L-leucine (L-Leu, 99 wt%) were purchased from ACROS. These reagents were used without further purification. Deionized water was used as the solvent.

5.4.2 Apparatus

Batch crystallizers with volumes of 50 and 200 mL were used with jackets for temperature control. A water bath (F32-ME, Julabo, Germany) was used to control the temperature of the jacket and therefore the crystallizers. A magnetic stirrer was used to stir the suspension.

The purity of solid products was analysed by HPLC (1260 Infinity, Agilent Technologies) with a Chirobiotic T column. The HPLC analysis was performed at 25°C using UV detection at 210 nm, the injection volume was 5 µL, using 40:60 vol% ethanol: water mixture as a mobile phase with flow rate 0.2 mL/min for experiments in section 5.4.3, and section 5.4.5 and using 70:30 vol% ethanol: water mixture as a mobile phase with flow rate 0.5 mL/min for experiments in section 5.4.4.

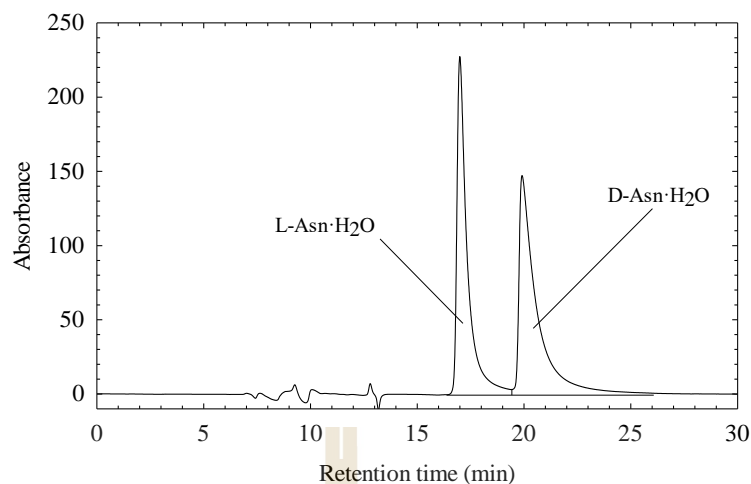


Figure 5.4 The analysis of D-/L-Asn·H₂O in water from HPLC using a Chirobiotic T column with a 40:60 vol% ethanol: water mobile phase.

5.4.3 Preferential Crystallization of L-Asn·H₂O in Batch Crystallization

We prepared a DL-Asn·H₂O solution with a supersaturation ratio (S) equal to 1.3 at 20°C in 150 g of water in a 200 mL crystallization vessel with a jacket to control the temperature. The solution was heated to 55°C, 20°C above the saturation temperature, for 20 min to completely dissolve the crystalline material. Subsequently, the solution was cooled down with a cooling rate of 1°C/min to the crystallization temperature of 20°C. L-Asn·H₂O seeds (150-180 micron) were added into the solution the moment the crystallization temperature was reached. A 5 mL sample of suspension was taken by syringe every 0.5 h to 1 h and filtered using a membrane filter. The solid product was kept in a desiccator for 1-2 days to completely dry the sample. The solid products were analysed for the product purity and yield using HPLC. The experiments were done using the conditions shown in Table 5.1.

Table 5.1 The conditions of preferential crystallization of L-Asn·H₂O.

Condition	Supersaturation ratio of DL-Asn·H ₂ O, S	L-Asn·H ₂ O seed amount (g)
A1	1.3	0.3
A2	1.1	0.3
A3	1.5	0.3
A4	1.3	0.075
A5	1.3	0.15

5.4.4 Tailor made Inhibition to the Preferential Crystallization of L-Asn·H₂O in a Small Batch Crystallization.

We prepared a solution of DL-Asn·H₂O with a supersaturation ratio (S) of 1.3 at 30°C in 40 g of water in a 50 mL crystallization vessel with a jacket to control the temperature. Additives, as shown in Table 5.2, were added to the solution at 5 mol% compared to the total amount of DL-Asn·H₂O. The solution was heated to 50°C, 15°C above the saturation temperature, for 20 min to completely dissolve the crystalline material. Subsequently, the solution was cooled down rapidly to the crystallization temperature of 30°C. L-Asn·H₂O seeds, 0.02 g (300-500 micron) were added into the solution the moment the crystallization temperature reached at 30°C. The process was stopped at a given time and the suspension was filtered to obtain crystal samples at different times from 1 h to 7 h after the addition of seeds. The solid product was kept in a desiccator for drying. The solid products were analysed the purity and yield by HPLC.

Table 5.2 The conditions of preferential crystallization of L-Asn·H₂O in small batch crystallization.

Condition	Supersaturation ratio of DL-Asn·H ₂ O, S	L-Asn·H ₂ O seed amount (g)	Additives	%additives
B1	1.3	0.3	-	-
B2	1.3	0.3	D-Asp	5%
B3	1.3	0.3	D-Glu	5%
B4	1.3	0.3	D-Val	5%
B5	1.3	0.3	D-Leu	5%

From the analysis by HPLC, we found the %enantiomeric excess (*e.e.*) which represents the enantiopurity of the product, as shown in Equation (5.1) and the % yield of L-Asn·H₂O in the solid product, as shown in Equation (5.2).

$$\%e.e. = \frac{C_L - C_D}{C_L + C_D} \times 100\% = \frac{A_L + A_D}{A_L + A_D} \times 100\% \quad (5.1)$$

where C_L and C_D are the concentration of L-Asn·H₂O and D-Asn·H₂O in the solid product respectively. A_L and A_D are HPLC peak area of L-Asn·H₂O and D-Asn·H₂O in the solid product.

$$\% yield = \frac{m_t}{m_{th}} \times 100\% \quad (5.2)$$

where m_t is the mass of preferred enantiomer produced and m_{th} is maximum mass of the preferred enantiomer obtainable at equilibrium. Since a mass m_s of seed crystals was introduced at the start of the preferential crystallization resulting in a mass m_p of

the preferred enantiomer product, the yield is further defined using $m_t = m_p - m_s$ in Equation (5.2).

5.4.5 Tailor made Inhibition to the Preferential Crystallization of L-Asn·H₂O in a Batch Crystallization.

From Section 5.5.4, we found that D-Asp and D-Glu additives clearly inhibit the nucleation of D-Asn·H₂O. Thus, this section studies the effect of the amount of additive using procedures similar to Section 5.4.3, and using the conditions shown in Table 5.3.

Table 5.3 The conditions of preferential crystallization of L-Asn·H₂O with Tailor-made additives inhibition.

Condition	Supersaturation ratio of DL-Asn·H ₂ O	Additives	% additives
C1	1.3	D-Asp	3%
C2	1.3	D-Asp	5%
C3	1.3	D-Asp	7%
C4	1.3	D-Glu	3%
C5	1.3	D-Glu	5%
C6	1.3	D-Glu	7%

5.5 Results and Discussion

5.5.1 The Preferential Crystallization of L-Asn·H₂O in DL-Asn·H₂O Solution.

The preferential crystallization of L-Asn·H₂O from the DL-Asn·H₂O solution (S=1.3) at 20°C was analyzed for the product purity by HPLC. The solid product concentration of D- and L-Asn·H₂O is shown in Figure 5.5. The amounts of both of the enantiomers increases with time, but the L-Asn·H₂O crystallizes first from

the crystal growth and secondary nucleation of L-Asn·H₂O seeds, and then the D-Asn·H₂O spontaneously nucleates since its degree of supersaturation is still high for an extended period. From this figure, only L-Asn·H₂O crystallizes from 0 h to 1 h and then both D- and L-Asn·H₂O crystallizes after 1 h. In the solution phase, the concentration decreased due to the mass transfer from the liquid phase to the solid phase by crystal growth for L-Asn·H₂O, and by nucleation and subsequent crystal growth for D-Asn·H₂O, as shown in Figure 5.6. Figure 5.7 shows the pathway of D- and L-Asn·H₂O solution from the preferential crystallization of L-Asn·H₂O in the ternary solubility phase diagram between D-Asn·H₂O, L-Asn·H₂O, and water. The pathway moves from a racemic mixture of DL-Asn·H₂O as the concentration of L-Asn·H₂O decreases during the period 0 h to 1 h, and then both D- and L-Asn·H₂O decrease to the racemic mixture at the equilibrium for this crystallization temperature. The %*e.e.* decreases from 100% after 1 h of crystallization as shown in Figure 5.8. In Figure 5.9, the yield of D- and L-Asn·H₂O solid product is shown, the yield of L-Asn·H₂O rapidly increases from the crystal growth of L-Asn·H₂O seed, and eventually the D-Asn·H₂O yield increases from the nucleation of the counter enantiomer and subsequent growth of these nuclei. Thus, the yield of L-Asn·H₂O increases faster than the yield of D-Asn·H₂O. The relationship between the %yield and %*e.e.* is shown in Figure 5.10. The %*e.e.* decreases when the %yield increases.

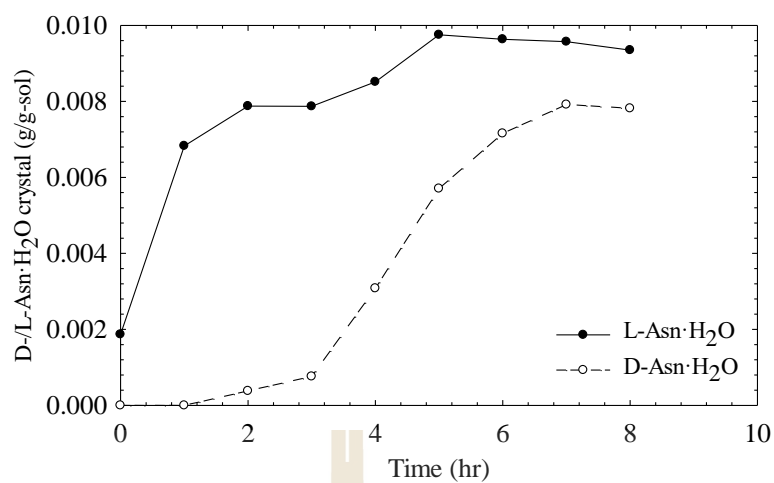


Figure 5.5 Solid crystal of D-/L-Asn·H₂O in the preferential crystallization of L-Asn·H₂O in DL-Asn·H₂O (S=1.3) at 20°C

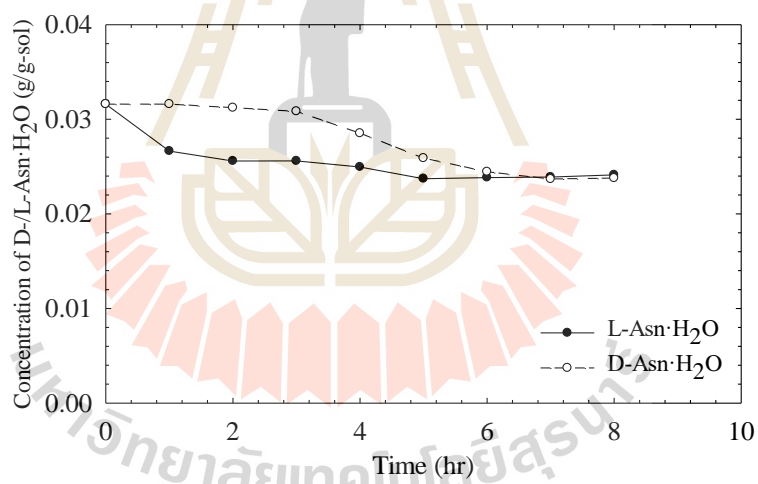


Figure 5.6 Concentration of D-/L-Asn·H₂O in the preferential crystallization of L-Asn·H₂O in DL-Asn·H₂O (S=1.3) at 20°C

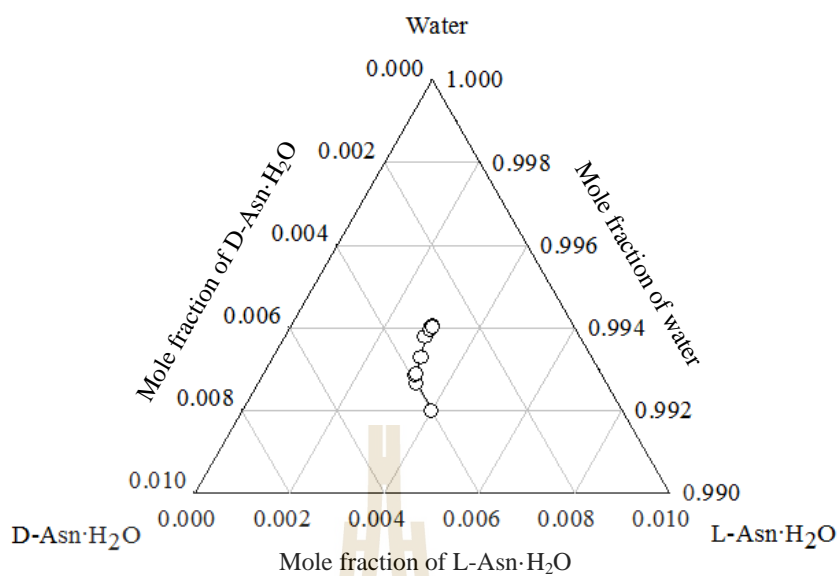


Figure 5.7 Ternary solubility phase diagram of D-/L-Asn·H₂O in DL-Asn·H₂O solution (S=1.3) during the preferential crystallization of L-Asn·H₂O at 20°C.

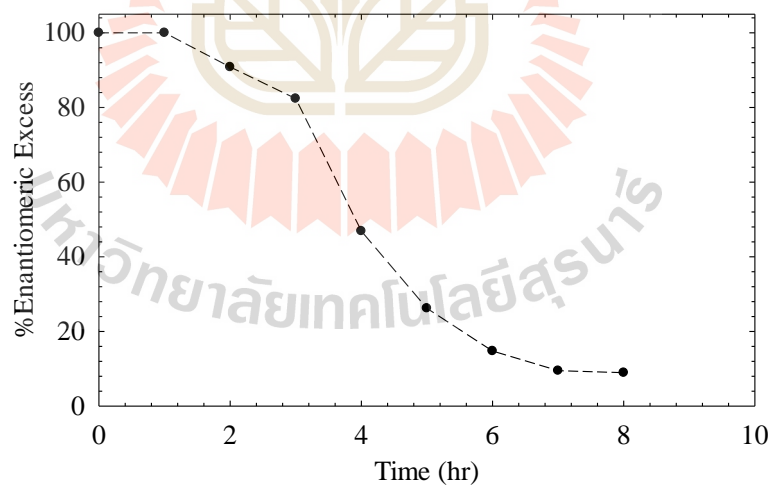


Figure 5.8 %*e.e.* of L-Asn·H₂O in the preferential crystallization of L-Asn·H₂O in DL-Asn·H₂O (S=1.3) at 20°C.

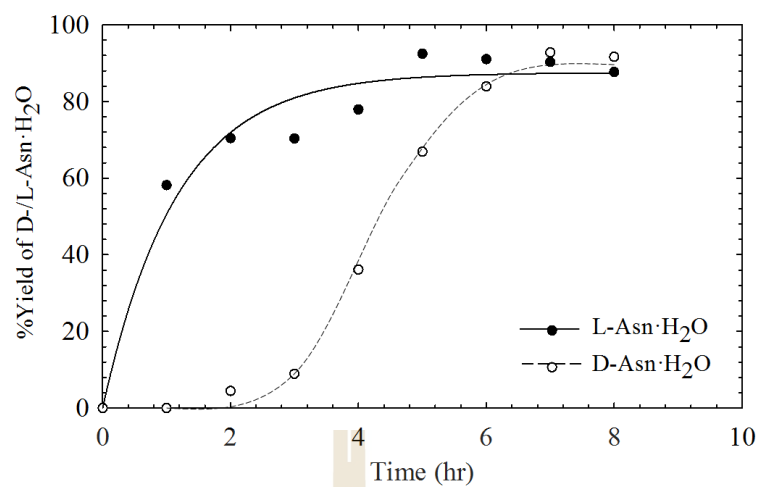


Figure 5.9 % Yield of D-/L-Asn·H₂O in the preferential crystallization of L-Asn·H₂O in DL-Asn·H₂O (S=1.3) at 20°C.

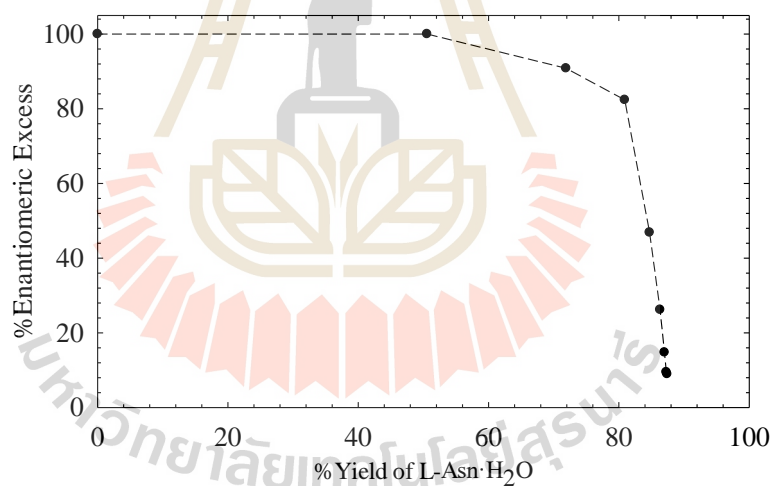


Figure 5.10 The relationship between % yield and % enantiomeric excess of L-Asn·H₂O in the preferential crystallization of L-Asn·H₂O in DL-Asn·H₂O (S=1.3) at 20°C.

5.5.2 Effect of Supersaturation Ratio to the Preferential Crystallization of L-Asn·H₂O from DL-Asn·H₂O.

The preferential crystallization of L-Asn·H₂O from DL-Asn·H₂O at 20°C and constant L-Asn·H₂O seed amount, for varying supersaturation ratio, are shown in this section. We compare supersaturation ratios (S) of 1.1, 1.3, and 1.5. The amount of L-Asn·H₂O crystal in the solution increases when the supersaturation increases, as shown in Figure 5.11, because a higher supersaturation ratio means a higher driving force and a higher amount of excess solute at a constant crystallization temperature. The results for the solid product of D-Asn·H₂O, as shown in Figure 5.12, have a similar trend to the solid product of L-Asn·H₂O as we discussed previously.

The results for %*e.e.* plotted in Figure 5.13 show that at the highest supersaturation ratio, S=1.5, %*e.e.* decreases rapidly within 1 h because the driving force is very high not only for L-Asn·H₂O, which is the preferred enantiomer, but also for D-Asn·H₂O which is the counter enantiomer. Thus, a high initial supersaturation is not optimum for the separation of enantiomers by preferential crystallization because spontaneous nucleation of the counter enantiomer occurs rapidly. In this figure, the %*e.e.* of L-Asn·H₂O from the supersaturation ratio, S=1.1, is 100% for 5.5 h, because it is a low supersaturation ratio. At S=1.1, the spontaneous primary nucleation of both L-Asn·H₂O and D-Asn·H₂O is slow to occur. Thus, the crystallization of D-Asn·H₂O is very slow in the absence of D-Asn·H₂O seeds. The time in which it is possible to create a pure L-Asn·H₂O product is longer. However, the %yield at S=1.1 is lower than the %yield at a higher supersaturation ratio because of the lower concentration and driving force as shown in Figure 5.14. However, when comparing

the maximum yield where the %*e.e.* (and therefore product enantiopurity) is still 100%, the supersaturation ratio, $S=1.1$ is highest, and $S=1.5$ is lowest, as shown in Figure 5.15.

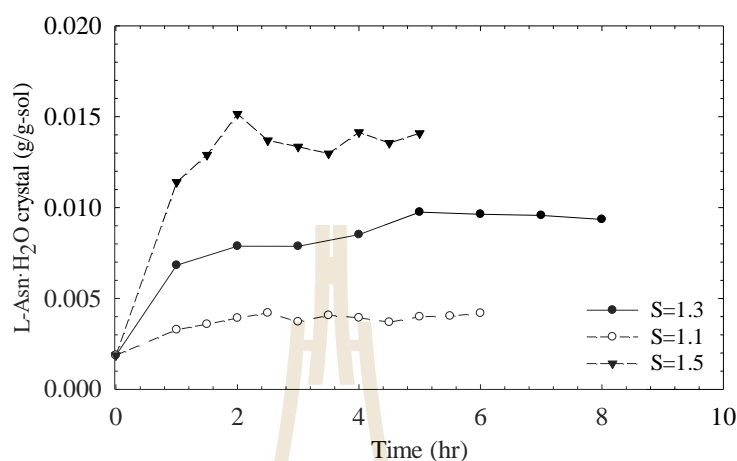


Figure 5.11 Amount of crystalline L-Asn·H₂O in the preferential crystallization of L-Asn·H₂O in DL-Asn·H₂O at 20°C by varying the supersaturation ratio.

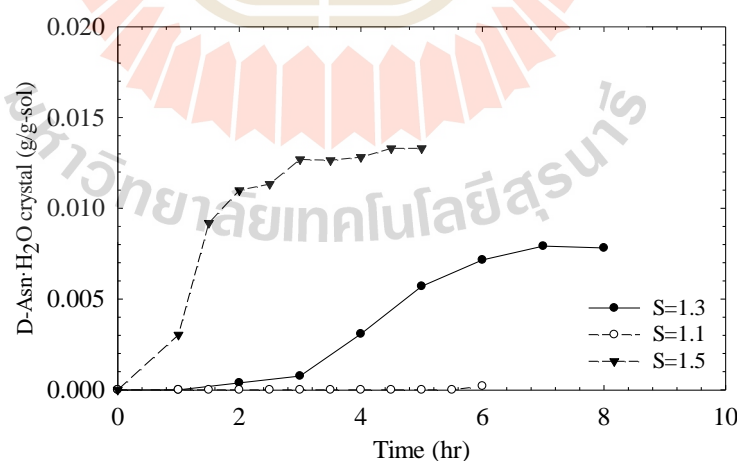


Figure 5.12 Amount of crystalline L-Asn·H₂O in the preferential crystallization of L-Asn·H₂O in DL-Asn·H₂O at 20°C by varying the supersaturation ratio.

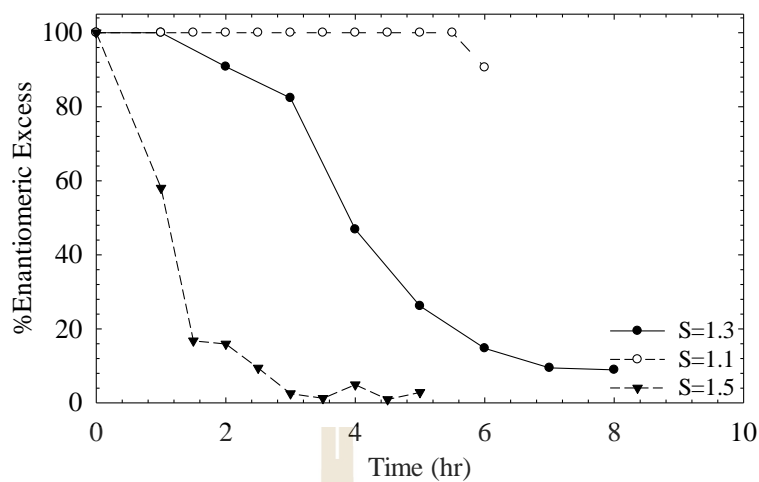


Figure 5.13 % *e.e.* of L-Asn·H₂O in the preferential crystallization of L-Asn·H₂O in DL-Asn·H₂O at 20°C by varying the supersaturation ratio.

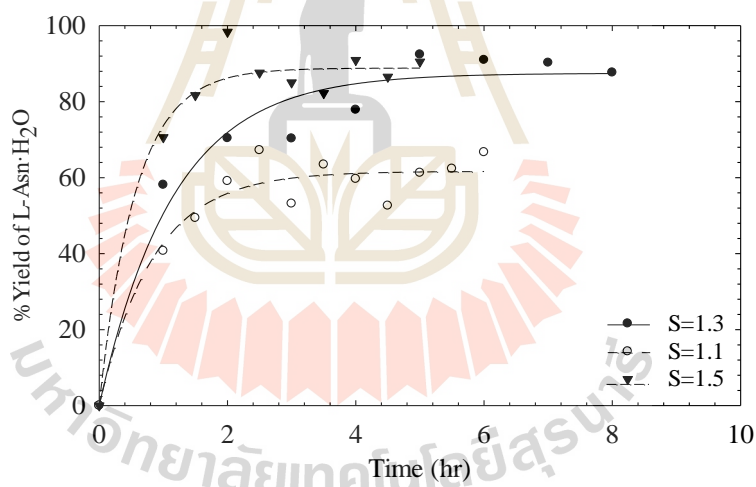


Figure 5.14 % Yield of L-Asn·H₂O in the preferential crystallization of L-Asn·H₂O in DL-Asn·H₂O at 20°C by varying the supersaturation ratio.

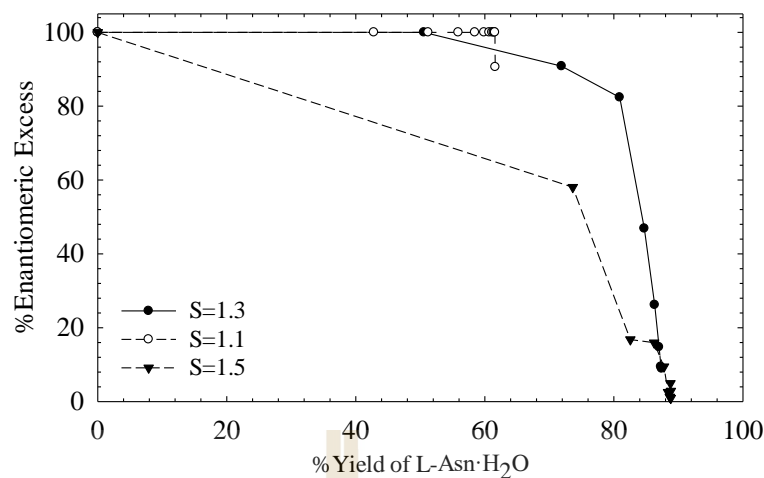


Figure 5.15 The relationship between % yield and % *e.e.* of L-Asn·H₂O in The preferential crystallization of L-Asn·H₂O in DL-Asn·H₂O at 20°C by varying the supersaturation ratio.

5.5.3 Effect of Seed Amount to the Preferential Crystallization of L-Asn·H₂O from DL-Asn·H₂O

A series of preferential crystallizations of L-Asn·H₂O from DL-Asn·H₂O in water, at 20°C, and with supersaturation ratio, $S=1.3$, were performed to determine the effect of variations in the amount of L-Asn·H₂O seeds. The results are presented in this section. The amount of seeds used were 0.075 g, 0.150 g, and 0.300 g based on a solvent content of 150 g water. In Figure 5.16, the amount of L-Asn·H₂O crystal in the suspension increases when time increases, with the highest seed amount (0.3 g of L-Asn·H₂O) giving the highest total L-Asn·H₂O crystal (which also includes the seed weight). The amount of L-Asn·H₂O product, with the seed weight subtracted, is shown in Figure 5.17. The amounts of L-Asn·H₂O crystal from the varying amounts of L-Asn·H₂O seeds are very similar, but the amount from the L-Asn·H₂O crystal product from 0.3 g seeds are slightly higher than the others. From Figure 5.18, in the

preferential crystallization by varying the amount of L-Asn·H₂O seeds, the D-Asn·H₂O crystals, which is the counter enantiomer, spontaneously nucleates at a very similar time and also the crystallization rate of D-Asn·H₂O 0.075 g, and 0.15 g of L-Asn·H₂O seeds. At preferential crystallization with 0.3 g seeds, the D-Asn·H₂O nucleated slightly faster than the others, so, the D-Asn·H₂O in the product is slightly higher than the others. However, the amount of L-Asn·H₂O seeds does not have a strong effect to the nucleation rate and induction time of D-Asn·H₂O.

The %*e.e.* of L-Asn·H₂O for these experiments is shown in Figure 5.19. At 0.3 g seeds, the %*e.e.* begins to decrease after 1 h. This is slightly faster than the other experiments, where the %*e.e.* decreases at 1.5 h. The %*e.e.* results for 0.15, and 0.075 g seeds are very similar. From this figure, D-Asn·H₂O, which is the counter enantiomer, nucleates at almost the same time; this means that the amount of seeds has almost no effect on the time of nucleation of the counter enantiomer.

The %yield of L-Asn·H₂O is shown in Figure 5.20. The %yield of L-Asn·H₂O is highest when using 0.3 g of seeds because it has the highest surface area for crystal growth. Hence, the L-Asn·H₂O can more rapidly transfer from the solution phase to the crystal phase. The relationship between the maximum yield of pure L-Asn·H₂O product (from the fitted curve) and %*e.e.* of L-Asn·H₂O is shown in Figure 5.21. The maximum yield of L-Asn·H₂O with 100% enantiomer excess for the different seed amounts are very close, but the total yield of L-Asn·H₂O with 0.3 g seeds is slightly higher than the others.

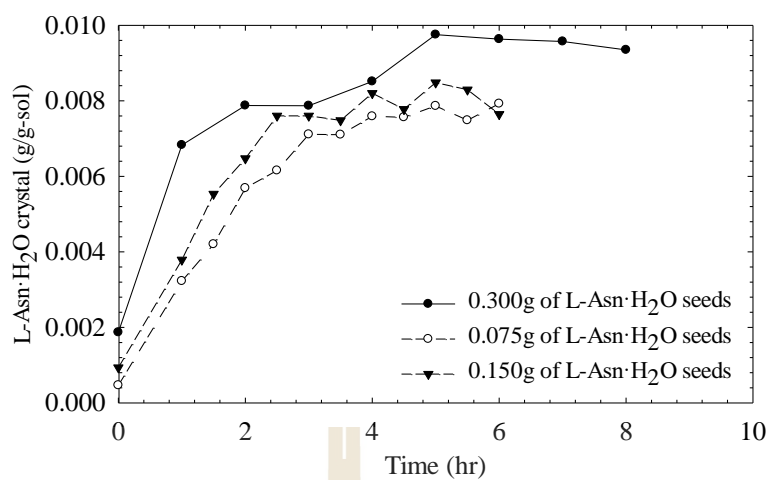


Figure 5.16 Amount of crystal L-Asn·H₂O in the preferential crystallization of L-Asn·H₂O in DL-Asn·H₂O (S=1.3) at 20°C by varying the L-Asn·H₂O seeds.

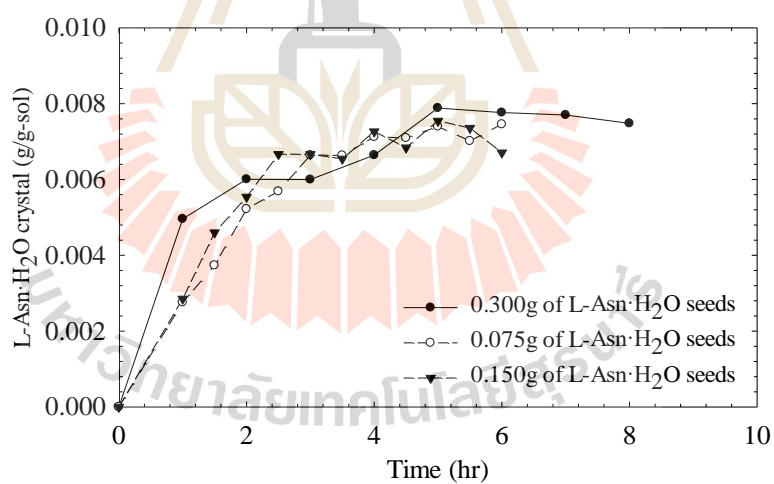


Figure 5.17 Amount of crystal L-Asn·H₂O (excluding seed weight) in the preferential crystallization of L-Asn·H₂O in DL-Asn·H₂O (S=1.3) at 20°C by varying the L-Asn·H₂O seeds.

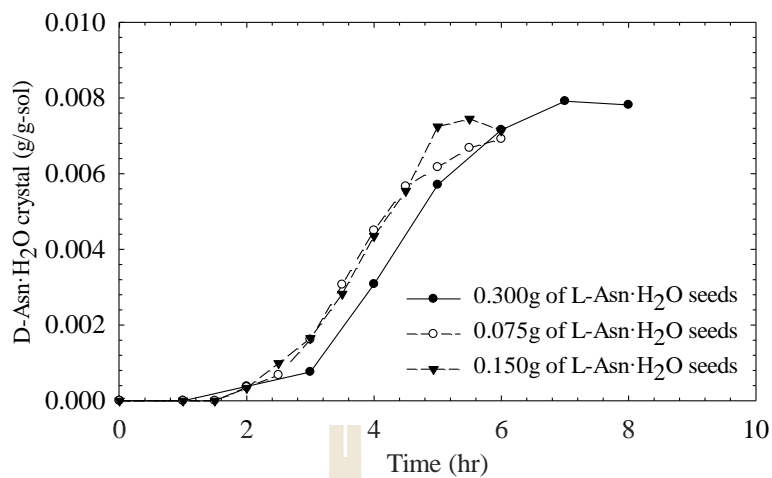


Figure 5.18 Amount of crystal D-Asn·H₂O in the preferential crystallization of L-Asn·H₂O in DL-Asn·H₂O (S=1.3) at 20°C by varying the L-Asn·H₂O seeds.

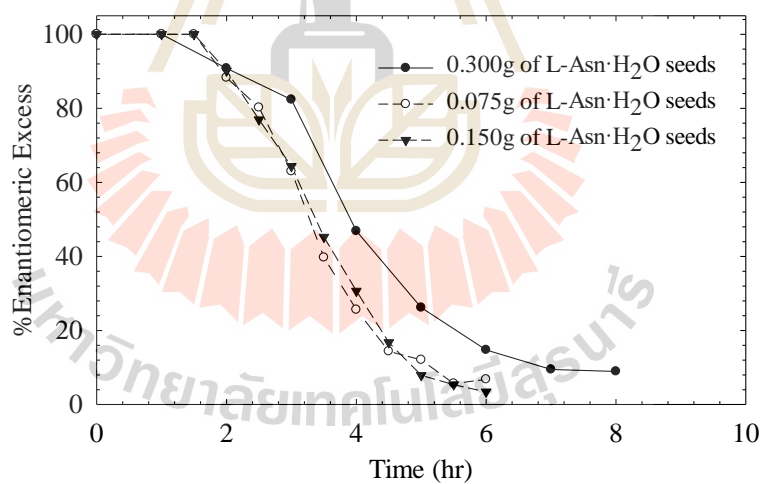


Figure 5.19 % e.e. of L-Asn·H₂O in the preferential crystallization of L-Asn·H₂O in DL-Asn·H₂O (S=1.3) at 20°C by varying the amount of L-Asn·H₂O seed.

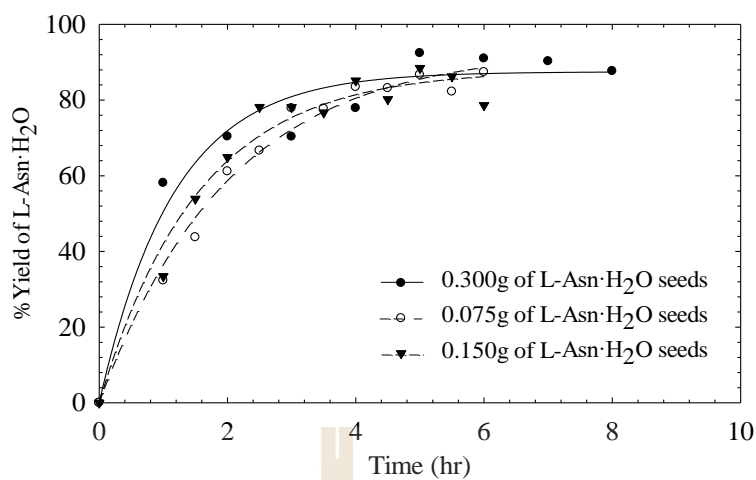


Figure 5.20 % Yield of L-Asn·H₂O in the preferential crystallization of L-Asn·H₂O in DL-Asn·H₂O ($S=1.3$) at 20°C by varying the amount of L-Asn·H₂O seed.

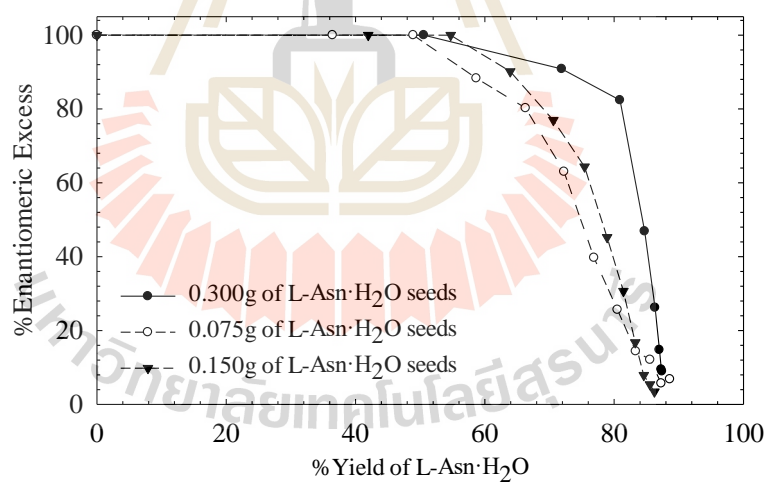


Figure 5.21 The relationship between % yield and % *e.e.* of L-Asn·H₂O in the preferential crystallization of L-Asn·H₂O in DL-Asn·H₂O ($S=1.3$) at 20°C by varying the amount of L-Asn·H₂O seed.

5.5.4 Effect of Tailor-Made Additives to the Preferential Crystallization of L-Asn·H₂O from DL-Asn·H₂O.

The effect of tailor-made additives to the preferential crystallization of L-Asn·H₂O from DL-Asn·H₂O in water was studied in a small crystallizer with supersaturation ratio $S=1.3$ at 30°C. The L-Asn·H₂O crystal in the suspension increases when time increases, as shown in Figure 5.22. The amount of L-Asn·H₂O crystal product from the preferential crystallization of L-Asn·H₂O in DL-Asn·H₂O without additives and with D-Val and D-Leu additives show a very similar trend, but with D-Glu and D-Asp additives there is a lower amount of the L-Asn·H₂O crystal in solution for an equivalent time in the experiment without additives. The amount of D-Asn·H₂O crystal in the suspension, as shown in Figure 5.23, from DL-Asn·H₂O solution without additives and with D-Val and D-Leu additives are very similar. This indicates that D-Leu and D-Val have almost no inhibiting effect on the nucleation of D-Asn·H₂O (which is the counter enantiomer). For preferential crystallization of L-Asn·H₂O from DL-Asn·H₂O with D-Glu and D-Asp additives, the D-Asn·H₂O solid crystal is retarded by D-Glu and D-Asp, especially for D-Asp which can inhibit the nucleation of D-Asn·H₂O for a period of 10 h. These effects follow the rule of reversal, where the additive inhibits the enantiomer with the same absolute configuration. However, from Figure 5.22, L-Asn·H₂O the amount of crystal from preferential crystallization of L-Asn·H₂O in DL-Asn·H₂O with D-Asp and D-Glu is lower than the others at the same time. This means that D-Asp and D-Glu not only inhibits the nucleation of D-Asn·H₂O as a counter enantiomer, but they also slightly inhibit the crystal growth rate of L-Asn·H₂O. These results do not follow to the rule of reversal, in that the additive do not only have an effect on the enantiomer with the same absolute

configuration. We also confirm the effect of D-Asp and D-Glu to L-Asn·H₂O from the crystal growth rate and nucleation results in Chapter III and Chapter IV respectively.

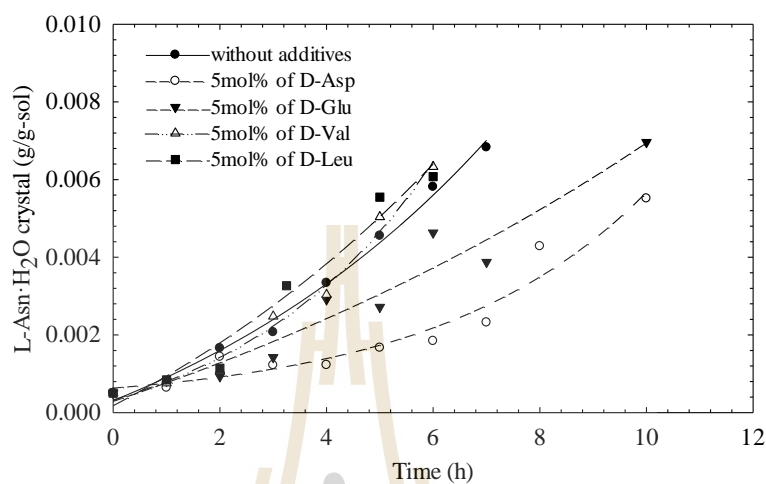


Figure 5.22 Amount of L-Asn·H₂O produced in the preferential crystallization of L-Asn·H₂O in DL-Asn·H₂O with 5 mol% of D-amino acid additives ($S=1.3$) at 30°C.

The %*e.e.* of the L-Asn·H₂O solid product from preferential crystallization of L-Asn·H₂O in DL-Asn·H₂O without and with D-Val and D-Leu additives decreases from 100%*e.e.* at around 4 h, but with the D-Glu additive the decrease occurs at 7 h, and with D-Asp additive the result is 10 h. Thus, the retarding of nucleation of the counter enantiomer is clear when using D-Glu and D-Asp as additives, as shown in Figure 5.24.

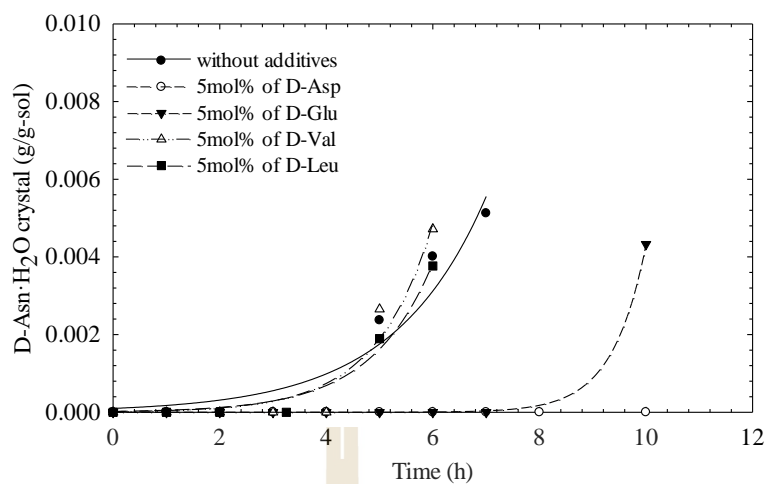


Figure 5.23 Amount of D-Asn·H₂O produced in the preferential crystallization of L-Asn·H₂O in DL-Asn·H₂O with 5 mol% of D-amino acid additives (S=1.3) at 30°C with D-amino acid additives.

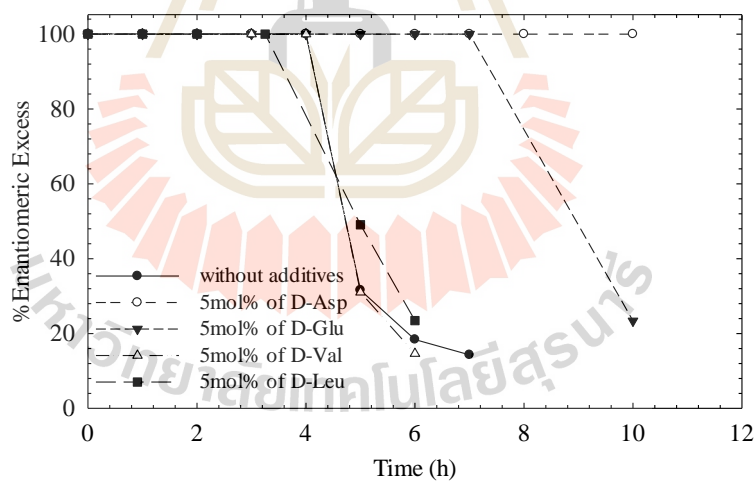


Figure 5.24 % e.e. of L-Asn·H₂O in the preferential crystallization of L-Asn·H₂O in DL-Asn·H₂O with 5 mol% of D-amino acid additives (S=1.3) at 30°C.

The % yield of L-Asn·H₂O from the PC experiments is shown in Figure 5.25. The yield of L-Asn·H₂O from preferential crystallization with D-Glu and D-Asp are lower than without additives, and also lower than when D-Val and D-Leu are used as additives. In Figure 5.26, the maximum yield of L-Asn·H₂O at 100% *e.e.* from preferential crystallization with D-Asp is 44% yield, and with D-Glu is 30%. The maximum yield of L-Asn·H₂O from DL-Asn·H₂O without additives, and when D-Val and D-Leu are used as additives is around 24%.

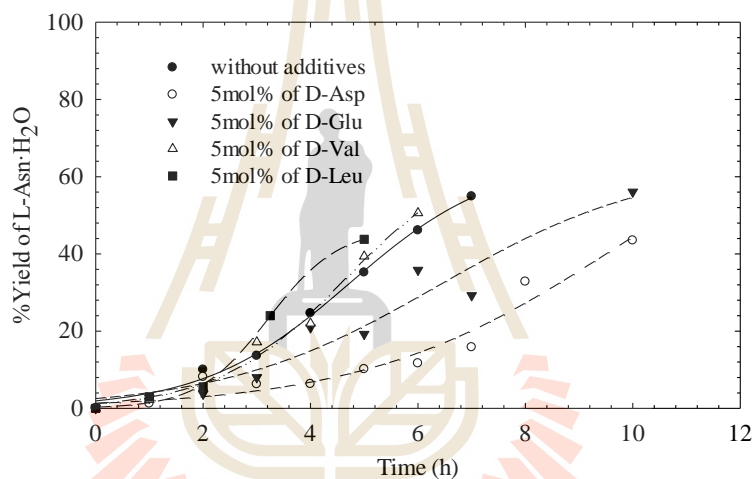


Figure 5.25 % Yield of L-Asn·H₂O in the preferential crystallization of L-Asn·H₂O in DL-Asn·H₂O with 5 mol% of D-amino acid additives (*S*=1.3) at 30°C.

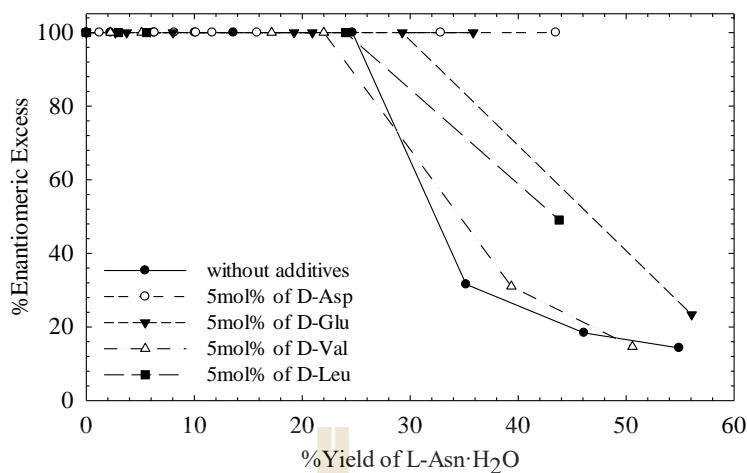


Figure 5.26 The relationship between % yield and % *e.e.* of L-Asn·H₂O in the preferential crystallization of L-Asn·H₂O in DL-Asn·H₂O with 5 mol% of D-amino acid additives (*S*=1.3) at 30°C.

5.5.5 Effect of Amount of Additive to the Preferential Crystallization of L-Asn·H₂O from DL-Asn·H₂O.

From the previous section, it is clear that the preferential crystallization of L-Asn·H₂O from DL-Asn·H₂O solutions with D-Glu and D-Asp additives increases the yield and crystallization time of the pure L-Asn·H₂O solid product. Thus, here we study the effect of the amount of these additives to the preferential crystallization.

5.5.5.1 Effect of D-Aspartic Acid Additives

We performed the preferential crystallization of L-Asn·H₂O from DL-Asn·H₂O with 3, 5, and 7 mol% of D-Asp additive compared to the total amount of DL-Asn·H₂O used. In Figure 5.27, the amount of L-Asn·H₂O crystal in DL-Asn·H₂O solution with and without D-Asp shows a similar trend, but for 7 mol% of D-Asp the amount of L-Asn·H₂O crystal is slightly lower than in the other experiments. In Figure 5.28, The amount of D-Asn·H₂O crystal in the DL-Asn·H₂O

suspension with the additive D-Asp is lower than from PC from DL-Asn·H₂O without additives, at an equivalent time, because of the inhibition of nucleation and crystal growth of D-Asn·H₂O by the D-Asp additive. Increasing amounts of D-Asp increases the time available to produce pure L-Asn·H₂O, with additional inhibition of D-Asn·H₂O nucleation. Concentrations of D-Asp of 3, 5, and 7 mol% increase the time available to crystallize pure L-Asn·H₂O from 1 h to 6, 7, and 10 h respectively.

The pathway of D- and L-Asn·H₂O solution from the preferential crystallization of L-Asn·H₂O from DL-Asn·H₂O with D-Asp additives can be described in the ternary solubility phase diagram between D-Asn·H₂O, L-Asn·H₂O, and water. Here, we assume that the mole fraction of the D-Asp additive is very small. The diagrams are shown in Figure 5.29 - 5.31 for 3, 5, and 7 mol% of D-Asp respectively. The pathway of the concentration in the ternary solubility phase diagram moves to the point that L-Asn in the solution decreases, but D-Asn in the solution is constant until the nucleation of D-Asn·H₂O occurs. These pathways show the longer trend of the line to a lower amount of L-Asn·H₂O in the solution when increasing the amount of the D-Asp additive. We also show Figure 5.32, which combines all the preferential crystallizations, with 3, 5, and 7 mol% D-Asp additive.

The time at 100% enantiomeric excess of L-Asn·H₂O with D-Asp additive increases when the amount of D-Asp increases from 3 mol% to 7 mol% from 1 h to 6 h, 7 h and 10 h for 3, 5, and 7 mol% of D-Asp respectively, as shown in Figure 5.33. In Figure 5.34, the yield of L-Asn·H₂O product from preferential crystallization of L-Asn·H₂O from DL-Asn·H₂O with 3 and 5 mol% additive is slightly lower than DL-Asn·H₂O without additives. It means that D-Asp also inhibits the crystal growth rate of L-Asn·H₂O, which we discussed in the previous section. However, in

the preferential crystallization of L-Asn·H₂O from DL-Asn·H₂O with 7 mol% of D-Asp additive, there is a low yield of L-Asn·H₂O because of the inhibition of D-Asp to L-Asn·H₂O, and also the effect of additives on the solubility of DL-Asn·H₂O; the additive at this level increases the solubility of the Asn species, so the yield is lower than in the other experiments. In Figure 5.35, the %*e.e.* decreases when the yield increases, however the yield of L-Asn·H₂O at 100%*e.e.* increases when the amount of D-Asp additives increases from 3 mol% to 5 mol% of D-Asp but the yield decreased when using 7 mol% of D-Asp. The maximum yield of L-Asn·H₂O solid product and maximum time of 100%*e.e.* in the preferential crystallization with D-Asp are shown in Figure 5.36. The maximum time of 100%*e.e.* increases when the D-Asp additive increases but the yield decreases when using 7 mol% of D-Asp because the inhibition of L-Asn·H₂O and solubility change, which we discussed previously.

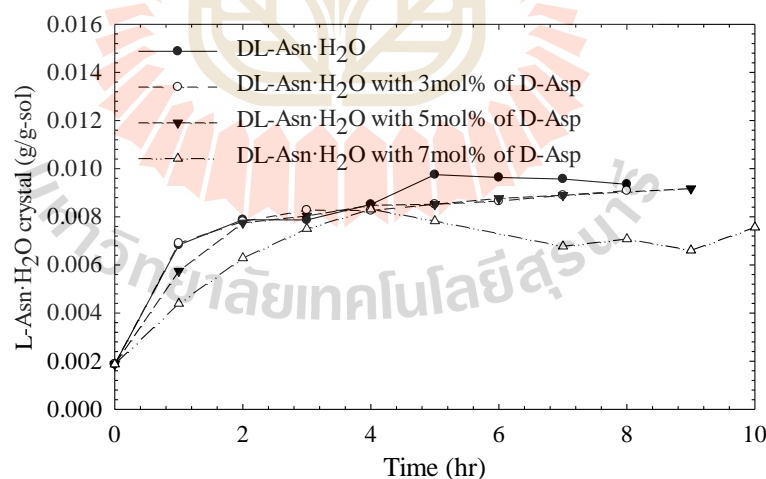


Figure 5.27 Amount of crystal of L-Asn·H₂O in the preferential crystallization of L-Asn·H₂O in DL-Asn·H₂O with D-Asp additives (S=1.3) at 20°C.

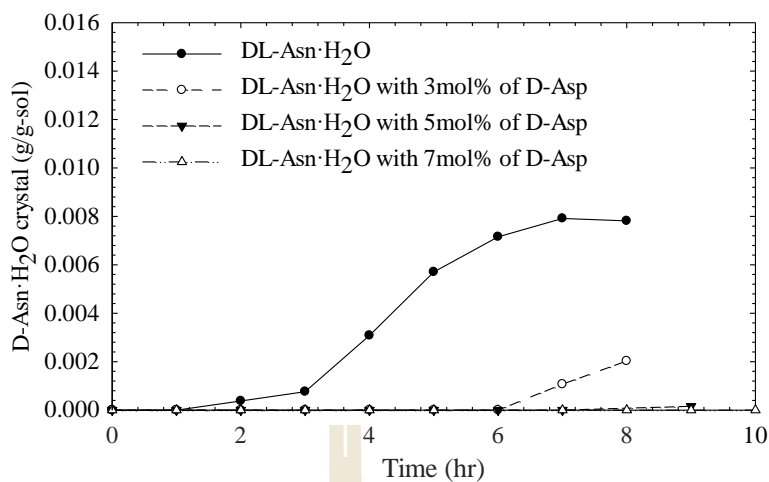


Figure 5.28 Amount of crystal of D-Asn·H₂O in the preferential crystallization of L-Asn·H₂O in DL-Asn·H₂O with D-Asp additives (S=1.3) at 20°C.

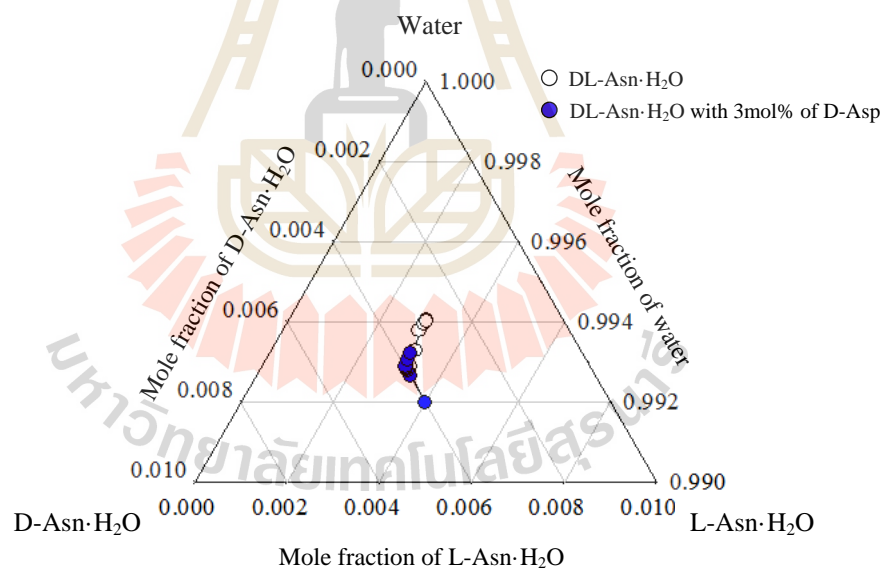


Figure 5.29 Ternary solubility phase diagram of D-/L-Asn·H₂O in DL-Asn·H₂O solution (S=1.3) during the preferential crystallization of L-Asn·H₂O at 20°C with 3 mol% of D-Asp additives.

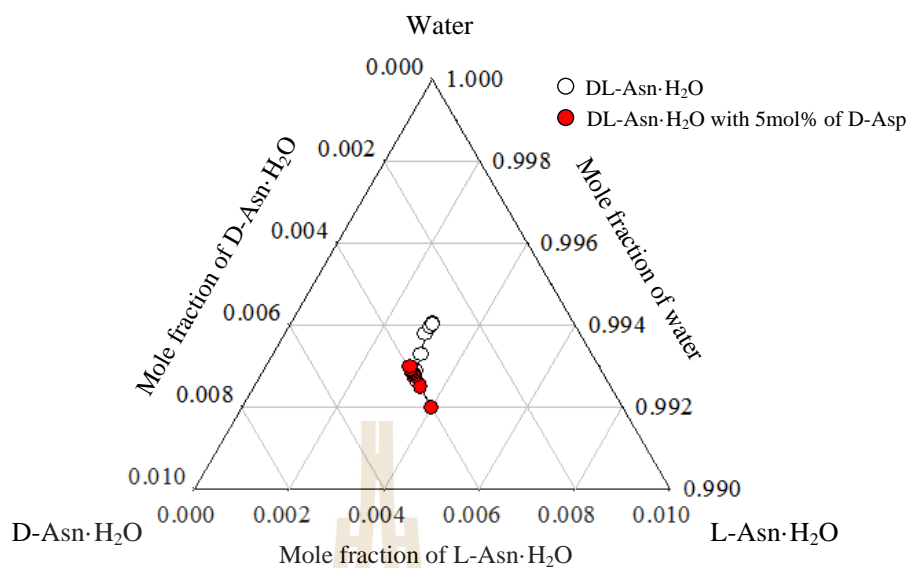


Figure 5.30 Ternary solubility phase diagram of D-/L-Asn·H₂O in DL-Asn·H₂O solution ($S=1.3$) during the preferential crystallization of L-Asn·H₂O at 20°C with 5 mol% of D-Asp additives.

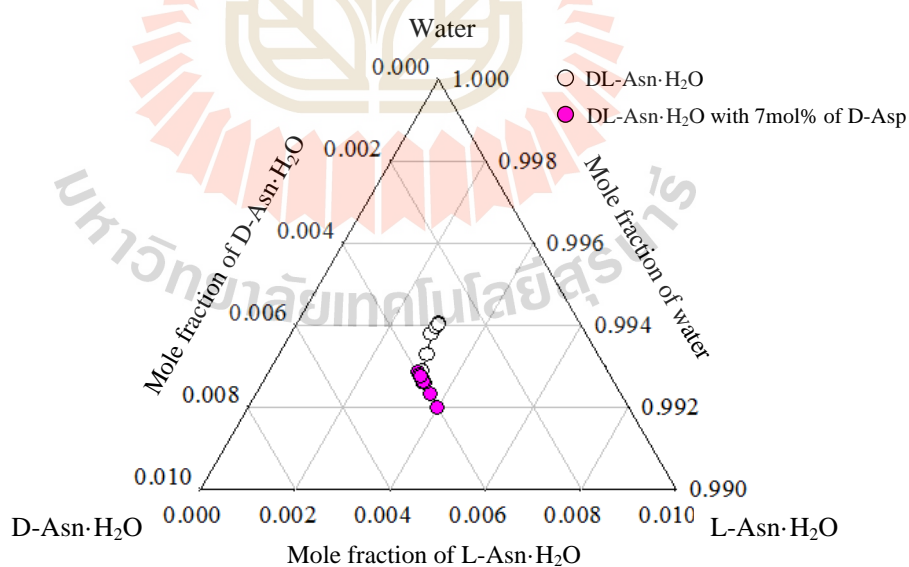


Figure 5.31 Ternary solubility phase diagram of D-/L-Asn·H₂O in DL-Asn·H₂O solution ($S=1.3$) during the preferential crystallization of L-Asn·H₂O at 20°C with 7 mol% of D-Asp additives.

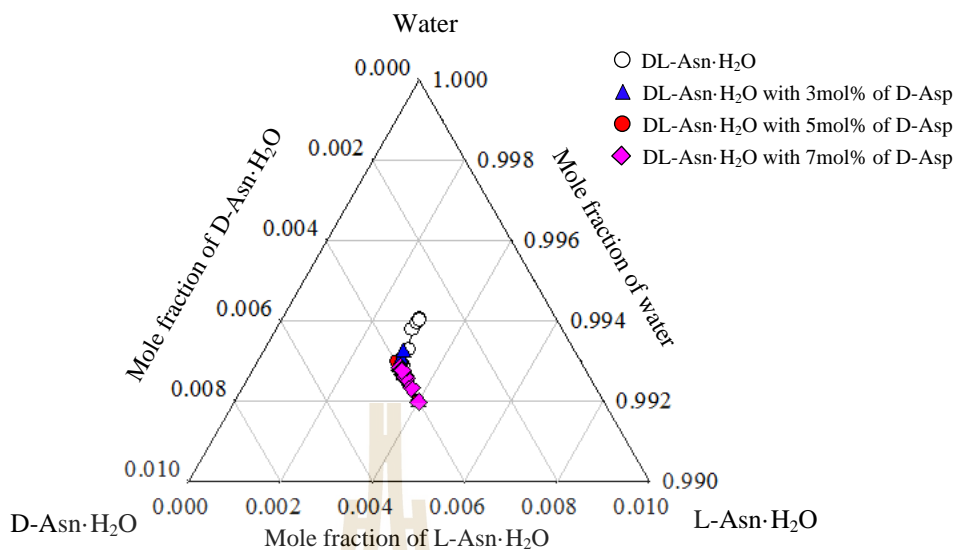


Figure 5.32 Ternary solubility phase diagram of D-/L-Asn·H₂O in DL-Asn·H₂O solution ($S=1.3$) during the preferential crystallization of L-Asn·H₂O at 20°C with D-Asp additives.

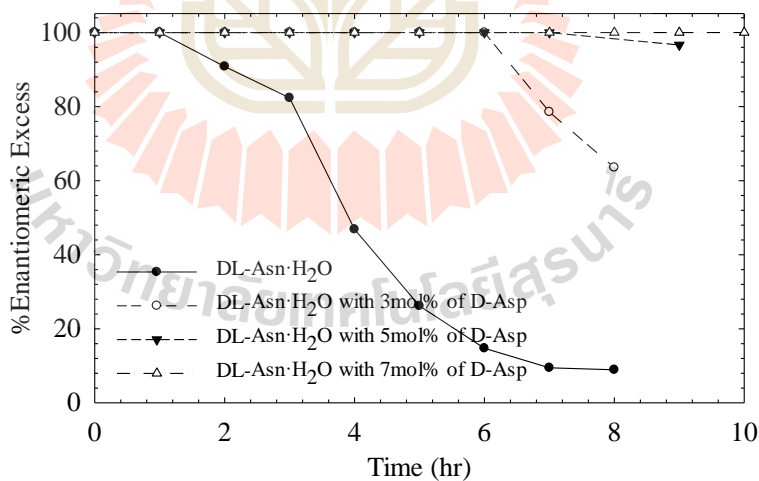


Figure 5.33 % e.e. of L-Asn·H₂O in the preferential crystallization of L-Asn·H₂O in DL-Asn·H₂O with D-Asp additives ($S=1.3$) at 20°C.

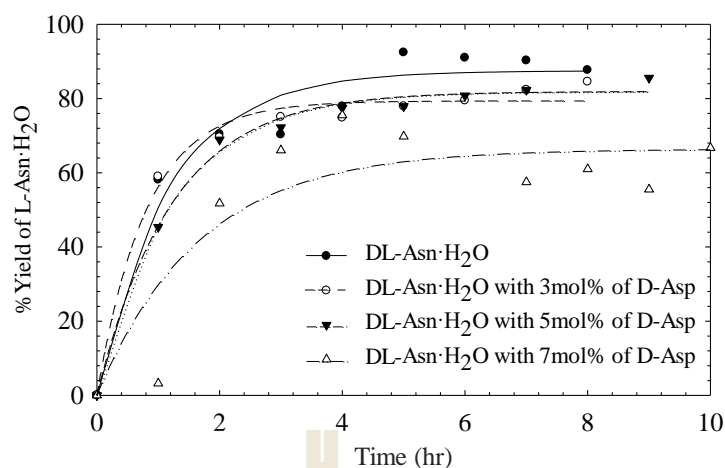


Figure 5.34 % Yield of L-Asn·H₂O in the preferential crystallization of L-Asn·H₂O in DL-Asn·H₂O with D-Asp additives (S=1.3) at 20°C.

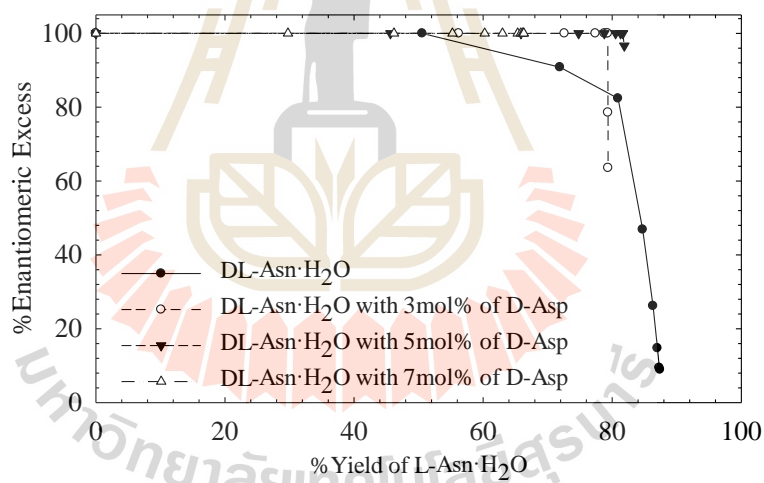


Figure 5.35 The relationship between % yield and % *e.e.* of L-Asn·H₂O in the preferential crystallization of L-Asn·H₂O in DL-Asn·H₂O with D-Asp additives (S=1.3) at 20°C.

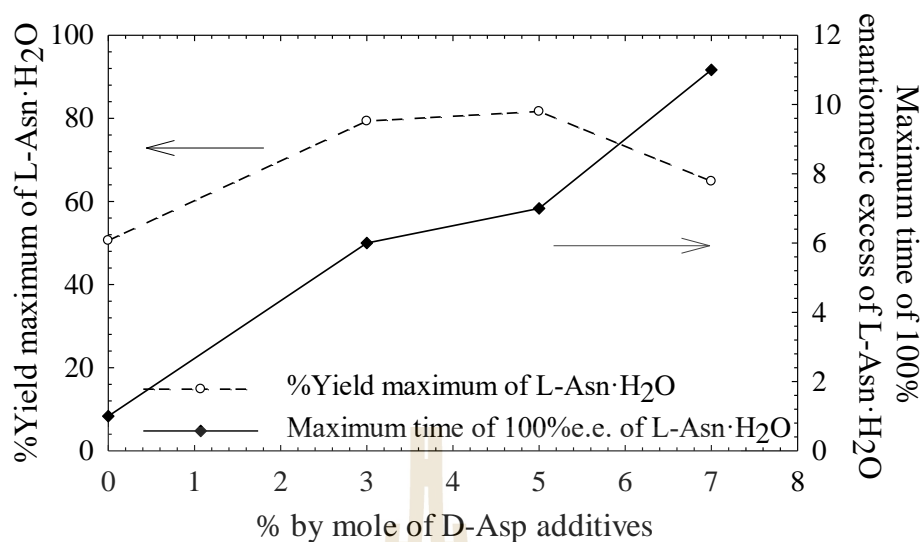


Figure 5.36 % Maximum of yield of L-Asn·H₂O in the preferential crystallization of L-Asn·H₂O in DL-Asn·H₂O without and with 3, 5, and 7% by mole of D-Asp additives at 20°C.

5.5.5.2 Effect of D-Glutamic Acid Additives

The effect of the amount of D-Glu additive to the preferential crystallization of L-Asn·H₂O in DL-Asn·H₂O is shown in this section. The L-Asn·H₂O solid crystal product in DL-Asn·H₂O without and with D-Glu are not significantly different, as shown in Figure 5.37. The D-Asn·H₂O solid crystal product in DL-Asn·H₂O with D-Glu are retarded because of the inhibition of D-Glu to the nucleation and growth of D-Asn·H₂O. The increase of D-Glu from 3 to 7 mol% increased the time of inhibition. Thus, D-Asn·H₂O crystallizes slower when a higher amount of D-Glu additives is used, as shown in Figure 5.38. The time of 100% enantiomeric excess of L-Asn·H₂O from DL-Asn·H₂O with 7 mol% of D-Glu is 3.5 h, and with 3, and 5 mol% D-Glu the time is 2.5 h. Thus, the 3 mol% and 5 mol% of D-Glu additives is quite similar, but in the case of 7 mol% the time of 100% *e.e.* is clearly increased, as shown

in Figure 5.39. In Figure 5.40, the yield of L-Asn·H₂O is lower when using a higher amount of D-Glu additives because the D-Glu not only inhibits the D-Asn·H₂O nucleation but it also inhibits the crystal growth of L-Asn·H₂O, as discussed in Chapters III and IV. In Figure 5.41, the %*e.e.* decreases when the %yield increases, however the %yield of L-Asn·H₂O at 100%*e.e.* increases when the amount of D-Glu additive increases. The maximum %yield of L-Asn·H₂O from DL-Asn·H₂O with D-Glu shows that the changes in the amount of D-Glu from 3 to 7 mol% does not significantly alter the maximum yield; the maximum yield is around 64-70%, but their %yield increases from the DL-Asn·H₂O without additives case, where %yield is approximately 50%.

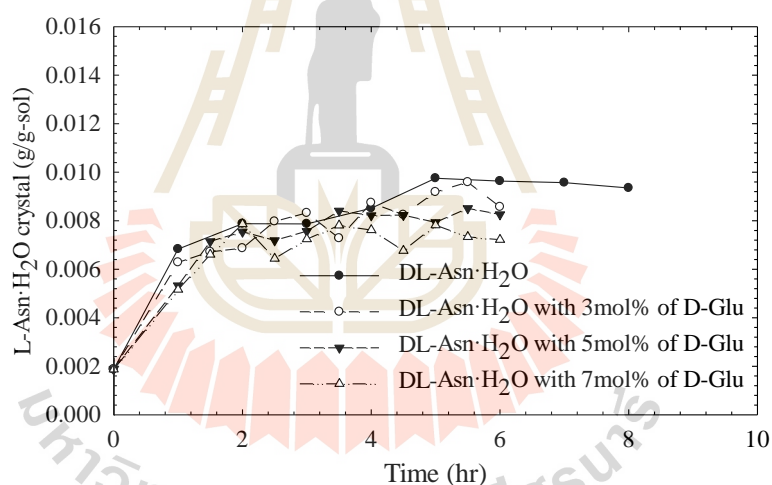


Figure 5.37 Amount of L-Asn·H₂O crystal in the preferential crystallization of L-Asn·H₂O in DL-Asn·H₂O with D-Glu additives (*S*=1.3) at 20°C.

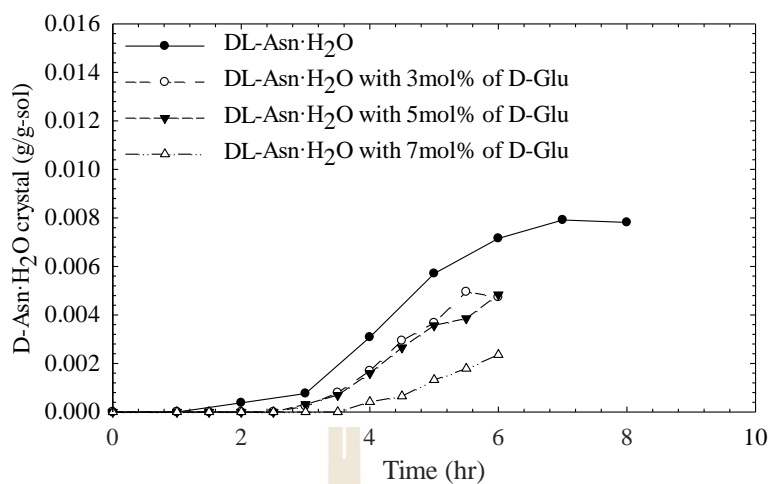


Figure 5.38 Amount of D-Asn·H₂O crystal in the preferential crystallization of L-Asn·H₂O in DL-Asn·H₂O with D-Glu additives (S=1.3) at 20°C.

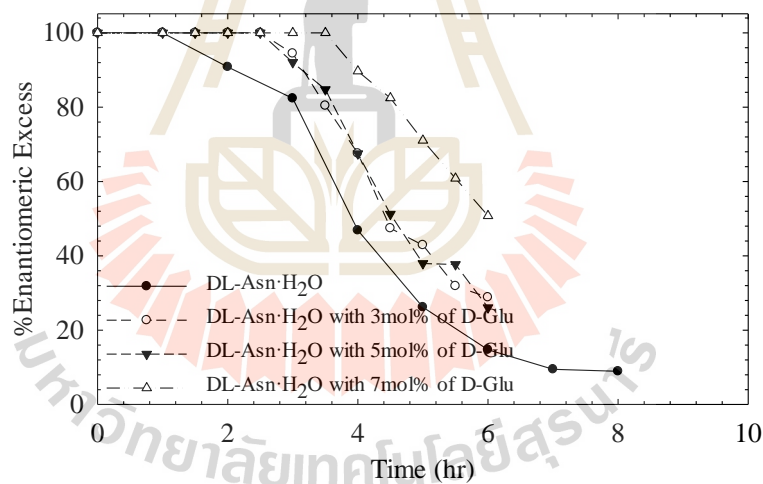


Figure 5.39 %e.e. of L-Asn·H₂O in the preferential crystallization of L-Asn·H₂O in DL-Asn·H₂O with D-Glu additives (S=1.3) at 20°C.

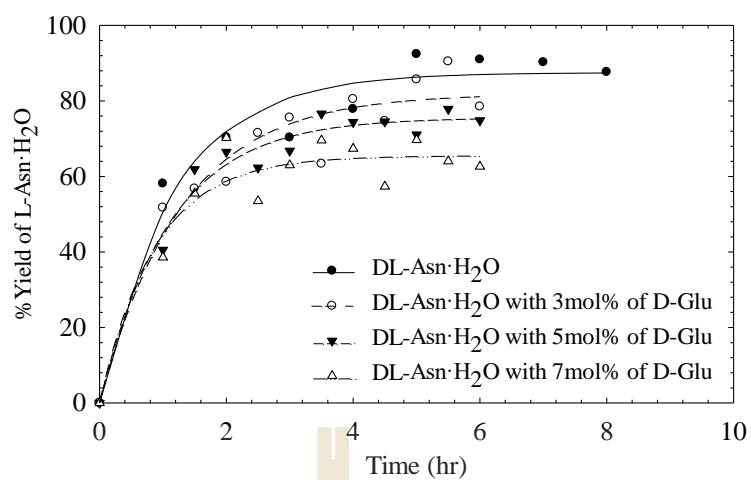


Figure 5.40 % Yield of L-Asn·H₂O in the preferential crystallization of L-Asn·H₂O in DL-Asn·H₂O with D-Glu additives ($S=1.3$) at 20°C.

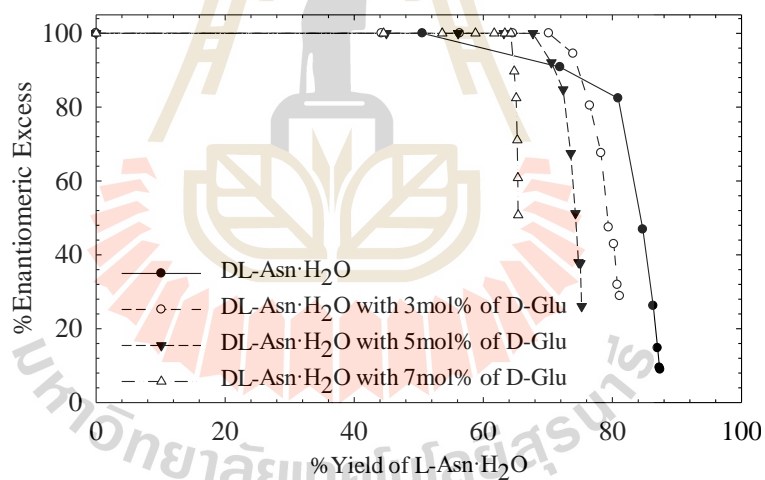


Figure 5.41 The relationship between % yield and % *e.e.* of L-Asn·H₂O in the preferential crystallization of L-Asn·H₂O in DL-Asn·H₂O with D-Glu additives ($S=1.3$) at 20°C.

5.6 Conclusions

The preferential crystallization of L-Asn·H₂O from DL-Asn·H₂O in water was studied. When the supersaturation ratio of DL-Asn·H₂O increases, the crystallization rate including nucleation and crystal growth rate increases. However, the purity of L-Asn·H₂O product from DL-Asn·H₂O and maximum %yield of pure L-Asn·H₂O product is lower than at a lower supersaturation ratio. However, at very low supersaturation ratio, the total yield of L-Asn·H₂O is very low. An increasing amount of L-Asn·H₂O seeds results in an increased yield of L-Asn·H₂O but did not make the nucleation of D-Asn·H₂O occur faster.

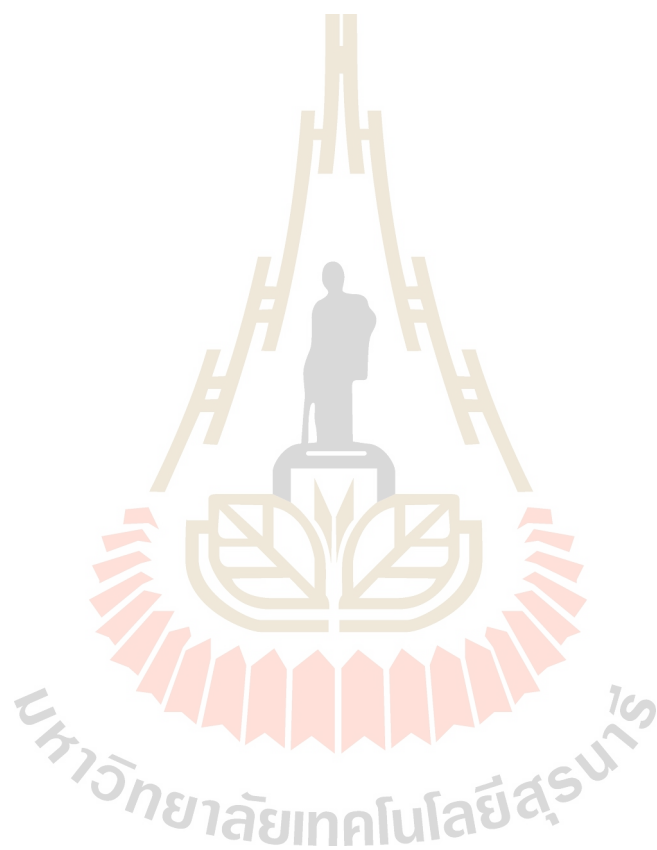
5 mol% of D-Val and D-Leu additives do not change the crystallization pathway of D- and L-Asn·H₂O in the preferential crystallization of L-Asn·H₂O from DL-Asn·H₂O solution. However, 5 mol% of D-Glu and D-Asp additives increase the time to produce pure L-Asn·H₂O solid product by inhibiting the nucleation of D-Asn·H₂O, which is the counter enantiomer. The %yield of L-Asn·H₂O also increases when using D-Glu and D-Asp additives especially for D-Asp additives. An increasing amount of D-Asp additives increases the time of pure L-Asn·H₂O crystallization. The total yield of L-Asn·H₂O decreases when using a higher amount of additives when compared to DL-Asn·H₂O without additives, because the D-Asp inhibits both D- and L-Asn·H₂O, and also changes the solubility. The time of crystallization of pure L-Asn·H₂O from the preferential crystallization of L-Asn·H₂O from DL-Asn·H₂O with D-Glu additives increases when the amount of D-Glu increases; nevertheless, the maximum yield of pure L-Asn·H₂O product is very similar for D-Glu 3-7 mol%.

5.7 References

- Angelov, I., Raisch, J., Elsner, M. P., and Seidel-Morgenstern, A. 2008. Optimal operation of enantioseparation by batch-wise preferential crystallization. **Chemical Engineering Science** 63 (5):1282-1292.
- Beilles, S., Cardinael, P., Ndzié, E., Petit, S., and Coquerel, G. 2001. Preferential crystallisation and comparative crystal growth study between pure enantiomer and racemic mixture of a chiral molecule: 5-ethyl-5-methylhydantoin. **Chemical Engineering Science** 56 (7):2281-2294.
- Buhse, T., Kondepudi, D. K., and Hoskins, B. 1999. Kinetics of chiral resolution in stirred crystallization of D/L-glutamic acid. **Chirality** 11 (4):343-348.
- Czapla, F., Haida, H., Elsner, M. P., Lorenz, H., and Seidel-Morgenstern, A. 2009. Parameterization of population balance models for polythermal auto seeded preferential crystallization of enantiomers. **Chemical Engineering Science** 64 (4):753-763.
- Eicke, M. J., Levilain, G., and Seidel-Morgenstern, A. 2013. Efficient Resolution of Enantiomers by Coupling Preferential Crystallization and Dissolution. Part 2: A Parametric Simulation Study to Identify Suitable Process Conditions. **Crystal Growth and Design** 13 (4):1638-1648.
- Elsner, M. P., Ziomek, G., and Seidel-Morgenstern, A. 2009. Efficient separation of enantiomers by preferential crystallization in two coupled vessels. **AIChE Journal** 55 (3):640-649.
- Jacques, J., Collet, A., and Wilen, S. H. 1981. **Enantiomers, Racemates, and Resolutions**. New York: Wiley.

- Levilain, G., Eicke, M. J., and Seidel-Morgenstern, A. 2012. Efficient Resolution of Enantiomers by Coupling Preferential Crystallization and Dissolution. Part 1: Experimental Proof of Principle. **Crystal Growth and Design** 12 (11):5396-5401.
- Matsuoka, M. 1997. Purity Drop in Optical Resolution of Racemic Mixtures. 667:59-72.
- Petruševska-Seebach, K., Seidel-Morgenstern, A., and Elsner, M. P. 2011. Preferential crystallization of L-asparagine in water. **Crystal Growth and Design** 11 (6):2149-2163.
- Petruševska-Seebach, K., Würges, K., Seidel-Morgenstern, A., Lütz, S., and Elsner, M. P. 2009. Enzyme-assisted physicochemical enantioseparation processes—Part II: Solid–liquid equilibria, preferential crystallization, chromatography and racemization reaction. **Chemical Engineering Science** 64 (10):2473-2482.
- Profir, V. M., and Matsuoka, M. 2000. Processes and phenomena of purity decrease during the optical resolution of dl-threonine by preferential crystallization. **Colloids and Surfaces A: Physicochemical and Engineering Aspects** 164 (2–3):315-324.
- Srimahaprom, W., and Flood, A. E. 2013. Crystal growth rates and optical resolution of dl-methionine hydrochloride by preferential crystallization from aqueous solution. **Journal of Crystal Growth** 362:88-92.
- Svang-Ariyaskul, A., Koros, W. J., and Rousseau, R. W. 2009. Chiral separation using a novel combination of cooling crystallization and a membrane barrier: Resolution of DL-glutamic acid. **Chemical Engineering Science** 64 (9):1980-1984.

Würges, K., Petrusevska, K., Serci, S., Wilhelm, S., Wandrey, C., Seidel-Morgenstern, A., Elsner, M. P., and Lütz, S. 2009. Enzyme-assisted physicochemical enantioseparation processes: Part I. Production and characterization of a recombinant amino acid racemase. **Journal of Molecular Catalysis B: Enzymatic** 58 (1-4):10-16.



CHAPTER VI

CRYSTAL SIZE DISTRIBUTION DURING THE PREFERENTIAL CRYSTALLIZATION OF L-ASPARAGINE MONOHYDRATE WITH THE INHIBITIONS BY TAILOR-MADE ADDITIVES

6.1 Abstract

The result of preferential crystallization is focused on the product yield and purity, but the crystal size distribution (CSD) is also important for industrial scale production because the size of crystals can have a significant impact in many aspects such as filtration and recovery of the product. This chapter investigates the particle size distribution of D- and L-Asn·H₂O during the preferential crystallization of L-Asn·H₂O from DL-Asn·H₂O with and without D-Glu and D-Asp additives. The experiments were studied in 300 g of water at a supersaturation ratio 1.3 at 20°C, with 0.6 g of L-Asn·H₂O seeds. The product yield and purity was analyzed by HPLC every 1 h from 1 h to 7 h for DL-Asn·H₂O with and without D-Glu additive, and from 1 h to 15 h for DL-Asn·H₂O with D-Asp additive. The CSD was measured in-situ by FBRM (Focused Beam Reflectance Measurement) every 5 s. The results from HPLC shows the higher yield and time for which a pure product can be produced when using D-Glu, and especially D-Asp additives, which can inhibit the nucleation of D-Asn·H₂O for 15 h. Nucleation of D-Asn·H₂O occurred after 3 h in the process without additives. However, the yield of L-Asn·H₂O from DL-Asn·H₂O with D-Asp and D-Glu additives is lower

than in DL-Asn·H₂O without additives (at a particular batch time) because the additives inhibit the crystal growth rate of L-Asn·H₂O. The peak of the CSD of L-Asn·H₂O from DL-Asn·H₂O moves to higher chord lengths during the crystallization, with both the crystal size and the total number of crystals increasing as time increases. The CSD from DL-Asn·H₂O with D-Glu and D-Asp additives moved slower than DL-Asn·H₂O without additives due to the inhibition. From the CSD, we could find the relationship between the relative supersaturation and crystal growth rate. The crystal growth rate decreases when the relative supersaturation decreases. The crystal growth rate of L-Asn·H₂O from DL-Asn·H₂O with D-Glu and D-Asp additives is lower than from DL-Asn·H₂O without additives.

6.2 Introduction

The crystal size distribution is important information for industrial crystallization because the final use of the compound depends on the size, morphology, dissolution properties, and polymorphic form (Lewis et al., 2015). For example the shape and size of ice crystals in ice cream is important to make a smooth texture and melt properties (Myerson, 2002; Lewis et al., 2015). Thus, many processes using crystallization must have a study concerning the crystal size distribution. Many analyzers can analyze the crystal size distribution in an offline mode, where a sample must be removed from the process to measure the CSD, however, this method is not suitable for a high crystallization rate or a small amount of sample. Currently, online measurement of CSD becomes more interesting because it does not disturb the crystallization process and it can measure in real-time, which makes it easy to control the crystallization pathway using, for example the stirrer speed or crystallization

temperature when the process does not follow the required path. Focused Beam Reflectance Measurement (FBRM) is an online particle size distribution analysis technique which is widely used for crystallization processes. FBRM has been used in many research projects for industrial crystallization; Chew et al. (2007) used FBRM to develop and optimize a crystallization process in unseeded and seeded crystallization mode for cooling crystallization of glycine and paracetamol. Doki et al. (2004a) used FBRM and FTIR to control the production of metastable α -glycine and was able to completely avoid production of γ -glycine crystal. Moreover, polymorphic transition has also been studied by using FBRM (Schöll et al., 2006). Barrett and Glennon (2002) used FBRM to find the solubility and metastable zone width. Doki et al. (2004b) studied the effect of L-cysteine (L-Cys) to the crystallization of DL-Asn using the FBRM to see the number of particles from nucleation of D- and L-Asn from the solution with and without additives, and HPLC to determine the purity of the solid product. The results show that increasing the amount of L-Cys clearly inhibits the nucleation of L-Asn, so the number of the crystals rapidly increases in two steps; the primary nucleation of D-Asn and then the primary nucleation of L-Asn. They also used FBRM to measure the particle size during the pulse heating of this crystallization process to see the crystal product which is only pure D-Asn for large crystal sizes (>400 microns) and only pure L-Asn for small crystal sizes (<200 microns).

In preferential crystallization, there are many steps in the crystallization, as shown in Figure 6.1. If we consider the preferential crystallization of L-Asn·H₂O from DL-Asn·H₂O, after the L-Asn·H₂O was seeded into the crystallizer the L-Asn·H₂O seeds will grow, and at some time the secondary nucleation of L-Asn·H₂O will begin. However, the spontaneous primary nucleation of D-Asn·H₂O will occur at some time

also, so the product purity will start to drop. If we consider the crystal size distribution during this process, with the seeded time being t_0 , then the L-Asn·H₂O will grow and secondary nucleation of L-Asn·H₂O occurs at time t_1 . At this time, the first peak from the L-Asn·H₂O seed moves to a higher crystal size and a new small peak from the secondary nucleation of L-Asn·H₂O will be created. At time t_2 , after the nucleation of D-Asn·H₂O occurs, there are three peaks of the distribution, which are from the growth of L-Asn·H₂O seeds, the growth of L-Asn·H₂O from secondary nucleation, and the primary nucleation of D-Asn·H₂O.

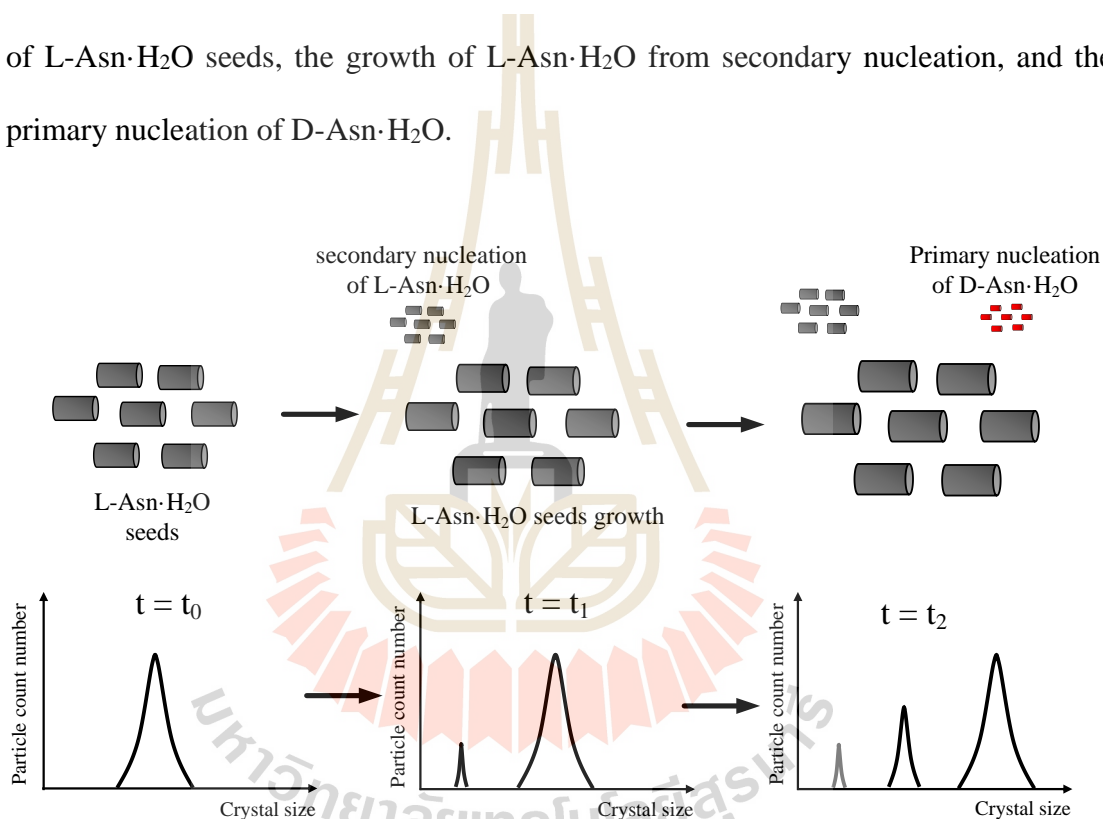


Figure 6.1 Model of particle size distribution of D- and L-Asn·H₂O from the preferential crystallization of L-Asn·H₂O in DL-Asn·H₂O solution (adapted from Elsner et al. (2005)).

From Chapter V, the preferential crystallization of L-Asn·H₂O in DL-Asn·H₂O with and without D-Glu and D-Asp additives was performed, focusing on

the product purity and yield. This chapter investigates the crystal size distribution during the preferential crystallization of L-Asn·H₂O in DL-Asn·H₂O with and without 5 mol% of D-Glu and D-Asp additives, and investigated the relationship between the crystal growth rate and the relative supersaturation of L-Asn·H₂O during the preferential crystallization.

6.3 Theory

6.3.1 Particle Size Distribution

Particle size distribution (PSD) or Crystal size distribution (CSD) is a function to describe the amount of crystal as a function of the size of crystal. The two main parameters given from the CSD are the mean crystal size and range of particle sizes (the spread of the distribution). The CSD usually considers the number distribution of crystals as a function of the linear crystal size. The number distribution is chosen because of the great significance of nucleation to crystal size distribution.

In Figure 6.2, the particle size distribution and cumulative oversize distribution are shown. The particle size distribution shows the normal distribution, and the cumulative oversize distribution represents the total number of crystals having a size greater than the minimum size of each range.

The cumulative oversize distribution is often used more than cumulative undersize because the particle size analyzer equipment cannot always measure the smallest particles, but it is usually not difficult to determine sizes for the largest particles (Flood, 2009).

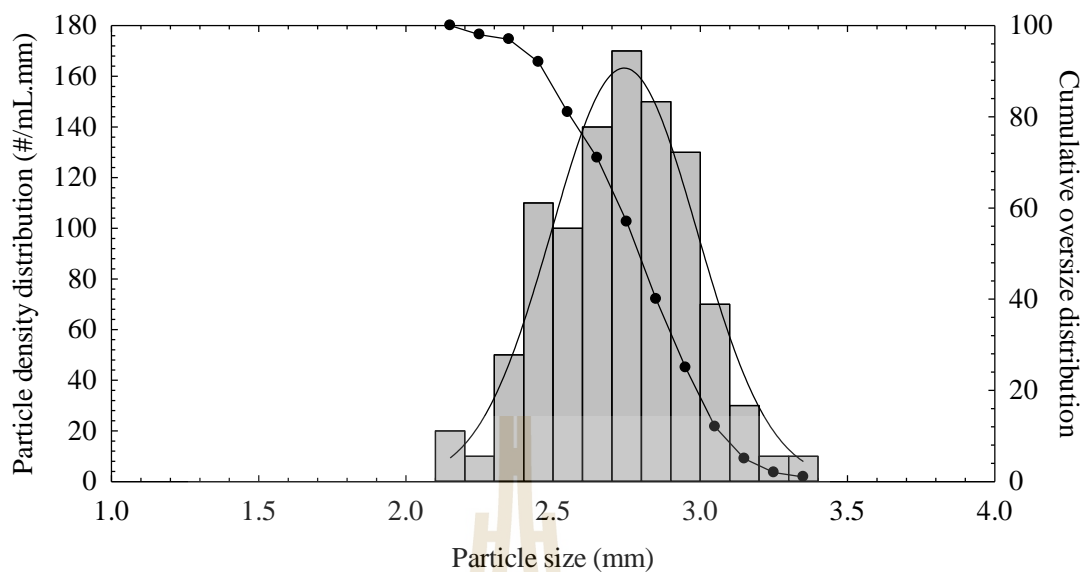


Figure 6.2 Particle size distribution and cumulative particle size distribution (Flood, 2009).

6.4 Materials and Methods

6.4.1 Materials

DL-asparagine monohydrate (DL-Asn·H₂O, 99+ wt%), L-asparagine monohydrate (L-Asn·H₂O, 99+ wt%) and D-asparagine monohydrate (D-Asn·H₂O, 99+ wt%), were purchased from Sigma-Aldrich. D-aspartic acid (D-Asp, 99+wt%), and D-glutamic acid (D-Glu, 99+wt%) were purchased from ACROS. These reagents were used without further purification. Deionized water was used as the solvent.

6.4.2 Apparatus

A 500 mL batch crystallizer was used. A water bath (F32-ME, Julabo, Germany) was used to control the temperature of the crystallizer. An overhead stirrer was used at 400 rpm to mix the suspension. The experimental set up is shown in Figure 6.3.

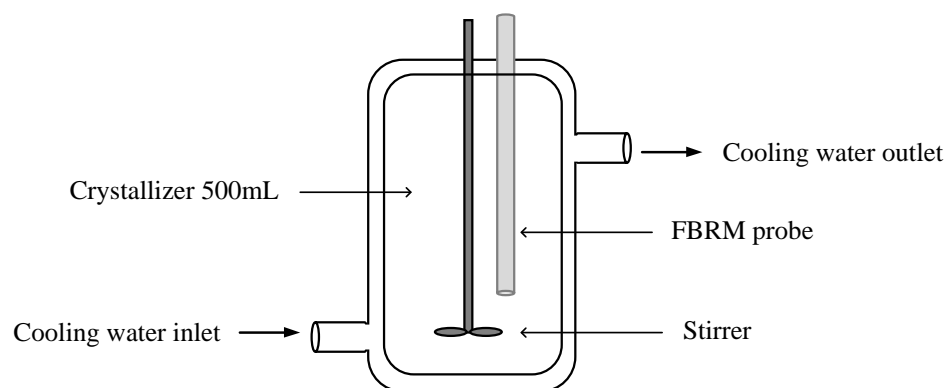


Figure 6.3 Experimental Setup.

The purity of solid products was analysed by HPLC (1260 Infinity, Agilent Technologies) with a Chirobiotic T column. The HPLC analysis was performed at 25°C using a 40:60 vol% ethanol: water mixture as a mobile phase with flow rate 0.25mL/min and using UV detection at 210 nm. The injection volume was 5 μ L.

For measuring the crystal size distribution (CSD), we used FBRM (Focused Beam Reflectance Measurement), as shown in Figure 6.4. The particle size distribution was measured every 5 seconds during the preferential crystallization process. The number of particles that is counted by FBRM is only the particles which are close to end of the FBRM probe; we can calculate the particle count number by using Equation (E.2) where the calculation is shown in Appendix E. The CSD from FBRM was calculated by the program icFBRM 4.3. A screenshot of the running program is shown in Figure 6.5. There are 3 screens consisting of the particle count number screen, particle size distribution screen, and statistics screen. The particle count number screen shows the particle count number at any time. The particle size distribution screen shows the particle size distribution at a fixed time. The statistics

screen shows the total result from the particle count number and particle size distribution.

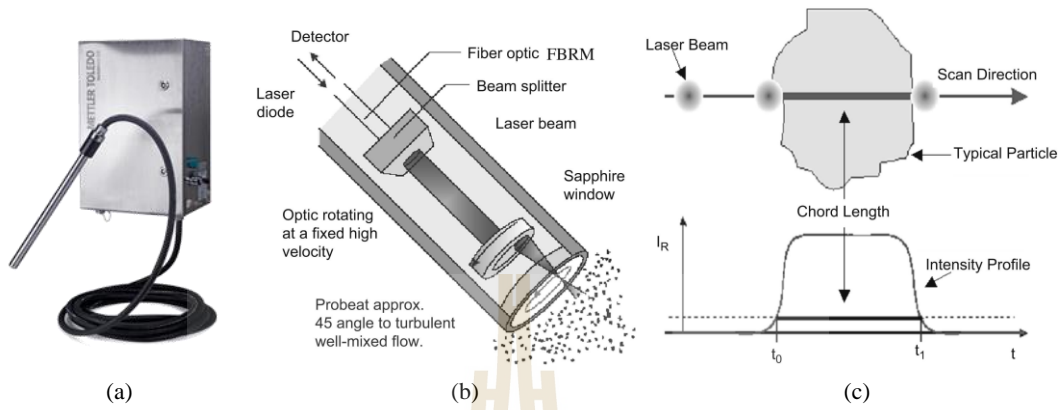


Figure 6.4 Focused Beam Reflectance Measurement (a) FBRM E25 model, (b) FBRM probe technique, and (c) Measurement of a particle chord length using the FBRM technique (Greaves et al., 2008).

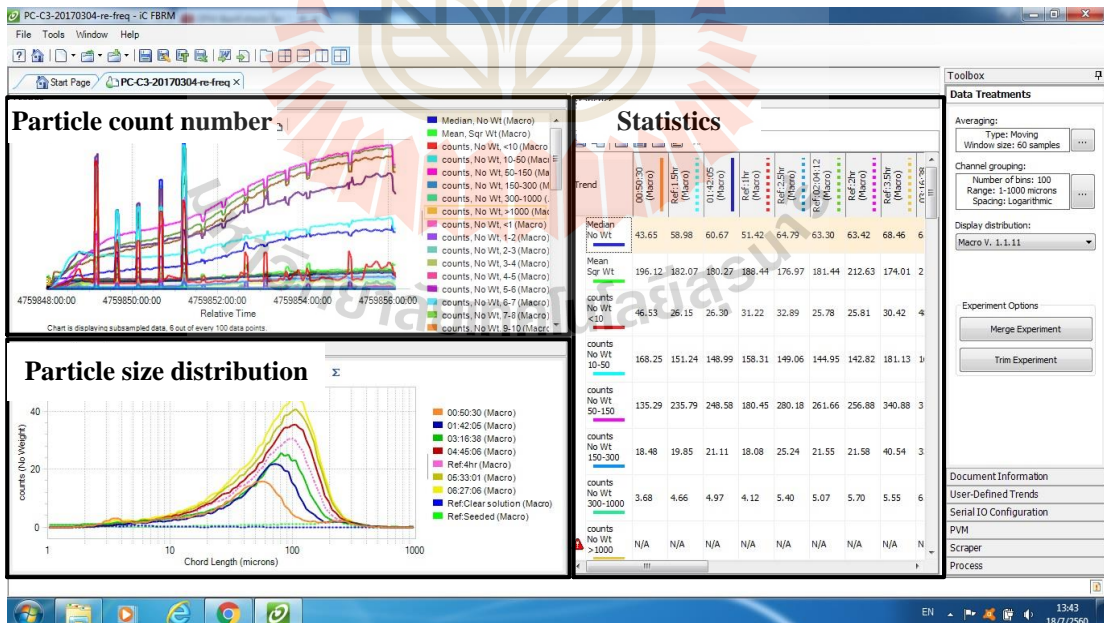


Figure 6.5 The screen of icFBRM 4.3 program for analysing the crystal size distribution.

6.4.3 Particle Size Distribution during the Preferential Crystallization of L-Asn·H₂O in Batch Crystallization

We prepared DL-Asn·H₂O solutions, with the conditions shown in Table 6.1, in 300 g of water in a 500mL crystallization vessel with a jacket to control the temperature. The solution was heated to 55°C to completely dissolve the crystalline material. Subsequently, the solution was cooled down rapidly to the crystallization temperature at 20°C. The FBRM (Focused Beam Reflectance Measurement) probe was placed into the solution to measure the particle size distribution every 5 s. A sample of 5 mL of suspension was taken by syringe every 0.5 h to 1 h, and then filtered using a membrane filter. The solid product was kept in a desiccator for 1-2 days to completely dry the liquid solution. The solid products were analysed for the %enantiomeric excess (%*e.e.*) and %yield of L-Asn·H₂O by HPLC, which were calculated by equation (6.1) and (6.2) respectively.

$$\%e.e. = \frac{C_L - C_D}{C_L + C_D} \times 100\% = \frac{A_L + A_D}{A_L + A_D} \times 100\% \quad (6.1)$$

where C_L and C_D are the concentration of L-Asn·H₂O and D-Asn·H₂O in the solid product respectively. A_L and A_D are HPLC peak area of L-Asn·H₂O and D-Asn·H₂O in the solid product.

$$\% \text{ yield} = \frac{m_t}{m_{th}} \times 100\% \quad (6.2)$$

where m_t is the mass of preferred enantiomer produced and m_{th} is maximum mass of the preferred enantiomer obtainable at equilibrium. Since a mass m_s of seed crystals is

introduced at the start of the preferential crystallization resulting in a mass m_p of the preferred enantiomer product, the yield is further defined using $m_t=m_p-m_s$ in Equation (6.2).

Table 6.1 The conditions for preferential crystallization of L-Asn·H₂O for finding the particle size distribution.

Condition	Supersaturation ratio of DL-Asn·H ₂ O	Additives	%additives
D1	1.3	-	-
D2	1.3	D-Glu	5%
D3	1.3	D-Asp	5%

6.5 Results and Discussion

6.5.1 The Analysis of Concentration and Product Purity

The concentration of L-Asn·H₂O from the preferential crystallization of L-Asn·H₂O in DL-Asn·H₂O with D-Glu and D-Asp additives decreases slower than without additives as shown in Figure 6.6. We also show the relative supersaturation of L-Asn·H₂O in DL-Asn·H₂O solution in Figure 6.7. The rate of L-Asn·H₂O concentration decrease from the DL-Asn·H₂O solutions with D-Glu and D-Asp additives decreases because these D-amino acids additives decrease the crystallization rate of L-Asn·H₂O even though there is a difference in the absolute configuration of the solute and the additive.

The concentration of D-Asn·H₂O from the preferential crystallization of L-Asn·H₂O in DL-Asn·H₂O with D-Glu and D-Asp additives is shown in Figure 6.8. The D-Asn·H₂O concentration starts to decrease 3 h, 6 h, and 15 h from the start of the preferential crystallization of L-Asn·H₂O in DL-Asn·H₂O without additives, and with

D-Glu and D-Asp additives respectively. These results show the effectiveness of the inhibition of D-Asn·H₂O from DL-Asn·H₂O solution by D-Glu and D-Asp.

The amount of L-Asn·H₂O solid product in the preferential crystallization of L-Asn·H₂O in DL-Asn·H₂O is shown in Figure 6.9. The amount of L-Asn·H₂O crystal increases when time increases. The amount of L-Asn·H₂O solid product from DL-Asn·H₂O without additives increases faster than it does in solutions with D-Glu and D-Asp additives. In Figure 6.10, the amount of D-Asn·H₂O crystal from DL-Asn·H₂O without additives increases faster than from DL-Asn·H₂O with D-Glu and (especially) D-Asp additives. In Figure 6.11, the %*e.e.* of L-Asn·H₂O solid product decreased fastest when crystallized from DL-Asn·H₂O without any additives, and the %*e.e.* of L-Asn·H₂O solid product decreases slowest when crystallized from DL-Asn·H₂O with D-Asp additive. These results also support the inhibition of D-Asn·H₂O through the use of D-Glu and D-Asp additives. Thus, the time available to produce product at 100%*e.e.* is increased when using the additives. The amount of L-Asn·H₂O solid product at a particular time decreases when using the additives, as shown in Figure 6.12. However, when comparing the yield of L-Asn·H₂O as a function of time with the %*e.e.* as a function of time, it is possible to create a plot of yield vs %*e.e.*, as shown in Figure 6.13. The maximum yield of L-Asn·H₂O at 100%*e.e.* in DL-Asn·H₂O without additives is 47%, in DL-Asn·H₂O with D-Glu is 53% and in DL-Asn·H₂O with D-Asp is 60%. Thus, the yield of L-Asn·H₂O at 100%*e.e.* of L-Asn·H₂O increases when using D-Glu and (especially) D-Asp additives.

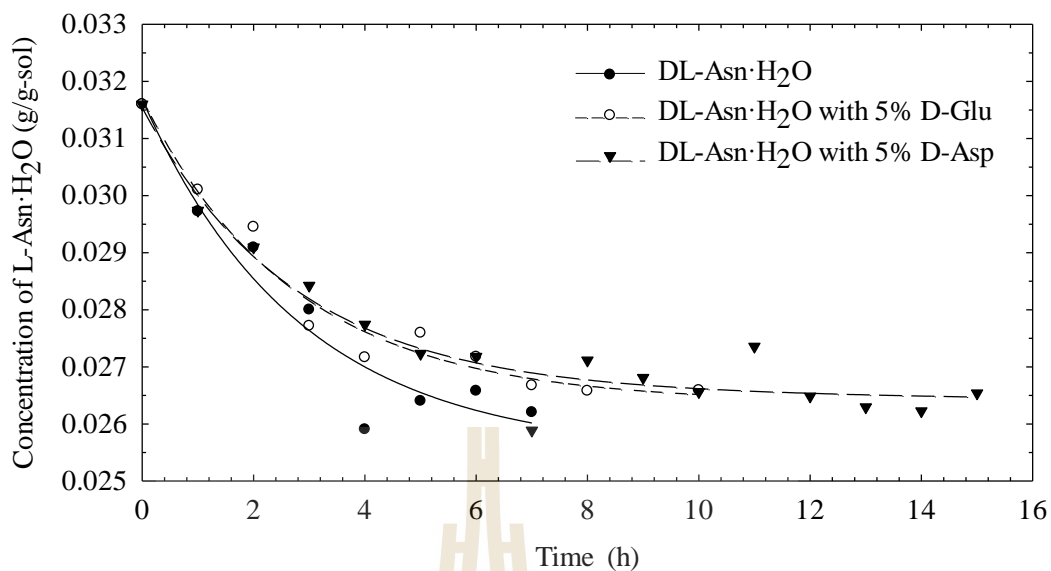


Figure 6.6 Concentration of L-Asn·H₂O in the preferential crystallization of L-Asn·H₂O in DL-Asn·H₂O with and without D-Glu and D-Asp additives.

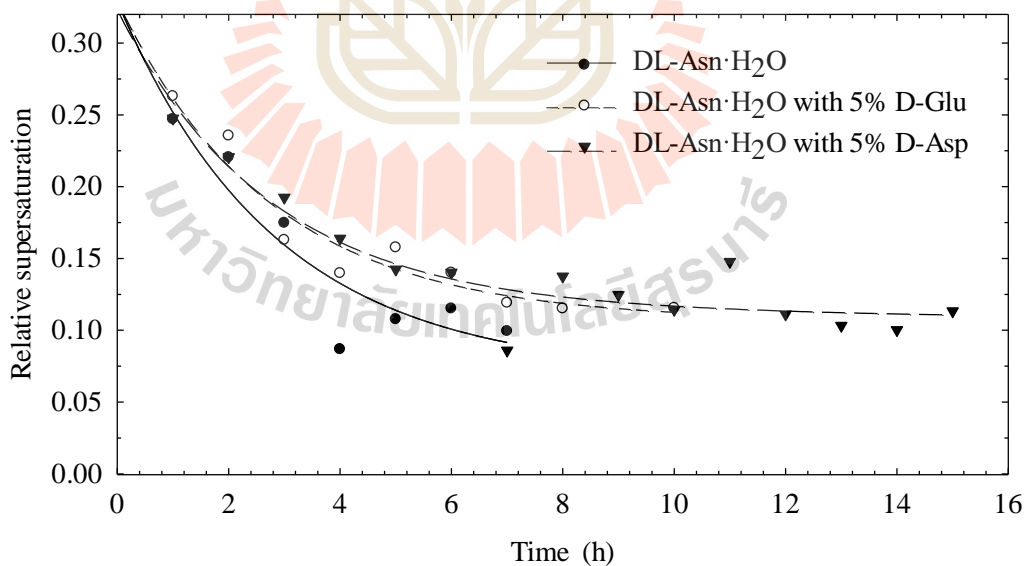


Figure 6.7 Relative supersaturation of L-Asn·H₂O in the preferential crystallization of L-Asn·H₂O in DL-Asn·H₂O with and without D-Glu and D-Asp additives.

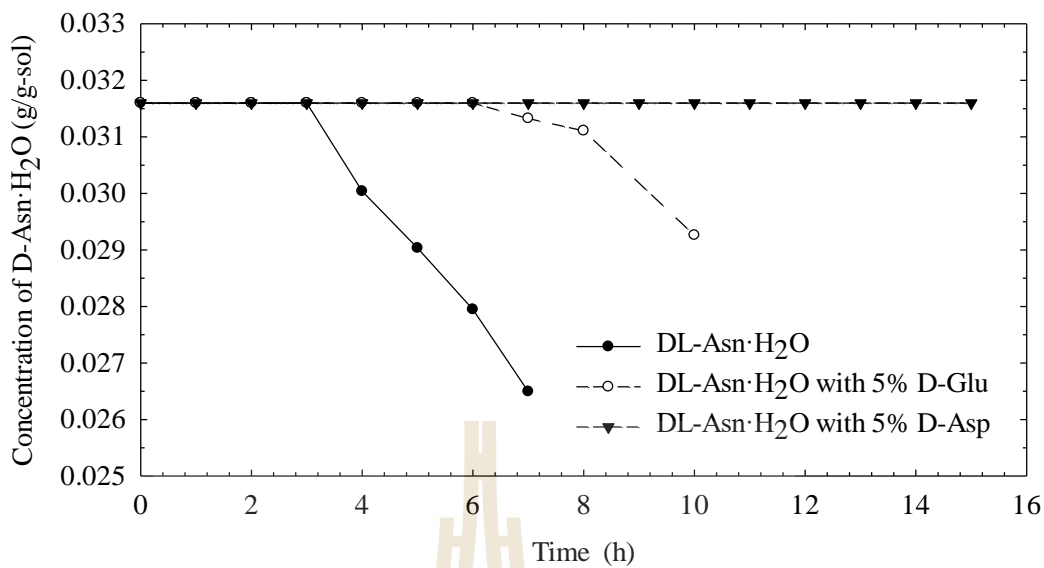


Figure 6.8 Concentration of D-Asn·H₂O in the preferential crystallization of L-Asn·H₂O in DL-Asn·H₂O with and without D-Glu and D-Asp additives.

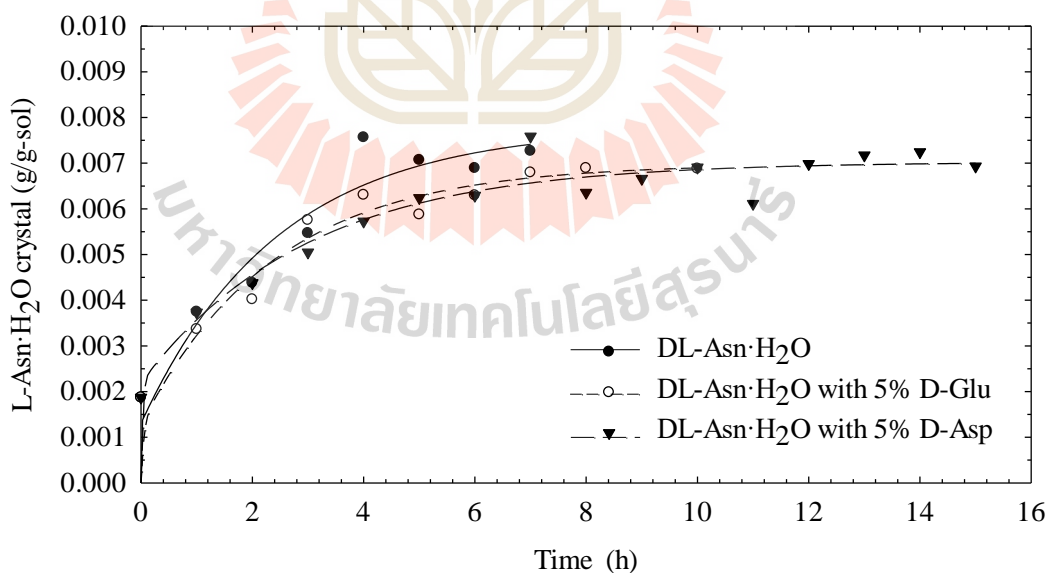


Figure 6.9 Amount of L-Asn·H₂O crystal in the preferential crystallization of L-Asn·H₂O in DL-Asn·H₂O with and without D-Glu and D-Asp additives.

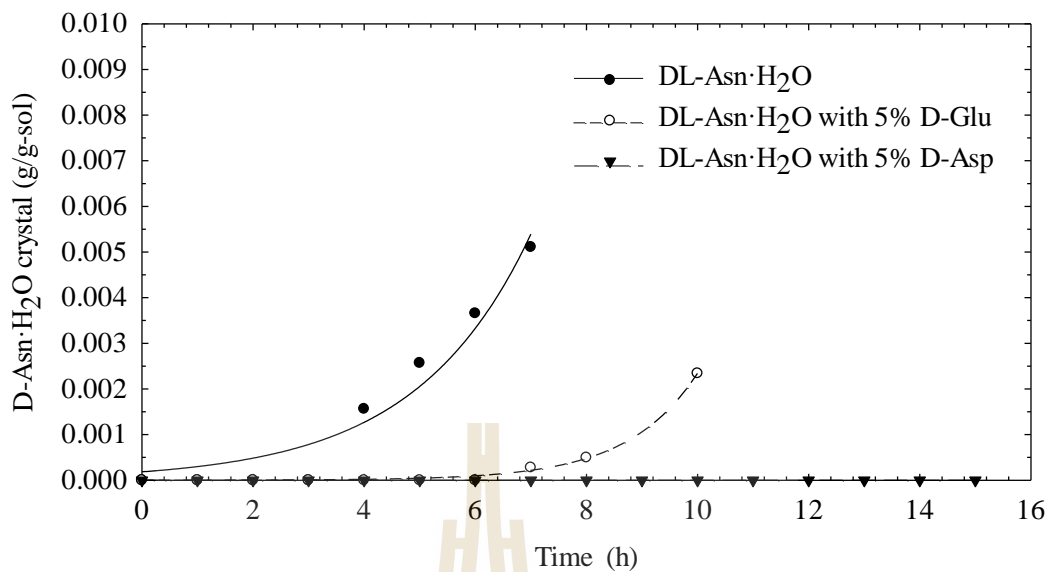


Figure 6.10 Amount of D-Asn·H₂O crystal in the preferential crystallization of L-Asn·H₂O in DL-Asn·H₂O with and without D-Glu and D-Asp additives.

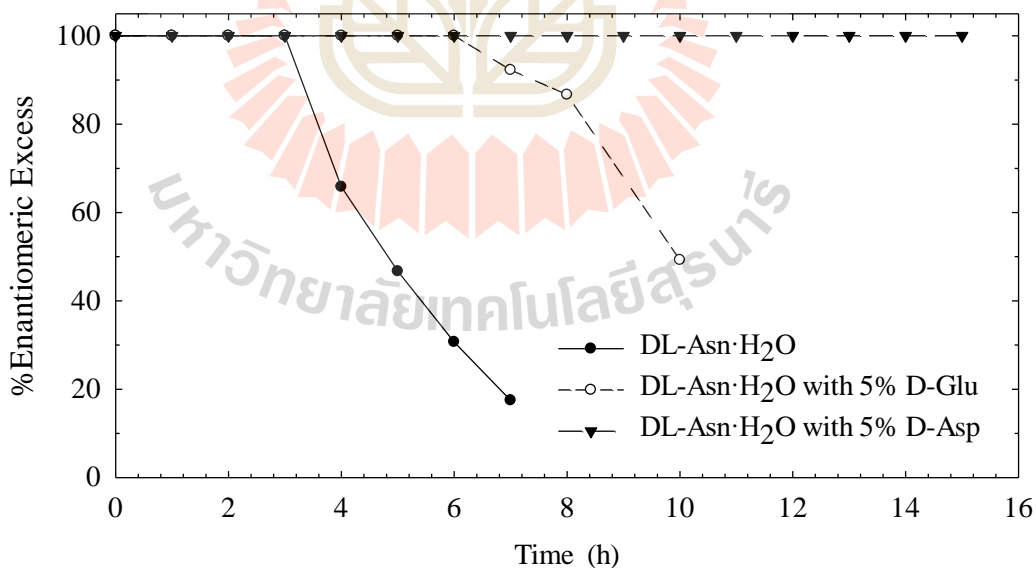


Figure 6.11 % e.e. of L-Asn·H₂O in the preferential crystallization of L-Asn·H₂O in DL-Asn·H₂O with and without D-Glu and D-Asp additives.

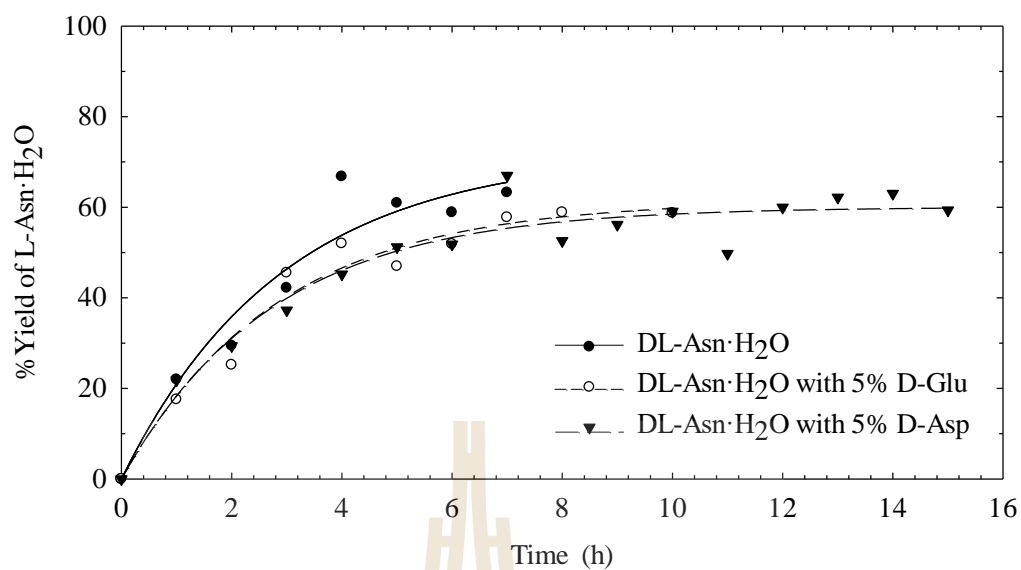


Figure 6.12 % Yield of L-Asn·H₂O in the preferential crystallization of L-Asn·H₂O in DL-Asn·H₂O with and without D-Glu and D-Asp additives.

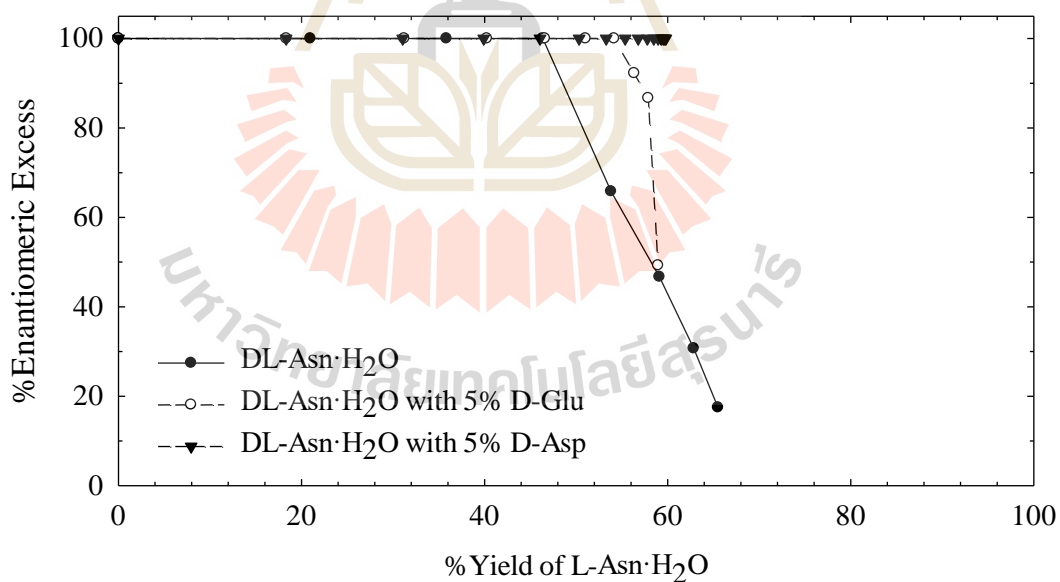


Figure 6.13 The relationship between % *e.e.* and % Yield of L-Asn·H₂O in the preferential crystallization of L-Asn·H₂O in DL-Asn·H₂O with and without D-Glu and D-Asp additives.

6.5.2 The Crystal Size Distribution

The crystal size distribution (CSD) of D- and L-Asn·H₂O in the preferential crystallization of L-Asn·H₂O in DL-Asn·H₂O with and without D-Glu and D-Asp additives is shown in this section to investigate the effect of additives to the CSD of the solid product (which potentially contains both L- and D-Asn·H₂O).

The crystal size distribution of the product crystals from the preferential crystallization of L-Asn·H₂O in DL-Asn·H₂O without additives is shown in Figure 6.14. The x-axis is chord length, which refers to the particle or crystal size, and the y-axis is the number of crystals in 1 g of solution. The number of crystals increased when the time increased, and the peak of the CSD also moved to higher chord length. The clear solution is the solution before seeding, 0 h refers to the seeding time and 1 h to 7 h are the crystallization time in the preferential crystallization process. When the crystallization time increases the number of particles increases due to nucleation and growth of both D- and L-Asn·H₂O. However, the CSD of this experiment shows only one peak, although there should be at least two peaks, the first from the L-Asn·H₂O seeds and the second due to the nucleation of D-Asn·H₂O. A third peak would appear if significant primary or secondary nucleation of L-Asn·H₂O occurred. The CSD shows only one peak because the crystal size distribution is so wide; therefore, this wide CSD combines all the small peaks from the primary nucleation of D-Asn·H₂O and also the secondary nucleation of L-/ D-Asn·H₂O. The width of the distribution may be due to both the initial width of the seed CSD and also the growth rate dispersion of L-Asn·H₂O.

In Figure 6.15, the cumulative oversize distribution of crystal in the preferential crystallization is shown. The normalized cumulative oversize distribution

is shown in Figure 6.16. At 0 h (at the seeding time), the mean chord length is highest, as shown in this figure and Figure 6.14, because the L-Asn·H₂O crystal seed size is around 150-180 microns, but after seeding the crystal size is smaller because of the secondary nucleation of seed crystals. The crystal size distribution, cumulative oversize distribution and normalized cumulative distribution during the preferential crystallization of L-Asn·H₂O in DL-Asn·H₂O with D-Glu additives are shown in Figure 6.17 – 6.18, and in DL-Asn·H₂O with D-Asp additives in Figure 6.20 – 6.22.

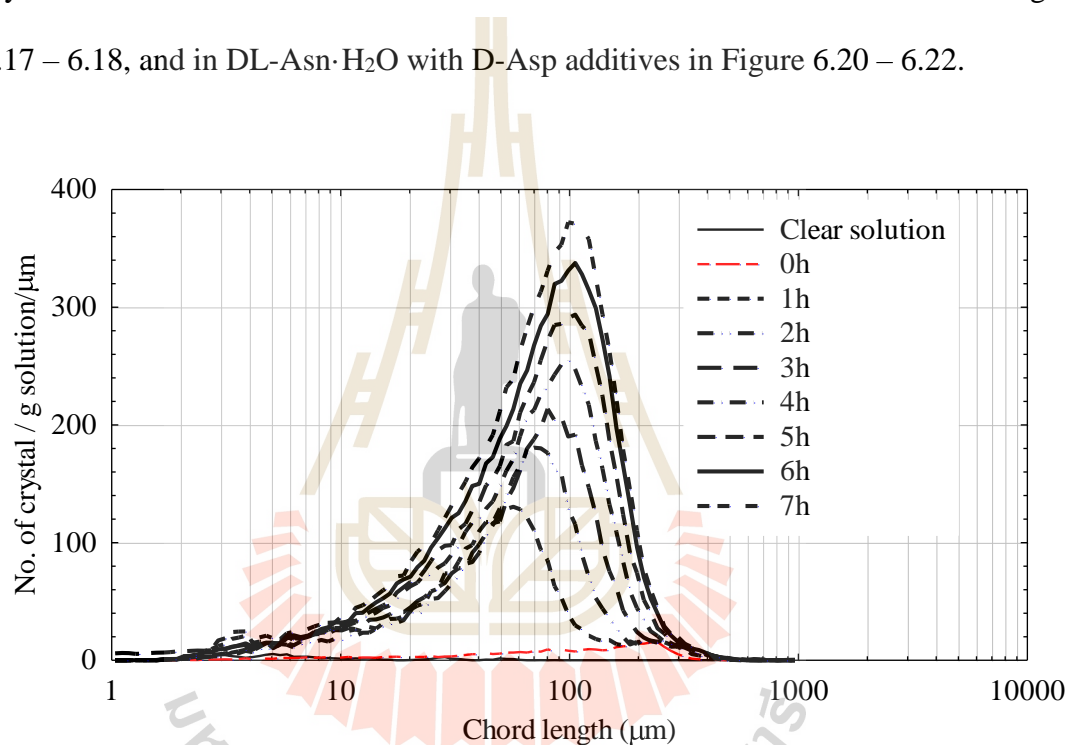


Figure 6.14 The crystal size distribution from the preferential crystallization of L-Asn·H₂O in DL-Asn·H₂O solution by FBRM.

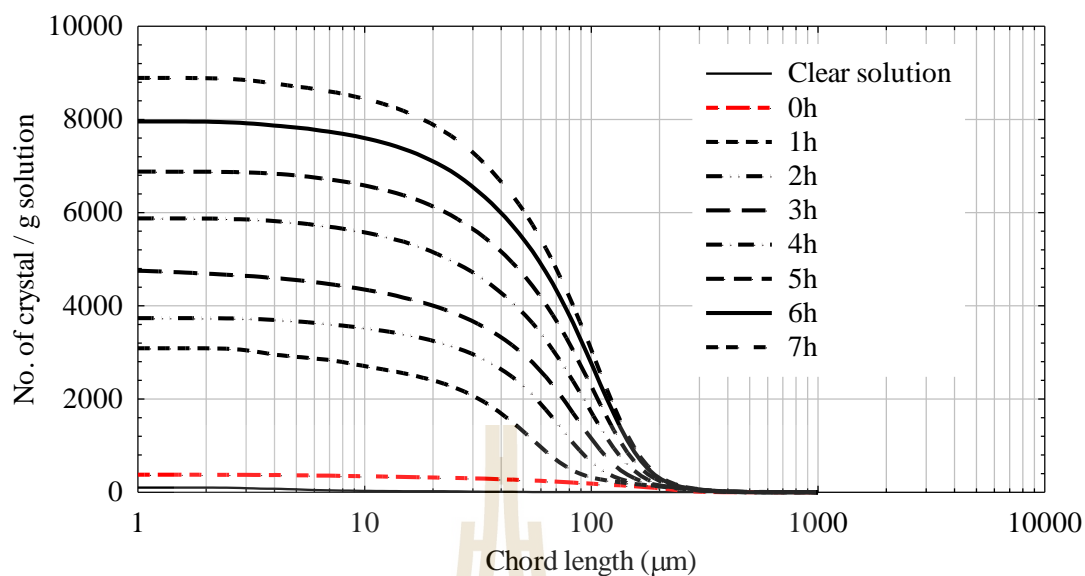


Figure 6.15 The cumulative oversize distribution of crystal in the preferential crystallization of L-Asn·H₂O in DL-Asn·H₂O solution by FBRM.

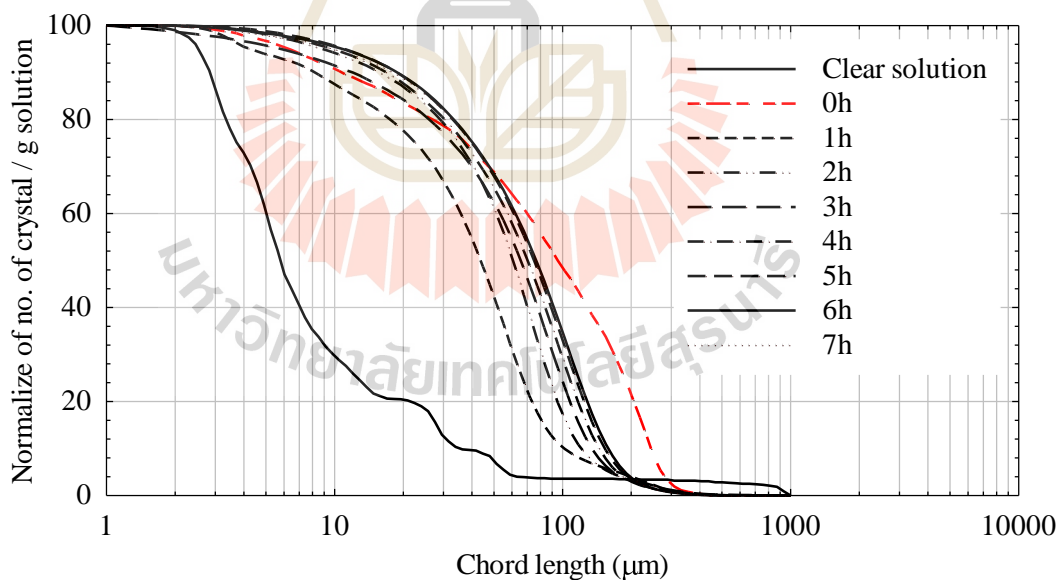


Figure 6.16 The normalized cumulative oversize distribution of crystals in the preferential crystallization of L-Asn·H₂O in DL-Asn·H₂O solution by FBRM.

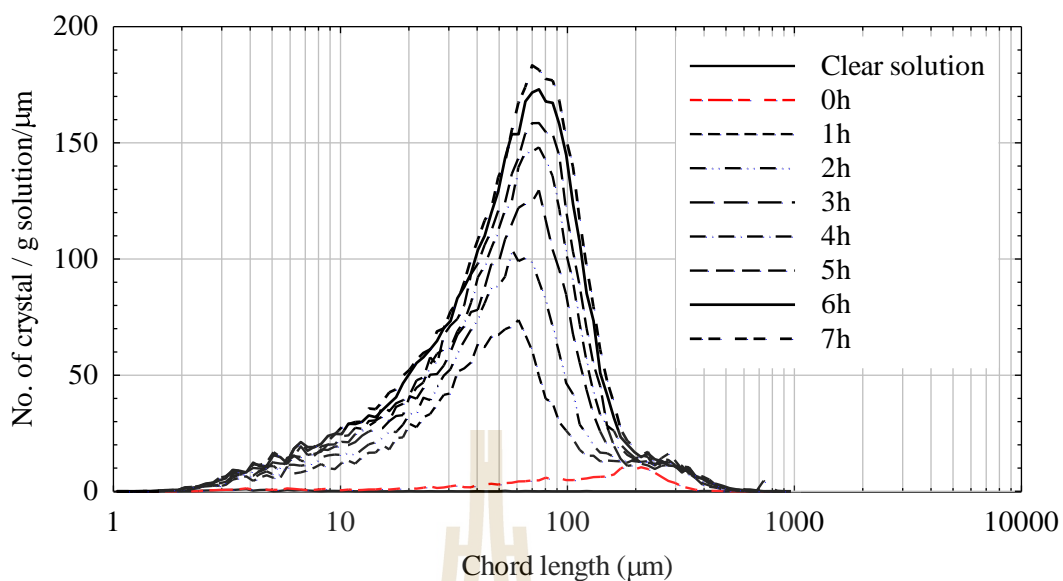


Figure 6.17 The crystal size distribution from the preferential crystallization of L-Asn·H₂O in DL-Asn·H₂O solution with 5 mol% D-Glu by FBRM.

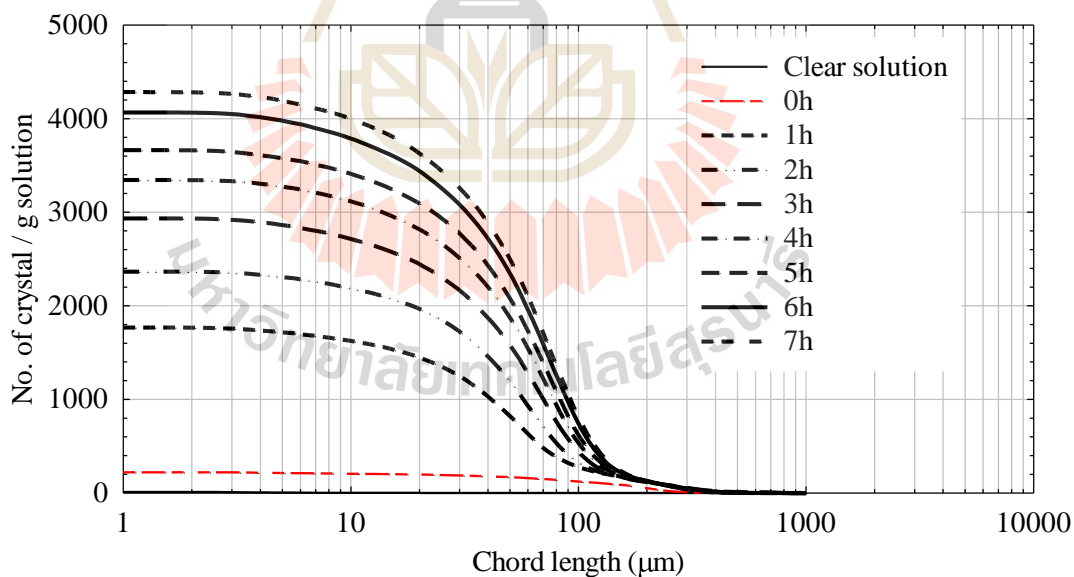


Figure 6.18 The cumulative oversize distribution of crystals in the preferential crystallization of L-Asn·H₂O in DL-Asn·H₂O solution with 5 mol% D-Glu by FBRM.

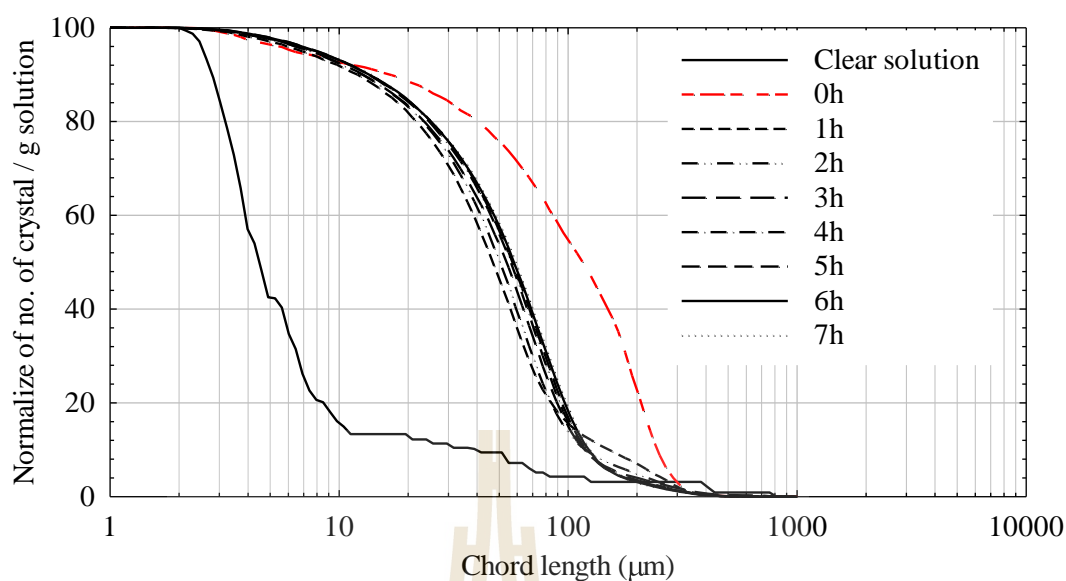


Figure 6.19 The normalized cumulative oversize distribution of crystals in the preferential crystallization of L-Asn·H₂O in DL-Asn·H₂O solution with 5 mol% D-Glu by FBRM.

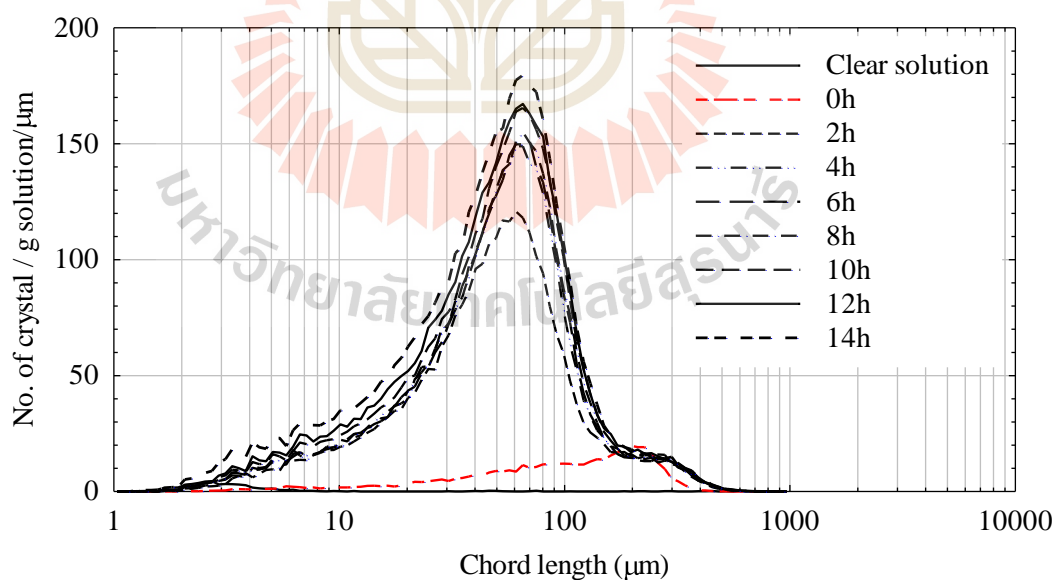


Figure 6.20 The crystal size distribution from the preferential crystallization of L-Asn·H₂O in DL-Asn·H₂O solution with 5 mol% D-Asp by FBRM.

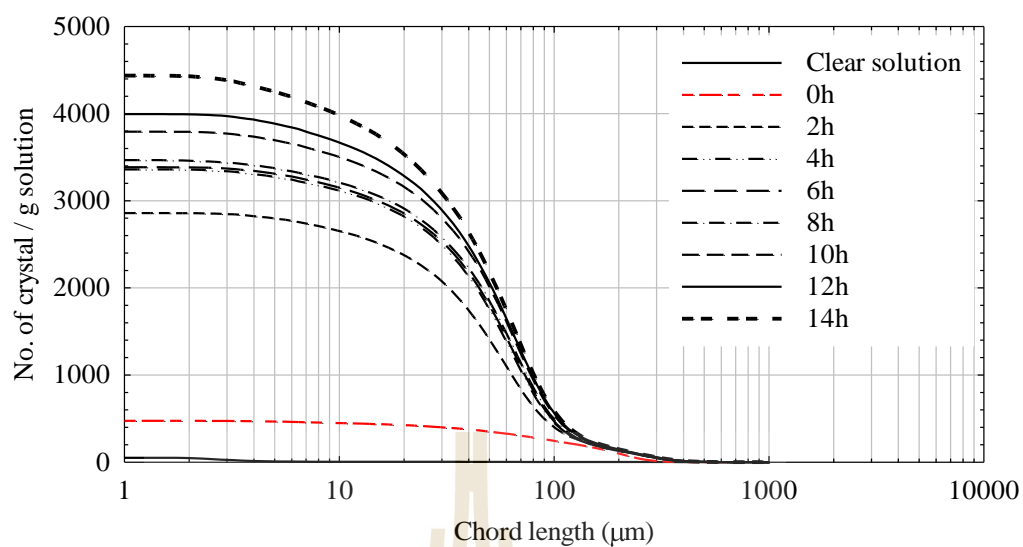


Figure 6.21 The cumulative oversize distribution of crystals in the preferential crystallization of L-Asn·H₂O in DL-Asn·H₂O solution with 5 mol% D-Asp by FBRM.

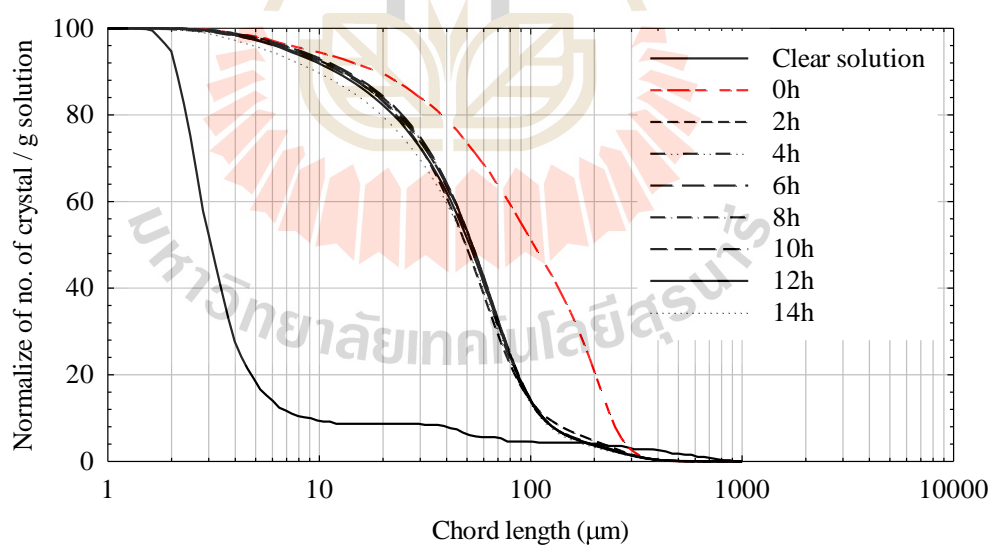


Figure 6.22 The normalized cumulative oversize distribution of crystals in the preferential crystallization of L-Asn·H₂O in DL-Asn·H₂O solution with 5 mol% D-Asp by FBRM.

6.5.3 Mean Crystal Size of L-Asn·H₂O and Crystal Growth Rate During the Preferential Crystallization

From the CSD results of D- and L-Asn·H₂O from preferential crystallization of L-Asn·H₂O in DL-Asn·H₂O with and without D-Glu and D-Asp additives in Section 6.5.2, the mean crystal growth rate of L-Asn·H₂O was calculated.

The mean crystal growth rate was found based on the mean crystal size of L-Asn·H₂O at 1 h, because from 0 h to 1 h the crystal size significantly decreases because the secondary nucleation of L-Asn·H₂O seeds, and the average size of the seeds is uncertain because of the small numbers of seed. Basing growth rates on the cumulative number for the mean crystal size at 1 h results in a more accurate measurement.

The mean crystal growth rate of L-Asn·H₂O was found by following these steps

(1) Find the mean crystal size of L-Asn·H₂O at 1 h by using the D50 value based on the total number of crystal from the normalized of number of crystal graph, for example the D50 from preferential crystallization of L-Asn·H₂O in DL-Asn·H₂O, as shown in Figure 6.16, is 43.6 microns.

(2) From this D50 value, we can find the sequence of the number of crystal at 1 h from the cumulative oversize distribution graph. For example, in Figure 6.15, is 1,545 from the total number of crystals being 3,090. We used this calculation because we preferred to measure the crystal growth rate of L-Asn·H₂O for a particular crystal; the crystal that is the D50 of the distribution at 1 h.

(3) Find the mean crystal size of L-Asn·H₂O from 2 h to 7 h by fixing the cumulative crystal number at 1,545. For example, in Figure 6.15, the mean crystal size of L-Asn·H₂O is shown in Table 6.2.

From Table 6.2, the relationship between the L-Asn·H₂O crystal size and time was constructed as shown in Figure 6.23. In this figure, the crystal size of L-Asn·H₂O increases when time increases. However, the crystal size of L-Asn·H₂O in DL-Asn·H₂O with D-Glu and D-Asp increases slower than without additives, because the D-Glu and D-Asp inhibit the crystal growth of L-Asn·H₂O as we discussed in Chapter III.

From the mean crystal size of L-Asn·H₂O results, the crystal growth rate is calculated from the change of crystal size per time. The crystal growth rate of L-Asn·H₂O from preferential crystallization of L-Asn·H₂O in DL-Asn·H₂O with and without D-Glu and D-Asp additives is shown in Figure 6.24. The crystal growth rate of L-Asn·H₂O from DL-Asn·H₂O with D-Asp is very low when compared with the growth rate of L-Asn·H₂O from DL-Asn·H₂O without additives because of the inhibition of D-Asp on the L-Asn·H₂O crystal (which does not follow to the rule of reversal, however its inhibition on D-Asn·H₂O is stronger according to results from previous chapters).

From Figure 6.7, the relationship between the relative supersaturation of L-Asn·H₂O and time, and from Figure 6.24, the relationship between the crystal growth rate and time, we constructed the relationship between the relative supersaturation and crystal growth rate. The relationship between relative supersaturation and crystal growth rate is shown in Figure 6.25. The growth rate of L-Asn·H₂O from DL-Asn·H₂O with D-Glu and D-Asp is very low when compared to DL-Asn·H₂O without any

additives because of the inhibition of D-Glu and D-Asp on the crystal growth of L-Asn·H₂O.

From Figure 6.25, the results were fitted with the crystal growth rate equation in Equation (6.3).

$$G = k_g \sigma^n \quad (6.3)$$

where G is the crystal growth rate, k_g is the growth rate constant, σ is relative supersaturation, and n is the growth rate order.

The fitting parameters with the growth rate equation are shown in Table 6.3. The growth rate order, n, is higher than 2 when using the D-Glu and D-Asp additives; normally an upper value for this parameter is 2. This is because the additives change the crystallization pathway; therefore, the growth rate order is higher when compared to the preferential crystallization of L-Asn·H₂O in DL-Asn·H₂O without additives.

Table 6.2 Mean crystal size of L-Asn·H₂O seed crystals in the preferential crystallization of L-Asn·H₂O in DL-Asn·H₂O from 1h to 7h.

Time (h)	Mean crystal size (microns)
1	43.65
2	68.94
3	87.63
4	105.05
5	119.28
6	129.88
7	134.15

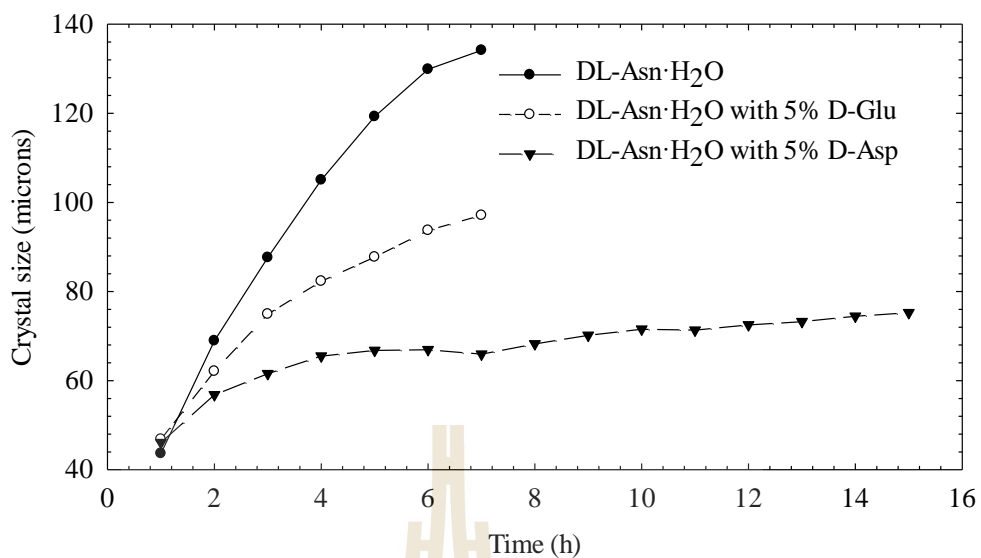


Figure 6.23 The relationship between the crystal size and time of L-Asn·H₂O crystal in the preferential crystallization of L-Asn·H₂O in DL-Asn·H₂O with and without D-Glu and D-Asp additives.

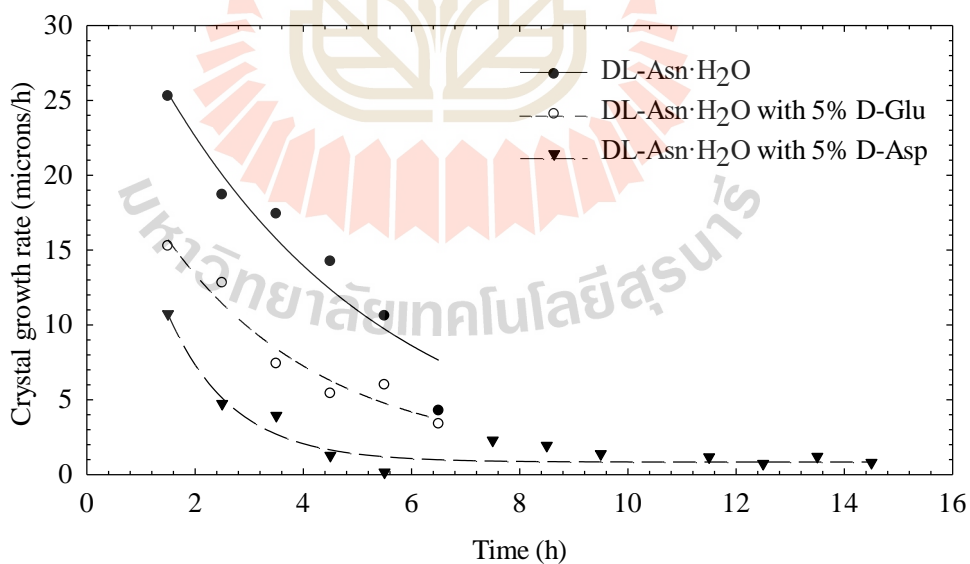


Figure 6.24 The relationship between the crystal growth rate and time for L-Asn·H₂O crystal in the preferential crystallization of L-Asn·H₂O in DL-Asn·H₂O with and without D-Glu and D-Asp additives.

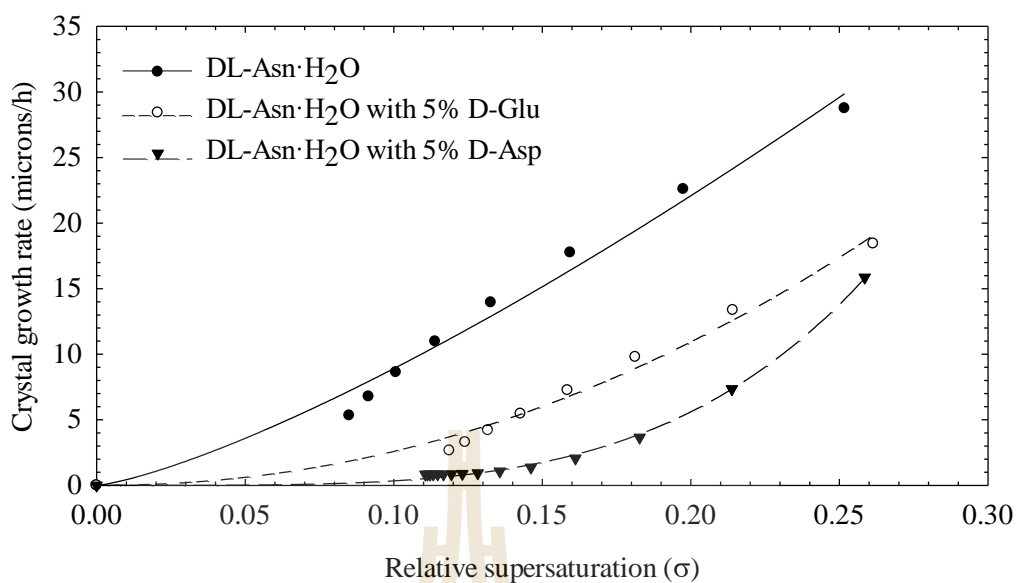


Figure 6.25 The relationship between the crystal growth rate and relative supersaturation of L-Asn·H₂O crystal in the preferential crystallization of L-Asn·H₂O in DL-Asn·H₂O with and without D-Glu and D-Asp additives.

Table 6.3 The fitting parameters of crystal growth rate of L-Asn·H₂O in preferential crystallization of L-Asn·H₂O in DL-Asn·H₂O with and without D-Glu and D-Asp additives.

Preferential Crystallization in	k_g	n
DL-Asn·H ₂ O	182.1	1.31
DL-Asn·H ₂ O with D-Glu	310.0	2.08
DL-Asn·H ₂ O with D-Asp	3709.4	4.04

6.6 Conclusions

The crystal size distribution of D-/L-Asn·H₂O showed the effect of D-Glu and D-Asp additives to crystal size, by the reduction in crystal growth rate of L-Asn·H₂O

when using D-Glu and D-Asp in DL-Asn·H₂O solution. However, the yield of the product is still high for pure L-Asn·H₂O when using the D-Glu, and especially for D-Asp additives. The D-Asp and D-Glu clearly inhibits the nucleation of D-Asn·H₂O which is the counter enantiomer, and they also inhibit the crystal growth rate of L-Asn·H₂O. Moreover, at all relative supersaturations, the crystal growth rate of L-Asn·H₂O from DL-Asn·H₂O with D-Glu and D-Asp additives is always lower than PC from DL-Asn·H₂O without the additives.

6.7 References

- Barrett, P., and Glennon, B. 2002. Characterizing the Metastable Zone Width and Solubility Curve Using Lasentec FBRM and PVM. **Chemical Engineering Research and Design** 80 (7):799-805.
- Chew, J. W., Chow, P. S., and Tan, R. B. H. 2007. Automated In-line Technique Using FBRM to Achieve Consistent Product Quality in Cooling Crystallization. **Crystal Growth & Design** 7 (8):1416-1422.
- Doki, N., Seki, H., Takano, K., Asatani, H., Yokota, M., and Kubota, N. 2004a. Process Control of Seeded Batch Cooling Crystallization of the Metastable α -Form Glycine Using an In-Situ ATR-FTIR Spectrometer and an In-Situ FBRM Particle Counter. **Crystal Growth & Design** 4 (5):949-953.
- Doki, N., Yokota, M., Sasaki, S., and Kubota, N. 2004b. Simultaneous crystallization of D- and L-asparagines in the presence of a Tailor-made additive by natural cooling combined with pulse heating. **Crystal Growth and Design** 4 (6):1359-1363.

- Elsner, M. P., Fernandez Menendez, D., Muslera, E. A., and Seidel-Morgenstern, A. 2005. Experimental study and simplified mathematical description of preferential crystallization. **Chirality** 17 Suppl:S183-195.
- Flood, A. E. 2009. **Industrial crystallization from solution: A primer**. Thailand: Suranaree University of Technology.
- Greaves, D., Boxall, J., Mulligan, J., Montesi, A., Creek, J., Dendy Sloan, E., and Koh, C. A. 2008. Measuring the particle size of a known distribution using the focused beam reflectance measurement technique. **Chemical Engineering Science** 63 (22):5410-5419.
- Lewis, A., Seckler, M., Kramer, H., and van Rosmalen, G. 2015. **Industrial Crystallization: Fundamentals and Applications**: Cambridge University Press.
- Myerson, A. S. 2002. **Handbook of Industrial Crystallization**. Second Edition ed. Woburn: Butterworth-Heinemann.
- Schöll, J., Bonalumi, D., Vicum, L., Mazzotti, M., and Müller, M. 2006. In Situ Monitoring and Modeling of the Solvent-Mediated Polymorphic Transformation of l-Glutamic Acid. **Crystal Growth & Design** 6 (4):881-891.

CHAPTER VII

CONCLUSIONS AND RECOMMENDATIONS

7.1 Conclusions

The main active pharmaceutical ingredients (APIs) produced currently should be in the form of a pure enantiomer and not in the form of racemic mixture. Therefore, many research groups have tried to separate enantiomers since this is important for the pharmaceutical and food industries. There are many methods to separate enantiomers such as chiral membrane separation, chiral chromatography, or separation via diastereomeric salts. Preferential crystallization is also a process to separate enantiomers, and this method is easy to operate, low cost, and gives a high yield. However, the problem of this method is the spontaneous primary nucleation of the counter enantiomer. This research fixed this problem using tailor-made additives. If these additives are chiral species they can inhibit the nucleation and growth of enantiomers that are the same absolute configuration as them. Therefore, this thesis focuses on the effect of additives to the crystallization process, including effects on the solubility, metastable zone width, nucleation, crystal growth, and the preferential crystallization in general. This research used the solute asparagine monohydrate ($\text{Asn}\cdot\text{H}_2\text{O}$) to study these effects, because this chemical is an amino acid that is widely used in many processes in the pharmaceutical industry. The following conclusions can be made for this thesis.

1. The solubility of L-, D-, and DL-Asn·H₂O with additives in water were studied. The solubility of D-/L-Asn·H₂O with 5 mol% of additives, consisting of D-/L-aspartic acid (Asp), D-/L-glutamic acid (Glu), D-/L-valine (Val), and D-/L-Leu (Leu), increases because the additives associate with the solute in the solution; so, the solubility is increased. Moreover, when the amount of additives increased the solubility increased. The solubility of DL-Asn·H₂O also increased when using the additives.

2. The width of the metastable zone increased when the cooling rate increased. The additives change the metastable zone width of D-/L-/DL-Asn·H₂O, but they did not show a clear trend in their effect to the metastable zone width because the metastable zone width is a process related to nucleation, which is a stochastic process.

3. The crystal growth rate of L-Asn·H₂O increased when the supersaturation ratio of L-Asn·H₂O and DL-Asn·H₂O increased, but the crystal growth rate of L-Asn·H₂O from DL-Asn·H₂O solution is lower than from L-Asn·H₂O solution at the same supersaturation ratio. D-Val, D-Leu and L-Leu have almost no effect on the crystal growth rate of L-Asn·H₂O in DL-Asn·H₂O solution – they are not effective additives for inhibition of growth. The crystal growth rate of L-Asn·H₂O from DL-Asn·H₂O with L-Val as an additive was promoted slightly. L-Asp and L-Glu clearly inhibit the crystal growth rate of L-Asn·H₂O from DL-Asn·H₂O solution because they have the same absolute configuration to L-Asn·H₂O, and their side chains are similar in size and structural features. D-Asp and D-Glu also inhibit the crystal growth rate of L-Asn·H₂O from DL-Asn·H₂O (but to a smaller extent than L-Asp and L-Glu) although their absolute configuration is different to the solute.

4. The crystallization of DL-Asn·H₂O without seeding was studied. D- and L-Asn·H₂O crystallized at the same rate from DL-Asn·H₂O supersaturated solutions

that did not contain additives. At any time, the yield of solid product increases when increasing the crystallization temperature and supersaturation ratio. The D-/L-Leu and D-/L-Val did have a scattered effect to the crystallization from DL-Asn·H₂O solutions; these additives sometimes inhibited D-Asn·H₂O and sometimes inhibited L-Asn·H₂O crystallization. This means the effect of these additives is very small for the inhibition of D-/L-Asn·H₂O. The L-Asp and L-Glu additives clearly inhibit nucleation of L-Asn·H₂O and D-Asp and D-Glu additives inhibit the nucleation of D-Asn·H₂O, which follows the rule of reversal; the enantiomer can have an effect on the solute molecule which has the same absolute configuration as the additive. However, L-Asp and L-Glu also slightly inhibit the nucleation of D-Asn·H₂O, although they are different in absolute configuration.

5. From the effect of additives to crystal growth rates and nucleation, D-Asp and D-Glu inhibit the growth and nucleation of D-Asn·H₂O and L-Asp and L-Glu inhibit the growth and nucleation of L-Asn·H₂O. These additives also slightly inhibit L-Asn·H₂O also although they are different in absolute configuration. D-Leu and D-Val have almost no effect to crystal growth rate and nucleation of D-Asn·H₂O.

6. The preferential crystallization of L-Asn·H₂O from DL-Asn·H₂O with and without additives was studied. An increasing of the supersaturation ratio of DL-Asn·H₂O caused an increasing crystallization rate, including increasing the nucleation and crystal growth rate. However, the purity of L-Asn·H₂O product from preferential crystallization from DL-Asn·H₂O solution at high supersaturation is lower than at a lower supersaturation ratio. However, at very low supersaturation ratio the yield is very low. Increasing the amount of L-Asn·H₂O seeds makes the yield of L-Asn·H₂O increase but did not make the nucleation of D-Asn·H₂O occur faster.

7. D-Leu and D-Val additives almost have no effect on the preferential crystallization of L-Asn·H₂O from DL-Asn·H₂O supersaturated solution. D-Glu and D-Asp additives inhibited the nucleation of D-Asn·H₂O as the counter enantiomer in the preferential crystallization of L-Asn·H₂O from DL-Asn·H₂O solution. The inhibition of D-Asn·H₂O as a counter enantiomer increased when the amount of D-Glu and D-Asp increased. However, the yield of L-Asn·H₂O product is lower when using these additives because these additives inhibited the crystal growth and nucleation of L-Asn·H₂O. The time of pure L-Asn·H₂O production increased when the amount of D-Glu and D-Asp additives was increased, but if the amount of additives is very high the yield of L-Asn·H₂O is lower than when a small amount of additives is used, because when the amount of additives increase the solubility of L- and DL-Asn·H₂O also increased.

8. The crystal size distribution (CSD) of D-/L-Asn·H₂O from the preferential crystallization of L-Asn·H₂O from DL-Asn·H₂O with and without D-Glu and D-Asp was studied. The size of crystals increased slowly when using these additives. The crystal growth rate of L-Asn·H₂O decreased when the relative supersaturation decreased. The crystal growth rate of L-Asn·H₂O from DL-Asn·H₂O with D-Glu and D-Asp is lower than from DL-Asn·H₂O without additives because D-Glu and D-Asp inhibited the crystal growth rate of L-Asn·H₂O, although their absolute configuration is different. However, the yield of enantiopure L-Asn·H₂O product is higher when using D-Asp and D-Glu additives because the time period when the pure species could be produced also increased.

7.2 Recommendations

1. We used the preferential crystallization process to separate the preferred enantiomer from the racemic mixture which contains an equimolar mixture of the preferred enantiomer and the counter enantiomer. Therefore, following the crystallization process in the crystallizer is important. Hence, the use of online analyzers such as polarimeters or density meters to measure the concentration in the solution phase during the preferential crystallization, the online microscope, which can record the picture or video inside the crystallizer to see the particle size and shape, would be very useful.

2. From the preferential crystallization of L-Asn·H₂O from DL-Asn·H₂O with and without additives, the effect of nucleation and crystal growth of L-Asn·H₂O should be modelled based on careful experiments to clearly see the mechanism by which tailor-made additives inhibit the nucleation and crystal growth of L-Asn·H₂O or another enantiomer.

3. The preferential crystallization in this research used asparagine monohydrate which is a conglomerate forming system, but racemic mixtures of chemicals are in this form only 5-10% of the total cases, and 90-95% are a racemic compound forming system. Therefore, the preferential crystallization of racemic a compound should be studied. However, the problem of this process for racemic compounds is in the phase equilibrium because it is difficult to produce pure enantiomer. Therefore, the preferential crystallization of racemic compounds by using the inhibition of tailor-made additives is interesting to increase the yield and product purity.



APPENDIX A

**RAW DATA OF SOLUBILITY AND METASTABLE
ZONE WIDTH OF ASPRAGINE MONOHYDRATE
WITH TAILOR-MADE ADDITIVES**

Table A.1 Solubility of DL-Asn·H₂O in water from Gravimetric Method.

T(°C)	DL-Asn (mg/gH ₂ O)	DL-Asn·H ₂ O (mg/gH ₂ O)
20	43.76	51.05
25	55.19	63.83
30	72.05	82.67
35	90.87	103.49
40	114.34	129.35

Table A.2 Solubility of L- and DL-Asn·H₂O in water from and Refractive Index Method.

T (°C)	DL-Asn·H ₂ O (mg/gH ₂ O)	L-Asn·H ₂ O (mg/gH ₂ O)
20	49.22	22.64
25	66.26	28.89
30	80.85	35.90
35	103.14	45.67
40	128.62	57.76

Table A.3 Solubility and Metastable Zone Limit (cooling rate 0.3°C/min) of DL-Asn·H₂O in water by Crystal16.

DL-Asn·H ₂ O (mg/gH ₂ O)	Saturation Temperature (°C)	Metastable Zone Limit at cooling rate 0.3°C/min (°C)
89.72	32.82	-
92.73	33.87	-
97.81	34.78	-
103.67	35.76	9.08
110.19	36.95	18.69
119.36	39.10	12.74
125.01	39.46	18.13
135.31	41.74	23.03
144.02	43.04	21.63
155.12	44.75	26.82
161.12	45.38	29.65

Table A.3 Solubility and Metastable Zone Limit (cooling rate 0.3°C/min) of
DL-Asn·H₂O in water by Crystal16. (cont.)

DL-Asn·H ₂ O (mg/gH ₂ O)	Saturation Temperature (°C)	Metastable Zone Limit at cooling rate 0.3°C/min (°C)
165.45	45.82	28.18
169.64	46.41	33.67
176.68	47.29	30.04
181.19	47.64	34.21
185.82	48.32	31.68
189.27	47.93	32.56
192.85	49.43	34.01
67.42	27.35	8.97
72.98	28.57	9.66
78.94	31.22	8.88
85.47	32.04	-
86.19	32.17	1.13
90.49	32.70	10.83
96.22	34.35	12.09
101.79	35.47	7.82
49.92	20.87	-
59.90	24.41	-

Table A.4 Solubility and Metastable Zone Limit (cooling rate 0.1°C/min) of
DL-Asn·H₂O in water by Crystal16.

DL-Asn·H ₂ O (mg/gH ₂ O)	Saturation Temperature (°C)	Metastable Zone Limit at cooling rate 0.1°C/min (°C)
59.90	24.61	8.58
79.89	29.65	13.78
99.44	34.70	16.03
120.50	39.16	20.05
140.18	41.58	25.67
159.24	44.73	29.45
178.28	46.48	34.40
186.86	47.93	34.01

Table A.5 Solubility and Metastable Zone Limit (cooling rate 0.3°C/min) ofL-Asn·H₂O in water by Crystal16.

L-Asn·H ₂ O (mg/gH ₂ O)	Saturation Temperature (°C)	Metastable Zone Limit at cooling rate 0.3°C/min (°C)
79.43	46.99	34.20
85.11	49.24	35.96
90.18	50.96	28.61
94.68	52.28	35.86
100.41	53.87	29.86
104.77	53.92	40.15
109.61	55.98	43.48
114.15	54.36	50.73
24.28	21.75	-
30.18	26.53	-
34.64	29.42	6.73
39.25	33.53	14.67
43.56	35.00	17.80

Table A.6 Solubility and Metastable Zone Limit (cooling rate 0.1°C/min) ofL-Asn·H₂O in water by Crystal16.

L-Asn·H ₂ O (mg/gH ₂ O)	Saturation Temperature (°C)	Metastable Zone Limit at cooling rate 0.1°C/min (°C)
30.18	25.62	9.21
39.62	31.80	12.34
50.17	37.04	24.10
59.59	41.21	25.28
69.97	44.71	36.52
80.45	47.11	38.58
90.02	50.34	31.23
99.72	53.87	42.89

Table A.7 Solubility and Metastable Zone Limit of D-Asn·H₂O in water with 5 mol% of D-Asp by Crystal16.

L-Asn·H ₂ O (mg/gH ₂ O)	Saturation Temperature (°C)	Metastable Zone Limit at cooling rate 0.1°C/min (°C)
29.87	27.99	12.60
40.57	32.00	5.74
59.98	40.68	26.91
69.64	43.61	31.59
79.34	47.06	28.19
89.86	49.48	35.95
99.26	51.37	41.00

Table A.8 Solubility and Metastable Zone Limit of L-Asn·H₂O in water with 5 mol% D-Asp by Crystal16.

L-Asn·H ₂ O (mg/gH ₂ O)	Saturation Temperature (°C)	Metastable Zone Limit at cooling rate 0.1°C/min (°C)
38.64	30.19	17.40
51.86	37.49	24.07
60.06	40.87	27.01
85.36	47.29	39.35
76.73	44.88	34.40
100.81	51.71	37.21
103.52	52.68	42.45
104.79	52.44	39.25

Table A.9 Solubility and Metastable Zone Limit of D-Asn·H₂O in water with 5 mol% D-Glu by Crystal16.

L-Asn·H ₂ O (mg/gH ₂ O)	Saturation Temperature (°C)	Metastable Zone Limit at cooling rate 0.1°C/min (°C)
29.98	24.21	-
39.64	29.90	13.29
49.27	34.50	23.09
59.85	38.62	24.56
69.63	44.49	28.09
79.78	47.11	36.53
89.91	50.31	36.53

Table A.10 Solubility and Metastable Zone Limit of L-Asn·H₂O in water with 5 mol% D-Glu by Crystal16.

L-Asn·H ₂ O (mg/gH ₂ O)	Saturation Temperature (°C)	Metastable Zone Limit at cooling rate 0.1°C/min (°C)
36.73	29.10	14.79
40.10	31.41	18.81
50.19	36.84	17.44
59.59	40.57	27.53
69.81	43.97	29.96
80.09	46.96	37.01
90.18	49.61	36.52
100.09	52.15	41.72

Table A.11 Solubility of L-Asn·H₂O in water with 10 mol% L-Asp and L-Glu by Crystal16.

L-Asn·H ₂ O (mg/gH ₂ O)	Saturation Temperature (°C)	
	10 mol% of L-Asp	10 mol% of L-Glu
30	21.87	18.37
40	26.60	20.67
50	34.50	31.80
70	43.27	40.33
90	49.63	47.67

Table A.12 Solubility and Metastable Zone Limit of D-Asn·H₂O in water with
5 mol% D-Val by Crystal16.

L-Asn·H ₂ O (mg/gH ₂ O)	Saturation Temperature (°C)	Metastable Zone Limit at cooling rate 0.1°C/min (°C)
32.42	28.07	-
39.64	34.15	10.19
50.36	38.41	19.60
59.86	41.40	24.40
69.59	45.00	24.27
89.38	50.98	37.21
100.80	53.62	44.85

Table A.13 Solubility and Metastable Zone Limit of L-Asn·H₂O in water with
5 mol% D-Val by Crystal16.

L-Asn·H ₂ O (mg/gH ₂ O)	Saturation Temperature (°C)	Metastable Zone Limit at cooling rate 0.1°C/min (°C)
30.28	25.33	10.04
48.30	36.60	18.29
58.39	40.57	25.02
66.18	45.86	23.84
76.79	46.52	27.47
80.02	47.99	24.04
90.05	50.24	32.70
100.18	52.79	38.92

Table A.14 Solubility and Metastable Zone Limit of D-Asn·H₂O in water with 5 mol% D-Leu by Crystal16.

DL-Asn·H ₂ O (mg/gH ₂ O)	Saturation Temperature (°C)	Metastable Zone Limit at cooling rate 0.1°C/min (°C)
30.62	28.07	12.54
39.75	32.22	11.46
49.91	37.12	14.21
59.39	40.15	18.22
69.36	44.46	36.42
79.90	47.84	23.19
89.73	50.34	31.33

Table A.15 Solubility and Metastable Zone Limit of L-Asn·H₂O in water with 5 mol% D-Leu by Crystal16.

L-Asn·H ₂ O (mg/gH ₂ O)	Saturation Temperature (°C)	Metastable Zone Limit at cooling rate 0.1°C/min (°C)
30.03	25.54	5.84
46.22	34.99	14.76
50.09	37.20	17.11
59.39	41.07	25.83
69.99	43.61	32.94
89.44	49.63	33.91
96.18	51.57	36.92

Table A.16 Solubility of DL-Asn·H₂O in water with 5 mol% L-Asp and L-Glu by Crystal16.

DL-Asn·H ₂ O (mg/gH ₂ O)	Saturation Temperature (°C)	
	5 mol% of L-Asp	5 mol% of L-Glu
60	22.83	22.83
80	28.40	28.57
100	32.83	32.80
140	40.80	41.20
180	46.53	46.67



APPENDIX B

**RAW DATA OF CRYSTAL GROWTH RATE OF
L-ASPARAGINE MONOHYDRATE FROM
L-/DL-ASPARAGINE MONOHYDRATE WITHOUT
AND WITH TAILOR-MADE ADDITIVES**

Table B.1 Crystal growth rate of L-Asn·H₂O in L-Asn·H₂O and DL-Asn·H₂O supersaturated solution.

Crystal growth rate range ($\mu\text{m}/\text{min}$)	Number of L-Asn·H ₂ O crystal					
	in L-Asn·H ₂ O supersaturation at various S			in DL-Asn·H ₂ O supersaturation at various S		
	1.05	1.1	1.15	1.05	1.1	1.15
0.0 - 0.1	0	0	0	0	0	0
0.1 - 0.2	0	0	0	3	0	0
0.2 - 0.3	0	0	0	16	0	0
0.3 - 0.4	4	0	0	14	1	0
0.4 - 0.5	13	0	0	1	7	0
0.5 - 0.6	15	0	0	0	9	2
0.6 - 0.7	4	0	0	0	13	4
0.7 - 0.8	0	3	0	0	4	8
0.8 - 0.9	0	7	0	0	0	9
0.9 - 1.0	0	14	0	0	1	10
1.0 - 1.1	0	8	0	0	0	7
1.1 - 1.2	0	3	2	0	0	2
1.2 - 1.3	0	1	3	0	0	2
1.3 - 1.4	0	0	12	0	0	0
1.4 - 1.5	0	0	9	0	0	1
1.5 - 1.6	0	0	6	0	0	0
1.6 - 1.7	0	0	2	0	0	0
1.7 - 1.8	0	0	2	0	0	0
1.8 - 1.9	0	0	0	0	0	0
1.9 - 2.0	0	0	0	0	0	0



APPENDIX C

**RAW DATA OF UNSEED CRYSTALLIZATION OF
DL-ASPARAGINE MONOHYDRATE WITH
TAILOR-MADE ADDITIVES**

มหาวิทยาลัยเทคโนโลยีสุรนารี

Table C.1 The purity of D-Asn·H₂O and yield of D-/L-Asn·H₂O in unseeded crystallization of DL-Asn·H₂O in water.

time (hr)	% Purity of D-Asn·H ₂ O				% Yield of D-Asn·H ₂ O				% Yield of L-Asn·H ₂ O			
	S=1.5 at 20°C	S=1.5 at 30°C	S=1.5 at 35°C	S=1.7 at 30°C	S=1.5 at 20°C	S=1.5 at 30°C	S=1.5 at 35°C	S=1.7 at 30°C	S=1.5 at 20°C	S=1.5 at 30°C	S=1.5 at 35°C	S=1.7 at 30°C
0	-	-	-	-	0.00	0.00	0.00	0.00	0.00	0.00	0.00	0.00
1	-	47.63	51.65	50.56	-	35.90	52.99	65.42	-	39.46	49.60	63.98
1.5	-	51.17	51.78	51.01	-	61.84	70.47	82.63	-	59.01	65.61	79.36
2	52.63	50.46	51.53	50.88	60.66	70.30	77.75	81.34	54.60	69.01	73.13	78.53
2.5	-	-	-	-	-	-	-	-	-	-	-	-
3	52.14	51.39	50.92	50.67	76.78	81.36	79.38	83.39	70.49	76.95	76.52	81.17
3.5	-	-	-	-	-	-	-	-	-	-	-	-
4	52.26	51.19	51.44	51.07	83.59	78.91	79.71	83.57	76.38	75.24	75.25	80.07

มหาวิทยาลัยเทคโนโลยีสุรนารี

Table C.2 The purity of D-Asn·H₂O and yield of D-/L-Asn·H₂O in unseeded crystallization of DL-Asn·H₂O with D-/L-Asp additives.

time (hr)	% purity of D-Asn				% yield of D-Asn				% yield of L-Asn			
	3% L-Asp	5% L-Asp	7% L-Asp	5% D-Asp	3% L-Asp	5% L-Asp	7% L-Asp	5% D-Asp	3% L-Asp	5% L-Asp	7% L-Asp	5% D-Asp
0	-	-	-	-	0.00	0.00	0.00	0.00	0.00	0.00	0.00	0.00
1	100.00	-	-	-	12.28	-	-	-	0.00	-	-	-
1.5	-	-	-	-	-	-	-	-	-	-	-	-
2	94.29	100.00	100.00	-	49.73	41.17	30.74	-	3.01	0.00	0.00	-
2.5	-	-	-	0.00	-	-	-	0.00	-	-	-	18.02
3	63.61	100.00	-	0.00	64.06	58.92	-	0.00	36.65	0.00	-	34.72
3.5	-	-	-	-	-	-	-	-	-	-	-	-
4	56.26	99.12	100.00	5.36	81.26	67.16	56.10	2.70	63.18	0.59	0.00	47.57
4.5	-	-	-	-	-	-	-	-	-	-	-	-
5	53.91	-	-	20.52	73.77	-	-	16.53	63.08	-	-	64.04
6	-	63.42	98.89	33.74	-	69.98	61.41	32.88	-	40.36	0.69	64.56
7	52.10	-	-	-	76.73	-	-	-	70.54	-	-	-
8	-	58.27	96.40	45.00	-	75.72	66.34	53.46	-	54.23	2.48	65.36
9	-	-	-	-	-	-	-	-	-	-	-	-
10	50.98	53.48	82.63	50.10	76.29	67.99	63.29	68.38	73.37	59.14	13.30	68.11

Table C.3 The purity of D-Asn·H₂O and yield of D-/L-Asn·H₂O in unseeded crystallization of DL-Asn·H₂O with D-/L-Glu additives.

time (hr)	% purity of D-Asn				% yield of D-Asn				% yield of L-Asn			
	3% L-Glu	5% L-Glu	7% L-Glu	5% D-Glu	3% L-Glu	5% L-Glu	7% L-Glu	5% D-Glu	3% L-Glu	5% L-Glu	7% L-Glu	5% D-Glu
0	-	-	-	-	0.00	0.00	0.00	0.00	0.00	0.00	0.00	0.00
1	69.77	85.15	94.79	9.68	18.98	3.99	11.31	2.51	8.22	0.70	0.62	23.38
1.5	55.62	65.91	-	25.35	48.25	34.18	-	12.94	38.50	17.68	-	38.12
2	52.26	53.91	65.61	43.02	63.39	57.53	48.98	39.56	57.91	49.18	25.67	52.40
2.5	-	-	-	49.01	-	-	-	51.47	-	-	-	53.55
3	51.53	51.56	54.25	51.26	71.83	72.14	64.08	64.39	67.57	67.79	54.03	61.23
3.5	-	-	-	-	-	-	-	-	-	-	-	-
4	52.03	50.83	52.83	-	78.00	79.47	69.59	-	71.91	76.89	62.13	-
4.5	-	-	-	-	-	-	-	-	-	-	-	-
5	-	-	51.03	-	-	-	75.78	-	-	-	72.72	-

Table C.4 The purity of D-Asn·H₂O in unseeded crystallization of DL-Asn·H₂O with D-/L-Leu additives.

time (hr)	%Purity of D-Asn·H ₂ O in DL-Asn·H ₂ O with 5% L-Leu 30°C						%Purity of D-Asn·H ₂ O in DL-Asn·H ₂ O with 5% L-Leu 30°C					
	Run 1	Run 2	Run 3	Run 4	Run 5	Run 6	Run 1	Run 2	Run 3	Run 4	Run 5	Run 6
0	-	-	-	-	-	-	-	-	-	-	-	-
1	4.53	6.74	-	-	-	-	48.89	18.24	0.00	-	-	-
1.5	39.14	31.99	9.38	-	93.78	50.53	51.64	34.10	21.18	15.63	-	55.73
2	50.03	49.38	42.21	-	65.64	53.77	50.92	48.40	42.75	40.84	-	52.87
2.5	-	-	51.12	46.80	57.19	52.54	-	-	-	50.79	-	52.93
3	51.23	53.61	50.86	52.91	54.10	53.73	51.97	48.00	51.67	51.06	73.86	52.25
3.5	-	-	-	52.16	-	-	-	-	-	-	56.92	-
4	50.92	52.16	52.16	53.15	53.42	53.62	51.76	51.42	51.46	51.39	53.05	52.76
4.5	-	-	-	-	-	-	-	-	-	-	53.76	-

มหาวิทยาลัยเทคโนโลยีสุรนารี

Table C.5 The purity of D-Asn·H₂O in unseeded crystallization of DL-Asn·H₂O with L-Val additives.

time (hr)	%Purity of D-Asn·H ₂ O in DL-Asn·H ₂ O with 5% L-Val 30°C							
	Run 1	Run 2	Run 3	Run 4	Run 5	Run 6	Run 7	Run 8
0	-	-	-	-	-	-	-	-
1	20.14	54.52	4.51	11.07	-	-	-	-
1.5	48.90	52.12	28.63	38.44	-	-	-	51.17
2	50.63	52.06	47.40	49.20	52.54	88.72	-	52.85
2.5	-	-	-	-	53.73	66.18	-	53.95
3	50.72	52.19	52.06	55.75	52.74	58.41	99.30	52.85
3.5	-	-	-	-	-	52.96	99.41	-
4	52.78	52.17	52.59	53.52	52.16	53.88	88.64	53.32
4.5	-	-	-	-	-	-	61.43	-

มหาวิทยาลัยเทคโนโลยีสุรนารี

Table C.6 The purity of D-Asn·H₂O in unseeded crystallization of DL-Asn·H₂O with D-Val additives.

time (hr)	%Purity of D-Asn·H ₂ O in DL-Asn·H ₂ O with 5% D-Val 30°C							
	Run 1	Run 2	Run 3	Run 4	Run 5	Run 6	Run 7	Run 8
0	-	-	-	-	-	-	-	-
1	-	-	-	-	45.75	-	-	-
1.5	-	-	48.68	0.00	50.29	69.74	53.48	57.22
2	-	-	49.88	2.80	51.30	52.14	52.25	52.20
2.5	-	-	-	-	-	51.21	-	52.64
3	100.00	0.00	49.56	31.33	52.09	51.33	52.59	52.06
3.5	-	-	-	-	-	-	-	-
4	64.31	21.68	48.91	50.94	52.14	-	52.61	53.03
4.5	-	-	-	-	-	50.77	-	-
5	53.46	46.24	49.87	51.13	-	-	-	-
6	51.87	42.41	-	-	-	-	-	-



APPENDIX D

**RAW DATA OF PREFERENTIAL CRYSTALLIZATION
OF L-SAPARAGINE MONOHYDRATE WITH THE
INHIBITIONS BY TAILOR-MADE ADDITIVES**

Table D.1 The conditions of preferential crystallization of L-Asn·H₂O.

Condition	Supersaturation ratio of DL-Asn·H ₂ O, S	L-Asn·H ₂ O seed amount (g)	Results
A1	1.3	0.3	Table D.2
A2	1.1	0.3	Table D.3
A3	1.5	0.3	Table D.4
A4	1.3	0.075	Table D.5
A5	1.3	0.15	Table D.6

Table D.2 The result of preferential crystallization of L-Asn·H₂O in DL-Asn·H₂O for condition A1.

Time (h)	Soild concentration (g/gsol)		%enantiomeric excess	%yield of L-Asn·H ₂ O	%yield fitting curve
	L-Asn·H ₂ O	D-Asn·H ₂ O			
0	0.0019	0.0000	100.00	0.00	0.00
1	0.0068	0.0000	100.00	58.13	50.56
2	0.0079	0.0004	90.82	70.40	71.91
3	0.0079	0.0008	82.38	70.33	80.92
4	0.0085	0.0031	46.86	77.88	84.72
5	0.0098	0.0057	26.19	92.42	86.32
6	0.0096	0.0072	14.76	91.02	87.00
7	0.0096	0.0079	9.48	90.28	87.29
8	0.0094	0.0078	8.94	87.69	87.41

Table D.3 The result of preferential crystallization of L-Asn·H₂O in DL-Asn·H₂O for condition A2.

Time (h)	Soild concentration (g/gsol)		%enantiomeric excess	%yield of L-Asn·H ₂ O	%yield fitting curve
	L-Asn·H ₂ O	D-Asn·H ₂ O			
0	0.0019	0.0000	100.00	0.00	0.00
1	0.0033	0.0000	100.00	40.74	42.81
1.5	0.0036	0.0000	100.00	49.39	51.24
2	0.0039	0.0000	100.00	59.13	55.90
2.5	0.0042	0.0000	100.00	67.24	58.48
3	0.0037	0.0000	100.00	53.18	59.90
3.5	0.0041	0.0000	100.00	63.46	60.69
4	0.0039	0.0000	100.00	59.67	61.13
4.5	0.0037	0.0000	100.00	52.64	61.37
5	0.0040	0.0000	100.00	61.29	61.50
5.5	0.0040	0.0000	100.00	62.37	61.58
6	0.0042	0.0002	90.62	66.72	61.62

Table D.4 The result of preferential crystallization of L-Asn·H₂O in DL-Asn·H₂O for condition A3.

Time (h)	Soild concentration (g/gsol)		%enantiomeric excess	%yield of L-Asn·H ₂ O	%yield fitting curve
	L-Asn·H ₂ O	D-Asn·H ₂ O			
0	0.0019	0.0000	100.00	0.00	0.00
1	0.0114	0.0030	58.05	70.60	73.63
1.5	0.0129	0.0092	16.80	81.67	82.55
2	0.0151	0.0110	15.92	98.35	86.24
2.5	0.0137	0.0113	9.43	87.59	87.77
3	0.0133	0.0127	2.53	85.04	88.40
3.5	0.0130	0.0126	1.27	82.20	88.66
4	0.0141	0.0128	4.93	90.93	88.77
4.5	0.0136	0.0133	0.94	86.52	88.81
5	0.0141	0.0133	2.87	90.51	88.83

Table D.5 The result of preferential crystallization of L-Asn·H₂O in DL-Asn·H₂O for condition A4.

Time (h)	Soild concentration (g/gsol)		%enantiomeric excess	%yield of L-Asn·H ₂ O	%yield fitting curve
	L-Asn·H ₂ O	D-Asn·H ₂ O			
0	0.0005	0.0000	100.00	0.00	0.00
1	0.0032	0.0000	100.00	32.34	36.46
1.5	0.0042	0.0000	100.00	43.77	48.95
2	0.0057	0.0004	88.29	61.18	58.70
2.5	0.0062	0.0007	80.22	66.64	66.31
3	0.0071	0.0016	62.99	77.85	72.26
3.5	0.0071	0.0031	39.69	77.76	76.90
4	0.0076	0.0045	25.61	83.46	80.52
4.5	0.0076	0.0057	14.37	83.18	83.35
5	0.0079	0.0062	12.07	86.69	85.56
5.5	0.0075	0.0067	5.67	82.24	87.29
6	0.0079	0.0069	6.79	87.40	88.64

Table D.6 The result of preferential crystallization of L-Asn·H₂O in DL-Asn·H₂O for condition A5.

Time (h)	Soild concentration (g/gsol)		%enantiomeric excess	%yield of L-Asn·H ₂ O	%yield fitting curve
	L-Asn·H ₂ O	D-Asn·H ₂ O			
0	0.0009	0.0000	100.00	0.00	0.00
1	0.0038	0.0000	100.00	33.44	41.97
1.5	0.0055	0.0000	100.00	53.90	54.71
2	0.0065	0.0003	90.14	64.91	63.93
2.5	0.0076	0.0010	76.96	78.14	70.60
3	0.0076	0.0016	64.36	78.12	75.42
3.5	0.0075	0.0028	45.23	76.69	78.91
4	0.0082	0.0044	30.67	85.14	81.43
4.5	0.0078	0.0055	16.77	80.19	83.26
5	0.0085	0.0072	7.91	88.45	84.58
5.5	0.0083	0.0074	5.37	86.23	85.53
6	0.0076	0.0071	3.41	78.63	86.23

Table D.7 The conditions of preferential crystallization of L-Asn·H₂O in small batch crystallization.

Condition	Supersaturation ratio of DL-Asn·H ₂ O, S	Additives	%additives	Results
B1	1.3	-	-	Table D.8
B2	1.3	D-Asp	5%	Table D.9
B3	1.3	D-Glu	5%	Table D.10
B4	1.3	D-Val	5%	Table D.11
B5	1.3	D-Leu	5%	Table D.12

Table D.8 The result of preferential crystallization of L-Asn·H₂O in DL-Asn·H₂O for condition B1.

Time (h)	Soild concentration (g/gsol)		%enantiomeric excess	%yield of L-Asn·H ₂ O	%yield fitting curve
	L-Asn·H ₂ O	D-Asn·H ₂ O			
0	0.0005	0.0000	100.00	0.00	1.95
1	0.0008	0.0000	100.00	2.23	3.94
2	0.0017	0.0000	100.00	10.04	7.71
3	0.0021	0.0000	100.00	13.62	14.22
4	0.0033	0.0000	100.00	24.64	23.95
5	0.0046	0.0024	31.59	35.18	35.63
6	0.0058	0.0040	18.38	46.10	46.53
7	0.0068	0.0051	14.29	54.91	54.53

Table D.9 The result of preferential crystallization of L-Asn·H₂O in DL-Asn·H₂O for condition B2.

Time (h)	Soild concentration (g/gsol)		%enantiomeric excess	%yield of L-Asn·H ₂ O	%yield fitting curve
	L-Asn·H ₂ O	D-Asn·H ₂ O			
0	0.0005	0.0000	100.00	0.00	1.34
1	0.0006	0.0000	100.00	1.21	2.03
2	0.0014	0.0000	100.00	8.13	3.06
3	0.0012	0.0000	100.00	6.25	4.59
4	0.0012	0.0000	100.00	6.31	6.82
5	0.0017	0.0000	100.00	10.15	10.00
6	0.0018	0.0000	100.00	11.67	14.38
7	0.0023	0.0000	100.00	15.81	20.15
8	0.0043	0.0000	100.00	32.82	27.32
10	0.0055	0.0000	100.00	43.49	44.43

Table D.10 The result of preferential crystallization of L-Asn·H₂O in DL-Asn·H₂O for condition B3.

Time (h)	Soild concentration (g/gsol)		%enantiomeric excess	%yield of L-Asn·H ₂ O	%yield fitting curve
	L-Asn·H ₂ O	D-Asn·H ₂ O			
0	0.0005	0.0000	100.00	0.00	2.57
1	0.0008	0.0000	100.00	2.69	4.12
2	0.0009	0.0000	100.00	3.73	6.49
3	0.0014	0.0000	100.00	8.03	10.01
4	0.0029	0.0000	100.00	20.93	14.93
5	0.0027	0.0000	100.00	19.24	21.32
6	0.0046	0.0000	100.00	35.83	28.83
7	0.0039	0.0000	100.00	29.26	36.69
10	0.0070	0.0043	23.36	56.07	54.68

Table D.11 The result of preferential crystallization of L-Asn·H₂O in DL-Asn·H₂O for condition B4.

Time (h)	Soild concentration (g/gsol)		%enantiomeric excess	%yield of L-Asn·H ₂ O	%yield fitting curve
	L-Asn·H ₂ O	D-Asn·H ₂ O			
0	0.0005	0.0000	100.00	0.00	1.30
1	0.0008	0.0000	100.00	2.23	2.95
2	0.0011	0.0000	100.00	5.12	6.49
3	0.0025	0.0000	100.00	17.16	13.40
4	0.0030	0.0000	100.00	21.99	24.65
5	0.0050	0.0027	31.01	39.36	38.49
6	0.0063	0.0047	14.62	50.58	50.69

Table D.12 The result of preferential crystallization of L-Asn·H₂O in DL-Asn·H₂O for condition B5.

Time (h)	Soild concentration (g/gsol)		%enantiomeric excess	%yield of L-Asn·H ₂ O	%yield fitting curve
	L-Asn·H ₂ O	D-Asn·H ₂ O			
0	0.0005	0.0000	100.00	0.00	0.34
1	0.0008	0.0000	100.00	2.97	1.51
2	0.0011	0.0000	100.00	5.57	6.25
3.25	0.0033	0.0000	100.00	24.01	23.86
5	0.0055	0.0019	49.07	43.79	43.82
6	0.0061	0.0038	23.47	48.37	46.05

Table D.13 The conditions of preferential crystallization of L-Asn·H₂O with Tailor-made additives inhibition.

Condition	Supersaturation ratio of DL-AsnH ₂ O	Additives	%additives	Results
C1	1.3	D-Asp	3%	Table D.14
C2	1.3	D-Asp	5%	Table D.15
C3	1.3	D-Asp	7%	Table D.16
C4	1.3	D-Glu	3%	Table D.17
C5	1.3	D-Glu	5%	Table D.18
C6	1.3	D-Glu	7%	Table D.19

Table D.14 The result of preferential crystallization of L-Asn·H₂O in DL-Asn·H₂O for condition C1.

Time (h)	Soild concentration (g/gsol)		%enantiomeric excess	%yield of L-Asn·H ₂ O	%yield fitting curve
	L-Asn·H ₂ O	D-Asn·H ₂ O			
0	0.0019	0.0000	100.00	0.00	0.00
1	0.0069	0.0000	100.00	59.01	56.22
2	0.0078	0.0000	100.00	69.57	72.62
3	0.0083	0.0000	100.00	75.07	77.40
4	0.0083	0.0000	100.00	74.85	78.80
5	0.0085	0.0000	100.00	77.93	79.20
6	0.0086	0.0000	100.00	79.46	79.32
7	0.0089	0.0011	78.55	82.33	79.36
8	0.0091	0.0020	63.54	84.54	79.37

Table D.15 The result of preferential crystallization of L-Asn·H₂O in DL-Asn·H₂O for condition C2.

Time (h)	Soild concentration (g/gsol)		%enantiomeric excess	%yield of L-Asn·H ₂ O	%yield fitting curve
	L-Asn·H ₂ O	D-Asn·H ₂ O			
0	0.0019	0.0000	100.00	0.00	0.00
1	0.0057	0.0000	100.00	45.38	45.64
2	0.0077	0.0000	100.00	68.91	65.85
3	0.0080	0.0000	100.00	72.21	74.81
4	0.0085	0.0000	100.00	77.49	78.77
5	0.0085	0.0000	100.00	77.93	80.52
6	0.0088	0.0000	100.00	80.78	81.30
7	0.0089	0.0000	100.00	82.32	81.65
9	0.0092	0.0002	96.66	85.56	81.87

Table D.16 The result of preferential crystallization of L-Asn·H₂O in DL-Asn·H₂O for condition C3.

Time (h)	Soild concentration (g/gsol)		%enantiomeric excess	%yield of L-Asn·H ₂ O	%yield fitting curve
	L-Asn·H ₂ O	D-Asn·H ₂ O			
0	0.0019	0.0000	100.00	0.00	0.00
1	0.0044	0.0000	100.00	3.24	29.76
2	0.0063	0.0000	100.00	51.75	46.18
3	0.0075	0.0000	100.00	66.05	55.24
4	0.0083	0.0000	100.00	75.51	60.24
5	0.0078	0.0000	100.00	69.79	62.99
7	0.0068	0.0000	100.00	57.47	65.36
8	0.0071	0.0000	100.00	60.99	65.82
9	0.0066	0.0000	100.00	55.49	66.07
10	0.0076	0.0000	100.00	66.71	66.21
11	0.0076	0.0000	100.00	67.59	66.29

Table D.17 The result of preferential crystallization of L-Asn·H₂O in DL-Asn·H₂O for condition C4.

Time (h)	Soild concentration (g/gsol)		%enantiomeric excess	%yield of L-Asn·H ₂ O	%yield fitting curve
	L-Asn·H ₂ O	D-Asn·H ₂ O			
0	0.0019	0.0000	100.00	0.00	0.00
1	0.0063	0.0000	100.00	51.75	44.23
1.5	0.0067	0.0000	100.00	56.81	56.36
2	0.0069	0.0000	100.00	58.57	64.58
2.5	0.0080	0.0000	100.00	71.55	70.16
3	0.0083	0.0002	94.48	75.60	73.94
3.5	0.0073	0.0008	80.40	63.38	76.51
4	0.0087	0.0017	67.55	80.52	78.25
4.5	0.0082	0.0029	47.43	74.70	79.43
5	0.0092	0.0037	42.89	85.71	80.23
5.5	0.0096	0.0050	31.88	90.47	80.77
6	0.0086	0.0047	28.84	78.53	81.14

Table D.18 The result of preferential crystallization of L-Asn·H₂O in DL-Asn·H₂O for condition C5.

Time (h)	Soild concentration (g/gsol)		%enantiomeric excess	%yield of L-Asn·H ₂ O	%yield fitting curve
	L-Asn·H ₂ O	D-Asn·H ₂ O			
0	0.0019	0.0000	100.00	0.00	0.00
1	0.0053	0.0000	100.00	40.54	44.98
1.5	0.0071	0.0000	100.00	61.87	56.10
2	0.0075	0.0000	100.00	66.49	63.18
2.5	0.0072	0.0000	100.00	62.31	67.69
3	0.0076	0.0003	92.07	66.78	70.55
3.5	0.0084	0.0007	84.74	76.60	72.38
4	0.0082	0.0016	67.48	74.40	73.54
4.5	0.0082	0.0027	51.23	74.53	74.27
5	0.0079	0.0036	37.96	71.08	74.74
5.5	0.0085	0.0039	37.68	77.85	75.04
6	0.0083	0.0048	26.08	74.85	75.23

Table D.19 The result of preferential crystallization of L-Asn·H₂O in DL-Asn·H₂O for condition C6.

Time (h)	Soild concentration (g/gsol)		%enantiomeric excess	%yield of L-Asn·H ₂ O	%yield fitting curve
	L-Asn·H ₂ O	D-Asn·H ₂ O			
0	0.0019	0.0000	100.00	0.00	0.00
1	0.0052	0.0000	100.00	38.56	44.54
1.5	0.0066	0.0000	100.00	55.49	53.64
2	0.0079	0.0000	100.00	70.23	58.78
2.5	0.0064	0.0000	100.00	53.51	61.69
3	0.0072	0.0000	100.00	62.97	63.34
3.5	0.0078	0.0000	100.00	69.57	64.27
4	0.0076	0.0004	89.70	67.36	64.79
4.5	0.0068	0.0007	82.45	57.33	65.09
5	0.0078	0.0013	71.05	69.68	65.26
5.5	0.0073	0.0018	60.82	64.02	65.35
6	0.0072	0.0024	50.75	62.62	65.41



APPENDIX E

**CALCULATION OF TOTAL CRYTAL COUNT BY
FOCUSED BEAM REFLECTANCE MEASUREMENT**

มหาวิทยาลัยเทคโนโลยีสุรนารี

Calculation of total crystal count by focused beam

The data of particle count number from Focused Beam Reflectance Measurement (FBRM) report the number of particle that pass and contact to the FBRM probe. Therefore, the total number of particle in the crystallizer is defined. We used the calcium carbonate (CaCO_3) to construct the relationship between the number of particle from FBRM and total number of particle in crystallizer.

CaCO_3 size 75-90 microns was prepared by sieve. The 500 mL of saturated solution of CaCO_3 in water at 25°C was also prepared in the crystallizer. Set up the process by put the FBRM probe into the crystallizer and using overhead stirrer 400 rpm to stir the solution. The 1 g of CaCO_3 was seeded into the crystallizer to measure the particle size distribution by FBRM which FBRM was programmed to measure the particle size every 5 s. After 10 min of measurement, the CaCO_3 was added again for 1 g to get 2 g until 5 g to measure the particle size distribution when increase total amount of particle number.

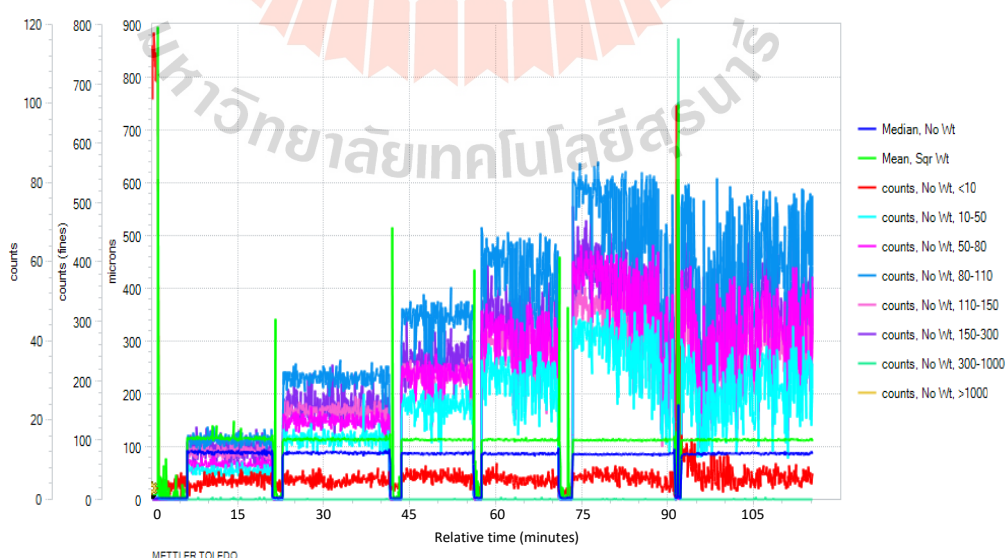


Figure E.1 The relationship between particle count number and time.

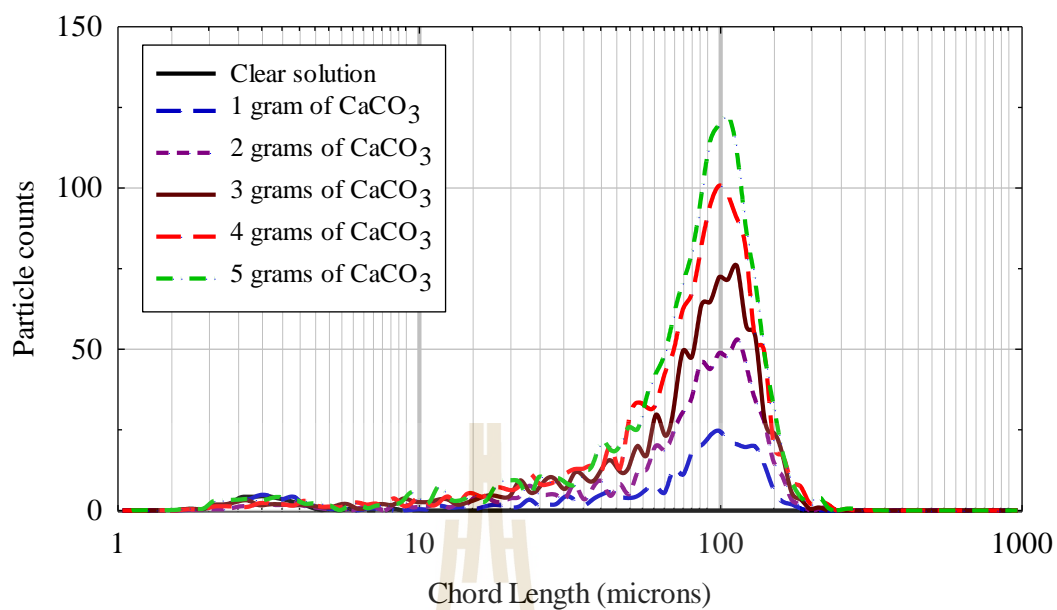


Figure E.2 The particle size distribution of CaCO_3 .

From the particle size distribution (PSD) in Figure E.2, the total number of particle can show the summarize in Table E.1. The relationship between the number of particle from FBRM and mass of CaCO_3 is plotted in Figure E.3 and fitting with linear equation in equation (E.1).

Table E.1 The number of CaCO_3 particle from FBRM.

Amount of CaCO_3 (g)	Number of particle from FBRM
1	335.27
2	664.38
3	973.92
4	1289.99
5	1498.08

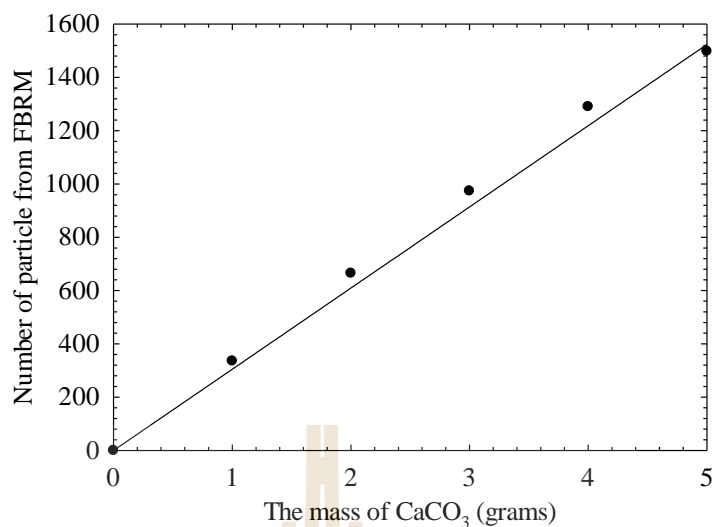


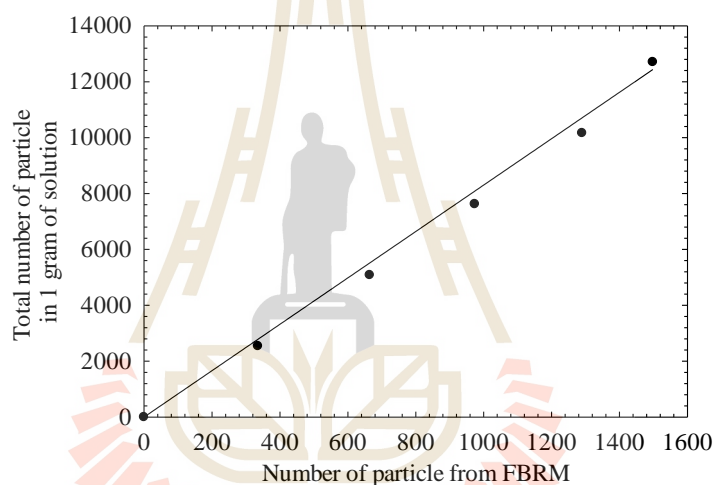
Figure E.3 The relationship between the number of particle from FBRM and mass of CaCO₃.

$$\text{Number of particle from FBRM} = \text{Mass of CaCO}_3 \text{ (g)} \times 304.690 \quad (\text{E.1})$$

From the information of CaCO₃ and the result from FBRM, the volume of particle is $2.905 \times 10^{-7} \text{ cm}^3$. The mass of CaCO₃ 1 particle is $7.872 \times 10^{-7} \text{ g}$. The total number of CaCO₃ are shown in Table E.2. The relationship between particle from FBRM and total number of particle in 1 g of solution is shown in Figure E.4 and the fitting curve with linear equation is shown in Equation (E.2).

Table E.2 The total number of CaCO₃ particles in 500 mL of solution.

Amount of CaCO ₃ (g)	Total number of particle (in 500 mL)	Total number of particle (no./g of solution)
0	0	0.00
1	1.270E+06	2540.57
2	2.541E+06	5081.15
3	3.811E+06	7621.72
4	5.081E+06	10162.29
5	6.351E+06	12702.86

**Figure E.4** The relationship between particle from FBRM and total number of particle in 1 gram of solution.

$$\text{Total no. of particle (no./g solution)} = 8.3016 \times \text{number of particle from FBRM} \quad (\text{E.2})$$



APPENDIX F

**RAW DATA OF CRYSTAL SIZE DISTRIBUTION
DURING THE PREFERENTIAL CRYSTALLIZATION
OF L-SAPARAGINE MONOHYDRATE WITH THE
INHIBITIONS BY TAILOR-MADE ADDITIVES**

Table F.1 The conditions for preferential crystallization of L-Asn·H₂O for finding the particle size distribution.

Condition	Supersaturation ratio of DL-AsnH ₂ O	Additives	%additives	Results
D1	1.3	-	-	Table F.2
D2	1.3	D-Glu	5%	Table F.3
D3	1.3	D-Asp	5%	Table F.4

Table F.2 The conditions of preferential crystallization of L-Asn·H₂O from DL-Asn·H₂O without additives (D1).

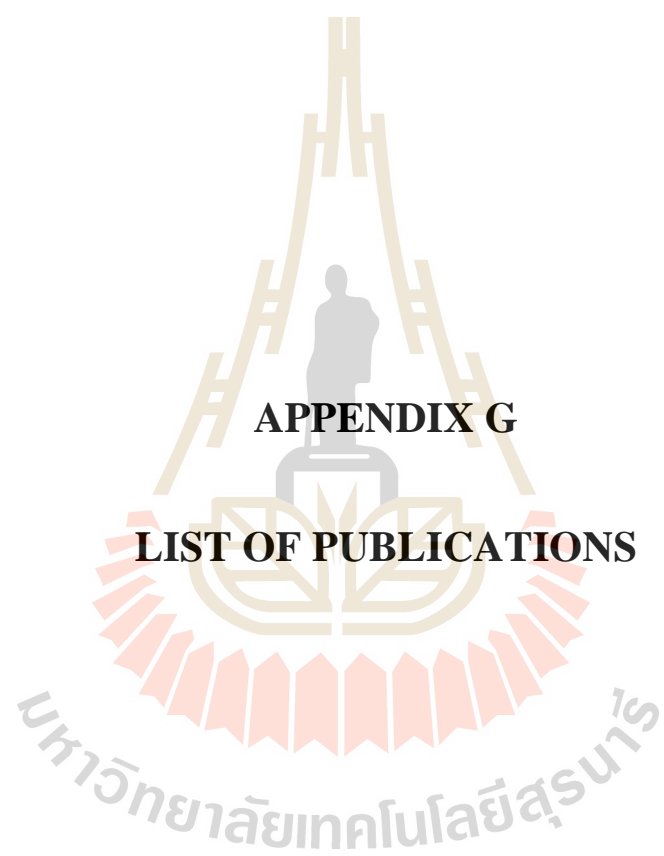
Time	Relative supersaturation of L-Asn·H ₂ O	Concentration (g/gsol)		Solid concentration (g/gsol)		% yield of L-Asn·H ₂ O		%Enantiomeric excess	Mean crystal size of L-Asn·H ₂ O
		L-Asn·H ₂ O	D-Asn·H ₂ O	L-Asn·H ₂ O	D-Asn·H ₂ O	Experiments	Fitting Curve		
0	0.3257	0.0316	0.0316	0.0019	0.0000	0.00	0.00	100.00	-
1	0.2470	0.0297	0.0316	0.0037	0.0000	21.99	20.98	100.00	43.65
2	0.2204	0.0291	0.0316	0.0044	0.0000	29.42	35.84	100.00	68.94
3	0.1747	0.0280	0.0316	0.0055	0.0000	42.19	46.37	100.00	87.63
4	0.0868	0.0259	0.0300	0.0076	0.0016	66.76	53.83	65.79	105.05
5	0.1076	0.0264	0.0290	0.0071	0.0026	60.93	59.11	46.70	119.28
6	0.1151	0.0266	0.0279	0.0069	0.0037	58.84	62.86	30.70	129.88
7	0.0993	0.0262	0.0265	0.0073	0.0051	63.25	65.51	17.46	134.15

Table F.3 The conditions of preferential crystallization of L-Asn·H₂O from DL-Asn·H₂O with D-Glu additives (D2).

Time	Relative supersaturation of L-Asn·H ₂ O	Concentration (g/gsol)		Solid concentration (g/gsol)		% yield		%Enantiomeric excess	Mean crystal size of L-Asn·H ₂ O
		L-Asn·H ₂ O	D-Asn·H ₂ O	L-Asn·H ₂ O	D-Asn·H ₂ O	Experiments	Fitting Curve		
0	0.3257	0.0316	0.0316	0.0019	0.0000	0.00	0.00	100.00	-
1	0.2629	0.0301	0.0316	0.0034	0.0000	17.53	18.35	100.00	46.85
2	0.2355	0.0295	0.0316	0.0040	0.0000	25.19	31.23	100.00	62.11
3	0.1628	0.0277	0.0316	0.0058	0.0000	45.51	40.26	100.00	74.92
4	0.1397	0.0272	0.0316	0.0063	0.0000	51.98	46.60	100.00	82.33
5	0.1577	0.0276	0.0316	0.0059	0.0000	46.94	51.04	100.00	87.74
6	0.1400	0.0272	0.0316	0.0063	0.0000	51.87	54.16	100.00	93.74
7	0.1191	0.0267	0.0313	0.0068	0.0003	57.73	56.35	92.25	97.12

Table F.4 The conditions of preferential crystallization of L-Asn·H₂O from DL-Asn·H₂O with D-Asp additives (D3).

Time	Relative supersaturation of L-Asn·H ₂ O	Concentration (g/gsol)		Solid concentration (g/gsol)		% yield		%Enantiomeric excess	Mean crystal size of L-Asn·H ₂ O
		L-Asn·H ₂ O	D-Asn·H ₂ O	L-Asn·H ₂ O	D-Asn·H ₂ O	Experiments	Fitting Curve		
0	0.3257	0.0316	0.0316	0.0019	0.0000	0.00	0.00	100.00	-
1	0.2476	0.0297	0.0316	0.0037	0.0000	21.83	18.32	100.00	46.11
2	0.2206	0.0291	0.0316	0.0044	0.0000	29.37	31.06	100.00	56.84
3	0.1924	0.0284	0.0316	0.0050	0.0000	37.24	39.90	100.00	61.58
4	0.1639	0.0277	0.0316	0.0057	0.0000	45.21	46.05	100.00	65.52
5	0.1424	0.0272	0.0316	0.0062	0.0000	51.21	50.32	100.00	66.80
6	0.1402	0.0272	0.0316	0.0063	0.0000	51.81	53.29	100.00	66.96
7	0.0860	0.0259	0.0316	0.0076	0.0000	66.98	55.36	100.00	65.96
8	0.1375	0.0271	0.0316	0.0064	0.0000	52.58	56.79	100.00	68.25
9	0.1247	0.0268	0.0316	0.0067	0.0000	56.16	57.79	100.00	70.19
10	0.1143	0.0266	0.0316	0.0069	0.0000	59.05	58.48	100.00	71.58
11	0.1477	0.0274	0.0316	0.0061	0.0000	49.74	58.96	100.00	71.36
12	0.1111	0.0265	0.0316	0.0070	0.0000	59.96	59.29	100.00	72.53
13	0.1032	0.0263	0.0316	0.0072	0.0000	62.18	59.53	100.00	73.27
14	0.1002	0.0262	0.0316	0.0072	0.0000	63.01	59.69	100.00	74.47
15	0.1133	0.0265	0.0316	0.0069	0.0000	59.33	59.80	100.00	75.27



APPENDIX G

LIST OF PUBLICATIONS

List of Publications

Kongsamai, P., Maneedaeng, A., Flood, C., ter Horst, J. H., and Flood, A. E. (2017). Effect of additives on the preferential crystallization of L-asparagine monohydrate. **The European Physical Journal Special Topics** 226 (5):823-835.

List of Proceedings

Kongsamai, P., Flood, C., and Flood, A.E. (2017). **The Effect of D-Glutamic Acid to the Preferential Crystallization of L-Asparagine monohydrate.** The 118th RGJ Seminar Series, Nakhon Ratchasima, Thailand. 1-2 May 2017.

Kongsamai, P., Flood, A.E, Maneedaeng, A., Flood, C., and ter Horst, J.H. (2016). **The Effect of D-Glutamic Acid to the Preferential Crystallization of L-Asparagine monohydrate.** The 17th RGJ-Ph.D. Congress, Chonburi, Thailand. 8-11 June 2016.

Flood, A.E., Kongsamai, P., Maneedaeng, A., Flood, C., and ter Horst, J.H. (2016). **Mechanisms of the Effect of Additives on the Preferential Crystallization of L-Asparagine Monohydrate.** The 12th International Workshop of the Crystal Growth of Organic Materials (GCOM12), Leeds, United Kingdom. 26-30 June 2016.

Flood, A.E., Kongsamai, P., Maneedaeng, A., and ter Horst, J.H. (2015). **Effect of D-Aspartic Acid on the Preferential Crystallization of L-Asparagine monohydrate.** The 22nd International Workshop on Industrial Crystallization (BIWIC 2015), Daejeon, South Korea. 9-11 September 2015.

Kongsamai, P., Maneedaeng, A., Flood, A.E, and ter Horst, J.H. (2014). **Additive effects on the preferential crystallization of L-asparagine monohydrate.**

The 19th International Symposium on Industrial Crystallization (ISIC), Toulouse, France. 16-19 September 2014.

Kongsamai P., Maneedaeng, A., and Flood A. E. (2013). **Effect of Tailor-Made Additives to Crystal Growth Rate.** Conference Proceedings of the 5th Regional Conference on Chemical Engineering, Chonburi, Thailand. 7-8 February 2013.



Effect of additives on the preferential crystallization of L-asparagine monohydrate

Peetikamol Kongsamai¹, Atthaphon Maneedaeng¹, Chalongsri Flood¹,
Joop H. ter Horst², and Adrian E. Flood^{3,a}

¹ School of Chemical Engineering, Suranaree University of Technology, 111 University Avenue, Nakhon Ratchasima, Thailand

² EPSRC Centre for Innovative Manufacturing in Continuous Manufacturing and Crystallisation (CMAC), Strathclyde Institute of Pharmacy and Biomedical Sciences, Technology and Innovation Centre, University of Strathclyde, 99 George Street, Glasgow G1 1RD, UK

³ Department of Chemical and Biomolecular Engineering, School of Energy Science and Engineering, Vidyasirimedhi Institute of Science and Technology, 555 Moo 1, Payupnai, Wang Chan, Rayong 21210, Thailand

Received 3 September 2016 / Received in final form 30 October 2016

Published online 18 April 2017

Abstract. Preferential Crystallization (PC) is a popular process to separate enantiomers, however the nucleation and growth of the counter enantiomer during the process can compromise the enantiopurity of the final crystalline product. This research investigates the use of additives to inhibit the nucleation and growth of the counter enantiomer. In this study, we use L-asparagine monohydrate (L-Asn·H₂O) as the preferred enantiomer in crystallization from DL-Asn·H₂O solutions. Additives include both pure enantiomers of several related amino acid species. This allows investigation of differences in inhibition caused by additives that are of the same chirality and different chirality as the preferred enantiomer. The additives had no discernible effect on the solubility but had a small effect on the metastable limit, with additives tending to slightly widen the metastable zone but also make the zone widths more disperse. D-additives have a small effect on the growth rate of L-Asn·H₂O but L-Asp and L-Glu strongly inhibit the growth rate of L-Asn·H₂O in DL-Asn·H₂O solution; there must also be a corresponding effect for D-Asp and D-Glu on D-Asn·H₂O. Indeed, PC experiments showed that in order to obtain L-Asn·H₂O from a PC while preventing the formation of D-Asn·H₂O, D-Asp and D-Glu are suitable additives, leading to high yield and purity of pure L-Asn·H₂O.

1 Introduction

Many products in pharmaceutical, food and agrochemical industries are chiral compounds. The two enantiomers of a chiral compound are two stereoisomers and the two

^a e-mail: adrian.f.vistec@gmail.com.

molecules are non-superimposable mirror images [1]. The pair of enantiomers have identical physical and chemical properties (apart from the optical rotation) in achiral solvents but are different in biological activities [2]. In the chemical synthesis of chiral materials the product of the synthesis is usually a racemic mixture of enantiomers; 50% is the preferred enantiomer and 50% is the counter enantiomer. Normally, the counter enantiomer has no beneficial effect but does increase the drug loading on the body. In some cases the counter enantiomer is harmful; R-thalidomide was used as a sedative and sleeping drug for pregnant women, however, S-thalidomide was found to be teratogenic and caused birth defects in thousands of babies [3]. Therefore the separation of enantiomers is essential in many industries, but particularly in the pharmaceutical industry.

There are many processes to separate enantiomers. Chiral membrane separation uses a chiral-modified membrane which allows the desired enantiomer to selectively diffuse through or adsorb onto the membrane [4]. Chiral chromatography separation uses an enantioselective chiral stationary phase to separate enantiomers [5,6]. However, crystallization has unprecedented selectivity and potentially leads to an enantiopure product within a single process step if the crystallization of the counter enantiomer can be avoided. This can be done through the formation of diastereomeric salts which changes the enantiomers to diastereomers which have different physical properties and enables separation by crystallization [7]. However, this requires an additional separation step to recover the resolving agent.

Preferential crystallization (PC) is a single step process that is easy and low cost for separating enantiomers. This process is suitable for separation of a racemic mixture that is a conglomerate forming system, meaning the equilibrium product is a mechanical mixture of the two enantiomorphs [8]. PC achieves separation in a single process step through seeding the preferred enantiomer to the supersaturated racemic solution; the preferred enantiomer will crystallize at a higher rate than the counter enantiomer, and significant yield and enantiopurity can be achieved if the nucleation and growth of the counter enantiomer from the supersaturated solution can be avoided. PC has been applied to chiral species such as glutamic acid [9], asparagine [10], threonine [11] and methionine hydrochloride [12]. However, this method has a serious problem which is the spontaneous nucleation and growth of the counter enantiomer. This may occur after prolonged batch times where the solution has a high supersaturation of the counter enantiomer in comparison to the preferred enantiomer [11]. Many researchers have tried to circumvent this problem, for instance by using coupled batch crystallizers – crystallizing the preferred enantiomer in one crystallizer and the counter enantiomer in another crystallizer, with exchange of solution between the two crystallizers [13], coupled batch crystallizers with seeding of the preferred enantiomer in one crystallizer and allowing nucleation of the counter enantiomer in another crystallizer maintained at a different temperature [14,15], coupled batch crystallizers with a membrane between the crystallizers to prevent transport of crystals from one crystallizer to another [16], and racemization of the solute species to equalize the concentrations of the preferred and counter enantiomer [17,18].

Another way to circumvent the crystallization of the counter enantiomer is to use tailor made additives to inhibit the nucleation and growth of the counter enantiomer. This will be convenient if the scale of the resolution is such that a fully batch system is most suitable and crystallization or recycling of the counter enantiomer is not required. A tailor made additive is any additive which is intelligently designed to change the crystallization process in a desired way. It may inhibit either growth or nucleation, or more rarely promote growth or nucleation, or it may alter the shape or morphology of the crystals. Addadi et al. proposed the rule of reversal, which suggests that additives most easily adsorb on the surface of the crystal that has the same absolute configuration as the additive [19,20]. The rule thus states that the chiral

additive will inhibit the crystallization of the enantiomorph similar in chirality to the additive. There are many studies about effect of tailor made additives to the crystallization such as effect of D- and L-lysine additives on DL-glutamic acid [9, 21, 22].

We are interested in the technique of preferential crystallization using tailor made additives because it uses only a small amount of additive and is easier to operate than other techniques. However the mechanism by which the additives affect the preferential crystallization, or more specifically the mechanism by which additives reduce the crystallization rate of the counter enantiomer is not known. The present research investigates the solubility and metastable zone width, and both the nucleation and crystal growth processes in the presence and absence of additives in an attempt to determine which of the crystallization mechanisms is altered by the presence of the additive.

Doki et al. investigated the effect of pure enantiomeric amino acid additives on the enantiomeric purity of asparagine crystals obtained from racemic solutions [23]. In these unseeded crystallizations they observed a significant delay in the crystallization of the counter enantiomer, indicating that asparagine is an interesting model compound to investigate the effect of chiral additives on asparagine PC. Therefore, following the rule of reversal, we further investigate the preferential crystallization process of L-asparagine monohydrate (L-Asn·H₂O) from DL-Asn·H₂O by using D- and L-amino acid additives which have a similar structure to asparagine. We also investigate the efficiency and yield of the preferential crystallization when using additives. To explain the observed effects we separately study the effect of additives on the solubility, metastable zone width and the growth rate.

2 Experimental methods

2.1 Materials

DL-asparagine monohydrate (99+ wt%), L-asparagine monohydrate (99+ wt%) and D-asparagine monohydrate (99+ wt%), were purchased from Sigma-Aldrich. D(-)-aspartic acid (99+ wt%), D(-)-glutamic acid (99+ wt%), D-valine (98+ wt%), D-leucine (99 wt%), L-(+)-aspartic acid (98+ wt%), L-(+)-glutamic acid (99+ wt%), L-valine (98+ wt%), and L-leucine (99 wt%) were purchased from ACROS. These reagents were used without further purification. Deionized water was used as the solvent.

2.2 Experimental procedure

2.2.1 Solubility and metastable zone width

The solubility and the metastable zone limit of L-Asn·H₂O with and without additives were determined using the Crystal16 (Technobis, Amsterdam). Samples were prepared with a known concentration of Asn·H₂O in 1 g of water. To determine the clear point temperature (the temperature at which the suspension turns into a clear solution upon heating), the suspension in the vial was heated with a heating rate of 0.1 °C/min up to 60 °C to complete dissolution. The temperature at which the turbidity reached zero was recorded. To determine the cloud point temperature (the temperature at which the clear solution turns into a suspension upon cooling), the clear solution was subsequently cooled down to 2 °C with a cooling rate of 0.1 °C/min. The clear point temperature was taken as the saturation temperature of the solution while the cloud point was taken as the metastable limit of the solution for the cooling rate used. The region between the saturation temperature and the highest metastable zone limit measured for a sample was taken as the metastable zone region. For the results, two or three measurements were performed subsequently with the same solution.

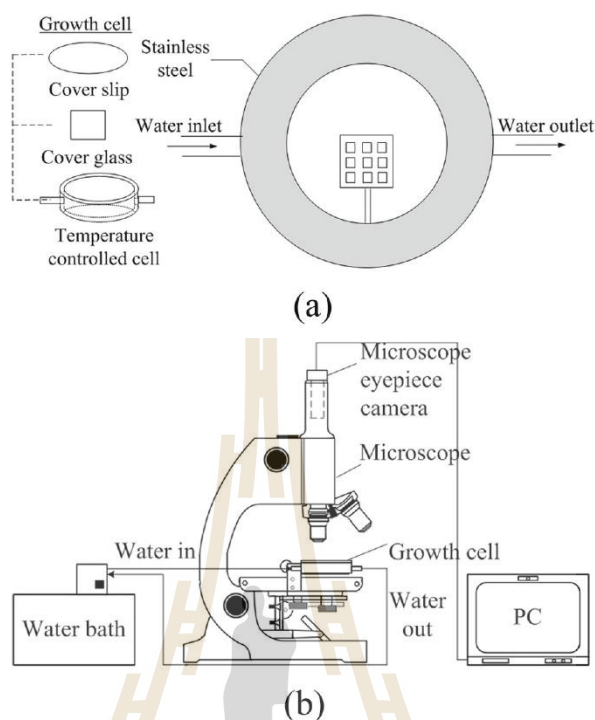


Fig. 1. The experimental set up of growth rate experiment (a) crystal growth cell and (b) experimental set up.

2.2.2 Single crystal growth rate experiments

Stock suspensions with various amounts of DL-Asn·H₂O in the presence and absence of various additives were prepared at 30 °C and heated up to 58 °C to completely dissolve the solute. When needed, the solution was cooled to the crystallization temperature, 30 °C. Nine crystals of L-Asn·H₂O were attached by glue to a cover glass that was placed in a 50 cm³ small cell which was temperature-controlled using a jacket on the cell which used water from a constant temperature bath. The experimental set up is shown in Figure 1. The growth process of L-Asn·H₂O was initiated when we added the solution to the cell. The size of the crystal was measured every 10 minutes until 80 minutes using a microscope and the DinoCapture 2.0 program. We analyzed the concentration in the cell using an automatic digital refractometer (RFM 340, Bellingham+Stanley Ltd., UK). We investigated the growth rate of L-Asn·H₂O crystals using supersaturation ratios (S) of 1.05, 1.10 and 1.15 for L-Asn·H₂O and DL-Asn·H₂O solutions. For investigation of the effect of additives we used 3 mol% of additives based on the total concentration of DL-AsnH₂O in solution at a supersaturation ratio (S) of 1.1.

2.2.3 Preferential crystallization

The preferential crystallization of L-Asn·H₂O (the preferred enantiomer) from DL-Asn·H₂O was performed, and additives were used to inhibit D-Asn·H₂O (the counter enantiomer). We prepared a solution of DL-Asn·H₂O with a supersaturation ratio (S) of 1.3 at 30 °C in 40 g of water in a 50 mL crystallization vessel with jacket to control the temperature. Additives were added to the solution at 5 mol% compared to the total amount of DL-Asn·H₂O. The solution was heated to 50 °C to completely dissolve

the crystalline material. Subsequently, the solution was cooled down rapidly to the crystallization temperature of 30 °C. L-Asn·H₂O seeds, 0.02 g (300–500 micron) were added into the solution the moment the crystallization temperature reached 30 °C. The process was stopped at a given time and the suspension was vacuum filtered to obtain crystal samples at different times from 1 h to 7 h after the addition of seeds. The solid product was kept in a desiccator for drying. The solid products were analysed by HPLC (1260 Infinity, Agilent Technologies) with a Chirobiotic T column. The HPLC analysis was performed at 25 °C using a 70:30 vol% ethanol:water mixture as a mobile phase at 0.4 mL/min, and using UV detection at 205 nm. The injection volume was 5 µL. Under these conditions the detection time for L-Asn·H₂O was 18 min and the retention time of D-Asn·H₂O was 27 min.

3 Results and discussion

First the solubility and metastable zone limit are presented, followed by the crystal growth rate experiments in the presence and absence of the additives. Finally, preferential crystallization of L-Asn·H₂O in DL-Asn·H₂O with and without additives is discussed.

3.1 Solubility and metastable zone width

Asparagine monohydrate is a conglomerate forming system [24] which is suitable for the PC process [6]. The solubility and metastable zone width of L-Asn·H₂O, DL-Asn·H₂O and L-Asn·H₂O with 5% additives is shown in Figure 2 where the solubility values are given in mg Asn·H₂O/g H₂O. The solubility of L-Asn·H₂O increases with increasing temperature. The solubility of DL-Asn·H₂O is slightly more than twice the L-Asn·H₂O solubility and thus only approximately follows the Meyerhoffer solubility rule [25]. The current data agrees well with the single data point for aqueous systems of Orella and Kirwan [26], 28.7 mg L-Asp·H₂O/g H₂O at 25 °C. However the data for the L-Asn·H₂O/g H₂O is around 4-5% lower than equivalent results of Dalton and Schmidt [27]: however that study is over 80 years old, and perhaps the purification of the amino acids was more difficult at that point. Solubility data over the entire range of temperatures measured agree very well with the recent data of Binev et al. [28].

Since D-Asn·H₂O and L-Asn·H₂O are a pair of enantiomers, the solubility and metastable zone width (MSZW) are the same for these species (in the absence of chiral additives, or if equivalent chiral additives are used). The solubility of D-Asn·H₂O with D-enantiomer additives is almost identical to the solubility of pure D-Asn·H₂O (by comparison to the solubility of pure L-Asn·H₂O). It was found that the D-enantiomer additives do have an effect on the MSZW of D-Asn·H₂O. The results are very scattered, but the additives appear to slightly increase the MSZW of D-Asn·H₂O, and also increase the range of possible values. Equivalent effects would be seen for the effect of L-additives on L-Asn·H₂O. The MSZWs for the DL-Asn·H₂O systems are significantly larger than those from the previous studies [28]. This is curious since both studies used identical techniques and equipment (the Crystal16, multiple reactor system). It is known that the MSZW is reliant on the nucleation rates of the solute, and so is very sensitive to small changes in the properties of the measurement device and also to the properties of the solution, for instance trace levels of impurity and dust.

3.2 Crystal growth rate of L-Asn·H₂O in L-/DL-Asn·H₂O with additives

The shape of crystals of L-Asn·H₂O grown from aqueous solution at various times is shown in Figure 3. We used the length of the principal axis of the crystal to find the

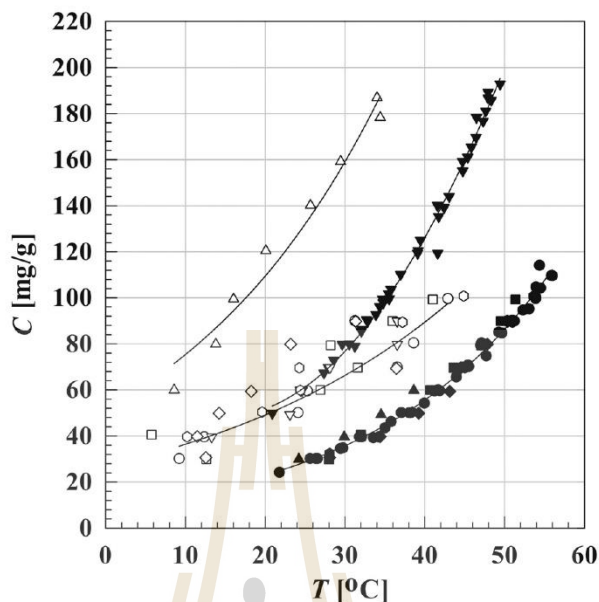


Fig. 2. The solubility and metastable limit of L-/DL-Asn-H₂O with and without additives in water. Solubility points consist of L-Asn-H₂O (●), DL-Asn-H₂O (▼), D-Asn-H₂O with D-Asp (■), D-Asn-H₂O with D-Leu (◆), D-Asn-H₂O with D-Glu (▲), D-Asn-H₂O with D-Val (●), and cloud points consist of L-Asn-H₂O (○), DL-Asn-H₂O (△), D-Asn-H₂O with D-Asp (□), D-Asn-H₂O with D-Leu (◇), D-Asn-H₂O with D-Glu (▽), and D-Asn-H₂O with D-Val (○). The lines are guide to the eye.

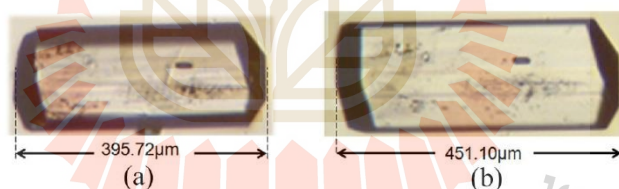


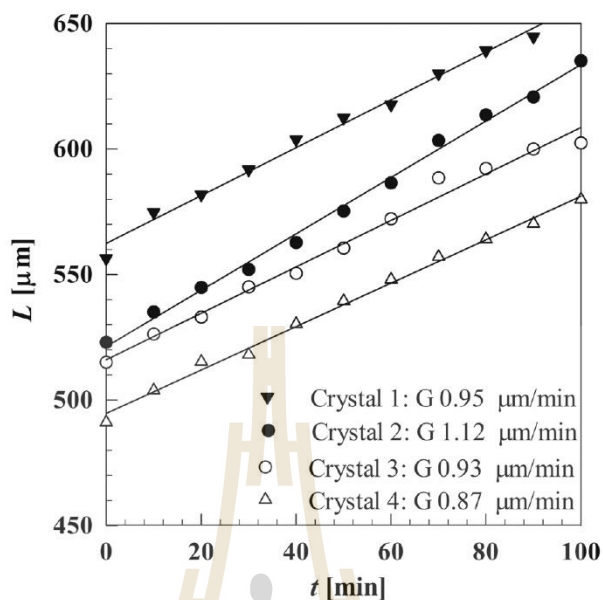
Fig. 3. Crystal shape of L-Asn-H₂O in DL-Asn-H₂O with supersaturation, S equal to 1.1 at (a) 0 min and (b) 80 min.

crystal growth rate. The crystal growth rate of each L-Asn-H₂O crystal in solution can be found from the slope of the plot between the length of crystal and time as shown in Figure 4.

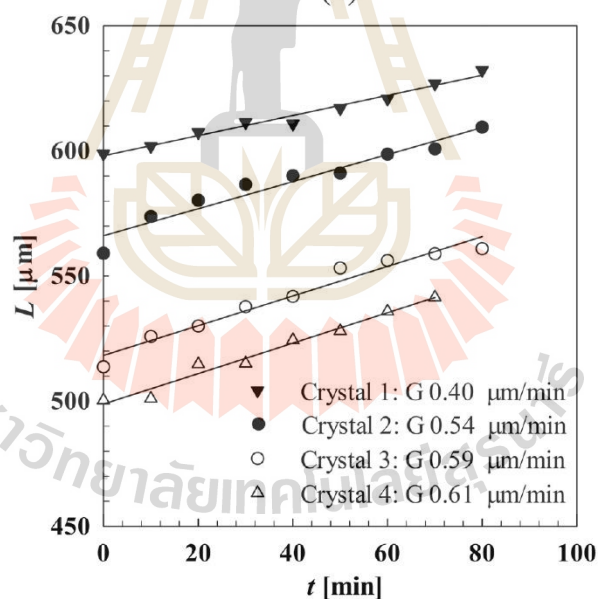
The crystal growth rate of L-Asn-H₂O crystals in supersaturated solutions of L- and DL-Asn-H₂O, and DL-Asn-H₂O with D/L- additives can be plotted as growth rate distributions, growth rate frequency vs growth rate of L-Asn-H₂O, as shown in Figure 5, and also modeled based on the normal distribution, equation (1).

$$f_G(G) = a \cdot \exp\left(-\frac{(G - G_0)^2}{2\sigma_G^2}\right) \quad (1)$$

where f_G is the growth rate frequency, G is the crystal growth rate, G_0 is the mean growth rate of the distribution, σ_G is the standard deviation of the growth rate distribution, and a is a parameter relating only to the total number of samples in the distribution [29]. While there is no *a priori* knowledge of the shape of the growth



(a)



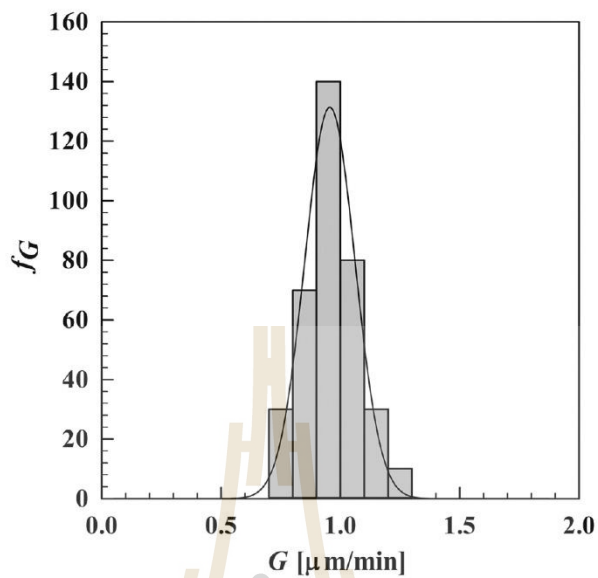
(b)

Fig. 4. Relationship between crystal size (length) of L-Asn·H₂O and time in supersaturated solution ($S = 1.1$) of (a) L-Asn·H₂O and (b) DL-Asn·H₂O at 30 °C.

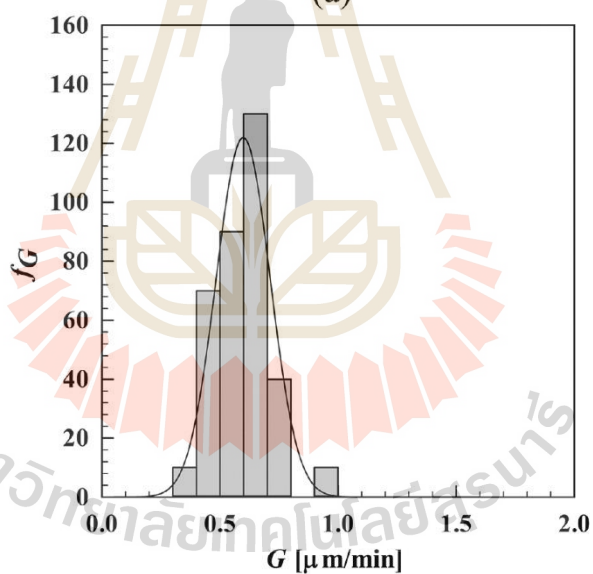
rate distributions, the distributions found are relatively narrow and fit the normal distribution quite well.

The fitting parameters for the crystal growth rate of L-Asn·H₂O crystals in various supersaturated solutions of L- and DL-Asn·H₂O are shown in Table 1 and in supersaturated solutions of DL-Asn·H₂O with 3 mol% of D-/L- additives in Table 2.

The growth rate of L-Asn·H₂O in L-Asn·H₂O solution was the highest; for the same supersaturation of L-Asn·H₂O the growth from DL-Asn·H₂O solutions was



(a)



(b)

Fig. 5. Relationship between growth rate frequency and growth rate of L-Asn·H₂O crystals in a solution with supersaturation, $S = 1.1$ of (a) L-Asn·H₂O (b) DL-Asn·H₂O at 30 °C.

Table 1. Fitting parameters for the crystal growth rate distribution of L-Asn·H₂O grown in solutions of L- and DL-Asn·H₂O in various supersaturation.

S	L-Asn·H ₂ O solution			DL-Asn·H ₂ O solution		
	1.05	1.1	1.15	1.05	1.1	1.15
$G_o(\mu\text{m}/\text{min})$	0.51	0.96	1.41	0.29	0.60	0.89
σ_G	0.09	0.11	0.12	0.07	0.11	0.18
R^2	0.9972	0.9835	0.9360	0.9985	0.9423	0.9765

Table 2. Fitting parameters for the crystal growth rate distribution of L-Asn·H₂O grown in solutions of DL-Asn·H₂O without and with 3 mol% (based on total concentration of DL-AsnH₂O) of various additives at a supersaturation $S = 1.1$.

Type of additives	No additives	D-Asp	D-Glu	D-Leu	D-Val	L-Asp	L-Glu	L-Leu	L-Val
$G_o(\mu\text{m}/\text{min})$	0.60	0.39	0.47	0.69	0.60	0.19	0.28	0.62	0.73
σ_G	0.11	0.07	0.09	0.11	0.08	0.06	0.06	0.12	0.07
R^2	0.9423	0.9903	0.9995	0.9824	0.9844	0.9643	0.9974	0.9829	0.8964

substantially reduced, with an almost 50% reduction in growth rates at low supersaturation values. One explanation for this difference is that the counter enantiomer acts as an inhibitor to the growth of the preferred enantiomer. It is possible that even in compounds where the conglomerate is the stable crystal form, the association of the preferred and counter enantiomer (as would be seen in the racemate form) is still strong enough that the counter enantiomer of the additive can also adsorb to the surface of the crystal and inhibit the growth of the conglomerate form. Another possible explanation is that racemic dimers of Asn (associations of D- and L-molecules) in solution hinders the supply of L-monomers to the surface of the crystal and thus lowers the crystal growth rate.

From Table 2, the mean growth rate of L-Asn·H₂O with D-Val and L-Leu additives are not statistically different from the growth rate without additives. Use of D-Leu as an additive increases the growth rate, however the change is only slightly larger than the 95% confidence limits. Use of L-Val as an additive increases the growth rate of L-Asn by a statistically significant amount. The reason for this is not known although the additive appears to have no significant effect on the solubility of L-Asn. It is possible that the molecule interrupts the associations between D- and L-Asn molecules in solution. D-Glu, D-Asp, L-Glu and L-Asp additives significantly reduced the crystal growth rate of L-Asn·H₂O. This is to be expected because of the greater similarity of the side chains of aspartic acid and glutamic acid to asparagine, in comparison to the side chains of valine or leucine. However, there is a more significant effect of additives of the same chirality as the growing crystal; the effect of L-Glu and L-Asp on L-Asn·H₂O was greater than the D-Glu and D-Asp additives because L-Glu and L-Asp additives have the same absolute configuration as L-Asn·H₂O. These additives are therefore likely to adsorb on the growing surface of L-Asn·H₂O and inhibit the propagation of the growth steps on the crystal.

For this experiment, we measured the growth in the length of the principal axis of the crystal, but the growth rate based on the spherical average diameter can be derived from this value based on the shape of the crystal. In the case investigated here it was found that there is minimal change in the shape of the crystal as the growth progresses even in experiments using additives, and therefore it seems that the additives cause a similar inhibiting effect for all important growth surfaces of the crystal.

Here L-Asn was used as the crystallizing species for convenience – it is easier to obtain commercially than D-Asn. In the preferential crystallizations of L-Asn·H₂O we use D-Asp and D-Glu to inhibit growth of D-Asn·H₂O.

3.3 Preferential crystallization of L-Asn·H₂O with D-aspartic acid additives

The preferential crystallization (PC) of L-Asn·H₂O from DL-Asn·H₂O with and without additives was studied. The enantiomeric excess e of the produced crystals and

yield y of the PC were measured to show the effectiveness of the additives.

$$e = \frac{C_L - C_D}{C_L + C_D} \times 100\% = \frac{A_L - A_D}{A_L + A_D} \times 100\% \quad (2)$$

where C_L is the concentration of L-Asn·H₂O in the solid product (g L-Asn·H₂O/g solid), C_D is the concentration of D-Asn·H₂O in the solid product, A_L and A_D are the peak areas of L-Asn·H₂O and D-Asn·H₂O from the solid product in the HPLC chromatogram.

$$y = \frac{m_t}{m_{th}} \times 100\%. \quad (3)$$

Here, m_t is the mass of preferred enantiomer produced (which does not include the mass of the counter enantiomer in the product if the e is less than 100%) and m_{th} is maximum mass of the preferred enantiomer obtainable at equilibrium (again, excluding the counter enantiomer). Since a mass m_s of seed crystals was introduced at the start of the preferential crystallization resulting in a mass m_p of the preferred enantiomer product, the yield is further defined using $m_t = m_p - m_s$ in equation (3).

$$y = \frac{m_p - m_s}{m_{th}} \times 100\%.$$

Figures 6 and 7 show the yield y and enantiomeric excess e of product in time respectively of the PC of L-Asn·H₂O in DL-Asn·H₂O with and without additives. The yield of the PC of L-Asn·H₂O with and without additives increases with time. The yield of the PC of L-Asn·H₂O without additives can reach 60% within 7 h. However, pure L-Asn·H₂O product can only be obtained within the initial 4 h, with a yield of only 25% at this time: After 4 h of the crystallization nucleation and growth of D-Asn·H₂O occurs decreasing the enantiomeric excess e .

Since the growth of the L-Asn·H₂O crystals was not close to completion at this time, the crystallization of D-Asn·H₂O should be inhibited to prolong the crystallization time through the use of additives. In the case of D-Leu and D-Val additives, similar yield and enantiomeric excess results are obtained compared to the PC without additives; this shows that they are not effective in inhibiting the crystallization of D-Asn·H₂O. However, D-Glu and D-Asp can extend the time period during which there is no crystallization of D-Asn·H₂O, which increases the period during which pure L-Asn·H₂O can be formed to longer than 7 h and 10 h respectively.

Although the time period of preferential crystallization is increased, the yield of L-Asn·H₂O is lower at the same crystallization time compared to the case where no additive is used. This indicates that these additives also seem to inhibit the crystallization of L-Asn·H₂O, which is consistent with the growth rate experiments. Nevertheless, the maximum yield of pure L-Asn·H₂O from PC with D-Glu additive is 30%, and with D-Asp additive is more than 44%, as shown in Figure 8, which is higher than the potential yield in the absence of additives. Therefore, the additives are helpful for the PC process in purity and yield. It is interesting that the main effect seen in the PC experiments was a significant increase in the induction time required for noticeable nucleation of the counter enantiomer while the MSZW experiments showed that the additives had only a small effect on the zone width. This may be due to the higher supersaturations at which crystals appear in the MSZW measurements compared to the PC and growth experiments. At these higher supersaturations additives might be less effective in blocking the crystal growth and since the MSZW is at least partially determined by growth no substantial effects of the impurities were measured. Since the MSZW is determined by nucleation and subsequent growth while no substantial effects of the impurities on the MSZW were measured this suggests that nucleation

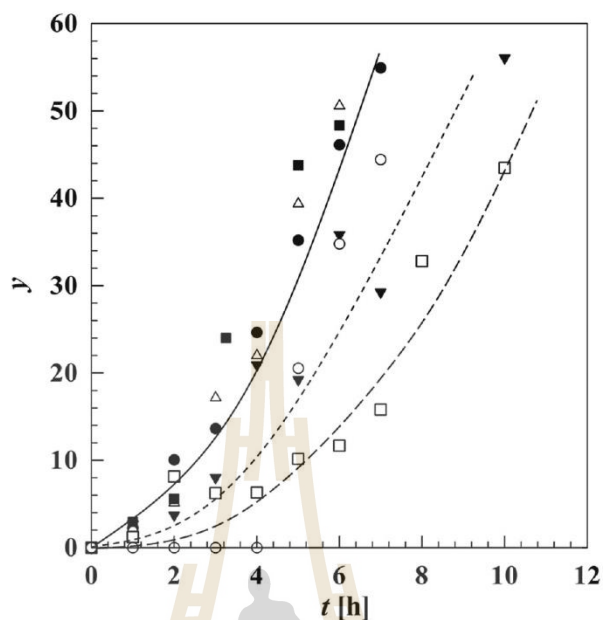


Fig. 6. The yield y of L-Asn·H₂O in the crystal phase during a preferential crystallization (PC) of L-Asn·H₂O from DL-Asn·H₂O in water in absence of additive (●), with 5% mol of D-Asp (□), with 5% mol of D-Glu (▼), with 5% mol of D-Val (△), with 5% mol of D-Leu (■), yield of D-Asn·H₂O from DL-Asn·H₂O in water in absence of additive (○). The lines are a guide to the eye.

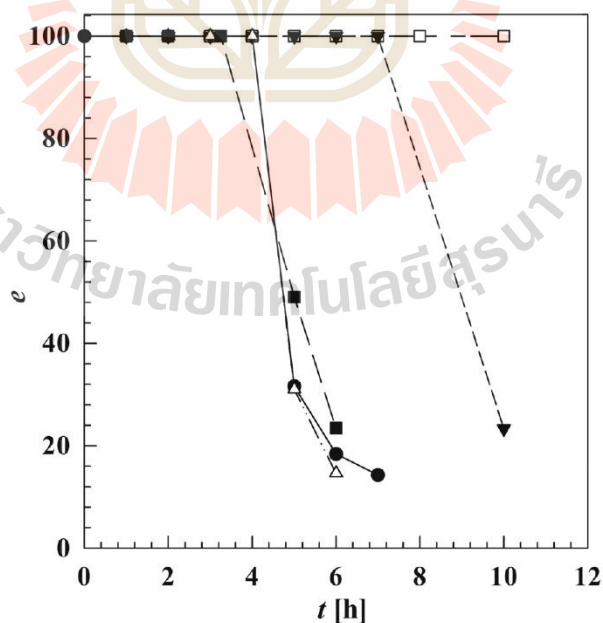


Fig. 7. The enantiomeric excess e of L-Asn·H₂O in the crystal phase during a preferential crystallization (PC) of L-Asn·H₂O from DL-Asn·H₂O in water in absence of additives (●), with 5% mol of D-Asp (□) with 5% mol of D-Glu (▼), with 5% mol of D-Val (△), with 5% mol of D-Leu (■). The lines are a guide to the eye.

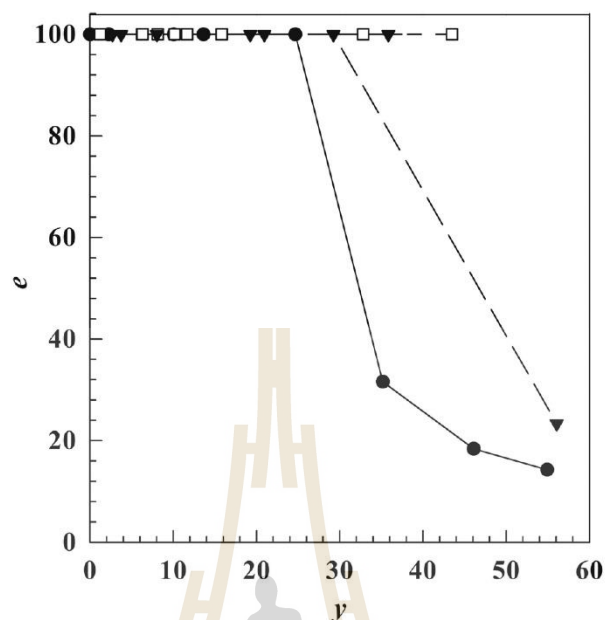


Fig. 8. The relationship between enantiomeric excess e and yield y of L-Asn·H₂O from DL-Asn·H₂O in water in absence of additive (●), with 5% mol of D-Asp (□), with 5% mol of D-Glu (▼). The lines are a guide to the eye.

only occurs at relatively high supersaturations at which the effect of the impurity on the growth is absent.

To increase yield and prolong the period for which the enantiomeric excess is close to 100% for the system using PC with additives, more seed crystals can be used. The current PC experiments were performed to investigate the mechanisms on which the additives act in order to improve the performance of the PC systems. In order to optimize PC processes it is also necessary to consider optimization in terms of all tunable parameters, including additive levels, temperature profiles during cooling, agitation levels, and the amount of seeds used.

4 Conclusions

The tested D-amino acids have almost no effect on the solubility of D-Asn·H₂O but have a slight effect on the metastable zone width of D-Asn·H₂O, largely increasing the scatter or uncertainty of this zone. The growth rate of L-Asn·H₂O strongly decreases when using L-Asp and L-Glu additives in DL-Asn·H₂O solutions. The converse must also be true, that D-Asp and D-Glu inhibit crystallization of D-Asn·H₂O: These additives effectively prevent the crystallization of the counter enantiomer in the preferential crystallization of L-Asn·H₂O. The success of these additives is likely due to the similarities in their side chains in comparison to asparagine. Leucine and valine have far less effect as additives; these two molecules have side chains that are alkanes, which are much less compatible with the side chain of asparagine which contains both carbonyl and amine functionality. However, at the same crystallization time the yield of L-Asn·H₂O decreases when D-Glu and D-Asp were used as additives. Therefore, the D-additives not only influence the crystallization of D-Asn·H₂O but also influence the crystallization of L-Asn·H₂O. Nevertheless, the yield of L-Asn·H₂O at the end of the period during which pure L-Asn·H₂O can be produced is higher when using D-Asp

and D-Glu additives, and can in principle be increased by adding more seed crystals. Therefore, these additives are promising for improving the preferential crystallization of this species.

The research was supported by the Thailand Research Fund (TRF) via the Royal Golden Jubilee Ph.D. program (PHD/0097/2552). PK thanks for the kind hospitality that he received upon his visit to the Intensified Reaction & Separation Systems group at the Delft University of Technology in the Netherlands. JtH thanks the EPSRC Centre for Innovative Manufacturing in Continuous Manufacturing and Crystallisation (<http://www.cmac.ac.uk>) for supporting this work (EPSRC funding under grant reference: EP/I033459/1).

References

1. P.Y. Bruice, *Organic Chemistry*, 4th edn. (Pearson Prentice Hall, New Jersey, 2004)
2. X.J. Wang, H. Wiehler, C.B. Ching, *J. Chem. Eng. Data* **48**, 1092 (2003)
3. T. Eriksson, S. Bjorkman, P. Hoglund, *Eur. J. Clin. Pharmacol.* **57**, 365 (2001)
4. M. Yoshikawa, A. Higuchi, in *Encyclopedia of Membrane Science and Technology*, edited by E.M.C. Hoek, V.V. Tarabara (John Wiley & Sons, Hoboken NJ, 2013)
5. E. Francotte, *J. Chromatogr A* **906**, 379 (2001)
6. H. Lorenz, A. Perlberg, D. Sapoundjiev, M.P. Elsner, A. Seidel-Morgenstern, *Chem. Eng. Process.* **45**, 863 (2006)
7. D. Kozma, *CRC Handbook of Optical Resolution via Diastereomeric Salt Formation* (CRC Press, Boca Raton, 2002)
8. J. Jacques, A. Collet, S. Wilen, *Enantiomers, Racemates and Resolutions* (John Wiley & Sons, New York, 1981)
9. T. Buhse, D.K. Kondepudi, B. Hoskins, *Chirality* **11**, 343 (1999)
10. K. Petruševska-Seebach, A. Seidel-Morgenstern, M.P. Elsner, *Cryst. Growth Des.* **11**, 2149 (2011)
11. V.M. Profir, M. Matsuoka, *Colloid Surface A.* **164**, 315 (2000)
12. W. Srimahaprom, A.E. Flood, *J. Cryst. Growth* **362**, 88 (2013)
13. M.P. Elsner, G. Ziomek, A. Seidel-Morgenstern, *AIChE J.* **55**, 640 (2009)
14. G. Levilain, M. Eicke, A. Seidel-Morgenstern, *Cryst. Growth Des.* **12**, 5396 (2012)
15. M.J. Eicke, G. Levilain, A. Seidel-Morgenstern, *Cryst. Growth Des.* **13**, 1638 (2013)
16. A. Svang-Ariyaskul, W.J. Koros, R.W. Rousseau, *Chem. Eng. Sci.* **64**, 1980 (2009)
17. K. Würges, K. Petruševska, S. Serci, S. Wilhelm, C. Wandrey, A. Seidel-Morgenstern, M.P. Elsner, S. Lütz, *J. Mol. Catal. B: Enzym.* **58**, 10 (2009)
18. K. Petruševska-Seebach, K. Würges, A. Seidel-Morgenstern, S. Lütz, M.P. Elsner, *Chem. Eng. Sci.* **64**, 2473 (2009)
19. L. Addadi, J. van Mil, M. Lahav, *J. Am. Chem. Soc.* **103**, 1249 (1981)
20. L. Addadi, S. Weinstein, E. Gati, I. Weissbuch, M. Lahav, *J. Am. Chem. Soc.* **104**, 4610 (1982)
21. D.K. Kondepudi, M. Culha, *Chirality* **10**, 238 (1998)
22. D.K. Kondepudi, K.E. Crook, *Cryst. Growth Des.* **5**, 2173 (2005)
23. N. Doki, M. Yokota, S. Sasaki, N. Kubota, *Cryst. Growth Des.* **4**, 1359 (2004)
24. S. Srisanga, J.H. ter Horst, *Cryst. Growth Des.* **10**, 1808 (2010)
25. T. Izumi, D.G. Blackmond, *Chem. Eur. J.* **16**, 3065 (2009)
26. C.J. Orella, D.J. Kirwan, *Ind. Eng. Chem. Res.* **30**, 1040 (1991)
27. J.B. Dalton, C.L.A. Schmidt, *J. Biol. Chem.* **109**, 241 (1935)
28. D. Binev, A. Seidel-Morgenstern, H. Lorenz, *Cryst. Growth Des.* **16**, 1409 (2016)
29. P. Kongsamai, A. Maneedaeng, A.E. Flood, in *Proceeding of the 5th Regional Conference on Chemical Engineering, Pattaya, Thailand, 2013*

BIOGRAPHY

Mr. Peetikamol Kongsamai was born on October 4, 1987 in Kanchanaburi. He earned his bachelor's degree in Chemical Engineering from Suranaree University of Technology (SUT), Nakhon Ratchasima, in 2010. He has received the RGJ-Ph.D. scholarship from the Thailand Research Fund (TRF) to study the doctoral degree in Chemical Engineering since 2010. He has also had additional laboratory experience as an exchange scholar at the intensified reaction and separation systems group at Delft University of Technology, Delft, the Netherlands, in 2013.

